THE UNIVERSITY *of* EDINBURGH

Function and organisation of actin and septins in *Neurospora crassa*

Adokiye Berepiki

Thesis presented for the degree of Doctor of Philosophy

University of Edinburgh

2013

Declaration

I declare that this thesis was written by myself and the research presented is my own work, except where stated otherwise. This work has not been submitted for any other degree or professional qualification except as specified.

Adokiye Berepiki

Acknowledgements

I would like to thank Nick Read for his supervision and guidance throughout my PhD, and in helping me develop as a researcher. Thanks to all the members of the Read lab for their input and help, particularly Alex Lichius and Jun-ya Shoji for passing on their expertise in molecular cloning. Thanks to Saskia du Pré who was responsible for generating plasmid pSP524, which was used to label MYO-5, and carried out the CCP and BDM experiments on the *lifeact-sgfp* strain. Thanks to Martin Barrios-Llerena and Thierry Le Bihan from the SynthSys Institute for the mass spectrometry analysis. I am eternally indebted to Dave Kelly for teaching me how to use various advanced microscopes and helping me in my live-cell imaging experiments. Thanks to my PhD committee for their advice and input. Finally, thanks to my partner, Sarah, for her continuous support over the last four years.

Abstract

This thesis deals with the organisation and function of actin and septins in the model filamentous fungus, *Neurospora crassa*. Firstly, study demonstrates the utility of the Lifeact peptide probe for the investigation of actin dynamics in *N. crassa*. Lifeact fused to fluorescent proteins allowed live-cell imaging of actin patches, cables and rings without interfering with cellular functions. Actin cables and patches localised to sites of active growth during the establishment and maintenance of cell polarity in germ tubes and conidial anastomosis tubes (CATs). Recurrent phases of formation and retrograde movement of complex arrays of actin cables were observed at growing tips of germ tubes and CATs. Two populations of actin patches exhibiting slow and fast movement were distinguished, and rapid (1.2 µm/s) saltatory transport of patches along cables was observed. Actin cables accumulated and subsequently condensed into actin rings associated with septum formation. F-actin organisation was markedly different between the tip regions of mature hyphae and germ tubes. Only mature hyphae displayed a sub-apical collar of actin patches and a concentration of F-actin within the core of the Spitzenkörper. Proper organisation of actin cables required the class-V myosin, MYO-5, and the frequency of rapid transport of actin patches was reduced in its absence, suggesting that MYO-5 participates in actin patch translocation. Deletion of *myo-5* caused gross morphological and polarity defects, demonstrating the importance of this motor for normal cell function. GFP-tagged MYO-5 localised as a crescent at germ tube tips and to the core of the Spitzenkörper in mature hyphae. Secondly, analysis of septin null mutants demonstrated that septins limit the emergence of germ tubes and are important for septation and conidiation in *N. crassa*. Septins showed different patterns of localisation at hyphal tips, with GFP-CDC-10 and CDC-11-GFP organised as a collar with lower signal intensity at the tip apex, CDC-3-GFP and CDC-12-GFP constituted as a cap at the tip apex and GFP-SPN-1 forming an extended collar. Septins formed a range of different higher-order structures in *N. crassa* – rings, loops, fibres, bar-like structures, and caps – which can co-exist within the same cell. Purification of the septin complex and mass spectrometry of isolated proteins revealed that the septin complex consists predominantly of CDC-3, CDC-10, CDC-11 and CDC-12. Immunoprecipitation of SPN-1 revealed that this septin interacts with the core septin complex.

Table of contents

Abbreviations

ABP	actin binding protein
ADWB	antibody-Dynabead wash buffer
ATP	adenine triphosphate
bp	base pair
BDM	2, 3-butanedione monoxime
CAR	contractile actomyosin ring
CAT	conidial anastomosis tube
CCCP	carbonyl cyanide *m*-chlorophenylhydrazone
CCD	charge-coupled device
CDC	cell division cycle
CSM	complete selection media
DAD	diaphonous-related formin autoregulatory domain
ddH_20	double deionised water
DID	diaphonous-related formin inhibitory domain
DMSO	dimethyl sulfoxide
dNTP	deoxyribonucleotide triphosphate
dTTP	deoxythymidine triphosphate
dUTP	deoxyuridine triphosphate
EDTA	ethylenediaminetetraacetic acid
EM	electron microscopy
ER	endoplasmic reticulum
FGSC	fungal genetics stock centre
FH1	formin homology domain 1
FH2	formin homology domain 2
FM4-64	N-(3-triethylammoniumpropyl)-4-(6-(4-(diethylamino)phenyl) hexatrienyl) pyridinium dibromide
FP	fluorescent protein
FRAP	fluorescence recovery after photobleaching
GFP	green fluorescent protein
GTP	guanine triphosphate
HAT	histidine affinity tag
HEPES	4-(2-hydroxyethyl)-1-piperazineethanesulfonic acid
HO	higher-order
HPLC	high-performance liquid chromatography

HTI	his tag isolation
IP	immunuprecipitation
kbp	kilo base pairs
kDa	kilo Daltons
Lat A	latrunculin A
LED	light emitting diode
LP	long pass
LTQ	linear trap quadrupole
MS	mass spectrometry
MT	microtubules
ORF	open reading frame
PAGE	polyacrylamide gel electrophoresis
PAK	p21-activated kinase
PEG	polyethylene glycol
PCR	polymerase chain reaction
PMSF	phenylmethylsulfonyl fluoride
RBD	rho-binding domain
RFP	red fluorescent protein
SDS	sodium sodecyl sulphate
SIMIBI	signal recognition particle related to MinD and BioD
Spk	Spitzenkörper
TAP	tandem affinity purification
TRAFAC	translation-factor-related
UTR	untranslated region
VMM	Vogel’s minimal medium
WT	wild-type
WASP	Wiskott-Aldrich syndrome protein
YRC	yeast recombinational cloning

List of figures and tables

Figures

Tables

Chapter 1:

Introduction

1.1 Morphogenesis in filamentous fungi

Filamentous fungi are of profound ecological, agricultural, medical and biotechnological importance (May and Adams, 1997). A key to the extraordinary success of these organisms has been the evolution of highly polarised, and predominantly tip-growing, tubular hyphae that determine the unique modes of morphogenesis and lifestyles of filamentous fungi as non-motile, heterotrophic organisms (Read, 2006). Several lines of evidence suggest that the ancestral form of fungi that gave rise to the budding and fission yeasts was filamentous (Liu and Hall, 2004).

The cytoskeleton plays a major role in the regulation of fungal cell morphogenesis (Berepiki et al., 2011; Lichius et al., 2011). The three main structural polymers constituting the fungal cytoskeleton are filamentous actin (F-actin), microtubules (MTs) and septins. Although somewhat contentious, septins can be considered as cytoskeletal elements for the following reasons: (1) they form nonpolar, heteropolymeric higher-order structures within the cell, the formation of which is fundamental for their role as scaffolds and barriers; (2) septin structures are not thought to have any catalytic functions, instead they compartmentalise the cell and support cellular architecture; (3) although not ubiquitous they are widespread in eukaryotes, and (4) deletion of one or more septins is lethal in many reported cases, highlighting their importance to normal cellular function (Barral et al., 2000; Gladfelter et al., 2001; Hartwell, 1971; Momany et al., 2001).

In common with other types of walled cells, morphogenesis in fungi is governed by wall construction (Bartnicki-Garcia, 2002). Hyphae grow by continual tip extension, which requires the localised delivery and fusion of secretory vesicles that supply the apical plasma membrane with membrane and enzymes for the synthesis of new cell wall, while turgor provides the primary driving force behind cell expansion (Bartnicki-Garcia, 2002; Bartnicki-Garcia et al., 2000). As such, targeted secretion underpins hyphal form and function, and the fungal cell achieves proper morphogenesis through the reorganisation, polarisation and

alignment of actin and microtubule cytoskeletal tracks along which secretory vesicles are translocated (Fuchs et al., 2005; Motegi et al., 2001; Pruyne et al., 1998; Schott et al., 2002; Seiler et al., 1997; Steinberg, 2007a; Weber et al., 2006). Both actin and microtubules are critical to the growth of hyphae and have different but complementary roles in their polarised extension (Harris et al., 2005; Lichius et al., 2011). Hyphal tips treated with anti-actin drugs immediately arrest apical extension and swell (Knechtle et al., 2006; Pantazopoulou and Penalva, 2009; Taheri-Talesh et al., 2008; Torralba et al., 1998) - suggesting that exocytosis still occurs but is no longer localised to the hyphal apex. Actin-mediated endocytosis also contributes to normal polar growth (Araujo-Bazan et al., 2008; Taheri-Talesh et al., 2008; Upadhyay and Shaw, 2008). In addition to the function of actin in exocytosis and endocytosis, pharmacological and genetic studies have revealed an essential role for actin in cytokinesis and organelle transport in fungi (Figure 1.1) (Ayscough et al., 1997; Barja et al., 1993; Harris et al., 1994; Novick and Botstein, 1985; Pantazopoulou and Penalva, 2009; Rida et al., 2006; Suelmann and Fischer, 2000; Taheri-Talesh et al., 2008; Torralba et al., 1998; Virag and Griffiths, 2004).

Also important to fungal morphogenesis is the generation of cellular asymmetry which permits the alignment of cytoskeletal tracks. Septins, which are filament-forming GTP-binding proteins, play key roles in cell polarity by localising to discrete regions on the plasma membrane where they form scaffolds and diffusion barriers which are crucial for the proper assembly of protein complexes such as the contractile actomyosin ring (CAR), polarisome and exocyst (Barral et al., 2000; Dobbelaere and Barral, 2004; Orlando et al., 2011). In filamentous fungi, the absence of septins leads to delayed septation, increased emergence of germ tubes and branches and decreased sporulation (Hernandez-Rodriguez et al., 2012; Lindsey et al., 2010a). These findings suggest that one of the key functions of septins in filamentous fungi is to prevent the inappropriate emergence of germ tubes and branches, which is in keeping with their known role as a diffusion barrier and scaffold in budding yeast.

The yeasts *Saccharomyces cerevisiae* and *Schizosaccharomyces pombe* are well-established models for the study of actin and septins in eukaryotic cells (Kovar et al., 2011; Moseley and Goode, 2006; Spiliotis and Gladfelter, 2012; Weirich et al., 2008). However, several aspects of the filamentous fungal lifestyle, such as the capacity to simultaneously maintain different foci of growth, rapid apical extension, and the production of a range of cell types suggests that there are likely to be important differences in actin and septin organisation and dynamics, as well as in associated regulatory mechanisms between unicellular and multicellular fungi (Harris and Momany, 2004). Indeed, a large scale-screen for proteins involved in hyphal morphogenesis in *Neurospora crassa* uncovered multiple regulators of actin dynamics but also several novel proteins lacking known homologues (Seiler and Plamann, 2003). The growing range of experimentally and genetically tractable, fully sequenced model filamentous fungi, such as *N. crassa*, *Aspergillus nidulans*, *Ashbya gossypii*, and *Ustilago maydis*, has expedited several recent investigations that have yielded new insights into the fungal actin and septin cytoskeletons, which are discussed below (Alvarez-Tabares and Perez-Martin, 2010; Araujo-Bazan et al., 2008; Berepiki et al., 2010; Delgado-Alvarez et al., 2010; DeMay et al., 2009; Lindsey et al., 2010a; Lindsey et al., 2010b; Taheri-Talesh et al., 2008).

1.2 The actin cytoskeleton

Actin is an abundant, highly-conserved protein found in all eukaryotes. The 43-kDa monomeric form (globular or G-actin) is a single polypeptide chain consisting of two major domains that form a deep cleft that participates in ATP binding (Dominguez and Holmes, 2011). G-actin can assemble into filaments (Figure 1.1A); two parallel proto-filaments form a double helix, known as a microfilament (filamentous actin or F-actin), with a diameter of 7 nm and the loop of the helix repeating every 37 nm. The process of self-assembly gives rise

to microfilaments with structural polarity, which is a crucial attribute for their cellular function. Assembly is dynamic, with individual filaments continually growing and shrinking, and is regulated by ATP hydrolysis and an enormous range of actin-binding proteins (ABPs). ABPs catalyse the gamut of regulatory events including severing, capping, nucleating, and cross-linking of F-actin.

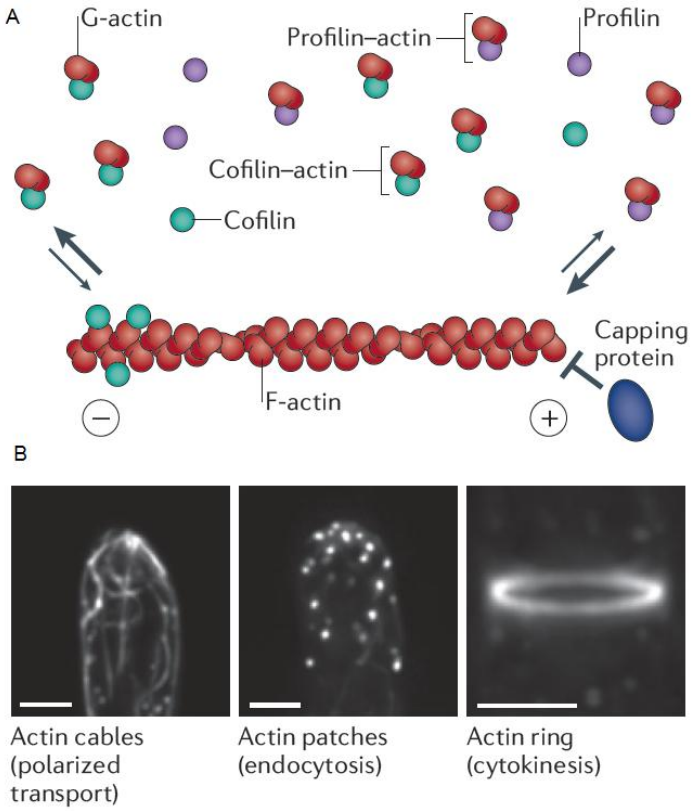

Figure 1.1 Properties of F-actin and higher order actin structures in filamentous fungi. (A) F-actin is an asymmetrical polymer. Within an actin filament the plus end (also known as the barbed end) of a G-actin subunit binds to the minus end (also known as the pointed end) of the neighbouring G-actin subunit. Two filaments form a helical microfilament. The plus end of a microfilament is the fast-growing end with net addition of subunits, whereas the minus end is slow-growing with net loss of subunits. Three important ABPs that regulate microfilament dynamics are cofilin (which disassembles F-actin), profilin (which sequesters G-actin) and capping protein (which caps the plus end of filaments, inhibiting their disassembly). (B) F-actin forms three higher order structures with different functional roles. Actin cables (extended lines) are important in polarised transport, actin patches (dots) mediate endocytosis and actin rings are contractile structures that guide septum formation during cytokinesis. Bar, 2 µm. Adapted from Berepiki et al. (2011).

The rapid assembly and disassembly of F-actin into higher-order structures, with differing functional roles, coupled to nucleotide hydrolysis, provides the cell with an energy-efficient means of cellular organisation (Figure 1.1B).

1.2.1 Imaging the actin cytoskeleton

A pioneering electron microscopy (EM) study by Howard (1981) using freeze-substitution provided one of the first insights into actin organisation in fungi. This study revealed a relative abundance of actin in hyphal tips, at septa and an accumulation of microfilaments in the Spitzenkörper (Spk), an apical multicomponent structure that contains a vesicle cluster involved in secretion. The Spitzenkörper, literally meaning 'apical body', was first identified in growing hyphae of filamentous fungi in the 1950s, using phase-contrast light microscopy, as a dynamic, phase-dark accumulation of material at the apex of hyphal tips (Girbardt, 1957). The Spk is a complex, multicomponent structure dominated by vesicles and in close proximity to the apical plasma membrane of mature hyphae (Verdin et al., 2009). New Spk arise at sites of branch initiation, and the position of the Spk within the hyphal tip predicts the subsequent direction of hyphal tip growth (Bracker et al., 1997; Girbardt, 1957). This evidence supports the idea that the Spk acts as a vesicle supply centre for targeted secretion of new plasma membrane and cell wall synthesising enzymes involved in cell surface expansion (Bartnicki-Garcia et al., 1989). The Spk has a unique role in spatially and temporally organising the polarity machinery, by moving within the apical dome and controlling the directionality and speed of polarised tip extension (Riquelme et al., 1998). The mechanism of Spk motility remains unknown, but might involve concerted action of the actin and microtubule cytoskeleton, in order to maintain the integrity of the Spk at the growing tip (Steinberg, 2007a). In *N. crassa* microtubules transiently extend into the Spk (Freitag et al., 2004), whereas actin localises to the core of the Spk and also forms a collar of endocytic

patches associated with the plasma membrane (Berepiki et al., 2010). The different distribution of MTs and F-actin at hyphal tips has led to the proposition that the Spk acts as a 'relay station' from long-distance transport along microtubules to short-distance F-actin-mediated targeted vesicle delivery to the apical plasma membrane of the hyphal tip (Harris et al., 2005). In addition, fidelity of polarised tip growth is thought to be increased through MT-mediated deposition of polarity factors at the apical plasma membrane (Takeshita et al., 2008), as has been shown for the formin For3 in *S*. *pombe*, which is delivered to cell tips by MTs where it assembles actin cables (Martin et al., 2005c).

It was suggested that the presence of F-actin within the Spk could mediate fusion between secretory vesicles and specific sites on the plasma membrane and, somewhat presciently, that "a possible role for actin filaments in secretion may be common to a wide variety of eukaryotic cell types" (Howard, 1981). Also reported was an aggregation of peripheral patches or plaques on or very close to the plasma membrane termed filasomes (Howard, 1981) that are vesicles coated in F-actin (Bourett and Howard, 1991; Roberson, 1992). Several years later, two seminal papers, utilising fluorescently-labelled phalloidin and actin antibodies, revealed the presence of three higher order F-actin structures in *S. cerevisiae*: patches, cables and rings (Adams and Pringle, 1984; Kilmartin and Adams, 1984). A close association of actin patches and cables with growing buds was described, suggesting that both structures participated in polarised growth. The presence of patches, cables and rings in the fission yeast *S. pombe* was confirmed shortly thereafter (Marks et al., 1986). Immunofluorescence microscopy confirmed the presence of actin patches (or plaques) and actin rings in hyphae of *A. nidulans*, *N*. *crassa*, and *C. albicans* (Barja et al., 1991; Garrill and Suei, 2008; Torralba et al., 1998; Yokoyama et al., 1990). It is likely that the filasomes reported by Howard (1981) and the actin patches in filamentous fungi are the same entity.

Imaging F-actin in living cells has proved to be challenging. Live-cell imaging of actin has been attempted by the microinjection of fluorescently labelled-phalloidin (or actin) or by expression of green fluorescent protein (GFP) -actin (Doyle and Botstein, 1996; Kreis et al., 1979; Wehland and Weber, 1981; Wu and Pollard, 2005). However, phalloidin is toxic to cells (Cooper, 1987) and microinjection allows only transient monitoring of actin dynamics. GFP-actin is unable to function as the sole source of cellular actin, is not incorporated into actin cables and perturbs actin dynamics (Doyle and Botstein, 1996; Riedl et al., 2008; Wu and Pollard, 2005). More recent approaches have relied on fusions of fluorescent proteins (FPs) to ABPs or actin binding domains. These approaches are preferable as there is generally less perturbation of F-actin dynamics *in vivo* but they may only reveal a subpopulation of F-actin and the fusion protein may compete with unlabelled endogenous ABPs. In an attempt to generate a suitable probe for F-actin, Riedl et al. (2008) truncated Abp140 from *S. cerevisiae*, first used for imaging the actin cytoskeleton in budding yeast (Yang and Pon, 2002), to yield a 17 aa peptide (called Lifeact) which gave the same staining pattern as the full length Abp140, when fused to GFP. The Lifeact peptide has proved to be a convenient F-actin probe and has been used to image F-actin in diverse organisms such as mice, plants, and filamentous fungi (Berepiki et al., 2010; Delgado-Alvarez et al., 2010; Riedl et al., 2010; Ueda et al., 2009; Vidali et al., 2009). Although Lifeact has proved to be an incredibly useful tool, there are some caveats with its use. Due to Lifeact's low binding affinity for F-actin, it cannot be utilised in microscopy techniques such as fluorescence recovery after photobleaching (FRAP) in order to measure F-actin dynamics, because FRAP requires the covalent attachment of a fluorophore to the protein of interest for accurate measurements of diffusion rates (Riedl et al., 2008). In addition, Lifeact has been shown to affect growth if expressed at high levels (Vidali et al., 2009) and care should be taken to ensure Lifeact-expressing cells are healthy and behave normally.

Recent studies with living filamentous fungi have unequivocally demonstrated the presence of actin cables (Berepiki et al., 2010; Delgado-Alvarez et al., 2010; Taheri-Talesh et al., 2008) and, therefore, it is likely that the previous failure to detect cables in some studies (Barja et al., 1991; Bourett and Howard, 1991; Howard, 1981; Roberson, 1992; Virag and Griffiths, 2004) was due to the use of unsuitable probes and/or poor preservation of labile F-actin structures during chemical fixation. We now know that the three higher-order F-actin structures all have distinct cellular roles, mechanisms of assembly, localisation patterns and dynamics (Figure 1.1B).

1.2.2 Actin patches

Actin patches are accumulations of F-actin complexed with over 60 other proteins that mediate endocytosis in fungal cells (Kubler and Riezman, 1993; Mulholland et al., 1994; Munn et al., 1995; Robertson et al., 2009b). Actin patches are initially assembled at the plasma membrane (Figure 1.2). Following invagination and scission, actin and other patch components that coat endocytic vesicles are gradually lost as the vesicles are transported away from the plasma membrane, and the uncoated vesicles eventually fuse with endosomal compartments (Huckaba et al., 2004). Endocytosis in growing regions of fungal cells is thought to provide a compensatory mechanism for exocytosis and aid the recycling of receptors and other membrane proteins (Altschuler et al., 2007; Penalva, 2010; Steinberg, 2007b). A pioneering study (Kaksonen et al., 2003), using pair-wise combinations of six patch proteins labelled with either GFP or red fluorescent protein (RFP), demonstrated that in *S. cerevisiae*, patch composition changes over time in a defined, predictable manner and that the alteration of protein composition correlates with different patterns of patch behaviour.

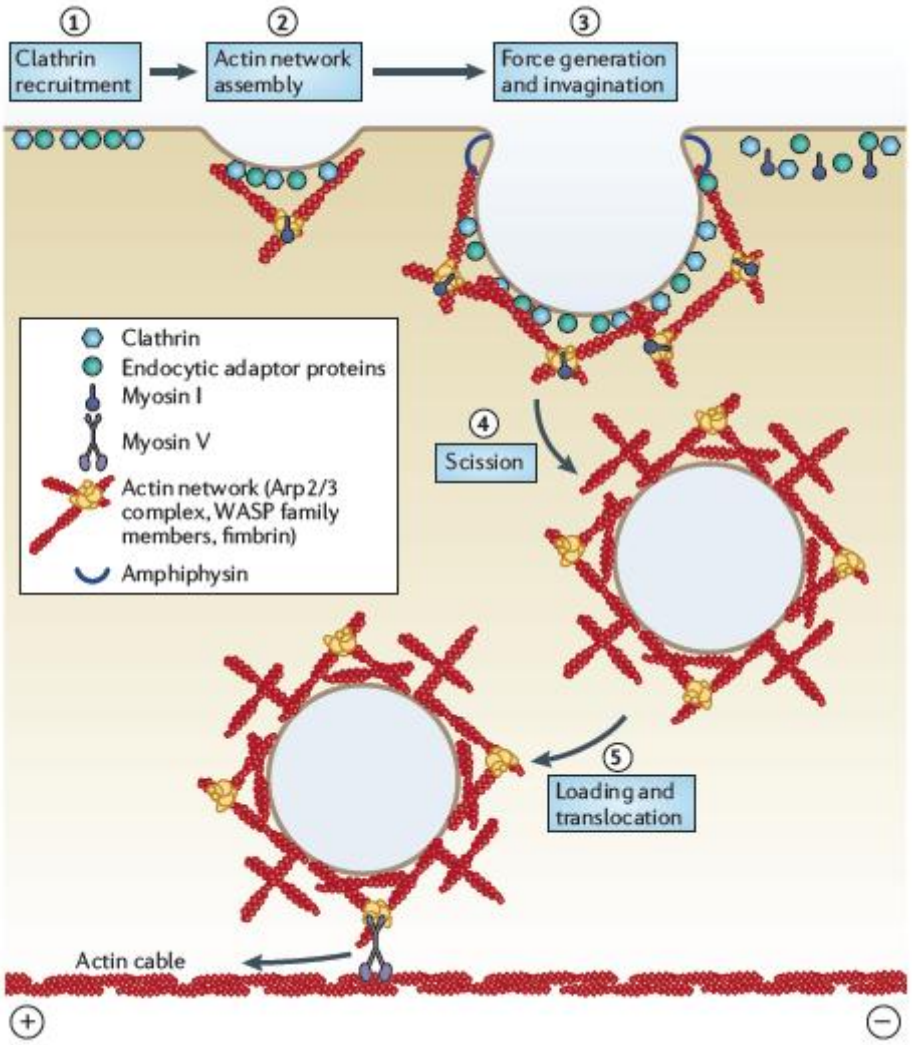

Figure 1.2. Model of Arp2/3-mediated actin nucleation and actin patch transport in filamentous fungi. Clathrin accumulation at the plasma membrane triggers the recruitment of endocytic adaptor proteins (step 1). Arp2/3 recruitment and activation by WASP and myosin-I catalyses the formation of an F-actin network cross-linked by fimbrin, leading to slow actin-dependent cortical movements (step 2). Further actin assembly together with amphyphysin and myosin-I activity promote invagination and scission of the endocytic vesicle (steps 3 and 4). Patch components left behind at the cell cortex include endocytic adaptor proteins and myosin-I. The mature patch is detached from the plasma membrane and loaded onto actin cables via an unknown mechanism (step 5). Patches can undergo rapid saltatory translocation along actin cables. The role of class V myosins in this mode of transport remains to be confirmed. Note that patches move in both directions within a hypha. As class-V myosins exclusively move towards the barbed ends of microfilaments, this suggests that actin cables are polarised or assembled from different sites and in opposite orientations. Adapted from Berepiki et al. (2011).

The composition of actin patches and details of their assembly has been the subject of several excellent reviews (Penalva, 2010; Robertson et al., 2009b; Sanchez-Ferrero and Peñalva, 2007). Briefly, in *S. cerevisiae* the accumulation of clathrin and endocytic adaptor proteins (such as Ede1, Eps15/Pan1, Sla1 and Sla2) at the plasma membrane triggers the recruitment of the Arp2/3 complex (Kaksonen et al., 2003; Kaksonen et al., 2005). The Arp2/3 complex employs structural mimicry to nucleate actin in patches (Moseley and Goode, 2006). Activation of Arp2/3 by the Wiskott-Aldrich syndrome protein (WASP) Las17 (also known as Bee1) (Li, 1997; Madania et al., 1999) and myosin-I (Jonsdottir and Li, 2004; Sun et al., 2006) stimulates actin assembly within patches to generate an F-actin network cross-linked by fimbrin (Ayscough et al., 2008; Kaksonen et al., 2005). Further actin assembly together with amphyphysin and myosin-I motor activity has been proposed to provide the force for plasma membrane invagination and scission of endocytic vesicles (Aghamohammadzadeh and Ayscough, 2009; Ayscough, 2000; Ayscough et al., 1997; Jonsdottir and Li, 2004; Robertson et al., 2009b; Sun et al., 2006).

Interestingly, actin is essential in *S. cerevisiae* for clathrin-dependent endocytosis, whereas in mammalian cells it merely facilitates endocytosis (Robertson et al., 2009b). Recent work has demonstrated that efficient actin polymerisation is required to overcome the internal turgor of fungal cells and drive membrane invagination during endocytosis (Aghamohammadzadeh and Ayscough, 2009). Furthermore, it has been suggested that in *S. cerevisiae* large, immobile, plasma membrane-associated protein assemblies called eisosomes are sites of endocytosis and it was initially shown that actin patch proteins colocalised with eisosome proteins (Walther et al., 2006). However, more recent studies have demonstrated that in *S. cerevisiae*, *A. gossypii* and *C. albicans* eisosome proteins fail to colocalise with actin patches and that eisosomes do not mark sites of endocytosis (Opekarova et al., 2008; Reijnst et al., 2011; Seger et al., 2011). The precise function of eisosomes remains elusive although it has been suggested they protect protein complexes

from endocytosis (Opekarova et al., 2008), and the eisosome protein Pil1 appears to be important for the polar growth of *A. gossypii* but not *A. nidulans* (Seger et al., 2011; Sophianopoulou et al., 2010).

The components of patches and the details of their assembly in filamentous fungi are probably similar to those found in *S. cerevisiae*, based on the high degree of ABP conservation between *S. cerevisiae*, *N. crassa* and *A. nidulans* (Borkovich et al., 2004; Sanchez-Ferrero and Peñalva, 2007). Initial studies have confirmed some similarities but have revealed interesting differences. Surprisingly, unlike other fungi where Arp2/3 is essential (Lees-Miller et al., 1992; Roca et al., 2010; Schwob and Martin, 1992), *C. albicans* cells lacking both Arp2 and Arp3 are viable and able to endocytose fluorescent dyes (FM4-64 and Lucifer yellow), albeit at a reduced rate (Epp et al., 2010). Distinct actin patches were not observed in Δ/Δ*arp2* Δ/Δ*arp3* cells whereas localisation of cables and rings, which are nucleated by formins (see below), was unaffected. Instead of patches, large filamentous aggregates were described similar to those observed in Arp2 and Arp3 temperature sensitive mutants and WASP Las17 null mutants of *S. cerevisiae*, which lack actin patches (Li, 1997; Martin et al., 2005a). The authors proposed the existence of an Arp2/3-independent endocytic pathway that requires actin polymerisation but uses a different nucleator, possibly a Ysc84 homolog or orthologous protein (Epp et al., 2010; Robertson et al., 2009a).

1.2.3 Actin patch dynamics

Actin patches display a predictable pattern of behaviour, i.e. they appear, mature, undergo a short period of undirected movement, and are subsequently translocated away from the membrane via actin cables (Berepiki et al., 2010; Huckaba et al., 2004; Pelham and Chang, 2001). Interestingly, two different patterns of patch behaviour have been observed in

filamentous fungi: slow-non linear, and rapid-linear (Berepiki et al., 2010; Upadhyay and Shaw, 2008).

The measured velocities and lifetimes of slow-non linear patches in *N. crassa* (0.26 µm/s and 14 s) (Berepiki et al., 2010) and *A. nidulans* (0.19 µm/s and 24 s) (Upadhyay and Shaw, 2008) were similar to values obtained for endocytic patches of *S. pombe* (0.31 µm/s and 19 s) (Pelham and Chang, 2001; Sirotkin et al., 2010) and *S. cerevisiae* (0.1-0.5 µm/s and 10-20 s) (Doyle and Botstein, 1996; Moseley and Goode, 2006; Smith et al., 2001; Waddle et al., 1996). Thus, these patches probably represent endocytic vesicles decorated with F-actin (Araujo-Bazan et al., 2008; Berepiki et al., 2010; Huckaba et al., 2004; Moseley and Goode, 2006; Sirotkin et al., 2010; Taheri-Talesh et al., 2008; Upadhyay and Shaw, 2008; Waddle et al., 1996).

Random, undirected movement of patches at the plasma membrane is driven by actin polymerisation (Kaksonen et al., 2003). In *S. cerevisiae*, subsequent patch transport along actin cables matches the rate of actin elongation, implying that polymerisation is the motive force (Huckaba et al., 2004; Pelham and Chang, 2001), whereas in *N. crassa* and *A. nidulans*, patches can undergo rapid, linear saltatory translocations along underlying actin cables, suggesting the involvement of myosin motors (Berepiki et al., 2010; Upadhyay and Shaw, 2008). In *N. crassa* and *A. nidulans*, linear patch movement proceeded at 1.2 µm/s and 0.56-0.59 µm/s, respectively, with patches moving towards and away from regions of active growth (Berepiki et al., 2010; Upadhyay and Shaw, 2008). Interestingly, although translocation along an individual cable was unidirectional, patches moved in both directions within a hypha suggesting that cables are nucleated from both basal and apical regions (Berepiki et al., 2010). Whether or not these patches fuse with endosomes remains to be determined. However, given the rapid motility of endosomes within fungal hyphae (Abenza et al., 2009; Wedlich-Soldner et al., 2000), it is conceivable that endocytic vesicles may

require transport to these organelles. Alternatively, fast patch transport could represent non-specific interactions with the underlying actin cable-myosin-V network.

1.2.4 Mutational studies of actin patches

Several putative components of the endocytic machinery have been analysed in filamentous fungi. Abp1 has a role in promoting the disassembly of endocytic structures in *S. cerevisiae* (Kaksonen et al., 2003; Kaksonen et al., 2005). In *A. nidulans*, deletion of the gene encoding the Abp1 homolog has no obvious effect on growth or endocytosis, in keeping with its partially redundant role in *S. cerevisiae* (Araujo-Bazan et al., 2008). *Aspergillus nidulans* mutants lacking the fimbrin FimA display abnormal hyphal growth, polarity defects during germination and are severely impaired in endocytosis (Upadhyay and Shaw, 2008). The prominent polarity defects of the Δ*fimA* mutants suggests that endocytosis is required to concentrate polarity markers, thus ensuring the maintenance of a stable growth axis and suppressing multipolarisation in hyphal cells (Upadhyay and Shaw, 2008). In *A. gossypii*, fimbrin supports fast polarised hyphal tip growth and endocytosis(Jorde et al., 2011). SlaB is the *A. nidulans* homolog of *S. cerevisiae* Sla2, which regulates actin dynamics in patches (Kaksonen et al., 2003). Deletion of *slaB* is lethal in *A. nidulans* (Araujo-Bazan et al., 2008) and conditional SlaB-deficient mutants of *Aspergillus oryzae* and *A. nidulans* show defects in endocytosis (Kitamoto et al., 2009; Penalva and Hervas-Aguilar, 2010). Amphyphysins are thought to contribute to endocytosis by inducing membrane curvature (Balguerie et al., 1999; Peter et al., 2004). The *C. albicans* amphiphysin homologs Rvs161 and Rvs167 are important for endocytosis, although not essential (Konopka et al., 2009). Wal1p, the homologue of *S. cerevisiae* WASP Las17, supports hyphal growth and is necessary for proper actin patch organisation in *C. albicans* and *A. gossypii*, suggesting that it has a

similar role to Las17 in Arp2/3-mediated endocytosis (Walther and Wendland, 2004a; Walther and Wendland, 2004b).

Class-I myosins have been shown to activate the *S. cerevisiae* Arp2/3 complex and are thought to participate in membrane invagination and scission during endocytosis (Jonsdottir and Li, 2004; Sun et al., 2006); several studies have confirmed the importance of this motor in filamentous fungi. In *C. albicans*, class I myosin Myo5 localises to actin patches (Oberholzer et al., 2002). *C. albicans* Myo5-deficient mutants can still undergo hyphal growth even though patches are depolarised, suggesting that patches are not necessary for polarised growth *per se*. Conversely, *A. nidulans* class-I myosin MyoA is essential for inducing polarised growth (Osherov et al., 1998; Yamashita et al., 2000). It has been suggested that the role of MyoA is mainly structural, as mutants devoid of motor motility can still support hyphal growth (Osherov et al., 1998; Yamashita et al., 2000). Interestingly, mutation of MyoA can render endocytosis constitutively active in *A. nidulans* (Yamashita and May, 1998).

1.2.5 Actin cables

Actin cables are bundles of formin-nucleated F-actin cross-linked by tropomyosin and fimbrin (Figure 1.3) (Evangelista et al., 2002; Moseley and Goode, 2006; Pruyne et al., 2002). In fungi, actin cables serve as tracks for the transport of various cargoes including secretory vesicles, actin patches, peroxisomes, Golgi equivalents, mitochondria, and vacuoles (Berepiki et al., 2010; Fehrenbacher et al., 2003; Motegi et al., 2001; Pantazopoulou and Penalva, 2009; Rida et al., 2006; Rossanese et al., 2001; Suelmann and Fischer, 2000; Upadhyay and Shaw, 2008). In both *C. albicans* and *A. nidulans* the polarisation and morphology of Golgi equivalents depends on actin (Hubbard and Kaminskyj, 2008; Pantazopoulou and Penalva, 2009; Rida et al., 2006) suggesting that these organelles move

along actin cables as has been demonstrated in budding yeast (Rossanese et al., 2001). Indeed, *C. albicans* cells lacking the formin Bni1, which mediates linear cable assembly (see below), form unpolarised disorganised Golgi equivalents (Rida et al., 2006). However, direct visualisation of Golgi equivalent transport along actin cables has not been demonstrated and it is possible that F-actin serves an organising function in Golgi equivalents in addition to or instead functioning as tracks for Golgi transport.

Targeted transport of cargoes is achieved via myosin-V-dependent translocation along an actin cable or attachment to a growing actin polymer (Fehrenbacher et al., 2003). Organelle transport in *S. cerevisiae* is almost entirely dependent on actin whereas in filamentous fungi both actin and microtubules contribute to organelle trafficking. Even within filamentous species differences exist. For example, in *N. crassa* mitochondria are transported via microtubules whereas in *A. nidulans* transport of mitochondria is actin-dependent (Fuchs et al., 2002; Suelmann and Fischer, 2000).

The roles of F-actin and microtubules can also change at different developmental stages; in *N. crassa*, cell fusion mediated by conidial anastomosis tubes (CATs) requires actin but not microtubules, whereas the normal growth of germ tubes and vegetative hyphae requires both cytoskeletal polymers (Barja et al., 1993; Roca et al., 2010).

Given that the key morphogenetic role of actin cables is to serve as tracks for secretory vesicle transport, where and when they are assembled in the cell is of considerable importance. The Rho family of small GTPases regulate the spatial organisation of the actin cytoskeleton (Harris, 2011). Loss–of-function studies of all six Rho GTPases identified in *Aspergillus niger*, have revealed how individual Rho GTPases contribute differently to growth and morphogenesis (Kwon et al., 2011). Interestingly, there appears to be a functional separation between small Rho GTPases involved in septation and those involved in tip growth. RHO-4, for example, has an exclusive function in actin ring organisation during septation, and is dispensable for polarised tip growth (Rasmussen and

Glass, 2005; Rasmussen and Glass, 2007). In contrast, Cdc42 and Rac1 are required for cell symmetry breaking and polarity maintenance, but dispensable for septum formation (Mahlert et al., 2006; Rolke and Tudzynski, 2008).

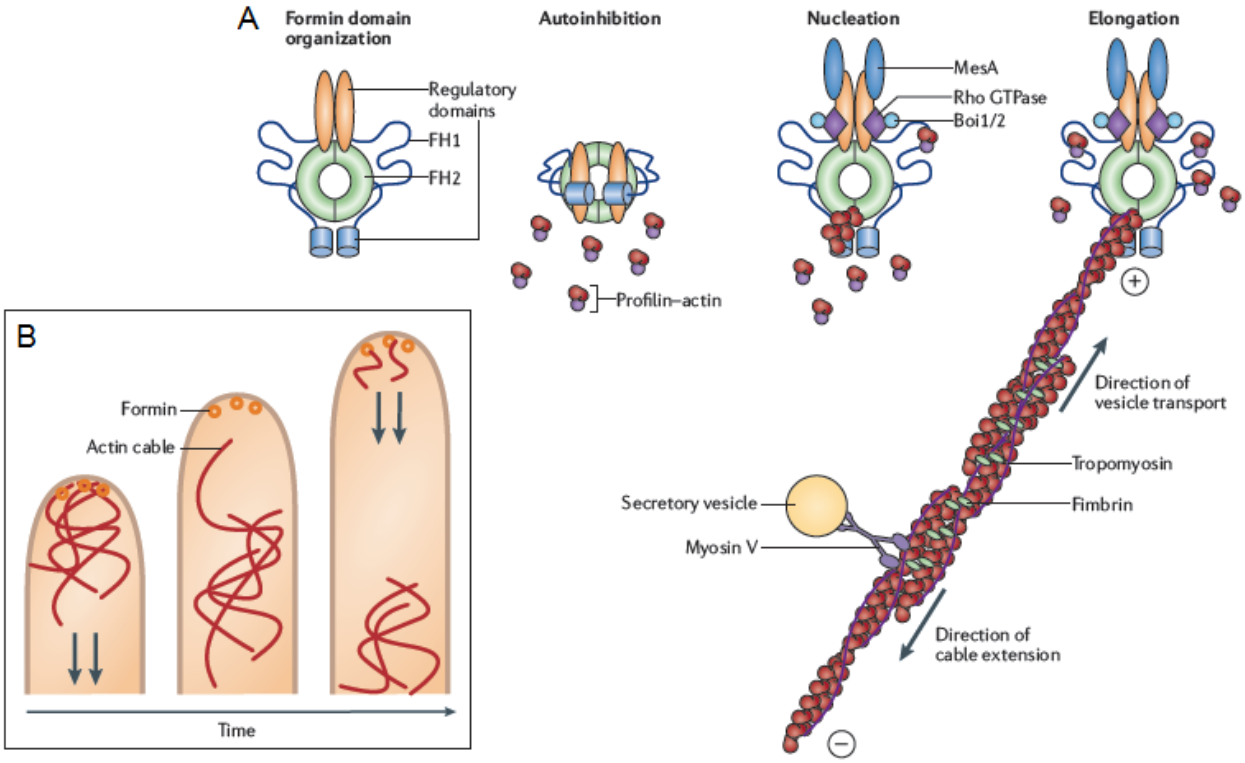

Figure 1.3. Actin cable assembly and dynamics. (A) Fungal formins are regulated by autoinhibitory interactions between a catalytic region (composed of FH1 and FH2 domains) and regulatory domains on the same protein. The inactive state is relieved by the binding of activated Rho GTPases allowing access of profilin-actin complexes to the FH1 and FH2 domains. Additional regulators, such as MesA and Boi1/2, contribute to formin activation and localisation in filamentous fungi. Profilin-G-actin complexes bind to the FH1 domain and are delivered onto the FH2 domain which catalyses F-actin nucleation in a processive manner forming the polymer chain. Assembled microfilaments are bundled into cables by fimbrin and tropomyosin and serve as tracks for the myosin-V-dependent transport of secretory vesicles. Cable extension and vesicle transport proceed in opposite directions. (B) In *N. crassa*, dense arrays of actin cables undergo retrograde movement from the tip during growth. Formin-mediated cable formation has been proposed to drive retrograde movement of actin cable arrays. Adapted from Berepiki et al. (2011).

Cdc42 and Rac1 are both crucial for proper hyphal morphogenesis in a range of filamentous fungi (Boyce et al., 2003; Kwon et al., 2011; Mahlert et al., 2006; Virag et al., 2007), which probably stems from their ability to modulate polarisome localisation and activity (Harris, 2011), as has been shown for *S. cerevisiae* Cdc42 (Evangelista et al., 1997). The polarisome is a multiprotein complex that forms at the sites of active growth and controls the assembly of actin cables (Pruyne and Bretscher, 2000). The formin Bni1 is a fundamental component of this complex because it catalyses *de novo* F-actin assembly (Figure 1.3).

1.2.6 Formins

Formins are conserved nucleators of actin filaments characterised by a formin homology 1 (FH1) domain, which contains binding sites for profilin-actin complexes, and a FH2 domain that controls actin nucleation and cable assembly (Chesarone et al., 2010; Evangelista et al., 1997; Evangelista et al., 2002; Kovar et al., 2003; Moseley et al., 2004; Pruyne et al., 2002; Sagot et al., 2002; Zigmond et al., 2003). Interaction between FH1 and profilin is required for actin recruitment at this site (Chang et al., 1997; Kovar et al., 2003; Kovar et al., 2005). Profilin-actin complexes arrive at the FH2 domain via FH1 and are delivered to the growing barbed end (also known as the plus end). The FH2 domain mediates actin filament assembly by the processive binding to the barbed end of a filament, thereby preventing access of capping proteins while allowing elongation (Kovar et al., 2003; Kovar et al., 2005; Moseley et al., 2004; Pruyne et al., 2002; Zigmond et al., 2003). Three other domains are typical in fungal formins: a Diaphonous-related formin inhibitory domain (DID); a Diaphonous-related formin autoregulatory domain (DAD) and a Rho-binding domain (RBD) (Chesarone et al., 2010). Autoinhibitory interactions between DID and DAD on the same protein, documented for some formins, are relieved by Rho GTPase binding to the RBD, although additional factors may be required for mouse and human formins (Chesarone et al.,

2010). Interestingly, *A. nidulans* and *N. crassa* possess only a single formin whereas the yeasts *S. cerevisiae* and *S*. *pombe* and the filamentous yeasts *A. gossypii* and *C. albicans* possess multiple formins that catalyse actin assembly from distinct cellular locations. For example, in *A*. *gossypii*, Bni1 localises to hyphal tips but not at septa, Bnr1 localises to septa but not at hyphal tips, and Bnr2 nucleates actin cables from the spindle pole body (the fungal equivalent of the metazoan centrosome) which is located on the nucleus (Kemper et al., 2011; Schmitz et al., 2006). The assembly of actin cables by Bnr2 from the spindle pole body during sporulation is thought to contribute to the morphogenesis of the long (30 µm) needle-shaped spores of *A. gossypii* (Kemper et al., 2011).

In *A. nidulans* and *N. crassa*, the formin gene (*SepA* and *bni-1*, respectively) is essential for cell viability (Harris et al., 1997; Justa-Schuch et al., 2010; Sharpless and Harris, 2002). The conditional SepA-deficient mutant of *A. nidulans* is aseptate, exhibits an aberrant growth pattern and has abnormally wide hyphae (Harris et al., 1997; Sharpless and Harris, 2002). In *A. nidulans* and *N. crassa*, SepA and BNI-1, respectively, are concentrated at hyphal tips and localises as a crescent at the extreme apex and as a dot posterior to the crescent, which colocalises with the fluorescent dye FM4-64 in the Spk (Lichius et al., 2012; Sharpless and Harris, 2002). SepA localisation in *A. nidulans* is dynamic, with the SepA-GFP spot and crescent tracking the direction of growth, and is dependent on actin (Sharpless and Harris, 2002). In *A. nidulans* and *N. crassa*, SepA and BNI-1, respectively, localise to septa where they catalyse actin ring formation (Justa-Schuch et al., 2010; Lichius et al., 2012; Sharpless and Harris, 2002), in contrast to Bni1 of *A. gossypii*, which seems to be specifically involved in tip growth (Schmitz et al., 2006). The *C. albicans bni1* null mutant is viable but shows major morphological defects and forms swollen abnormal hyphae (Li et al., 2005; Martin et al., 2005b). *Ashbya gossypii* Bni1 is essential for cell viability; the null mutant is unable to form hyphae and spores expand to large deformed cells (Schmitz et al., 2006). In all of the mutational studies on Bni1 and SepA, actin cables are absent, confirming

that formins mediate cable assembly in filamentous fungi (Harris et al., 1997; Li et al., 2005; Martin et al., 2005b; Schmitz et al., 2006; Sharpless and Harris, 2002). Swollen conidia and hyphae are a common feature of formin mutants, demonstrating that in the absence of actin cables, growth is no longer confined to a distinct region and highlighting the strict requirement for actin cables in targeted secretion (Harris et al., 1997; Li et al., 2005; Martin et al., 2005b; Schmitz et al., 2006; Sharpless and Harris, 2002).

In addition to the conserved functions of Rho GTPases and the polarisome in controlling cable assembly, several additional regulators have been identified in filamentous species. Recent studies in *A. nidulans* have demonstrated that small GTPases from the Ras family play an important role in actin organisation. The Ras activator GapA is recruited to the incipient site of germ tube emergence and deletion of *gapA* resulted in a disorganised cortical actin cytoskeleton (Harispe et al., 2008). Lack of GapA did not affect microtubule organisation, indicating a specific role for Ras GTPase in F-actin organisation at the cell cortex. Interestingly, MesA, a protein containing several predicted transmembrane domains, localises to hyphal tips in *A. nidulans* and participates in the recruitment and stabilisation of SepA at hyphal tips but not at septation sites (Pearson et al., 2004). Septation is completely unaffected in MesA-deficient mutants of *A. nidulans*, which fail to form actin cables and show altered lipid domain staining pattern. In *S. cerevisiae* and *S. pombe*, deletion of the gene encoding the MesA homolog (*YOR129c* (also known as *AFI1*) and *SPBC776.06c*, respectively), causes negligible morphological defects, and *SPBC776.06c* fails to complement the *A. nidulans* MesA-deficient mutant (Pearson et al., 2004; Ren et al., 2000). Cumulatively, these data suggest that MesA has evolved specific roles in hyphal morphogenesis.

Boi1/2 is another conserved protein found in both yeasts and filamentous fungi that has specific roles in hyphal morphogenesis. In *A. gossypii*, Boi1/2 regulates actin cable formation thereby ensuring maximal hyphal extension rates and preventing non-polar growth

in hyphal tips (Knechtle et al., 2006). Boi1/2 localises to tips and septa, although its localisation to septa is not important for permanent polar growth. The Rho GTPase Rho3, previously implicated in maintaining hyphal growth, interacts with both Boi1/2 and the formin Bni1 in *A. gossypii*, and GTP-bound Rho3 binds to the RBD of Bni1, suggesting that Boi1/2 and Rho3 cooperate to modulate Bni1-mediated actin cable assembly (Knechtle et al., 2006).

1.2.7 Actin cable dynamics

Actin cables were first visualised in living *S. cerevisiae* cells using an Abp140-GFP fusion (Yang and Pon, 2002). It was shown that assembly of actin cables occurs in the bud, with cables polarised along the mother-bud axis and that during *de novo* assembly and elongation cables undergo retrograde flow into the mother cell, in complete agreement with current models of formin-mediated F-actin assembly (Chesarone et al., 2010). Recent studies in *N. crassa* have revealed subtle but important differences in cable organisation between *S. cerevisiae* and filamentous fungi (Berepiki et al., 2010). Long actin cables (5-10 µm) are commonly observed in *N. crassa* germlings, and occasionally cables that cover the entire length of a 25 µm germ tube can be detected. Long actin cables such as these seem well suited to their proposed roles in vesicle/organelle transport. Actin cables in *N. crassa* also display transient cable-cable interactions and regularly undergo bending, buckling and kinking (Berepiki et al., 2010). Cables and patches are exquisitely sensitive to inhibitors of actin polymerisation implying a rapid turnover of filaments in these structures (Berepiki et al., 2010; Yang and Pon, 2002).

In *N. crassa*, a dense meshwork of actin cables, termed an ‘actin array’, marks the site of outgrowth of germ tubes, CATs and hyphal branches (Berepiki et al., 2010). During germ tube emergence and elongation, actin arrays undergo recurrent retrograde movement

from the tip, probably driven by BNI1-mediated F-actin assembly (Figure 1.3). It is likely that tip-directed secretory vesicle transport can still proceed, as the velocity of myosin-V transport is great enough to counter retrograde cable flow; in *S. cerevisiae*, myosin-V movement along actin cables is approximately ten times more rapid than the rate of retrograde cable extension (Moseley and Goode, 2006; Yang and Pon, 2002). A direct role for class-V myosins in secretion has not yet been demonstrated in filamentous fungi but they have been shown to be crucial for hyphal growth in *C. albicans* and *U. maydis* (Weber et al., 2003; Woo et al., 2003). In *U. maydis*, class-V myosin Myo5 is non-essential but is needed for normal cell separation, mating, hyphal growth and pathogenicity (Weber et al., 2003) . Similarly, in *C. albicans* and *A. nidulans*, class-V myosins are not essential but are required for correct polarisation of the actin cytoskeleton, efficient secretion and normal hyphal growth (Taheri-Talesh et al., 2012; Woo et al., 2003; Zhang et al., 2011). These data imply that myosin-V-dependent secretion supports hyphal growth but is not needed for secretion *per se*.

Interestingly, the dense actin arrays present in growing germ tubes are not found in mature hyphae; rather, actin cables mark the site of branch outgrowth and are found at the cell cortex but arrays are not present in tips. Instead, a spot of F-actin just behind the apex is present, colocalising with the Spk, followed by a collar of actin patches associated with the plasma membrane several microns posterior to the spot (Berepiki et al., 2010; Delgado-Alvarez et al., 2010). This observation confirms an emerging theme of hyphal growth: the rearrangement of the tip growth apparatus to support rapid extension (Figure 1.4). Filamentous fungi show a rapid acceleration in apical extension during the transition from germ tube to mature vegetative hypha. Rates of apical extension in mature hyphae can be up to 20 fold greater than that during initial germ tube emergence (Koehli et al., 2008). In *A. gossypii*, the transition from slow-growing to fast-growing hyphae is regulated by the paxillin homolog Pxl1 and the PAK (p21-activated kinase) Cla4 (Ayad-Durieux et al., 2000;

Philippsen et al., 2008). *Cla4* is epistatic to *pxl1* and *A. gossypii* cells lacking either of these components do not undergo hyphal maturation.

Endocytosis and exocytosis occur at the apex of a germ tube, whereas in mature vegetative hyphae secretion remains confined to the apex but endocytosis occurs in a circular band or collar several microns behind the tip apex (Araujo-Bazan et al., 2008; Berepiki et al., 2010; Koehli et al., 2008; Taheri-Talesh et al., 2008). Taken together, these findings support the view that subapical compensatory endocytosis underlies hyphal growth (Altschuler et al., 2007; Penalva, 2010; Steinberg, 2007b), and that endocytosis and exocytosis become spatially segregated to achieve the rapid growth rates exhibited by mature vegetative hyphae. Additional developmental changes to the tip growth apparatus include the transition from a crescent-like to spheroid localisation of exocyst and polarisome markers in *A. gossypii* (Koehli et al., 2008), and the formation of a Spk, enriched in formin, the polarisome component SPA-2, and F-actin, in *N. crassa* and *A. nidulans* (Araujo-Palomares et al., 2009; Berepiki et al., 2010; Delgado-Alvarez et al., 2010; Sharpless and Harris, 2002; Virag and Harris, 2006). Interestingly, in the trimorphic pathogen *C. albicans*, the Spk is present in hyphae but not in yeast cells , and the exocyst and polarisome display different patterns of localisation and distinct dynamics at hyphal tips (Jones and Sudbery, 2010).

The actin spot that is located in the hyphal tip has been described in living cells of *A. nidulans* and *N. crassa* and localised to the core of the Spk (Berepiki et al., 2010; Delgado-Alvarez et al., 2010; Taheri-Talesh et al., 2008), confirming ultrastructural observations made with freeze-substituted cells over 30 years ago (Howard, 1981). The enrichment of F-actin and formin as a spot suggests that the Spk acts as an actin-organising centre and could be considered as a fourth type of higher-order F-actin structure.

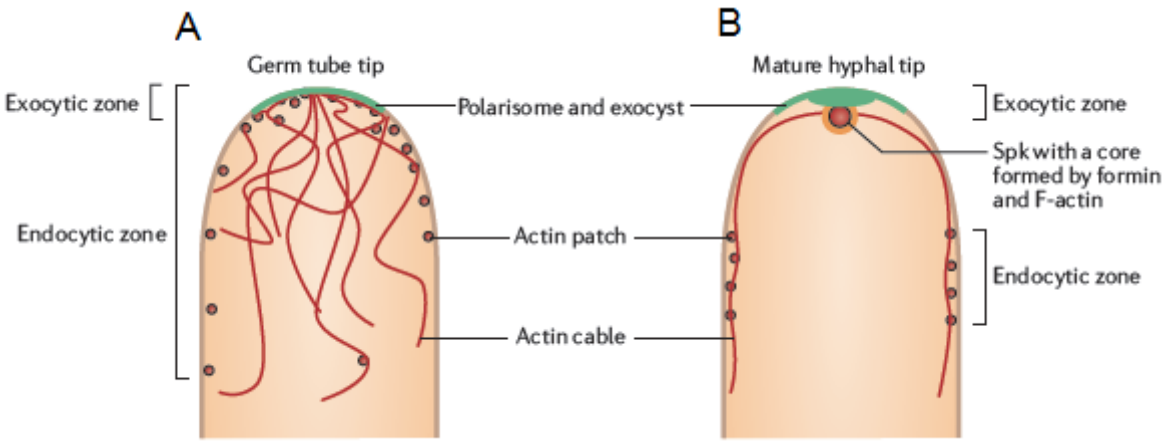

Figure 1.4. Rearrangement of tip growth apparatus. (A) The actin cytoskeleton in germ tubes. Dense arrays of actin cables are present at the apex and are thought to serve as tracks for myosin-V dependent secretory vesicle transport to the tip. The polarisome and exocyst both localise as a crescent at the apex of germ tubes. Actin patches are found at regions of exocytosis in germ tubes suggesting that exocytosis and endocytosis are spatially coupled at this stage. Actin patches are also translocated to and from the tip along actin cables. (B) In rapidly growing mature vegetative hyphae, the Spitzenkörper (Spk) contains a variety of components including secretory vesicles, the polarisome proteins Spa2 and Bni1, and a core of F-actin. Actin cables are no longer found as dense arrays but instead are mostly associated with the cell cortex, and can be observed emanating from the Spk. Endocytosis as shown by actin patch localisation becomes confined to a sub-apical collar several microns behind the tip apex. The polarisome and exocyst maintain their crescent shape but are now also present as a diffuse sphere between the apex and Spk. Adapted from Berepiki et al. (2011).

Interestingly, ABPs involved in actin patch formation, such as Arp2/3, fimbrin, and Abp1 do not localise to the Spk (Araujo-Bazan et al., 2008; Delgado-Alvarez et al., 2010; Taheri-Talesh et al., 2008; Upadhyay and Shaw, 2008). It is likely that actin filaments or cables, assembled by formin at the Spk and/or the apical plasma membrane, allow vesicles to reach the cell tip via myosin-V-dependent transport. Cortical actin cables appear to converge on the Spk; however, recent studies have so far failed to clearly visualise actin microfilaments or cables bridging the gap between the Spk and apical membrane in living hyphae (Berepiki et al., 2010; Delgado-Alvarez et al., 2010; Taheri-Talesh et al., 2008). It is likely that the strong fluorescence signal from the Spk hinders detection of actin

microfilaments and cables in this region. Conversely, actin microfilaments or cables simply may not be present in the gap between the Spk and the plasma membrane, and vesicles once concentrated in the Spk diffuse and preferentially dock at the apex. Which scenario occurs awaits further experimental analysis.

1.2.8 Actin rings

The contractile actomyosin ring is a key constituent of the cytokinetic machinery in fungi. Consisting of actin, myosin-II and other associated proteins, the CAR forms a force-generating ring linked to the plasma membrane (Pollard, 2010). Sliding of actin filaments by myosin-II leads to contraction of the ring, guiding membrane invagination and cell wall synthesis. The utilisation of a contractile ring is an ancient mechanism present in fungi, animals, and protists (Pollard, 2010). Although the central contractile mechanism is conserved between yeasts and filamentous fungi, differences in the regulation of the placement and assembly of the CAR exist (Seiler and Justa-Schuch, 2010).

In various fungi, anillin-like proteins provide the spatial clues for ring placement (Seiler and Justa-Schuch, 2010). In *N. crassa*, the anillin-like protein BUD-4 functions upstream of the Rho GTPase RHO-4 and its effectors (Figure 1.5) (Justa-Schuch et al., 2010; Rasmussen and Glass, 2005; Rasmussen and Glass, 2007). BUD-4 localises as dots at the plasma membrane at incipient sites of septum formation, forms a ring during septation, and is required for correct RHO-4 placement (Justa-Schuch et al., 2010). Although the localisation of BUD-4 dots at the plasma membrane is independent of RHO-4, BUD-4 dots do not coalesce into a ring in the absence of RHO-4 (Justa-Schuch et al., 2010). RHO-4 and its activator BUD-3 are proposed to localise and activate the formin BNI-1, thereby regulating CAR placement and assembly. A similar Rho4-Bud3 module regulates formin recruitment prior to CAR formation in *A. nidulans* (Si et al., 2010). Additionally, an

actinin-like protein, AcnA, localises to septation sites and has been shown to contribute to cytokinesis in *A. nidulans* (Wang et al., 2009).

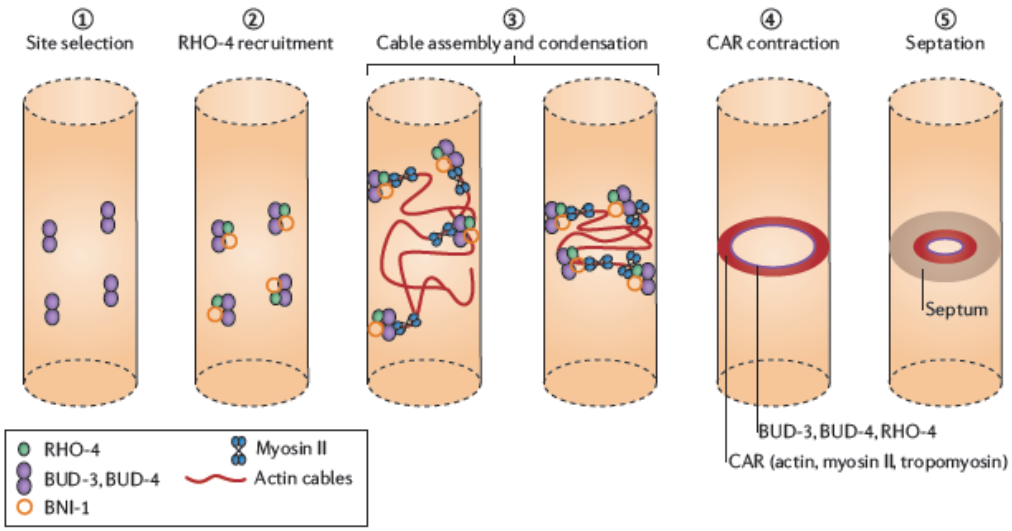

Figure 1.5. Model of contractile actomyosin ring (CAR) assembly in *N. crassa*. (Step 1) The site of CAR formation is determined by the anillin-like protein BUD-4 which assembles as dots at the inner perimeter of the cell cortex in a RHO-4-independent manner. (Step 2) Localisation of the Rho GTPase RHO4 depends on BUD-4. RHO-4, activated by BUD3, is thought to localise and activate the formin BNI-1 (Step 3). Formin mediated F-actin assembly leads to a meshwork of actin cables between formin nodes. (Step 4) The 'search, capture, pull and release' model proposes that myosin-II-dependent contraction leads to the condensation of the cable meshwork into a ring. The actomyosin ring is formed, consisting of actin, myosin-II and tropomyosin, with BUD-3, BUD-4, and RHO-4 localising to the inner perimeter of the CAR. (Step 5) The actomyosin ring contracts and guides membrane invagination and cell wall synthesis, which results in septum formation; the actomyosin ring eventually dissipates. In *N. crassa* the septum is not completed, and a septal pore is formed that retains BUD-3, BUD-4, and RHO-4, which suggests additional roles for this complex. Adapted from Berepiki et al. (2011).

The sites of BNI1-mediated cable assembly in *N. crassa*, as shown by cable localisation prior to ring formation, are dispersed within the hyphae and gradually coalesce into an actin ring (Berepiki et al., 2010; Delgado-Alvarez et al., 2010). The most convincing hypothesis to explain cable condensation into rings is the search, capture, pull, and release model developed by Pollard and colleagues from studies in *S. pombe* (Lord et al., 2005; Vavylonis et al., 2008; Wu and Pollard, 2005). In this organism, the anillin-like protein Mid1 localises as nodes in a broad band on the plasma membrane prior to septum formation (Pollard et al., 2006; Vavylonis et al., 2008; Wu and Pollard, 2005). Mid1 and associated proteins recruit the formin Cdc12, which then assembles actin filaments or cables from these nodes (Wu et al., 2009). Contraction of the nodes into a ring is thought to be mediated by myosin-II-dependent capture and tensioning of actin filaments that emanate from neighbouring nodes: Myo2 binds to a filament and 'walks' towards the barbed end, pulling nodes together (Lord et al., 2005; Vavylonis et al., 2008). Class-II myosins localise to the CAR in both *N. crassa* and *A. nidulans* (Calvert et al., 2011; Taheri-Talesh et al., 2012). Random breaks in the connecting filaments allow for numerous rounds of experimentation and correction, and computer simulations based on known physiological parameters closely mimic microscopic observations (Vavylonis et al., 2008). However, this hypothesis is contested, and *S. pombe mid1*-null mutants do not form detectable nodes yet are still able to form CARs, which suggests that other ring assembly mechanisms exist in this organism (Oliferenko and Mishra, 2008).

1.3 Septins

Septins are found in a range of eukaryotes from animals to yeasts but are absent from plants. They form oligomeric filaments that assemble into a variety of higher order structures. Septins are a family of proteins that interact with actin, microtubules and membranes and

are involved in regulating cytoskeletal dynamics, secretion and membrane remodelling (Spiliotis and Gladfelter, 2012). The term septin was coined by John Pringle because of the role played by these polymers in septation and cytokinesis (Hall et al., 2008). The septins were first discovered in *S. cerevisiae* in a mutant screen by Hartwell and colleagues (Hartwell, 1971). In *S. cerevisiae*, conditional *cdc3*, *cdc10*, *cdc11*, and *cdc12* mutants fail to complete cytokinesis at the restrictive temperature and cells eventually become multinucleate and form multiple elongated buds. A subsequent ultrastructural study revealed that septins form a highly ordered ring of 10 nm filaments on the cytoplasmic face of the plasma membrane at the bud neck (Byers and Goetsch, 1976). *In vitro*, septins purified from Drosophila, mammals, and budding yeast form short (~32 nm long) filaments, which can assemble end to end into >1500 nm long paired filaments upon dialysis into physiological (75 mM) salt (Frazier et al., 1998). Additionally purified mammalian septins self-assemble into rings 0.6 μM in diameter and in the presence of the adaptor protein anillin organises actin filaments into bundles while recruiting septin filaments to the bundles (Kinoshita et al., 2002). An ultrastructural study using unroofed yeast sphaeroplasts demonstrated that septins are found as rings and as ordered gauzes (Rodal et al., 2005).

1.3.1 Septin domain organisation

Septins typically contain an N-terminal GTP binding domain (G domain) and a coiled-coil C-terminal domain that is thought to participate in oligomerisation. A 53 aa sequence known as the septin unique element (SUE) flanks the G domain. Other extensions located at the N- or C-terminus are also found. Differences in N- and C-terminal extensions/domains permit interactions with a diverse range of proteins (Nakahira et al., 2010). Septins are part of the GTPase superclass of P‑loop NTPases. On the basis of phylogenetic studies, this superclass is divided into two classes, called SIMIBI (signal recognition particle, MinD and

BioD) and TRAFAC (translation factor). Septins are part of the TRAFAC class, which includes the Ras-type superfamily of small GTPases, translation factors, the OBG/HflX superfamily, and the structurally-related myosin-kinesin superfamily of ATPases (Leipe et al., 2002). P-loop GTP-binding proteins have a core α-β-α structure and conserved GTP-interacting motifs. Within this class, septins are most closely related to a subfamily of broadly distributed proteins called paraseptins, which are present in both prokaryotes and eukaryotes. The limited distribution of paraseptins among eukaryotes suggests that an ancestral protein was horizontally transferred from bacteria to eukaryotes and subsequently evolved in fungi and metazoans (Leipe et al., 2002).

Within and between species septins generally show at least 30% overall amino acid identity (Pan et al., 2007). Septins have been divided into 5 groups based on phylogenetic analysis (Pan et al., 2007). Group 1 includes *S. cerevisiae*, Cdc10, *Neurospora crassa* CDC-10 and human Sept9. Group 2 includes *S. cerevisiae* Cdc3, *N. crassa* CDC-3 and human Sept7. Group 1 and 2 septins are found in both fungi and animals whereas groups 3, 4 and 5 are only found in fungi. Group 3 septins contains *S. cerevisiae* Cdc11 and *N. crassa* CDC-11 and group 4 includes *S. cerevisiae* Cdc12 and *N. crassa* CDC-12 (Pan et al., 2007). Group 5 septins, which contains the fewest number of septins, are found only in filamentous fungi. The lack of orthologs in *S. cerevisiae* and *S. pombe* suggests that group 5 septins arose early in fungal evolution and were lost from unicellular yeasts or arose after the separation of yeast and filamentous fungi (Pan et al., 2007). Generally, ascomycete genomes contain five to eight septins whereas basidiomycetes have four or five. All fungal genomes contain a single group 1 and group 2 septin whereas multiple groups 3, 4 and 5 septins are found in some fungi. For example, *S. cerevisiae* and *S. pombe* both contain three group 3 septins (Cdc11, Sep7/Shs1, Spr28 in *S. cerevisiae* and Spn3, Spn5, and Spn7 in *S. pombe*).

1.3.2 Geometry of septin complexes

Recent EM studies have begun to reveal the polarity, subunit arrangement and binding interactions of septins during their assembly into oligomeric complexes. The relatively simple two-subunit septin assemblies of *Caenorhabditis elegans* has been utilised for this purpose (John et al., 2007). The *C. elegans* septins UNC-59 and UNC-61 form a non-polar tetramer in the order UNC-59–UNC-61–UNC-61–UNC-59. *In vitro*, *C. elegans* septin filaments are formed by end-to-end joining of the core tetramers, resulting in filaments that are also non-polar along the direction of filament extension (John et al., 2007). The mammalian SEPT3–SEPT5–SEPT7 complex forms an elongated hexamer, the order of which is SEPT7–SEPT6–SEPT2–SEPT2–SEPT6–SEPT7 (Lukoyanova et al., 2008; Sirajuddin et al., 2007). The *S. cerevisiae* core septin complex, consisting of Cdc3, Cdc10, Cdc11, and Cdc12, forms an elongated linear octamer with septin subunits arranged in the following order: Cdc11–Cdc12–Cdc3–Cdc10–Cdc10–Cdc3–Cdc12–Cdc11 (Bertin et al., 2008). The core tetramer is composed of proteins with clear metazoan homologues, whereas the peripheral core septins (Cdc11 and Cdc12) belong to fungus-specific groups. The proposed yeast core assembly order (Cdc11–Cdc12–Cdc3–Cdc10–Cdc10–Cdc3–Cdc12–Cdc11) mediates higher-order assembly via the NC-dimer interface of Cdc11 (Figure 1.6) (Bertin et al., 2008), conversely the *C. elegans* and mammalian core complexes form higher order structures via a G-dimer interface dimerisation between UNC-59–UNC-59 and SEPT7–SEPT7 (John et al., 2007; Sirajuddin et al., 2007). It is possible that the observed differences in the binding sites in higher order structure assembly reflects the distinct cellular role and resulting higher order structures formed (Weirich et al., 2008).

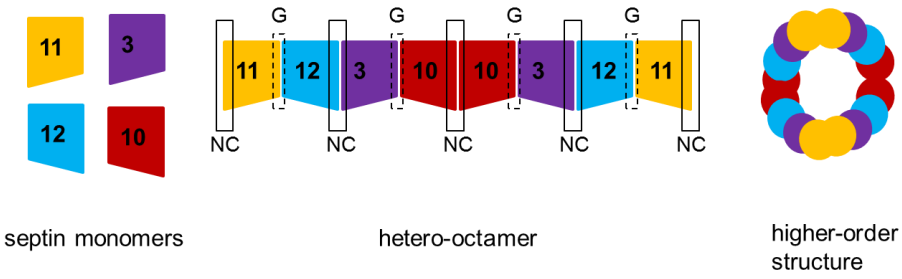

Figure 1.6. Core architectures of septin complexes. Diagram showing the arrangements of septin groups 1 (red, Cdc10), 2 (purple, Cdc3), 3 (yellow, Cdc11) and 4 (blue, Cdc12) in *S. cerevisiae*. Septins polymerise end to end to form a single hetero-octamer (composed of eight septin proteins). The individual subunits are labelled with numbers based on the *S. cerevisiae* nomenclature corresponding to Cdc10, Cdc3, Cdc12 and Cdc11. The interaction between septin monomers forms an elongated filament with alternating G‐ (black dashed boxes) and NC‐dimer (solid black boxes) interfaces. Hetero-octameric filaments assemble into higher-order structures that form diffusion barriers and scaffolds.

1.3.3 Role of GTP hydrolysis

The role of GTP binding and hydrolysis in septin complex assembly, function and dynamics is unclear. It has been demonstrated that septin filament assembly does not require associated GTP hydrolysis (Mitchison and Field, 2002). Additionally, isotope-labelling of *S. cerevisiae* has demonstrated that the majority of septin proteins do not hydrolyse GTP over the course of the cell cycle (Vrabioiu et al., 2004), and biochemical studies have shown GTPase activity only for Cdc10 and Cdc12 (Versele and Thorner, 2004); however, these reports are contested by findings which show that GTP binding contributes to the assembly of recombinant septins into filaments (Mendoza et al., 2002) and that GTP induces conformational changes of septins *in vivo* (Sirajuddin et al., 2007). The presence of the GTP binding domain at the interface of subunit interaction in the metazoan septin core has been proposed to link GTP binding and filament assembly (Mendoza et al., 2002). The situation is different in fungi however, as the interaction between subunits is governed by the N- and C-terminal interaction (Bertin et al., 2008; Weirich et al., 2008). It has been suggested that GTP

binding regulates interactions with non-septin proteins and/or membranes (Casamayor and Snyder, 2003).

1.3.4 Septin dynamics

In mammalian cells, subunit turnover within a septin filament is more rapid than in intermediate filaments but 2-3 times slower than in MTs or F-actin (Hu et al., 2008). In *S. cerevisiae*, exchange can occur in higher-order (HO) assemblies and individual septin subunits can also undergo substitution within an individual hetero-octamer (McMurray and Thorner, 2008). Subunit exchange has also been documented in *A. gossypii* using fluorescence recovery after photobleaching (FRAP) - septin rings recovered approximately 40% of their septin subunits after photobleaching, with a $t_{1/2}$ of 3 min (DeMay et al., 2010).

In *S. cerevisiae*, Cdc10 and Cdc12 persist through multiple cell divisions and are incorporated with new molecules into septin complexes without any bias between old and new subunits (McMurray and Thorner, 2008). During meiosis and sporulation, Cdc10 dynamics is normal but Cdc12 is irreversibly excluded from septin filaments and HO assemblies and replaced by Spr3 (McMurray and Thorner, 2008). Polarised fluorescence microscopy has been used to determine the orientation of septin filaments in various higher-order structures. Polarised fluorescence microscopy takes advantage of the physical properties of fluorescent molecules. Excitation of the fluorophore with polarised light induces the maximal fluorescence emission of fluorophores whose absorption vectors are aligned parallel to the polarisation vector of the exciting light. A change of orientation or rotation of the fluorophore leads to a loss in anisotropy and thus reduced fluorescence emission. Using this technique Mitchison *et al*. (Vrabioiu and Mitchison, 2006; Vrabioiu and Mitchison, 2007), and more recently DeMay *et al*. (2011), showed that septin-GFP fusion proteins displayed strongly polarised fluorescence *in vivo*, suggesting a distinct orientation. It was also found

that *S. cerevisiae* HO structures are not polarised along the mother-bud axis and that during cytokinesis, septin filaments rotate 90° from the plane of the membrane at the bud neck to a circumferential arrangement. Mechanistic details for this transition remain unknown (Spiliotis and Gladfelter, 2012). Septin filaments have also been shown to be organised into pairs in mammalian cells and fungi (DeMay et al., 2011).

1.3.5 Regulation of septin dynamics

Septins are regulated by phosphorylation. Three kinases, Gin4, Cla4, Cdc28, regulate septins by phosphorylation. Phosphorylation of septins by Gin4 and Cla4 is thought to control filament assembly and dynamics during septin collar formation at the bud neck in *S. cerevisiae* (Longtine et al., 2000; Mortensen et al., 2002; Versele and Thorner, 2004). Cdc28 has been suggested to control septin-ring disassembly by phosphorylation (Tang and Reed, 2002).

Sumoylation of septins has been documented during mitosis in *S. cerevisiae* but the functional role of these modifications is unknown. In *S. cerevisiae*, before mitosis Cdc3, Cdc11 and Shs1 are sumoylated and then this modification is removed as the ring is split into two rings (Johnson and Blobel, 1999). It has been proposed that sumoylation regulates septin dynamics (Weirich et al., 2008).

The interaction of septin filaments with membranes (Barral et al., 2000; Dobbelaere and Barral, 2004; Zhang et al., 1999), actin (Kinoshita et al., 2002; Kinoshita et al., 1997) and tubulin (Spiliotis et al., 2005; Surka et al., 2002) is well-documented in eukaryotic cells and is important for septin function. The mechanistic details governing these interactions and the proteins involved remain to be described, but Borg proteins, which bind Rho GTPases, have been implicated in this process (Kinoshita, 2003; Sheffield et al., 2003). In addition, a polybasic tract in *S. cerevisiae* Cdc11 has been shown to be required for phospholipid

interactions *in vitro* and for proper assembly of septin HO structures *in vivo* (Casamayor and Snyder, 2003). Interestingly, septins have also been shown to participate in the localisation of Bnr1, the formin that nucleates actin cable at the cytokinetic ring in *S. cerevisiae* (Pruyne et al., 2004). Additionally, a septin binding protein, Bni5, is responsible for the recruitment of Myo1 to the bud neck in budding yeast (Fang et al., 2010).

Post-translation modifications are removed from septin subunits, which are reused in further HO assemblies (McMurray and Thorner, 2008). Proteolytic degradation is negligible in *S. cerevisiae*. Also because new and old subunits are equally incorporated, this suggests that old septin complexes do not serve as a 'seed' or a template for new ones (McMurray and Thorner, 2009).

1.3.6 Septin function

The interaction of septins with the plasma membrane is intimately linked to their function. In budding yeast Cdc11, a polybasic tract is important for phospholipid binding *in vivo* and mutations in this region cause defects in septin ring formation at the bud and during cytokinesis (Casamayor and Snyder, 2003). Septins demarcate areas of the plasma membrane and scaffold proteins, which are crucial for the proper assembly of protein complexes such as the CAR and polarisome (Barral et al., 2000; Dobbelaere and Barral, 2004; Orlando et al., 2011). The bud ring acts a as a diffusion barrier for polarisome components in the bud and during cytokinesis the septin ring scaffolds the CAR and acts as a diffusion barrier to maintain diffusible exocyst and polarisome proteins at the cleavage site and as a scaffold for other cytokinetic proteins (Barral et al., 2000; Dobbelaere and Barral, 2004; Orlando et al., 2011).

Various mRNAs have been shown to be asymmetrically distributed in the budding yeast cell, a process that often involves actomyosin-mediated transport (Bertrand et al.,

1998). Septins have been shown to limit diffusion of plasma membrane protein-encoding *Ist2* mRNA thereby compartmentalising the plasma membrane (Takizawa et al., 2000). Additionally, a septin-dependent diffusion barrier forms in the nuclear envelope and limits the movement of extant nuclear pores into the bud (Shcheprova et al., 2008). The barrier also contributes to the segregation of other ageing factors, such as carbonylated proteins and DNA circles, thereby ensuring the asymmetric inheritance of age during cell division (Shcheprova et al., 2008).

During yeast budding a functional septin ring is required to maintain polar localisation of endoplasmic reticulum (ER) proteins and impedes the free movement of integral ER proteins (Luedeke et al., 2005; Shcheprova et al., 2008). In this instance, HO septin structures are proposed to localise the membrane-associated protein Bud6 to the bud neck which in turn restricts the diffusion of ER membrane proteins (Shcheprova et al., 2008).

1.3.7 Septins in filamentous fungi

Septins have been well studied in budding yeast and to a lesser extent in *S. pombe*. Research on these organisms suggests that the importance of septins to cellular function is linked to the geometry and morphology of the organism being studied; in spherical *S. cerevisiae* cells, which grow by budding the four core septins - Cdc3, Cdc10, Cdc11, and Cdc12 - are required for proper morphogenesis and cytokinesis (Hartwell, 1971), whereas in *S. pombe* cells which are cylindrical and divide by fission, the core septins are entirely dispensable, although in the absence of any or all of them cytokinesis is delayed (Berlin et al., 2003; Tasto et al., 2003). Interestingly, expression of the *A. nidulans* septin AspC induced highly elongated atypical pseudohyphae and spore-producing structures in *S. cerevisiae* (Lindsey et al., 2010b). This altered morphology was suppressed in yeast mutant backgrounds lacking either the septin Cdc10 or the formin Bni1, suggesting that AspC interacts with the budding yeast septin complex by binding to Cdc10, and that the

introduction of AspC into the complex can alter Bni1 regulation and activity. This remarkable study demonstrates that the introduction of a single heterologous septin from a filamentous species can alter growth patterns to reproduce aspects of hyphal morphogenesis and conidiation in yeast. The filamentous fungus *A. gossypii* is closely related to *S. cerevisiae* but grows in a hyphal instead of a yeast form (Wendland and Walther, 2005). *Ashbya gossypii* has the same set of septin genes as *S. cerevisiae* but with an additional tandem duplication of *cdc11* (DeMay et al., 2009). Septins are not essential in *A. gossypii* - again highlighting the link between septin function and cellular form - but contribute to mitosis, sporulation, hyphal morphology and septation (DeMay et al., 2009; Gladfelter, 2006; Helfer and Gladfelter, 2006). Unlike budding yeast, various HO septin assemblies can coexist within an *A. gossypii* cell and these structures utilise different signalling pathways for their assembly and maintenance (DeMay et al., 2009). For example deletion of Gin4 or Elm1 kinases completely abolished the formation of inter-region septin rings (IR rings - septin rings in the middle of a hyphal cell) but not tip-associated septin filaments or septin rings at branch points (DeMay et al., 2009).

In the trimorphic pathogen *C. albicans*, *cdc3* and *cdc12* are essential whereas Δ*cdc10*/Δ*cdc10* and Δ*cdc11*/Δ*cdc11* null mutants were viable but displayed conditional defects in cytokinesis, cell wall deposition and bud morphology (Warenda and Konopka, 2002). *Candida albicans* Δ*cdc10*/Δ*cdc10* and Δ*cdc11*/Δ*cdc11* deletion mutants formed abnormal hyphae and the Δ*cdc11*/Δcdc11and Δ*cdc10*/Δ*cdc10* null mutants were defective for invasive growth and virulence (Warenda et al., 2003; Warenda and Konopka, 2002). Interestingly in *C. albicans*, septin localisation in germ tubes is different from that observed during budding or pseudohyphal growth. Septins localise to a tight ring at the bud and pseudohyphal necks whereas in emerging germ tubes septins localise as a diffuse collar or cap at the site of outgrowth (Warenda and Konopka, 2002). Additionally, a faint cap of septins is also present at the tips of *C. albicans* hyphae but not pseudohyphae (Warenda

and Konopka, 2002). Analysis of septin gene expression in *C. albicans* has demonstrated that none of the septins are hyphal specific, which suggests that the change in septin localisation is due to changes in septin regulation during morphogenetic transitions (Warenda and Konopka, 2002).

In the dimorphic plant pathogen *U. maydis* none of the four septin genes are essential, however, all single septin deletion mutants show conditional lethality when grown at 34°C (Alvarez-Tabares and Perez-Martin, 2010). At restrictive temperatures septin null mutants were swollen and regularly lysed; both defects could be rescued by the addition of sorbitol (Alvarez-Tabares and Perez-Martin, 2010). Additionally, septin deletion mutants were hypersensitive to compounds known to affect cell wall integrity (caffeine, calcofluor white and chlorpromazine) suggesting that the primary defect in these mutants is in cell wall construction and possibly osmoregulation (Alvarez-Tabares and Perez-Martin, 2010). Septins in *U. maydis* were also shown to have role in infection (Alvarez-Tabares and Perez-Martin, 2010; Boyce et al., 2005) similar to septins in *C. albicans* and *Cryptococcus neoformans* (Kozubowski and Heitman, 2010; Warenda et al., 2003). The septins formed three HO structures in *U. maydis*: bud neck collars, band-like structures at the growing hyphal tip and long septin fibres that partially colocalised with microtubules (Alvarez-Tabares and Perez-Martin, 2010). Only Sep4 (*S. cerevisiae cdc10* ortholog) formed long septin fibres in *U. maydis* (Alvarez-Tabares and Perez-Martin, 2010). Cdc10 septin fibres have also been shown to occasionally colocalise with MTs in dikaryotic hyphae of *C. neoformans* (Kozubowski and Heitman, 2010). Interestingly in the plant pathogen *Magnaporthe oryzae*, the location of the appressorium septum is determined by the site of septin ring assembly (Saunders et al., 2010). During appressorium formation the septin ring functions as both a scaffold for Tea-1-mediated F-actin assembly and as a diffusion barrier for the Rvs167 I-BAR protein, which is thought to induce membrane curvature at the tip of the emerging penetration peg (Dagdas et al., 2012).

The genome of *A. nidulans* encodes a complement of five septins, four of which, *aspA*, *aspB*, *aspC*, *aspD*, are orthologous to the *S. cerevisiae* septins *cdc11*, *cdc3*, *cdc12* and *cdc10*, respectively. The *aspE* gene is a member of group 5 septins and orthologs are restricted to other filamentous fungi. All five septins are expressed during vegetative growth, demonstrating a lack of sporulation-specific septins, with *aspB* (*cdc3* ortholog) having the highest expression level (Westfall and Momany, 2002). Deletion of *aspA*, *aspB*, or *aspC* in *A. nidulans* leads to delayed septation, increased emergence of germ tubes and hyphal branches and decreased asexual sporulation (Hernandez-Rodriguez et al., 2012; Lindsey et al., 2010a). These findings suggest that one of the key function of septins in filamentous fungi is to prevent the inappropriate emergence of germ tubes and branches, which is in keeping with their known role as a diffusion barrier and scaffold in budding yeast; presumably cell polarity components are concentrated at a specific site by HO septin structures and are prevented from diffusing freely. Defects in conidiation and septation in septin null mutants demonstrate that septins play a minor role in cytokinesis. In *A. nidulans* and *A. fumigatus,* septins localise as rings in forming septa and emerging branches and germ tubes (Juvvadi et al., 2011; Lindsey et al., 2010a; Westfall and Momany, 2002). At hyphal tips, AspA and AspC localise as a diffuse collar and during conidiation septins localise to the interface between emerging conidiophore layers. Also present are cytoplasmic dots and fibres of septins. In *A. fumigatus*, maintenance of septin fibres depends on actin and MTs but whether or not these fibres associate with MTs or F-actin is unclear.

1.4 Questions to address

This thesis deals with the role and organisation of actin and septins in the model filamentous fungus *N. crassa*. *Neurospora crassa* has been utilised as a model eukaryote for over seventy years and research on this organism has yielded significant contributions to photobiology, circadian rhythms, development, DNA repair and recombination and cell polarity (Davis and Perkins, 2002). One notable discovery with this fungus include Beadle and Tatum's development of the "one gene one enzyme" hypothesis from their work on nutritional mutants of *N. crassa* (Beadle and Tatum 1941). A range of molecular tools are available for its genetic manipulation (Honda and Selker, 2009; Larrondo et al., 2009). However, one important limitation in the manipulation of *N. crassa* and other filamentous fungi is the low rate of homologous recombination in wild-type strains, a situation similar to most eukaryotes with the notable exception of yeast – this factor prohibits facile manipulation of a genome to generate a modified gene. However, recently it was found that in *N. crassa*, non-homologous integration of foreign exogenous DNA is entirely dependent on the Ku70/Ku80-Lig4 DNA repair pathway and that the deletion of any of these components dramatically increases the frequency of homologous recombination (Ishibashi et al., 2006; Ninomiya et al., 2004). This important discovery has led to the development of several fungal strains lacking these elements to facilitate the disruption, modification, or replacement of a target gene (Krappmann et al., 2006; Lebrun et al., 2008; Nayak et al., 2006; Ram et al., 2007).

Actin and septins have been particularly well studied in budding yeast. However, there are likely to be important differences between budding yeast and filamentous fungi in actin and septin architecture and dynamics, as budding yeast only display a short period of polarised growth during bud formation, which is followed by isotropic growth over the bud surface (Bretscher, 2003). These cytoskeletal elements are likely to have an important role in generating the range of cell morphologies in filamentous fungi. Sustained polarised growth

during hyphal morphogenesis is a defining feature of filamentous fungi (Harris, 2006) making them attractive models for studying the role of the actin and septins in cell polarity, tip growth and intracellular organisation. When commencing this thesis, live-cell imaging of actin and septin architecture and dynamics had not been accomplished in *N. crassa*, yet was expected to yield key insights into these cellular processes. The questions addressed in this thesis are as follows:

- Is the recently developed Lifeact probe suitable for imaging actin in *N. crassa*?
- Does the Lifeact probe bind to actin or cause any perturbation of cell function?
- How is F-actin organised in *N. crassa* and are F-actin dynamics similar to other systems?
- Are there any differences in F-actin organisation between germ tubes and mature hyphae?
- Is Lifeact suitable for dual-labelling experiments?
- What roles do septins fulfil in *N. crassa* and how are they organised?
- Do the six septins in *N. crassa* perform identical roles and share the same pattern of organisation?
- How does loss of septins affect cell morphology, the formation of higher-order septin structures, and the actin cytoskeleton?
- What components constitute the septin complex and do differences in septin localisation, if any, reflect differences in associated proteins?

1.5 Experimental techniques

I addressed the above questions with three main experimental techniques: (1) genetic manipulation, (2) live-cell imaging, and (3) protein purification combined with mass spectrometry. Fluorescence and differential interference contrast (DIC) microscopy were incredibly important techniques for the analysis of strains. Widefield fluorescence microscopy was utilised instead of confocal modalities because of the relatively thin imaging subject (*N. crassa* cells vary in thickness from ~ 5 to 15 µM), reduced phototoxicity and photobleaching during sample illumination, and superior quantum efficiency of CCD detectors (60-70% for CCD detectors compared to 10% for photo multiplier tube [PMT] detectors) (Murray et al., 2007; Spring, 2007; Waters, 2007). Typically, 3-D image stacks were acquired instead of a single plane to allow removal of out-of-focus blurring by image deconvolution (Swedlow, 2007; Wallace et al., 2001). Finally, mass spectrometry has emerged as a powerful method to identify interacting components in multiprotein complexes (Trinkle-Mulcahy et al., 2008; Walther and Mann, 2010). Mass spectrometry is a technique used to accurately determine the mass-to-charge ratio (m/z) of peptides and selected fragmented peptides, which in turn permits the identification of proteins by comparison of obtained peptide sequence profiles to a protein database of the organism in question. To isolate septin complexes individual septins were tagged with two epitopes and purified by tandem affinity purification (TAP) then analysed by tandem mass spectrometry to identify complex constituents.

Chapter 2:

Materials and Methods

2.1 Strains, media and culture conditions

Neurospora crassa strains used and generated in this study are listed in the Appendix (Table A.1). *Neurospora crassa* strains generated during this study were derived from FGSC #4200 (WT *a*), FGSC #2489 (WT *A*), FGSC #11972 (*Δcdc-3::hph a*), FGSC #11727 (*Δcdc-10::hph Δmus-51::bar A*), FGSC #11971 (*Δcdc-11::hph A*), FGSC #11442 (*Δmyo-5::hph A*), FGSC #9717 (*his-3*$^{-}$ *Δmus-51*::*bar A*), FGSC #6103 (*his-3*$^{-}$ *A*), FGSC #9717 (*his-3*$^{-}$ *Δmus-51*::*bar A*), FGSC #9718 (*Δmus-51*::*bar a*), and FGSC #9719 (*Δmus-52*::*bar a*) which were obtained from the Fungal Genetics Stock Center (FGSC; School of Biological Sciences, Kansas City, MO). Strains were maintained on Vogel's minimal medium (VMM) plates with 2% sucrose and 1.5% agar and cultured at 35°C. All manipulations were according to standard *N. crassa* techniques (Davis, 2000). Transformants were selected either on low nitrogen complete selection media (Low N_2 CSM; 1 M Sorbitol, 0.5% proline, 1% glucose, 0.025% fructose, 0.025% sorbose, 1× Vogel's nitrogen free salts, 1.5% agar) containing Ignite (phosphinothricin; Sigma-Aldrich) or on complete selection media (CSM; 1M Sorbitol, 1% glucose, 0.025% fructose, 0.025% sorbose, 1× Vogel's salts, 1.5% agar) containing either hygromycin or nourseothricin or on unsupplemented CSM for selection of transformants that had recovered histidine prototrophy. Hygromycin B (Calbiochem), nourseothricin (Werner BioAgents), and Ignite were used at concentrations of 200, 25, and 800 µg/ml, respectively. To isolate genomic DNA, strains were grown in liquid VMM with shaking for 2 days at 35°C.

2.2 Plasmid construction

All primers and synthetic oligonucleotides used in this study are listed in the Appendix (Table A.2). Plasmids constructed in this study are listed in the Appendix (Table A.3). All PCRs were carried out using Phusion polymerase (Finnzymes), with the exception of genotyping PCRs which were carried out using Phire polymerase (Finnzymes). Cycling conditions for

both polymerases were as follows: initial denaturation at 98°C for 45 s, followed by 30 cycles of 98°C for 10 s, annealing at 60-70°C (depending on t_m of primer set) for 10 s, extension at 72°C for 20 s per kb of amplicon, and then a final extension at 72°C for 60 s. Wild-type genomic DNA was used a template to amplify genomic sequences.

To visualise Lifeact-GFP in *N. crassa*, we constructed a synthetic gene for integration at the *his-3* locus. To construct the Lifeact-GFP plasmid, I designed *N. crassa*-codon optimised oligonucleotides, LA Fw and LA Rv, which contain the Lifeact sequence, an *Xba*I site at one end and a *Pac*I site at the other end. After boiling for 5 min, the oligos were incubated at room temperature for 30 min to anneal then digested with *Xba*I and *Pac*I and inserted into an *Xba*I- and *Pac*I-digested GFP expression vector, pCCG::C-Gly::GFP (Honda and Selker, 2009), yielding pAB221.

I found that expression of the Lifeact construct from the *ccg-1* promoter did not allow satisfactory visualisation of Lifeact-GFP in mature vegetative hyphae. Therefore, the 0.9 kb upstream regulatory region of the *N. crassa* locus NCU02003 (transcriptional elongation factor-1 homolog, *tef-1*) was amplified by PCR and exchanged for *Pccg-1* in the pAL1 GFP expression vector, yielding pTEFsG-2. Following confirmation that the putative *tef-1* promoter provided GFP expression throughout the *N. crassa* life cycle, the *Ptef-1* sequence was amplified from pTEFsG-2 using the primers TEF1 IF Fw and TEF1 IF Rv and purified using a DNA clean and concentrator kit (Zymo Research) then integrated into *Not*I- and *Xba*I-digested pAB221 using the In-Fusion PCR cloning kit (Clontech), yielding pAB261.

To facilitate dual labelling studies I developed a Lifeact-tagRFP-T fusion construct. The Lifeact-tagRFP-T fusion was made from the plasmid pAB261 which contains Lifeact-GFP under the control of the *tef-1* promoter. The tagRFP-T ORF was amplified from pAL5 (Lichius and Read, 2010) with the primers TAGRFPT IF Fw and TAGRFPT IF Rv. GFP was excised from pAB261 by digestion with *Pac*I and *Eco*RI and the linearised plasmid was gel-extracted. The tagRFP-T PCR product was purified using a DNA clean and concentrator kit

(Zymo Research) then integrated into *Pac*I- and *Eco*RI-digested pAB261 with the In-Fusion PCR cloning kit to yield plasmid pAB271 (*Ptef-1-lifeact-tagrfpt*). DNA sequencing was carried out by the GenePool at the University of Edinburgh on all vectors to confirm in-frame cloning of the fusion constructs. Thus, Lifeact-GFP constructs were expressed under the control of the *ccg-1* or *tef*-1 promoter, and consisted of the Lifeact sequence fused to GFP at its C-terminus via a 10 glycine linker.

2.3 Engineering of deletion cassettes and epitope-tagging cassettes

Yeast recombinational cloning (YRC) was used to generate deletion cassettes (knock-out) and epitope-tagging cassettes (knock-in) (Honda and Selker, 2009; Larrondo et al., 2009; Oldenburg et al., 1997). Three epitopes, GFP, mCherry and V5-HAT, were used to modify genes at their native loci. GFP and mCherry serve as markers for protein localisation whereas the V5-HAT epitope consists of two distinct epitopes (V5 is a viral epitope and HAT [histidine affinity tag] is a natural 19-aa poly histidine tag derived from chicken lactate dehydrogenase) and was utilised for tandem affinity purification of septin complexes. An outline of the strategy for generating knock-in and knock-out cassettes is shown in Figure 2.1. DNA fragments consisting of targeting flanks, a selection marker and, for knock-in constructs, an epitope were co-transformed into the yeast strain FY834 (Winston et al., 1995), along with the yeast shuttle vector pRS426 (Sikorski and Hieter, 1989) digested with *Xho*I and *Eco*RI, for assembly in yeast via its endogenous recombination system (Oldenburg et al., 1997). Yeast transformations were carried out with the lithium acetate/PEG method (Gietz and Woods, 2001). After 3 days of growth at 30°C, yeast colonies were harvested and pooled, then plasmid DNA was recovered and resuspended in 20 µL of 10 mM Tris-Cl pH 8.0, as described previously (Robzyk and Kassir, 1992). Two microliters of the DNA suspension was then introduced into *Escherichia coli* strain DH5α by electroporation.

Following restriction digest screening of *E. coli* clones and confirmation of the correct vectors by DNA sequencing, the cassette was cut out with the appropriate restriction enzymes and transformed into *Δmus*-51 or *Δmus*-52 *N. crassa* strains by electroporation.

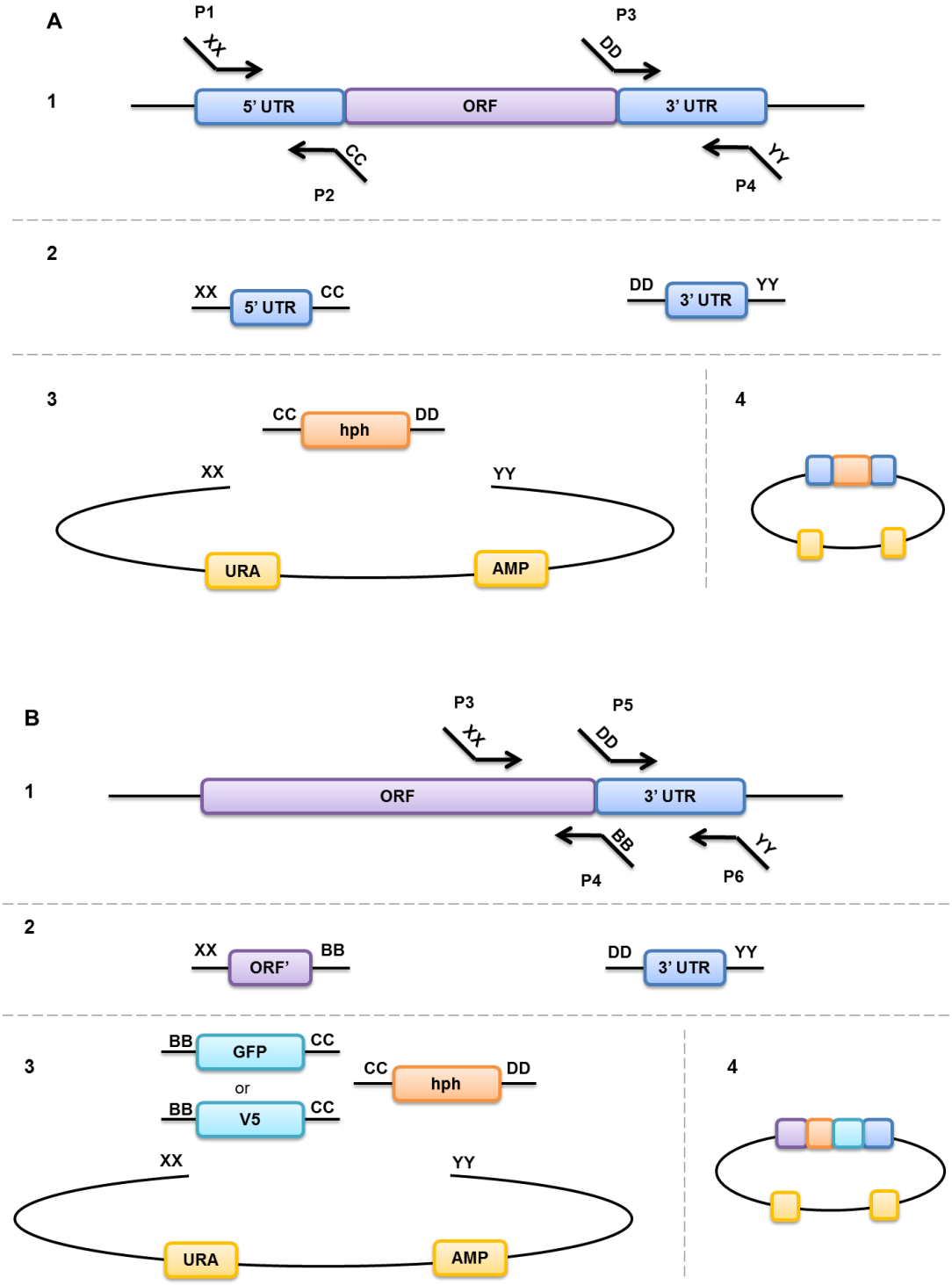

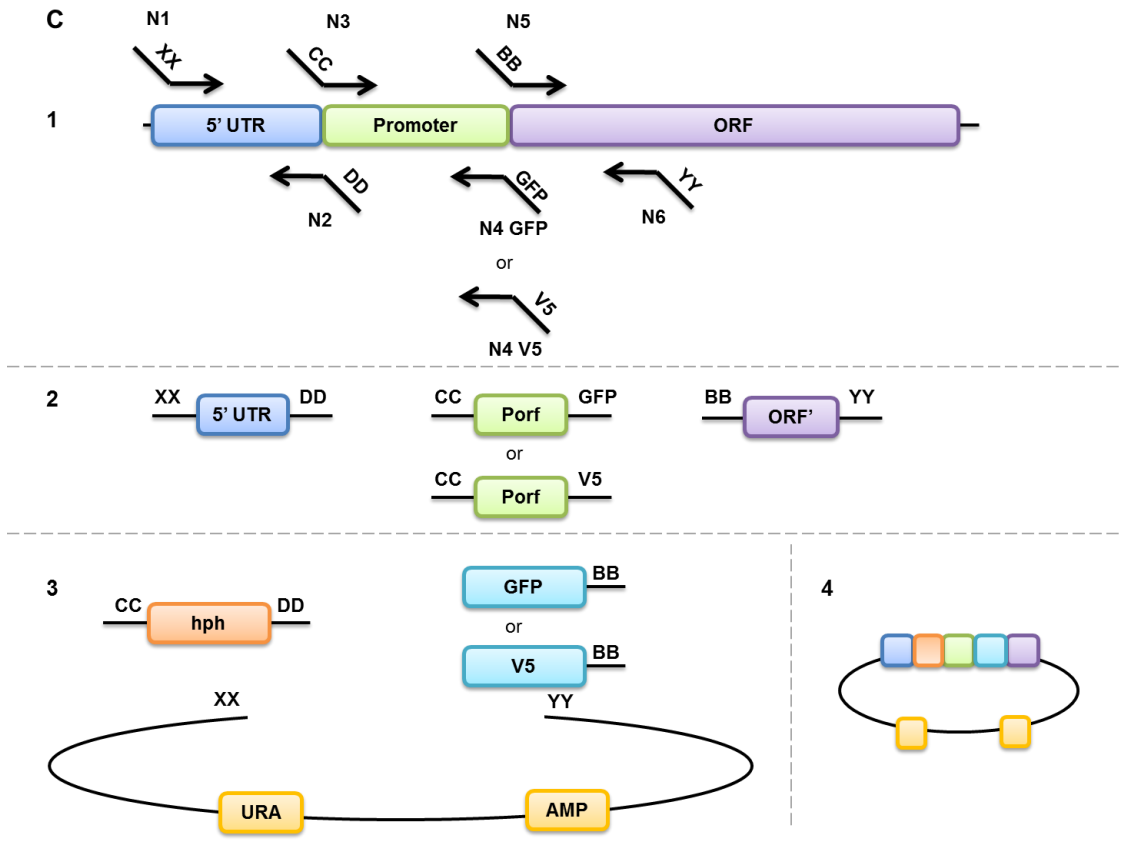

Figure 2.1. Strategy for creating integration cassettes with yeast recombinational cloning. (A) Elements required for deletion cassettes. (B) Elements required for C-terminal integration cassettes. (C) Elements required for N-terminal integration cassettes. The steps followed to generate the integration cassettes are the same regardless of the type of cassette to be constructed. (Step 1) Targeting flanks are amplified from genomic DNA with chimeric primers (shown as arrows) which contain 30 bp extensions at the 5' (shown as two letters). (Steps 2 and 3)Targeting flanks (blue, purple and green) are combined with a resistance marker module (orange) and, if required, an epitope tag module (turquoise), both of which have defined extensions at the 5' and 3' (shown as two letters) and transformed into *S. cerevisiae* along with a linearised shuttle vector for assembly in yeast via its endogenous recombination system. (Step 4) The correctly assembled plasmid is isolated from yeast then the functional integration cassette is released form the plasmid by digestion with *Not*I and transformed into *N. crassa* to integrate via homologous recombination at the desired locus.

The final vectors consisted of targeting flanks specific for the gene of interest and functional elements (henceforth referred to as modules) such as dominant selection markers and epitopes (for integration cassettes). The procedure was simplified by generating standardised modules via PCR which contain defined regions of homology at the 5' and 3' end of the DNA fragment. This allows a variety of knock-out and knock-in cassettes to be created with the same targeting flanks by swapping in or out different modules (*i.e.* substituting the *hph* selection module for the *nat* selection module or substituting the GFP module for the V5-HAT module).

To generate targeting flanks, three ~ 1kb regions were amplified from the genes of interest (*myo-5*, *cdc-3*, *cdc-10*, *cdc-11*, *cdc-12*, *asp-1*, and *asp-2*). Approximately ~ 1kb upstream of the gene of interest was amplified using primers P1 and P2 to yield flank A. Flank B consists of ~ 1kb of the region upstream of the gene's stop codon and was amplified using primers P3 and P4. Flank C contains ~ 1kb of the UTR region downstream of the gene's stop codon and was amplified using primers P5 and P6. Flanks A and C together with a marker module were used to create deletion cassettes whereas flanks B and C, in addition to a marker module and epitope module were used to create C-terminal epitope tagging cassettes.

For four genes (*myo-5*, *cdc-10*, *asp-1*, and *asp-2*) C-terminal tagging by knock-in was unsuccessful; therefore, we constructed C-terminal and N-terminal overexpression constructs using the In-Fusion PCR cloning kit (Clontech). For C-terminal overexpression constructs, the *myo-5*, *cdc-10*, *asp-1*, and *asp-2* genes were amplified, without the stop codon, with the primers MYO5 IF Fw and MYO5 IF Rv, CDC10 IF Fw and CDC10 P4 Rv, ASP1 IF Fw and ASP1 P4, or ASP2 IF Fw and ASP2 P4, respectively. The PCR products were purified using a DNA clean and concentrator kit (Zymo Research) then integrated into *Xba*I- and *Pac*I-digested pCCG::C-Gly::GFP using the In-Fusion PCR cloning kit to give plasmids pAB224 (*Pccg-1-myo-5-sgfp*), pAB226 (*Pccg-1-cdc-10-sgfp*), pAB229 (*Pccg-1-asp-*

1-sgfp), and pAB222 (*Pccg-1-asp-2-sgfp*). Similarly, for N-terminal overexpression constructs the *myo-5*, *cdc-10*, *asp-1*, and *asp-2* genes were amplified with the primers MYO5 IF NT Fw and MYO5 IF NT Rv, CDC10 IF NT Fw and CDC10 IF NT Rv, ASP1 IF NT Fw and ASP1 IF NT Rv, or ASP2 IF NT Fw and ASP2 IF NT Rv, respectively. The purified PCR products were then integrated into *Xba*I- and *Asc*I-digested pCCG::N-GFP (Honda and Selker, 2009) using the In-Fusion PCR cloning kit to yield plasmids pAB324 (*Pccg-1-sgfp-myo-5*), pAB326 (*Pccg-1-sgfp-cdc-10*), pAB329 (*Pccg-1-sgfp-asp-1*), and pAB322 (*Pccg-1-sgfp-asp-2*). For *myo*-5, *cdc-10*, *asp-1*, and *asp-2*, C-terminal tagging by overexpression was unsuccessful. N-terminal overexpression gave an adequate signal-to-noise ratio for *cdc-10*, *asp-1*, and *asp-2* but not for *myo*-5. Given that N-terminal tagging by overexpression was successful I generated N-terminal epitope-tagging cassettes for integration in the native loci of *myo*-5, *cdc-10*, *asp-1*, and *asp-2*.

To generate N-terminal knock-in cassettes different targeting flanks were required. Flank D contains ~ 1 kb of the region between base -2500 and -1500 upstream of the genes start codon and was amplified using primers N1 and N2. Approximately ~ 1 kb directly upstream of the gene of interest was amplified using primers N3 and N4 to yield flank E. Flank F contains ~ 1 kb of the region downstream of the gene's start codon and was amplified using primers N5 and N6. N-terminal knock-in cassettes were constructed with these three flanks (D, E, and F), a marker module and an epitope module. All targeting flanks were amplified with a 30 bp extension which corresponds to a region of homology at the 5'- and 3'-end of the various modules or the linearised pRS426 (see Figure 2.1)

The two dominant selection markers used in YRC, the *hph* gene and *nat* gene, confer hygromycin resistance and nourseothricin resistance in *N. crassa*, respectively. The *hph* module was amplified from pGFP::hph::loxP (Honda and Selker, 2009) with the primers HPH YRC CC Fw and HPH YRC DD Rv. The *nat* module was amplified from pD-Nat (Kück and Hoff, 2010) with the primers NAT YRC CC Fw and NAT YRC DD Rv. The GFP module

for C-terminal tagging was amplified from pGFP::hph::loxP with the primers GFP YRC BB Fw and GFP YRC CC Rv. For N-terminal tagging the GFP module was amplified from pGFP::hph::loxP with the primers GFP YRC NT Fw and GFP YRC NT BB Rv. The mCherry module for C-terminal tagging was amplified from pRset-mCherry (Shaner et al., 2004) with the primers MCH YRC BB Fw and MCH YRC CC Rv. The V5-HAT epitope was constructed *de novo* with *N. crassa*-codon optimised oligonucleotides V5HAT YRC A, V5HAT YRC B, and V5HAT YRC C which are partially overlapping and contain a 10x glycine linker at the 5'-end, the V5 and HAT sequences joined by a 5x glycine-alanine linker, and a region of defined homology at the 3'-end. After boiling for 5 min, the oligos were incubated at room temperature for 30 min to anneal then co-transformed into yeast along with *cdc-3* targeting flanks B and C, the *hph* module and pRS426 linearised with *Xho*I and *Eco*RI. The resulting plasmid, pAB455, was checked by DNA sequencing then used as a PCR template to generate the V5-HAT module for C-terminal tagging with primers V5HAT YRC BB Fw and V5HAT YRC CC Rv. For N-terminal tagging the V5-HAT module was amplified from pAB455 with primers V5HAT YRC NT Fw and V5HAT YRC NT BB Rv. For transformation the appropriate fragments were co transformed into yeast strain FY834 along with the *Eco*RI and *Xho*I-digested yeast shuttle vector pRS426 and the correct plasmids recovered as described above.

To visualise septins simultaneously with microtubules we created a tubulin-mCherry fusion construct. The tubulin-mCherry fusion was made with YRC. The 2647 bp *Pccg-1-bml* sequence was amplified from plasmid pMF309 (Freitag et al., 2004) with the primers BTUB YRC Fw, which contains 30 bp of homology at the 3'-end of the linearised pRS426, and BTUB YRC Rv, which contains 30 bp of homology at the 5'-end of the mCherry module. The *Pccg-1-bml* sequence was co-transformed into yeast along with the mCherry module, the linearised pRS426 shuttle vector and a *nat* selection module modified to include a 30 bp region of homology to the 5'-end of the linearised pRS426. The resulting plasmid, pAB46BT,

was isolated from yeast and screened as described above. DNA sequencing was carried out on all vectors by the GenePool at the University of Edinburgh to confirm in-frame cloning of the fusion constructs and correct amplification by PCR.

2.4. Transformation and transformant selection.

Electroporation of *N. crassa* was performed as described previously (Margolin et al., 1997). When required homokaryotic strains were obtained from heterokaryotic transformants by back-crossing to wild-type (Davis, 2000) or by the induction of microconidiation (Ebbole and Sachs, 1990).

To generate strains expressing Lifeact-GFP, *Nde*I-digested pAB221 and pAB261 were targeted to the *his-3* locus of FGSC #6103 (*mat A his-3*$^{-}$) to generate strains *Pccg-1-lifeact-sgfp* and *Ptef-1-lifeact-sgfp*, respectively. A Lifeact-tagRFP-T-expressing strain was created by introducing *Nde*I-digested pAB271 into the *his-3* locus of FGSC#6103 (*mat A his-3*$^{-}$) to generate strain *lifeact-rfp*.

To create single and double septin deletion strains, knock-out cassettes were released from their respective plasmids by digestion with *Not*I and then transformed into strain FGSC #9718 (*Δmus-51::bar*) or FGSC #9719 (*Δmus-52::bar*). Transformants were screened by PCR (see below) then back-crossed to the wild-type to restore the *mus-51* or *mus-52* gene and provide homokaryotic null mutants. One of the deletion strains obtained from the FGSC (FGSC #11727) was supplied as a heterokaryon and was back-crossed to the wild-type to acquire a homokaryotic deletion strain. Additionally, strain FGSC #11972 was crossed to FGSC #9719 strain to yield strain *Δcdc-3*, *Δmus-52*. FGSC #11971 was crossed to FGSC #9717 and to *Pccg-1-lifeact-sgfp* to yield strains *Δcdc-11*, *Δmus-51* and *Δcdc-11*, *lifeact-sgfp*, respectively. The Δ*myo-5* strain, FGSC #1144, was crossed to *Pccg-1-lifeact-sgfp* to generate strain Δ*myo-5*, *lifeact-sgfp*.

To generate strains expressing epitope-tagged proteins from their native loci, plasmids containing knock-in cassettes were digested with *Not*I and transformed into strain FGSC #9718 (*Δmus-51::bar*) with the exception of *cdc-3* integration cassettes which were digested with *Kpn*I and transformed into strain FGSC #9719 (*Δmus-52::bar*). The *cdc-11-sgfp::nat* and *cdc-12-sgfp::nat* integration cassettes were transformed into *Δmus-51* or *Δmus-52* septin null mutants to analyse their localisation in the absence of other septins.

C-terminal and N-terminal overexpression constructs for *myo-5*, *cdc-10*, *asp-1*, and *asp-2*, were digested with *Nde*I (or *Ssp*I for pAB222 and pAB322) and targeted to the *his-3* locus of strain FGSC #6103 (*his-3*$^{-}$). To visualise septins simultaneously with microtubules, strain *Pccg1-sgfp-cdc-10* was transformed with undigested pAB46BT to yield strain *sgfp-cdc-10, bml-mch*. An actin/septin co-labelled strain was generated by transforming FGSC #9717 with *NdeI*-digested pAB271 and then transforming the resulting *lifeact-rfp*, *Δmus-51* strain with *NotI*-digested pAB427 (*cdc-11-sgfp* integration cassette) to yield strain *cdc-11-sgfp*, *lifeact-rfp*. The dual-labelled GFP-MYO-5 and Lifeact-tagRFP-T strain was created by transforming pAL5 into strain *sgfp-myo-5* to give strain *sgfp-myo-5*, *lifeact-rfp*.

FP expression was examined in multiple transformants using a Nikon SMZ1500 stereomicroscope with a GFP (excitation 470/40 nm, 505 nm dichroic mirror, emission 530/40 nm) or RFP filter set (excitation 545/30 nm, 570 nm dichroic mirror, emission 620/60 nm). FP expression was analysed in at least eight transformants per plasmid construct by widefield fluorescence microscopy. Transformants exhibiting FP expression were selected for subsequent live-cell imaging studies. Expression of V5-HAT-tagged proteins was determined by immunoblotting (see below).

2.5 PCR-based genotyping

To verify the genetic make-up of strains generated in this project, multiplex PCR and Southern blotting were employed. A diagram showing the general positions of primers used for genotyping is shown in Figure 2.2. Genotyping primers are listed in the Appendix (Table A.2). Primers sets were chosen to confirm the presence of the wild-type gene (primers sets G1+G2 = PCR1 and G3+G4 = PCR2), integration of the deletion or epitope cassette (primers sets G1 + HPH2 = PCR3, G4 + HPH1 = PCR4, G1 + NAT2 = PCR5, G4 + NAT1 = PCR6), or to check the integration of *his-3 Pccg-1-sgfp* overexpression cassette (primers sets GFP Fw + His3 Rv = PCR7, and GFP Rv + His3 Fw = PCR8). The presence of *mus-51* (primers set MUS-51 Fw + MUS-51 Rv = PCR9) and mus-*52* (MUS-51 Fw + MUS-51 Rv = PCR10) was assessed following backcrossing of heterokaryotic deletion strains to the wild-type. Finally, a primer pair specific to the actin locus (NCU04173.3) were added to each PCR tube to serve as an internal positive control to confirm the presence of genomic DNA. Genomic DNA was isolated for PCR-based genotyping as described previously (Irelan et al., 1993).

2.6 Southern blotting

In addition to PCR-based genotyping, Southern blots were carried out on deletion strains to confirm the correct integration of the deletion cassette and to demonstrate that the deletion cassette has not been integrated ectopically elsewhere in the genome – a scenario that cannot be determined by PCR alone. A schematic showing the outline of the Southern blot strategy is shown in Figure 2.3. Plasmids encoding the appropriate deletion cassettes were used as templates to generate the probe. The restriction enzymes and predicted fragments sizes are given in Table 2.1. A Qiagen DNeasy plant mini kit was used to isolate genomic DNA for Southern blots, according to the manufacturer's instructions.

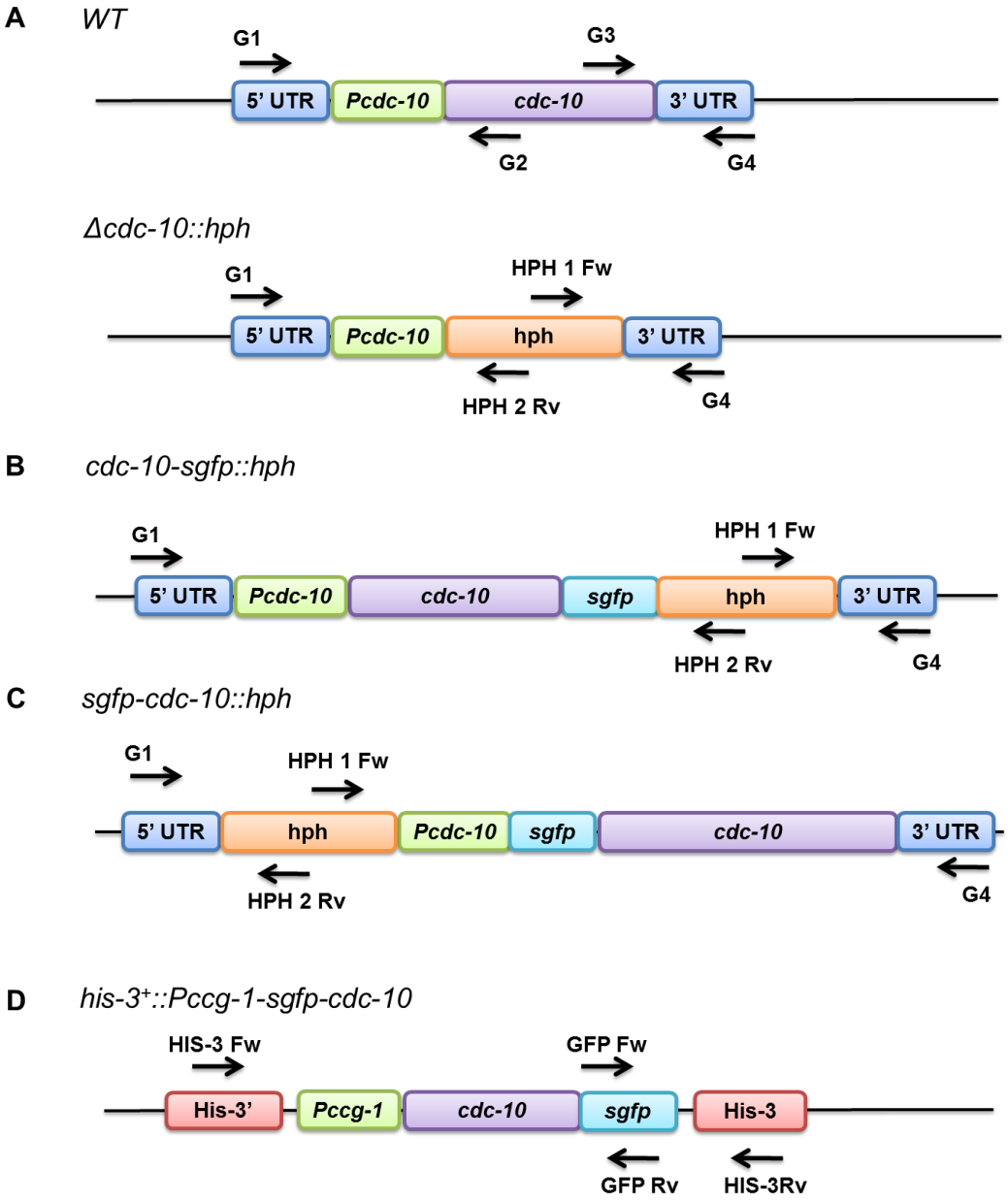

Figure 2.2. Schematic representation of genotyping strategy. Names of strains are in italics. An identical scheme was also used to genotype other *N. crassa* strains using the appropriate primers. (A) Location of primer binding sites used to confirm correct integration of *hph*- or *nat*-based deletion cassettes. Primers were used in the following combinations: G1 + G2, G3 + G4, G1 + HPH2 and G4 + HPH1 for strains selected with the *hph* gene; G1 + G2, G3 + G4, G1 + NAT2 and G4 + NAT1 for strains selected with the *nat* gene. (B) Location of primer binding sites used to confirm the correct C-terminal integration of *hph-sgfp* or *hph-v5-hat* cassettes. Primers were used in the following combinations: G1 + HPH2, G4 + HPH1. (C) Location of primer binding sites used to confirm the correct N-terminal integration of *hph-sgfp* or *hph-v5-hat* cassettes. Primers were used in the following combinations: G1 + HPH2, G4 + HPH1. (D) Location of primer binding sites used to confirm the correct integration of *his-3-Pccg-1-sgfp* cassettes. Primers were used in the following combinations: GFP Fw + HIS3 Rv, GFP Rv + HIS3 Fw.

Probes were generated using Phusion polymerase (Finnzymes) and a modified dNTP nucleotide mix in which dTTP was replaced with a mix of 50% unmodified dTTP and 50% biotin-16-dUTP (Roche). The following cycling parameters were used for probe amplification: initial denaturation at 98°C for 45 s, followed by 30 cycles of 98°C for 10 s, 60°C for 10 s, and 72°C for 60 s, and then a final extension at 72°C for 60 s. The probe was purified using a DNA clean and concentrator kit (Zymo Research).

Following isolation and digestion of genomic DNA, DNA fragments were separated on a 0.8% agarose gel. A xylene cyanol loading buffer (6x loading buffer = 0.1% xylene cyanol, 30% glycerol) was used instead of bromophenol blue to reduce background during detection.

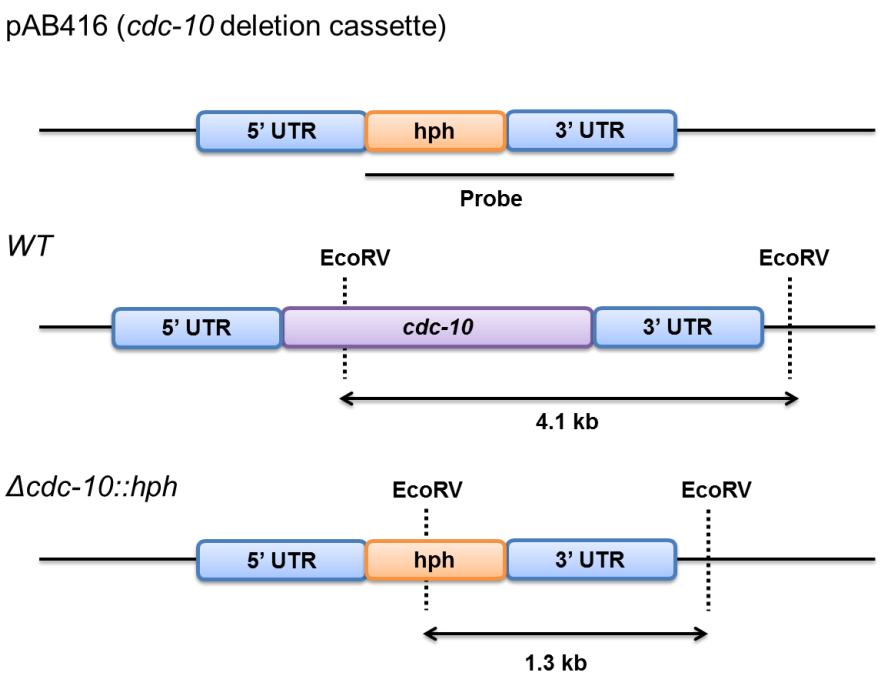

Figure 2.3. Schematic representation of Southern blotting strategy. A similar strategy was also used to determine the correct integration of deletion cassettes at other loci. The probe was amplified from deletion cassettes and designed to bind to the resistance marker and 3'UTR of the target gene. DNA fragments generated by digestion with *Eco*RV are indicated by arrows. The restriction enzymes and predicted fragments sizes for Southern blotting analysis are given in Table 2.1.

The gel was depurinated in 0.25 M HCL for 30 min with gentle shaking then DNA fragments were transferred to a Amersham Hybond N+ membrane overnight using 0.4 M NaOH. Hybridisation (at 60°C), washing, blocking and detection with streptavidin-IRDye 800CW conjugate (LiCOR) was carried out according to the manufacturer's instructions. Membranes were imaged using a LiCOR Odyssey scanner.

Table 2.1. Predicted DNA fragment sizes and restriction enzymes for Southern blots

Strain	**Restriction enzyme**	**Fragment size (kb) for WT control**	**Fragment size (kb) for null mutants selected with *hph* gene**
Δmyo-5	*Eco*RI	3.4	1.5
Δcdc-3	*Eco*RI	4.3	1.4
Δcdc-10	*Eco*RV	4.1	1.3
Δcdc-11	*Pvu*II	1.4	3.1
Δcdc-12	*Sac*I	2.1	1.7,1.1
Δasp-1	*Pst*I	3.2	1.7
Δasp-2	*Nde*I	4	2.2
Δcdc-10 Δcdc-11	*Eco*RV	4.1	1.3
Δcdc-10 Δcdc-12	*Eco*RV	4.1	1.3
Δcdc-11 Δcdc-12	*Pvu*II	1.4	3.1
Δcdc-3 Δcdc-10	*Eco*RI	4.3	1.4
Δcdc-3 Δcdc-11	*Eco*RI	4.3	1.4
Δcdc-3 Δcdc-12	*Eco*RI	4.3	1.4
			Fragment size (kb) for null mutants selected with *nat* gene
Δcdc-10 Δcdc-11	*Eco*RV	1.1	1.6
Δcdc-10 Δcdc-12	*Xba*I	1.5	4.1
Δcdc-11 Δcdc-12	*Xba*I	1.5	4.1
Δcdc-3 Δcdc-10	*Eco*RV	4.1	1.9
Δcdc-3 Δcdc-11	*Eco*RV	1.1	1.6
Δcdc-3 Δcdc-12	*Xba*I	1.5	4.1

2.7 Protein extraction, affinity purification and immunoblotting

All protein purification steps were performed at 4°C. *Neurospora crassa* strains expressing V5-HAT-tagged proteins were grown at 35°C for 2 days in 2 l flasks containing 500 ml of liquid VMM. The cultures were harvested by filtration through Mira-cloth (Calbiochem), washed twice with 250 ml ddH_2O, and pressed between paper towels to remove excess water. The collected mycelium (~ 10 g) was then frozen in liquid nitrogen and ground into a fine powder in a pre-cooled pestle and mortar. Ice-cold HG extraction buffer (50 mM HEPES [pH 7.4], 137 mM NaCl, 10% glycerol freshly supplemented with a protease inhibitor cocktail [complete, EDTA-free tablet, Roche] and 1 mM PMSF) was added to the frozen grindate (5 ml of buffer/g of grindate) which was resuspended by vortexing for three 20 s pulses, inverted once every minute for 5 min and then centrifuged for 2370 x g at 4°C for 10 min. The supernatant was carefully removed and used immediately for affinity purification. For affinity purification, two types of Dynabeads were used: His tag isolation (HTI) Dynabeads (Invitrogen) and anti-V5 conjugated Dynabeads (Invitrogen). Anti-V5 monoclonal antibody (Invitrogen) was coupled to M-270 epoxy Dynabeads (Invitrogen) at a concentration of 10 mg/ml according to the manufacturer's instructions. Both types of Dynabeads were washed three times in HG extraction buffer before adding to supernatants. For tandem affinity purification 100 µl of HTI Dynabeads was added to 10 ml of supernatant and incubated on a roller at 4°C for 10 min. HTI Dynabeads were collected with a Dynal magnet (Invitrogen), washed three times in HTI wash buffer (50 mM HEPES [pH 7.4], 300 mM NaCl, 0.01% Tween-20) and the complex eluted from the beads with two washes of 100 µl HTI elution buffer (50 mM HEPES [pH 7.4], 150 mM NaCl, 300mM imidazole, 0.01% Tween-20). The eluate was added to 100 µl anti-V5 Dynabeads and incubated on a roller at 4°C for 1 h. Anti-V5 Dynabeads Beads were collected with a Dynal magnet and washed twice in antibody-Dynabead wash buffer (ADWB; 50 mM HEPES pH 7.4, 150 mM NaCl, 0.02% Tween-20), once in ADWB minus Tween-20 and the proteins eluted twice in 20 µl 100 mM glycine-HCl

(pH 2.5). For single step affinity purifications with anti-V5 Dynabeads, 250 µl anti-V5 Dynabeads were added to 4 ml of cell extract. The remaining purification steps were carried out exactly as described for the immunoprecipitation stage of the tandem purification.

Purified protein samples were mixed with one-quarter volume of 4x sample buffer (0.2 M Tris-HCl, pH 6.8, 8% (w/v) SDS, 40% glycerol, 10% β-mercaptoethanol, 0.025% bromophenol blue) for SDS–PAGE. Samples were boiled for 5 min, and then separated by 10% SDS–PAGE. Gels were stained with either SYPRO Ruby (Invitrogen) or Safe blue (Invitrogen). For immunoblots, equal amounts of protein (100 µg) were separated by 10% SDS-PAGE, transferred to an Amersham Hybond nylon membrane in CAPS transfer buffer (10 mM CAPS [pH 11], 10% methanol) for 80 min at 80 V and the membrane was then blocked in PBS, 2% skimmed milk, 0.2% Tween-20. V5-HAT-tagged proteins were probed using mouse monoclonal anti-V5 antibody (Invitrogen; diluted to 1:10,000) and goat anti-mouse IgG- IRDye 800CW conjugate (LiCOR; diluted to 1:20,000) in PBS, 2% skimmed milk, 0.02% Tween-20. Membranes were washed for 30 min in PBS then imaged using a LiCOR Odyssey scanner.

2.8 Mass spectrometry

Destained SDS-PAGE gel bands were digested with sequencing grade modified porcine trypsin (Promega, ~ 5-10 ng/µl) solutions in 50 mM ammonium bicarbonate, and evaporated to dryness by vacuum centrifugation. Micro-HPLC/MS/MS analyses were performed using an online system consisting of a micro-pump Agilent 1200 binary HPLC system (Agilent) coupled to a hybrid LTQ Orbitrap XL instrument (Thermo-Fisher). The LTQ was controlled through Xcalibur 2.0.7 and LTQ Orbitrap XL MS2.4SPI. Capillary Picotip columns (10 cm long, 360 mm outer diameter, 75 mm inner diameter) with a 15 mm tip opening and fitted with a borosilicate frit were obtained from New Objective (Presearch). Fused-silica tubing

was from Composite Metal (UK). Samples were analysed on a 2 h gradient for data dependent analysis. MS/MS data were searched using Mascot version 2.2 (Matrix Science Ltd.), against the Neurospora genome and annotations database (http://www.broad.mit.edu/annotation/fungi, accessed January 2012).

2.9 Live-cell imaging

Conidia were collected from 3- to 5-day-old cultures and suspended in VMM. In all experiments, unless stated otherwise, conidia were used at a concentration of 10^6 cells per ml. Cells were incubated at 35˚C in VMM in Lab-Tek 8-well chamber-slides (Nalge-Nunc International) for 3-5 h in 250 µl of VMM at a concentration of 10^6 cells/ml then imaged. To image mature hyphae, conidia were grown in Petri dishes containing VMM solidified with 1.5% agar for 16-20 h at 24˚C then prepared for imaging using the "inverted agar block method" (Hickey et al., 2002). Imaging was carried out at room temperature. Two microscope setups were used: (1) a DeltaVision microscope (Applied Precision) consisting of: an Olympus IX70 base; Olympus 100x/1.4 NA Plan-Apo objective; 75W HBO illuminator; Chroma Sedat Quad ET filter set (for GFP: excitation 490/20 nm, emission 528/38 nm; for RFP: excitation 545/30 nm, emission 610/75 nm; for FM4-64: excitation 490/20 nm, emission 685/40 nm; for calcofluor white: excitation 360/40 nm, emission 457/50 nm; Chroma Technology Corp.); CoolSnap HQ CCD camera (Photometrics); and SoftWorx software (Applied Precision) for image acquisition; or (2) a Nikon TE2000 microscope consisting of: a Nikon100x/1.4 NA Plan-Apo objective; CoolLED PE-2 illuminator with LED excitation centred at 380 nm, 470 nm, and 550 nm; Chroma filter sets (for GFP: excitation 470/40 nm, 495 nm LP dichroic mirror, emission 525/50 nm; for RFP: excitation 535/50 nm, 565 nm LP dichroic mirror, emission 590 nm LP; for calcofluor white: excitation 355/50 nm, 400 nm LP dichroic

mirror, emission 420 nm LP); Hammamatsu Orca-ER CCD camera; and MetaMorph software (Universal Imaging) for image acquisition.

Exposure times ranged from 100-400 ms. To acquire 3D (x,y,z) images, 15-30 optical sections were obtained at 0.2-0.4 µm steps. For 4D imaging (x,y,z and t), 10-15 optical sections were obtained at 0.6 µm steps and 30-120 s intervals. Certain images were processed through 10 iterative deconvolutions using SoftWorx or AutoQuant image analysis software (Media Cybernetics). To image actin patch and GFP-MYO-5 particle dynamics, time-lapse sequences were captured in one focal plane using 2 x 2 camera binning at 100-300 ms intervals. Extension rates, patch/particle velocities and lifetimes were measured manually using the track object function of the Image Pro analysis software (version 7.0; Media Cybernetics, Bethesda, MD). The (x,y) coordinates of individual patches/particles or hyphal tips were recorded, and the velocities of objects were calculated as the sum of the distance between points divided by time. The velocities of individual patches/particles were averaged to obtain the mean velocity. Patch lifetimes were determined by multiplying the frame interval by the number of frames in which an individual patch was visible before it moved out of the focal plane. The size of the F-actin-depleted zone was determined using the measurements option of Image Pro. Projections and further processing steps were carried out with ImageJ software (*rsbweb.nih.gov/ij/)*. Some single-plane time-lapse (x,y,t) sequences were processed with an 'unsharp mask' filter to aid visualisation of fine cytoskeletal details.

2.10 Fluorescent staining

Mature hyphae and germlings were labelled for 30 min with either 2 µM FM4-64 (prepared from 200 µM stock in dimethyl sulfoxide [DMSO]; Molecular Probes), which stains the

plasma membrane and organelle membranes, or 0.1 µg/ml calcofluor white (prepared from 1 mg/ml stock in ethanol; Sigma-Aldrich) which stains cell walls.

2.11 Pharmacological treatments

Latrunculin A (Lat A; Invitrogen) was stored as a 1 mM stock in DMSO. Benomyl (Fluka) was stored as a 3 mg/ml stock in DMSO. Carbonyl cyanide 3-chlorophenylhydrazone (CCCP, Sigma-Aldrich) was stored as a 100 mM stock in DMSO. 2,3-Butanedione monoxime (BDM, Sigma-Aldrich) was stored as a 10 M stock in DMSO. 10x working solutions were made in ddH_20 for each of the inhibitors and DMSO control. For experimental procedures, cells of the GFP-MYO-5 and the Lifeact-GFP strains were incubated in Lab-Tek 8-well chamber slides in 250 µl of VMM at a concentration of 10^6 cells/ml. After 3 h of incubation, 25 µl of VMM was removed from the observation chamber and replaced with 25 µl of Lat A, benomyl, CCCP, BDM or DMSO working solutions. The final concentrations used were 10 µM Lat A, 3 µg/ml benomyl, 10 µM CCCP, 10 mM BDM or 0.1% DMSO. The effect of Lat A treatment on Lifeact-GFP localisation was monitored with time-lapse microscopy for 10 minutes, 1 minute after its addition. Cells were scored for the presence or absence of patches or cables at 1 minute intervals by visual inspection of time-lapse sequences. The effect of CCCP and BDM on Lifeact-GFP localisation was monitored with time-lapse microscopy for 20 s, 30 minutes after addition. To quantify the effects of treatment the number of rapid actin patch movements was counted in the time courses. The effect of Lat A, Benomyl, CCCP and BDM on GFP-MYO-5 localisation was monitored with time-lapse microscopy for 20 s, 30 minutes after addition. To quantify the effects of treatment, cells were divided into three categories – crescent, gradient, and cytoplasmic – on the basis of GFP-MYO-5 distribution.

2.12 Quantification of germination, cell fusion, germ tube emergence, unseparated conidia and septation

Conidial germination was quantified as the percentage of conidia possessing one or more protrusions/hyphae whilst cell fusion was quantified as the percentage of conidia or conidial germlings involved in fusion. Cell fusion during colony initiation involves the fusion of specialised cell protrusions termed conidial anastomosis tubes (CATs) (Read et al., 2009; Roca et al., 2005). The number of unseparated conidia was quantified as the percentage of cells attached to another cell at time 0 h. Septation was quantified as the percentage of cells with a septum and cells were scored as having multiple germ tubes if more than one germ tube had emerged from conidia. Statistical analysis (t-test) was performed using 'R' (http://www.r-project.org/).

Chapter 3:

F-actin dynamics and organisation in *Neurospora crassa*

3.1 Results

3.1.1 Lifeact-GFP and Lifeact-TagRFP label F-actin in N. crassa

The recently developed live-cell imaging probe for F-actin, Lifeact (Riedl et al., 2008), was utilised to study F-actin organisation in *N. crassa*. Lifeact is a 17-amino-acid peptide derived from the N-terminus of the budding yeast actin-binding protein Abp140 (Asakura et al., 1998; Yang and Pon, 2002), and has recently been demonstrated to be a universal live-cell imaging marker for F-actin in eukaryotes (Riedl et al., 2008). Immunofluoresence studies in *N. crassa* have shown that F-actin localises to hyphal tips as 'clouds' and 'plaques' (Barja et al., 1993; Heath et al., 2000; Virag and Griffiths, 2004). However, immunolabelling has failed to reveal actin cables in *N. crassa* and offers limited insights into F-actin dynamics.

I constructed two synthetic genes consisting of Lifeact fused to sGFP (S65T variant, henceforth termed GFP)(Chiu et al., 1996) or tagRFP-T (Merzlyak et al., 2007; Shaner et al., 2008) and expressed these constructs under the control of the *ccg-1* or *tef-1* promoter in various *N. crassa* strains. All clones chosen for live-cell imaging studies grew, germinated and fused at wild-type rates, were healthy and conidiated normally at 25˚C and 35˚C, and possessed colony morphologies similar to wild-type (Figure 3.1 and Table 3.1). Lifeact-tagRFP-T gave a pattern of actin localisation identical to Lifeact-GFP and was of comparable brightness and photostability. Henceforth, I refer to Lifeact-GFP or Lifeact-tagRFP-T interchangeably as Lifeact-FP. To image Lifeact-FP, I used widefield fluorescence microscopy combined with image deconvolution. Lifeact-FP gave robust labelling of actin patches, cables and rings (Figure 3.2) and displayed a localisation pattern of F-actin consistent with previous studies in *N. crassa* using immunofluorescent labelling (Barja et al., 1993; Heath et al., 2000). Latrunculin A treatment, which disrupts the actin cytoskeleton, confirmed F-actin labelling (see below).

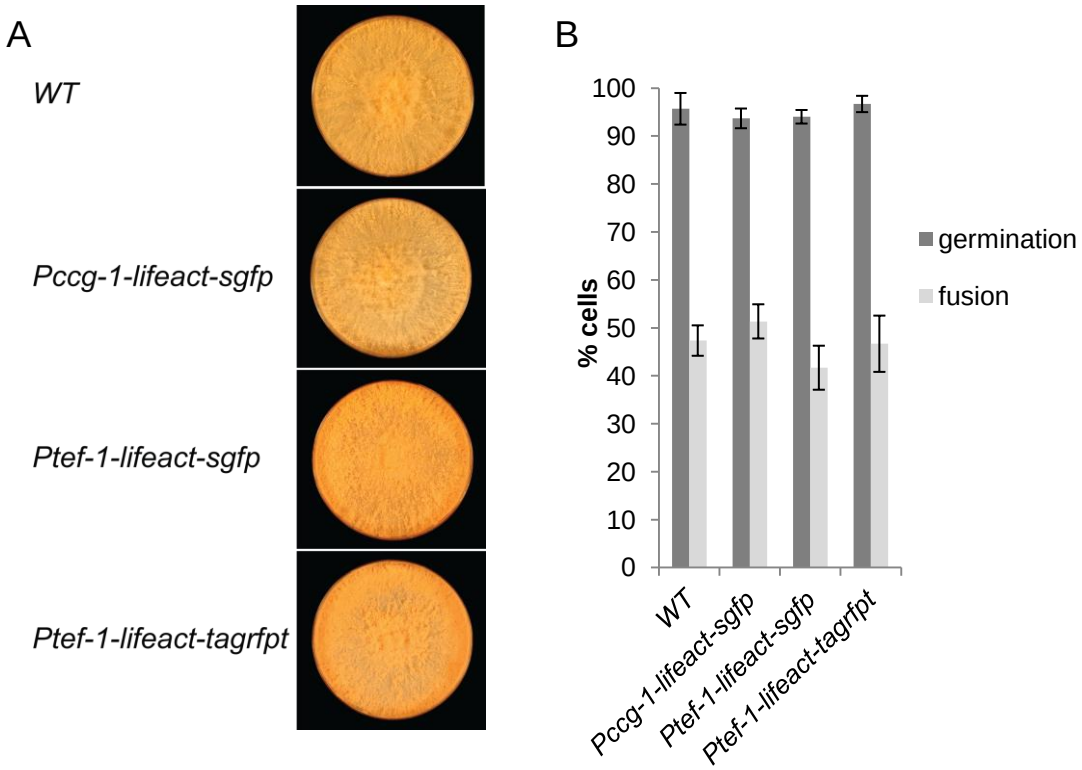

Figure 3.1. Expression of Lifeact-GFP or Lifeact-tagRFP-T does not affect growth or development in *N crassa*. (A) Colony morphologies of Lifeact-FP transformants in comparison to wild-type. Strains were inoculated onto solid VMM, incubated for four days at 24°C then photographed. All strains displayed wild-type colony morphologies. (B) Quantification of germination and cell fusion rates of transformants after 5 h incubation in liquid VMM at 35°C. For each strain, germination and cell fusion rates was assessed (*n* = 300 cells). Germination was scored as the number of conidia with any protrusion emerging from the spore body and cell fusion was scored as the number of cells that had fused with another cell. Differences in the assed parameters between transformant strains and wild-type were statistically not significant (all p > 0.1). The error bars indicate standard deviations.

Table 3.1 Radial extension of *N. crassa* strains

Strain	**Extension rate ± Stdev (mm/hour)***
WT	2.1±0.2
Pccg-1-lifeact-sgfp	2.1±0.1
Ptef-1-lifeact-sgfp	2.2±0.3
Ptef-1-lifeact-tagrfpt	2.3±0.2

*The radial extension of mycelia was assessed after 8 h growth on VMM plates at 35°C. Colony extension was measured along four randomly chosen radii on duplicate plates; *n* = 8 for each.

3.1.2 F-actin localises in complex arrays during the establishment and maintenance of polarised growth

Three distinct phases are associated with conidial germination leading to germ tube formation: (1) hydration and isotropic growth, (2) germ tube emergence, and (3) germ tube extension (Araujo-Palomares et al., 2007; Harris et al., 2005). During isotropic growth, actin cables were unpolarised and mostly associated with the cell cortex (Figure 3.2A and B). Similarly, actin patches were found at the cell periphery but showed no accumulation at particular sites in ungerminated conidia. Prior to germ tube emergence, I observed a strong accumulation of fluorescence that formed a polar cap marking the site of germination (Figure 3.2C). Individual cables in this highly dynamic array of F-actin were generally not orientated along the future longitudinal axis but rather followed the curvature of the polarising cell (Figure 3.2C and D). In some instances this cap disappeared and reformed at a different site on the cell cortex, suggesting that the axis of polarity had not been stably established.

In growing germ tubes, actin cables were mostly found at the cell cortex and organised longitudinally throughout the length of the cell, terminating in a dense meshwork-like array at growing tips (Figure 3.2E and F). During conidial anastomosis tube (CAT) - mediated cell fusion, actin cables and patches localised to CAT tips (Figure 3.2G and H). When two CATs were homing towards each other, an equal accumulation of fluorescence in either cell protrusion was typically observed. If only one of the interacting CATs was growing, pronounced actin arrays were only observed in this one.

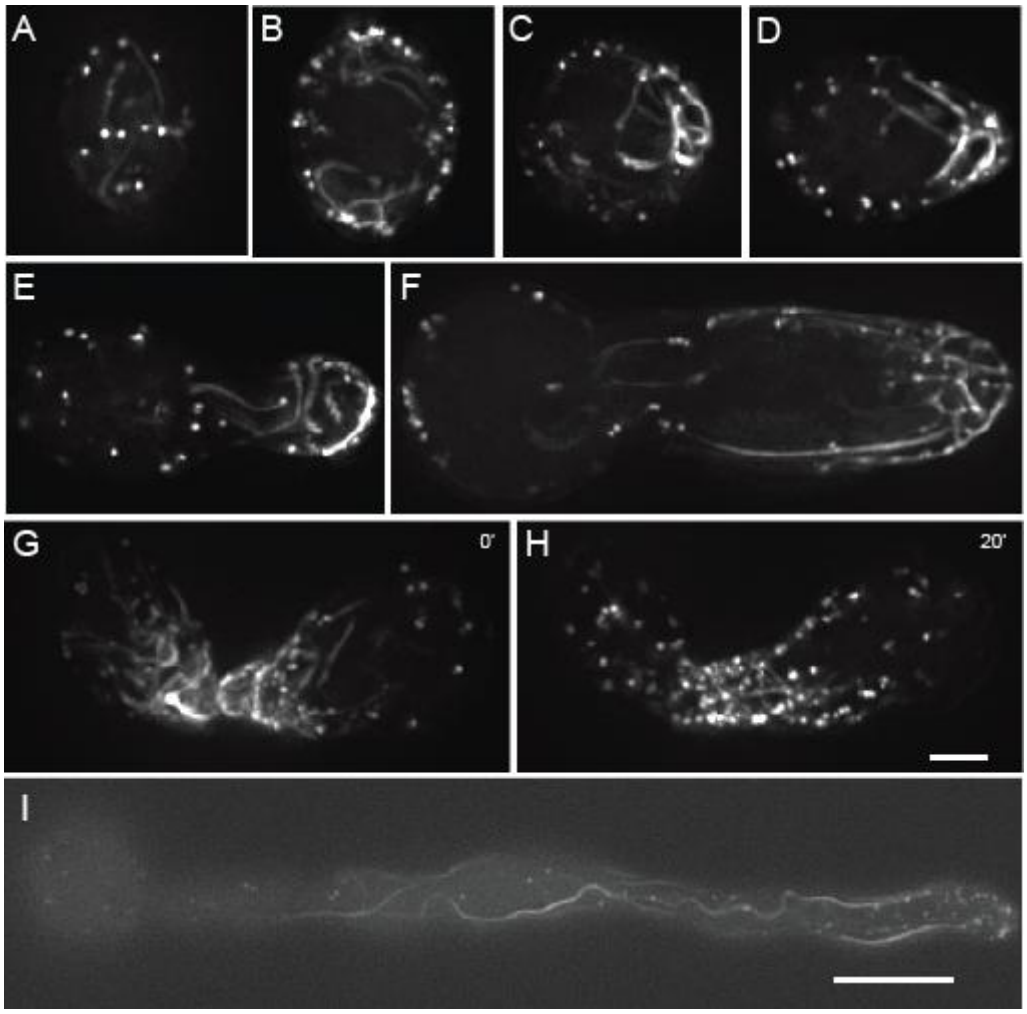

Figure 3.2. Lifeact-GFP localisation during germ tube emergence and CAT-mediated cell fusion. Maximum intensity projections of 5-10 planes of different conidia at various stages of development are shown. Maximum intensity projections of 6 optical planes from the top (A) and middle (B) of an ungerminated spore. Actin patches and cables are mostly associated with the cell cortex. (C, D) A meshwork-like actin array always marks the site of germ tube emergence. (E, F, G) Actin arrays persist at sites of active growth. Maximum intensity projections of a time-lapse sequence showing enrichment of cables and patches at CAT tips before cell fusion (G) and loss of actin cables 20 minutes after fusion (H). (I) Long actin cables extend through germ tubes. The longest actin cable in this germ tube is ~25 µm in length. Images A-H (bar, 2 µm) are displayed at a different scale than image I (bar, 5 µm).

Upon contact, actin cables gradually disappeared from the fusion site (Figure 3.2H), which was coincident with the cessation of polarised tip growth.

Long (5-10 µm) actin cables were commonly observed in germ tubes (Figure 3.2F). Occasionally, cables that spanned the entire length of a 25 µm germ tube were visible (Figure 3.2I). Cortical actin patches were present along the whole length of germ tubes although, as with cables, they were concentrated at sites of active growth. These observations indicate a close association of actin patches and actin cable arrays with active tip growth. I often observed co-localisation of patches and cables at the cell periphery and occasionally observed movement of patches along the length of a cable (see below; Figure 3.5A and B; Supplementary movie 1). The germ tubes analysed in this study had extension rates of 0.05-1.5 µm/min (n = 30).

3.1.3 Latrunculin A causes a rapid loss of Lifeact-FP labelled structures

Although Lifeact-FP localisation observed here was consistent with previous reports of F-actin distribution in yeast and filamentous fungi, I confirmed F-actin specificity of the probe using Latrunculin A. Latrunculins are potent inhibitors of F-actin polymerisation and have been shown to cause rapid disruption of the actin cytoskeleton in fungi spector ref (Ayscough et al., 1997; Barja et al., 1993; Coue et al., 1987; Heath et al., 2000; Knechtle et al., 2006; Pelham and Chang, 2001; Taheri-Talesh et al., 2008; Wu and Pollard, 2005). F-actin dynamics in a growing germ tube was monitored for 10 min before and after the addition of 10 µM Lat A (Figure 3.3A). Treatment with Lat A led to a rapid loss of Lifeact-FP fluorescence associated with patches and cables. This confirmed that Lifeact-FP binds to F-actin in *N. crassa*.

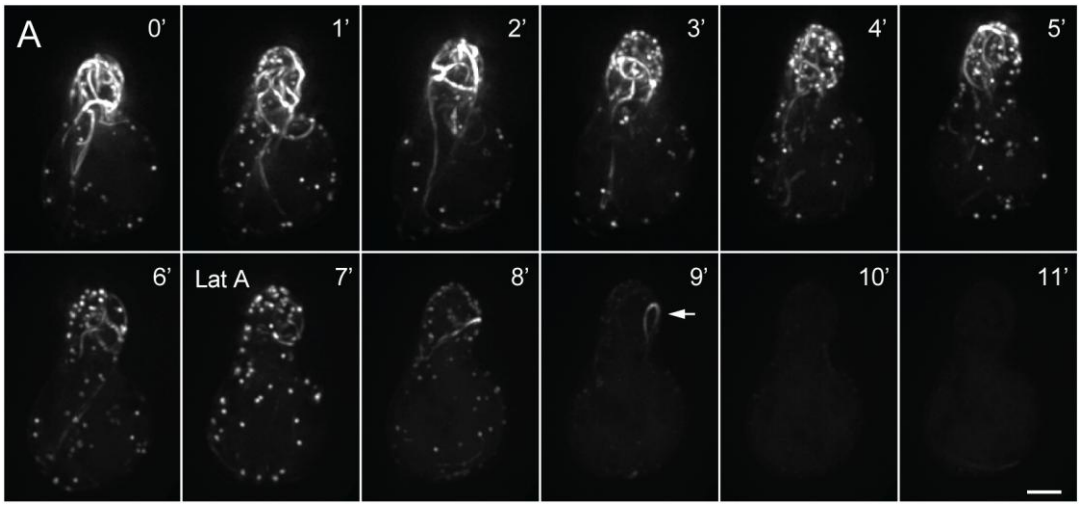

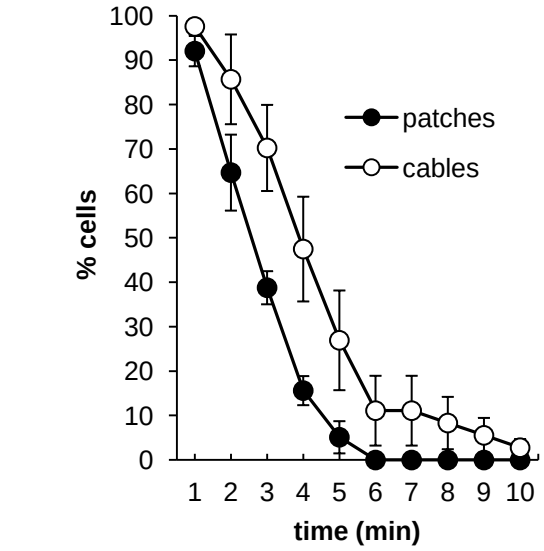

Figure 3.3. Lifeact-GFP localisation is sensitive to Latrunculin A. Growing germ tubes of *N. crassa* were treated with 10 µM Lat A dissolved in DMSO. (A) Maximum intensity projections of a time-lapse sequence of an elongating germ tube before and after Lat A treatment. 11 min of the full 25 min sequence is shown. Lat A was added at the 7 min time point and caused a loss of Lifeact-GFP-labelled structures within 4 min. The arrow at the 9 min time point shows a cable that is not tethered to a particular site. The extension rate in the 10 min before Lat A addition was 0.24 µm/min. Following treatment the extension rate was reduced to 0.005 µm/min. Incubation with an equivalent amount of DMSO (1%) had no effect on Lifeact-GFP localisation (not shown). (B) Percentages of cells containing actin patches and actin cables after treatment with 10 µM Lat A (*n* = 39 cells). Bar, 2 µm. The error bars indicate standard deviations.

Germ tube elongation was abrogated by Lat A emphasising the importance of F-actin for tip growth (Figure 3.3A). Interestingly, upon treatment with Lat A I occasionally observed a sub-population of cables that did not appear to be tethered to a particular site (Figure 3.3A, arrow at 9 min) and displayed random motion. These cables eventually disassembled but their initial insensitivity to Lat A shows that the rate of F-actin depolymerisation varied within the population of cables. Quantification of the presence of patches and cables following Lat A treatment showed that patches are more sensitive to Lat A, with 83% of cells lacking patches after 4 min compared to 52% of cells lacking cables (*n* = 39 germlings; Figure 3.3B). Assuming that Lat A only affects actin polymerisation (Ayscough et al., 1997), this finding also indicates that complete turnover of F-actin in patches and most cables occurs within 4-6 min, with cables generally having a longer half-life.

3.1.4 Retrograde movement of actin arrays accompanies polarised growth

Actin cables have been shown to be highly dynamic structures in budding yeast (Yang and Pon, 2002). In *N. crassa* the actin cytoskeleton was in a constant state of flux with individual actin cables displaying regular bending along their length. I also observed numerous transient cable-cable interactions and the apparent 'exploratory' movement of the untethered ends of individual cables after being detached or severed (Supplementary movie 1).

Another striking aspect of cable dynamics was observed during germ tube emergence and elongation (2-4 h of incubation). Actin arrays were associated with sites of polarised growth in germlings; intriguingly, these arrays were not static but formed within germ tube tips and underwent recurrent retrograde movement back from the elongating tips (Figure 3.4).

This behavior was commonly observed during germ tube elongation but not during tip extension in mature hyphae (see below; Supplementary movies 2, 3, and 4). The whole process of actin array formation, retrograde movement and dissolution generally occurred over a 2-10 min period.

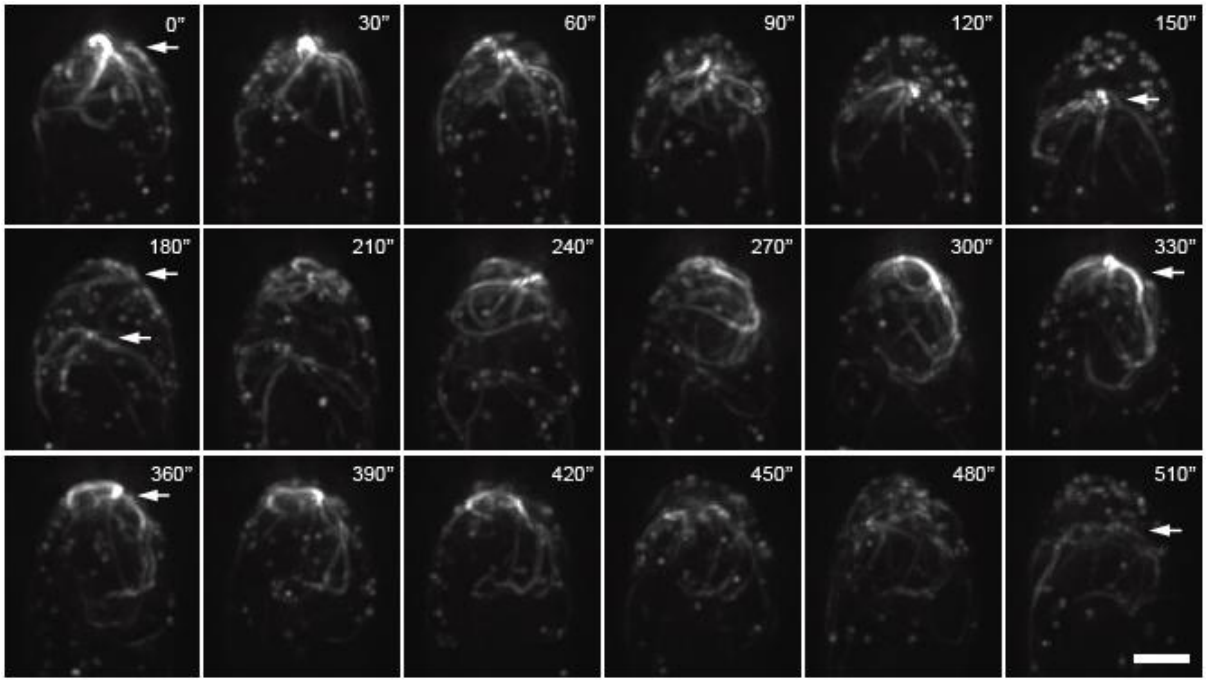

Figure 3.4. Retrograde movement of actin cables accompanied germ tube elongation. Maximum intensity projections of a time-lapse series showing actin cable dynamics. The arrow at the 0 s time point shows an actin array characterised by a bright focal point with cables emanating from it. At the 60 s time point the actin array started to move back, and by 180 s the array was no longer present at the germ tube tip. At the 180 s time point a new actin array (arrow) has begun to form and subsequently undergoes retrograde movement from the tip, as can be seen at the 510 s time point. The extension rate of the germling was 0.18 µm/min. Bar, 2 µm.

Given the dynamic nature of actin cables, I attempted to measure the extension rate of cables from the tips. Yang and Pon (2002) used 'fiduciary' marks on actin cables to assess cable extension rates. I was unable to find similar stable reference points suitable for such analysis, and generally quantitative analysis was hindered by the complicated architecture of actin arrays and their highly irregular movements. However, it was apparent that array formation involved the polymerisation of cables and that cable extension pushed back the array while tip growth was occurring (Supplementary movies 2 and 3).

3.1.5 Actin patches exhibit different types of behavior

Actin patches were visualised throughout the length of germlings but were concentrated at sites of active growth. Due to the rapid movement of actin patches, time-lapse observations of patch dynamics were limited to a single focal plane. Consistent with reports from other fungi (Araujo-Bazan et al., 2008; Huckaba et al., 2004; Pelham and Chang, 2001; Taheri-Talesh et al., 2008; Upadhyay and Shaw, 2008) in *N. crassa* two types of actin patch movement could be distinguished: slow/non-linear and fast/linear (Figure 3.5; Supplementary movie 5). Slow/non-linear patches formed at the plasma membrane and, following a short period of undirected movement, tracked along actin cables and left the plane of focus presumably moving to the interior of the cell (Figure 3.5A). The mean velocity and lifetimes of slow/non-linear patches was determined to be 0.26 ± 0.08 µm/s and 14 s (n = 23, 6 germlings), respectively. In contrast, the mean velocity of fast/linear patches was 1.2 ± 0.21 µm/s (n = 14, 4 germlings). Fast/linear movement of patches was discontinuous and occurred along the length of actin cables, with patches travelling towards and away from the growing tip (Figure 3.5B). In some instances actin patches appeared on the plasma membrane and subsequently underwent directed linear movement along actin cables (Supplementary movie 5).

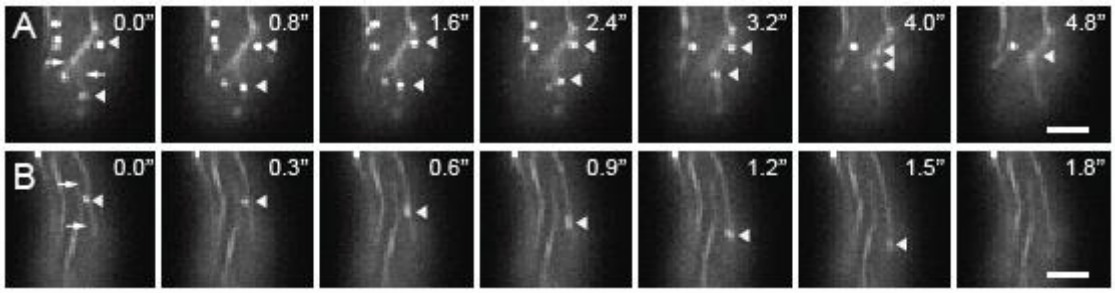

Figure 3.5. Actin patches show a close association with actin cables. Movement of Lifeact-GFP-labelled patches was monitored by time-lapse microscopy in a single focal plane. (A) Patches (arrowheads) formed at the plasma membrane, exhibited a short period of slow/non-linear movement and then tracked along actin cables (arrows) out of the plane of focus. (B) Fast/linear movement of an actin patch (arrowhead) along an actin cable (arrows). Bar, 2 µm.

3.1.6 Actin rings assemble prior to septum formation

The formation and dissipation of actin rings was studied with Lifeact-FP (Figure 3.6). Dual-labelling with Lifeact-GFP and the cell wall stain, calcofluor white, showed that ring formation preceded septum formation and that as the septum matured the actin ring was cleaved into two separate accumulations of F-actin and eventually dissipated (Figure 3.6A). The time duration from initiation to dissipation varied between 30 and 60 min. Formation of these rings occurred by an initially loose accumulation of actin cables in a small area of the hypha, which gradually condensed and shaped into an actin ring. Actin cables did not persist around the newly formed ring but appeared to be incorporated into its structure (Figure 3.6B).

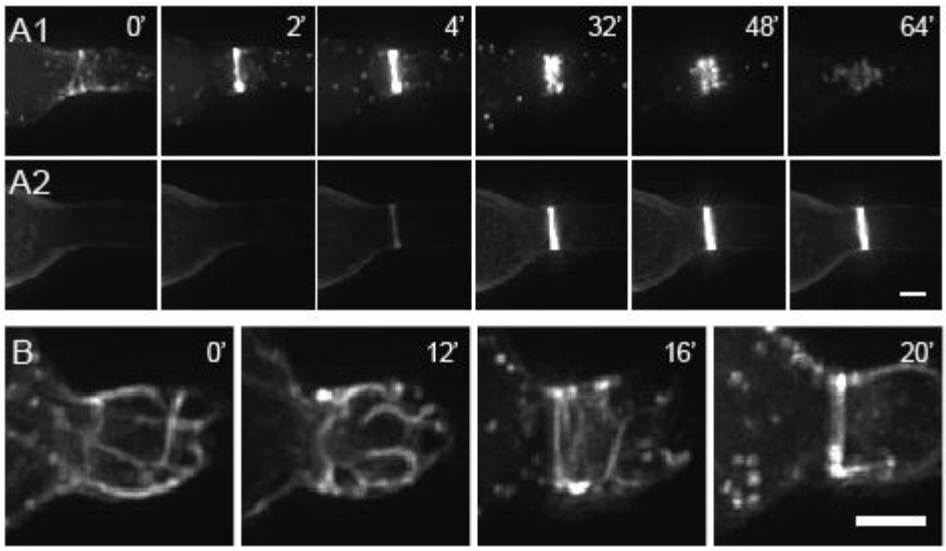

Figure 3.6. Actin cables condense to form actin rings. (A1 and A2) Maximum intensity projection of a time-lapse series showing Lifeact-FP (A1) and calcofluor white (A2) localisation during septation. A septum was formed after the appearance of an actin ring. Ring cleavage is visible at the 48 min time point and F-actin gradually dissipated thereafter. (B) Maximum intensity projections of a time-lapse series showing actin ring formation. A dense network of actin cables is visible around the future site of ring formation between the 0 and 12 min time points. At 16 min, cables gradually condensed into an actin ring which is fully formed 4 min later. Bar, 2 µm.

3.1.8 F-actin localisation in mature hyphae is distinct from germ tubes

Lifeact-FP revealed marked differences in F-actin localisation between the tip regions of mature hyphae and germ tubes. Filamentous fungi show a rapid acceleration in apical extension during the transition from germ tube to mature vegetative hypha. Rates of apical extension in mature hyphae can be up to 10 fold greater than that during initial germ tube emergence (Araujo-Palomares et al., 2007). In mature hyphae, I observed a concentrated spot of F-actin, at the extreme apices of hyphal tips followed by an F-actin-depleted zone and a collar of actin patches 3.51 ± 1.21 µm (n = 15) from the F-actin spot (Figure 3.7).

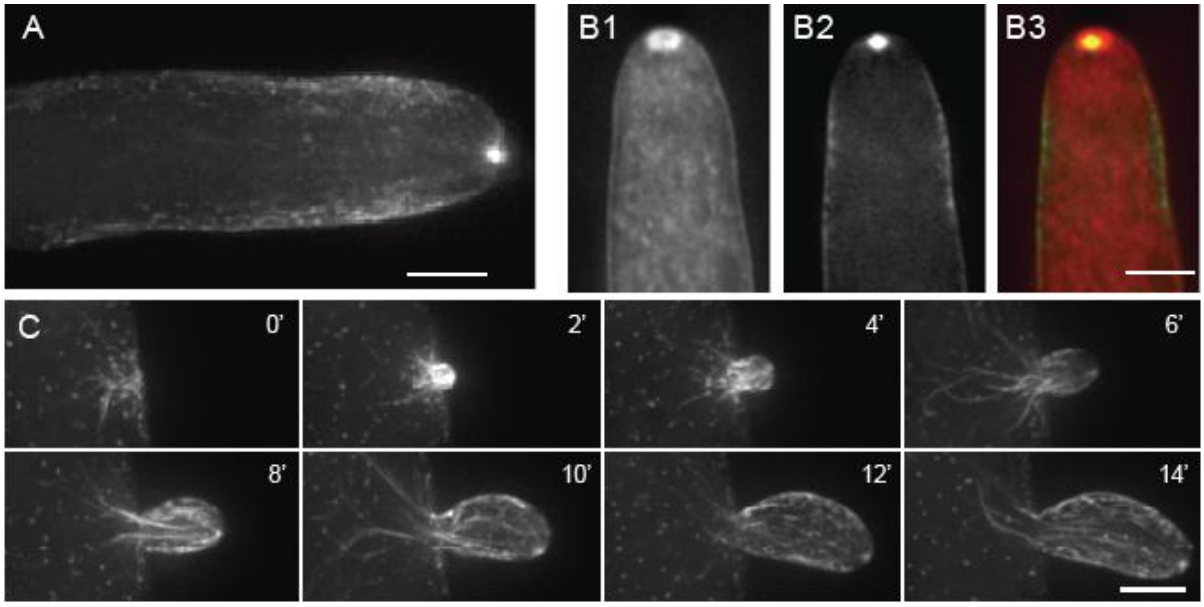

Figure 3.7. Lifeact-GFP localises to the Spk in mature hyphae. (A) Maximum intensity projection of a hyphal tip. F-actin is concentrated in a spot at the tip and patches are localised in a subapical collar around the hypha. (B1, B2, and B3) Lifeact-GFP and FM4-64 co-labelling of a hyphal tip. (B1) FM4-64, (B2) Lifeact-GFP, (B3) merged image of both channels with Lifeact-GFP in green and FM4-64 in red. Lifeact-GFP localises to the core of the Spitzenkörper, and is shown in yellow where it co-localises with FM4-64. (C) Maximum intensity projections of a time-lapse sequence showing branch formation. Actin cables were present during early stages of branch outgrowth but F-actin organisation changed as the new branch developed. Bar, 5 µm.

The F-actin exclusion zone and spot were present in all actively growing mature hyphae that were observed (*n* = 27). The membrane-selective dye FM4-64 was used to determine whether the F-actin spot localised to the Spk. The Spk is readily stained by FM4-64 and localises to the tip region of actively growing mature hyphae but is absent from sites of polarised growth in germlings of *N. crassa* (Araujo-Palomares et al., 2007; Fischer-Parton et al., 2000; Hickey et al., 2002). Lifeact-FP/FM4-64 co-labelling demonstrated that the F-actin spot localised to the core of the Spk indicating that this may be a centre for F-actin organisation (Figure 3.7B).

Notably, actin cables were not visualised in the tip regions of actively growing mature hyphae, although I did observe an accumulation of cables prior to branch formation (Figure

3.7C). Cables were present in the new branch for a short period (< 10 min) after which the F-actin spot and collar of patches developed and the branches had achieved a linear rate of extension. The leading mature hyphae analysed in this study exhibited extension rates of 9.1 - 12.4 µm/min (*n* = 15).

3.1.8 MYO-5 participates in rapid actin patch movement

Actin patches were shown to move rapidly along actin cables, suggesting the involvement of motor proteins, most likely class-V myosins (Berepiki et al., 2010). Only one class-V myosin (NCU01440; termed *myo-5*) has been identified in the genome of *N. crassa* (Borkovich et al., 2004). I hypothesised that if actin patches were translocated along actin cables in a myosin-5-dependent manner, perturbing MYO-5 function by gene deletion or with pharmacological inhibitors would affect rapid actin patch movement. To study the role of the single class-V myosin in rapid actin patch movement, I obtained the Δ*myo-5* mutant from the FGSC. Genotyping of the deletion strain by PCR and Southern analysis confirmed the correct integration of the deletion cassette (Figure 3.8). The Δ*myo-5* null mutant strain grew poorly in a biomass assay in liquid VMM and also displayed defects in colony growth and morphology (Figure 3.9 and Table 3.2).

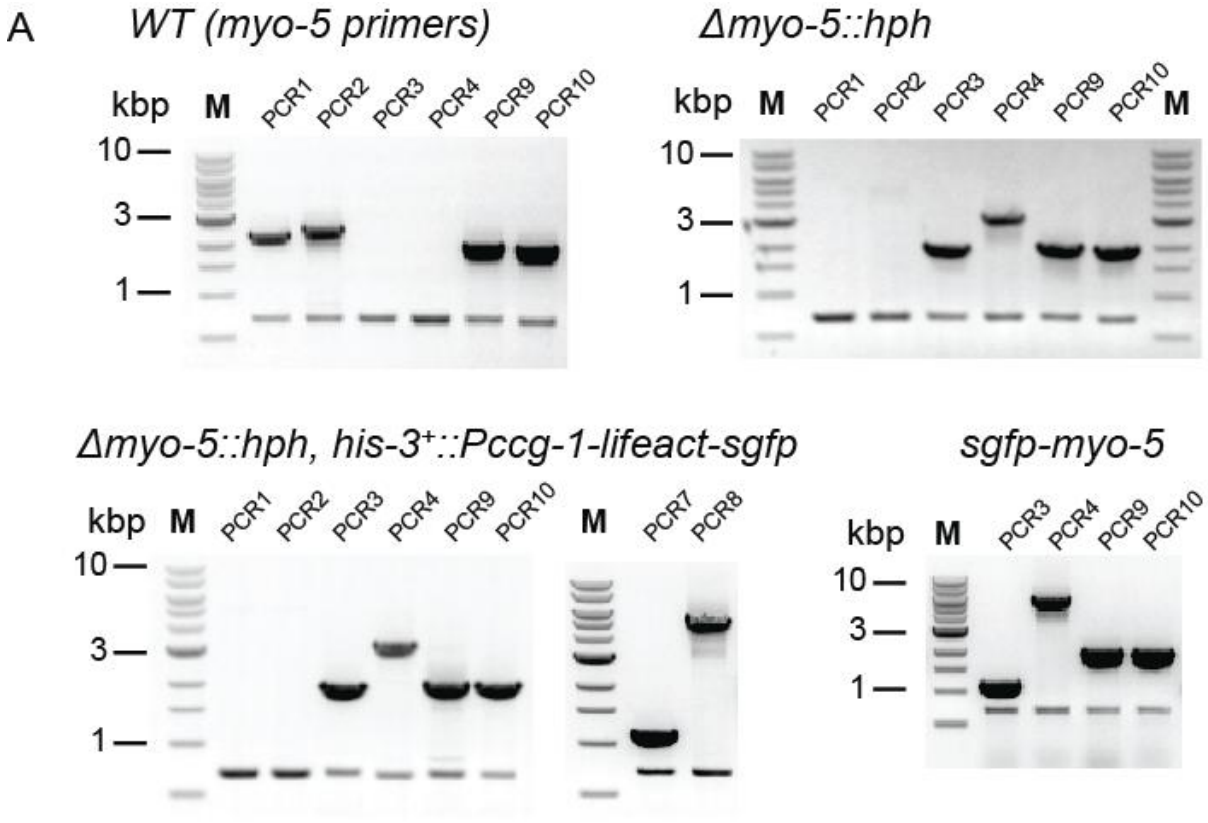

Figure 3.8. Genotyping of *myo-5* null mutants and the *sgfp-myo-5* strain. Primers sets were chosen to confirm the presence of the wild-type gene (primers set G1+G2 = PCR1 and primers set G3+G4 = PCR2), integration of the deletion or epitope cassette (primers set G1 + HPH2 = PCR3, primers set G4 + HPH1 = PCR4, primers set G1 + NAT2 = PCR5, primers set G4 + NAT1 = PCR6), integration of *his-3 Pccg-1-sgfp* overexpression cassette (primers set GFP Fw + His3 Rv = PCR7, primers set GFP Rv + His3 Fw = PCR8) or to check the presence of *mus-51* (primers set MUS-51 Fw + MUS-51 Rv = PCR9) and *mus-52* (MUS-51 Fw + MUS-51 Rv = PCR10). For strains with two integration events two gel pictures are shown – on the left is confirmation of integration of the hygromycin resistance cassette while on the right is shown the absence of the second deleted gene and confirmation of integration of the *his*-3-based cassette. The lower band in the gels is an actin amplicon internal control to confirm the presence of genomic DNA. The positions of DNA size markers (M, in kbp) are shown at the left or right of the panels and the template DNA used for the PCR is in italics above the gel. (A) PCR-based genotyping of wild-type genomic DNA to confirm lack of non-specific primer binding and genotyping PCRs on *myo-5* null mutants and the *sgfp-myo-5* strain. (B) Southern blotting analysis of the *myo-5* null mutant. The positions of DNA size markers (M, in kbp) are shown at the left or right of the panels. Genomic DNA from wild-type and septin deletion strains generated with a hygromycin resistance cassette was probed with *hph*-3'UTR-based probe. Lane 1, WT DNA; Lane 2, *Δmyo-5::hph* DNA. DNA fragments detected in the *myo-5* null mutant (1.5 kbp band) and wild-type (3.4 kbp band) match the predicted fragment sizes (Table 2.1).

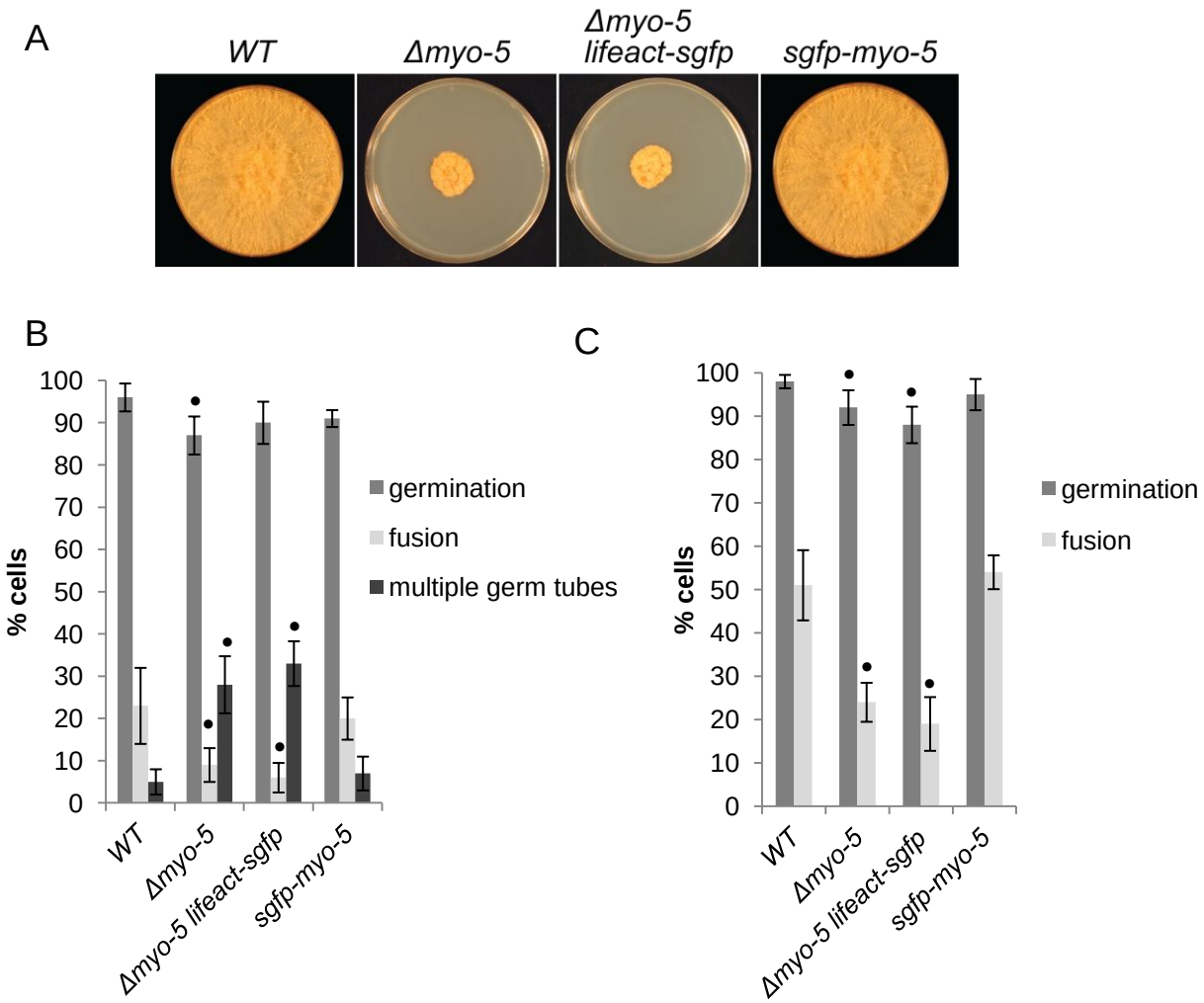

Figure 3.9. Colony morphology, growth, germination and cell fusion is altered in *myo-5* null mutants. (A) Strains were inoculated onto solid VMM, incubated for four days at 24 °C then photographed. The *myo-5* deletion strains displayed gross defects in colony morphology and did not produce as many aerial hyphae as wild-type. (B, C) Strains were incubated in liquid VMM for 3 h (B) or 5 h (C) then counted for germination, cell fusion and the number of cells with more than two germ tubes (*n* = 300). Germination was scored as the number of conidia with any protrusion emerging from the spore body and cell fusion was scored as the number of cells that had fused with another cell. A black dot above bars indicate a significant difference (p = <0.05) compared to the wild-type control. The error bars indicate standard deviations.

Table 3.2. Dry weight biomass in mg/ml of *N. crassa* strains after 24, 48, and 72h of growth in liquid VMM at 30 °C.

Strain	24h	48h	72h
WT	1.6	3.4	5.2
Δmyo-5	0.9	2.0	2.3
Δmyo-5 lifeact-sgfp	0.7	2.2	2.5
sgfp-myo-5	1.9	3.2	5.4

The phenotype of the Δ*myo*-5 strain was analysed with light microscopy. In the absence of *myo-5*, a significant percentage of cells (28%; p = <0.05) produce multiple germ tubes (Figure 3.9B) compared to the wild-type (5%). In addition, the germ tubes produced by Δ*myo*-5 were swollen and misshapen (Figure 3.10), suggesting that MYO-5 participates in cell polarity. The germination rate and the number of cell fusion events of the Δ*myo-5* null mutant were determined and compared to the wild-type (Figure 3.9B and C). Germination rates were slightly reduced when *myo-5* was deleted whereas cell fusion was significantly reduced (p = <0.05). The number of cell fusion events for the Δ*myo-5* null mutant (24%) was significantly lower (p = <0.05) than in the wild-type (51%), implying that MYO-5 plays a role in cell fusion.

To study the involvement of MYO-5 in rapid actin patch movement the Δ*myo-5* null mutant was crossed with a Lifeact-GFP-expressing strain (strain *Pccg-1-lifeact-sgfp*) (Berepiki et al., 2010; Riedl et al., 2008). The progeny of this cross, strain Δ*myo*-5, *lifeact-sgfp* had a phenotype indistinguishable from the Δ*myo-5* parent and expressed Lifeact-GFP. Genotyping of Δ*myo*-5, *lifeact-sgfp* by PCR confirmed the absence of *myo*-5 (Figure 3.8).

The formation of actin patches and rings was unaffected in the absence of *myo-5*; however, actin cables were concentrated at hyphal tips in a dense crescent and did not extend throughout the cell, while there appeared to be a reduction in the number of rapid linear movements by actin patches. The control Lifeact-GFP strain *Pccg-1-lifeact-sgfp* showed normal actin localisation; actin cables extended throughout the cell and rapid actin patch movement was commonly observed (Figure 3.11). I quantified the number of rapid actin patch movements in the Δ*myo*-5 mutant in 20 second time courses. The number of rapid actin patch movements was reduced by 41% in the Δ*myo*-5 mutant compared to the control, implying that MYO-5 participates in the translocation of actin patches but is not wholly responsible for their transport.

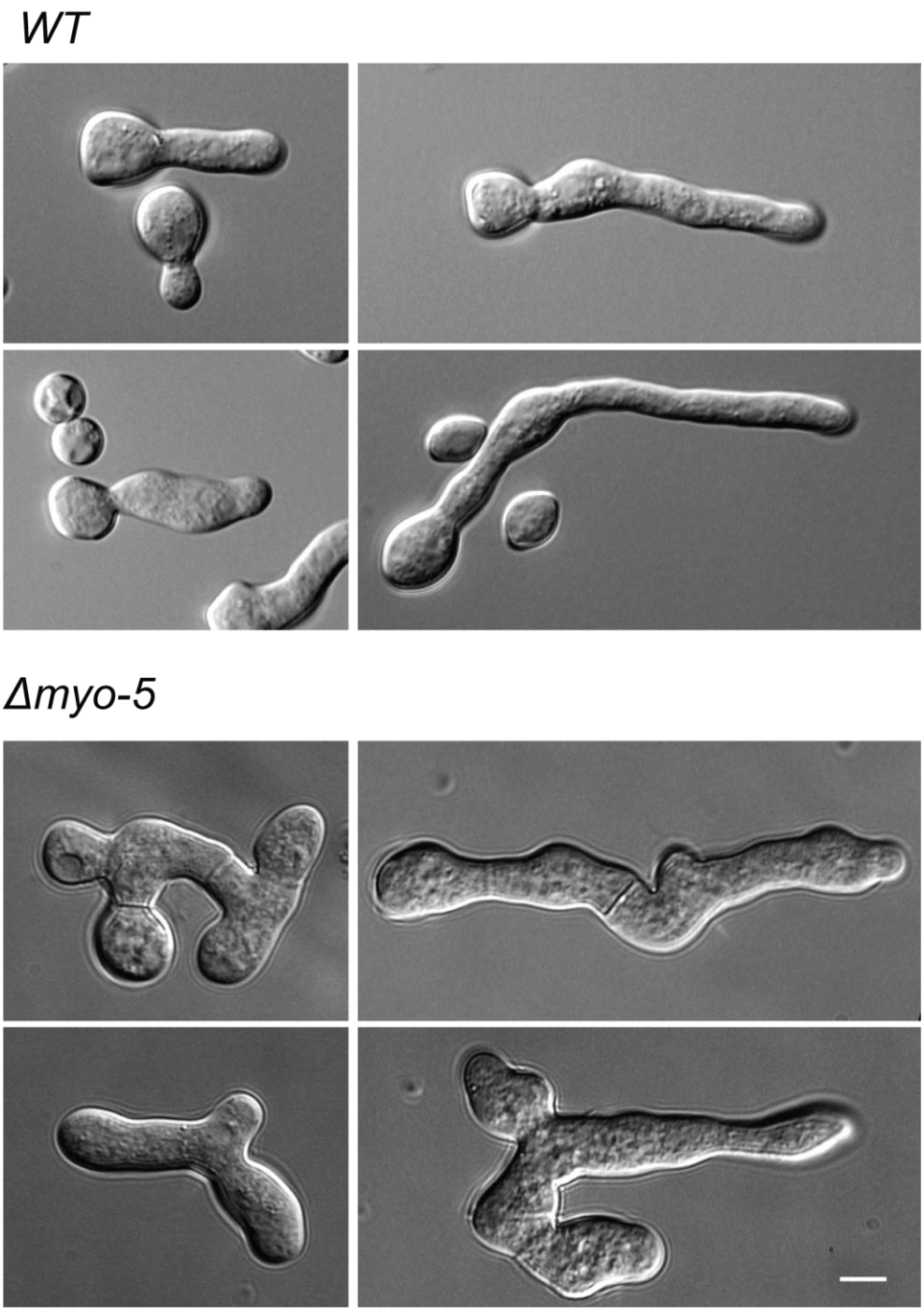

Figure 3.10. The *myo-5* deletion strain displays altered cell morphology. Wild-type and the *myo-5* null mutant were incubated in liquid VMM for up to 5 h then imaged by DIC microscopy to obtain representative images of germination and development. The *myo-5* null mutant displayed gross polarity defects and germ tubes often appeared swollen and misshapen. Bar, 5 µm.

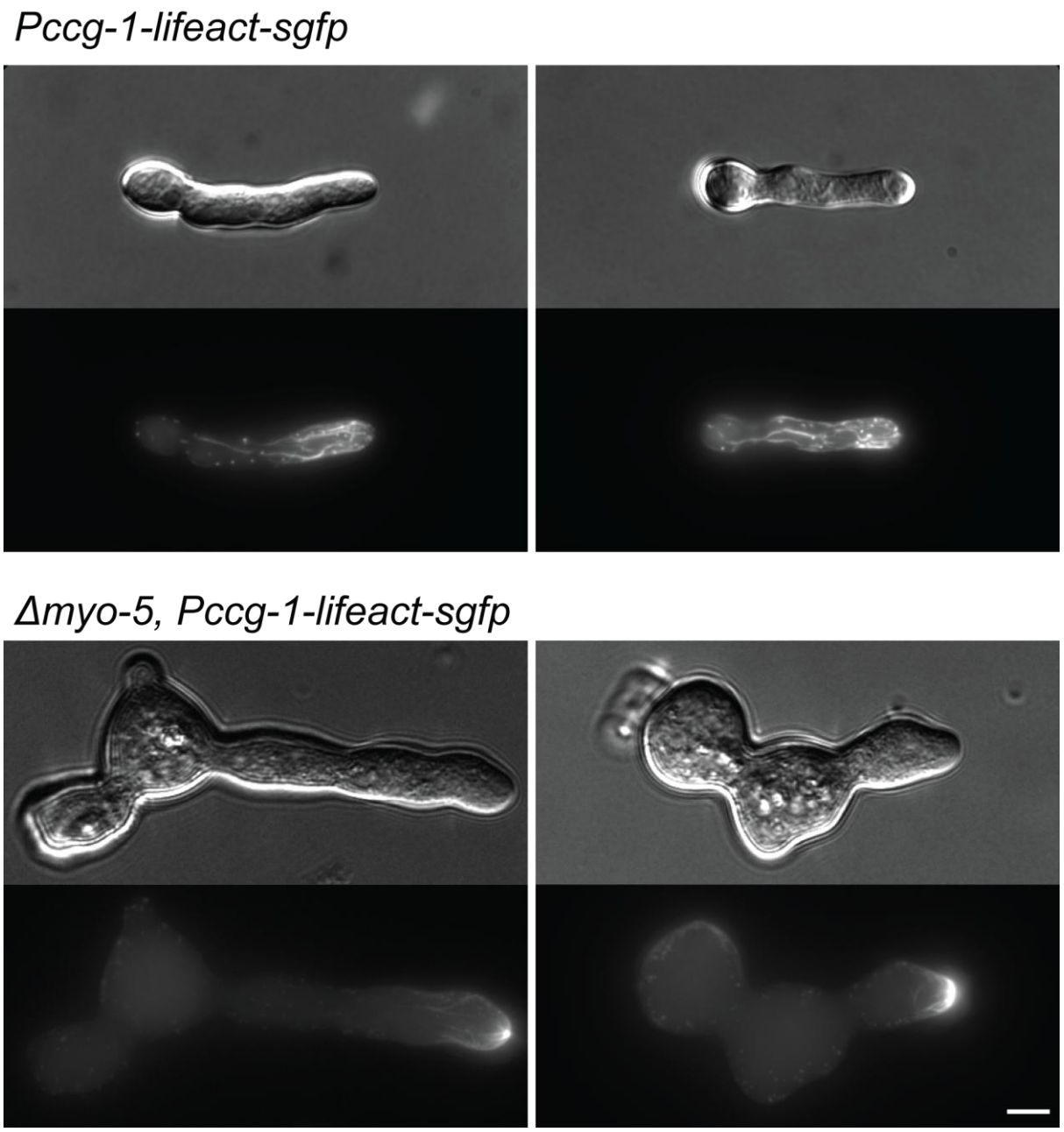

Figure 3.11. F-actin organisation is altered in the absence of *myo-5*. Lifeact-GFP-expressing wild-type and *Δmyo-5* strains were incubated in liquid VMM for 3 h then imaged with fluorescence and DIC microscopy. In the wild-type actin cables extend throughout the length of the cell but are concentrated at the tips of germ tubes in *Δmyo-5* mutants. Bar, 5 µm.

The role of MYO-5 in rapid actin patch movement was assessed by treating the Lifeact-GFP expressing strain *Pccg-1-lifeact-sgfp* with two pharmacological agents: carbonyl cyanide *m*-chlorophenylhydrazone (CCCP; depletes ATP) and 2,3-butanedione monoxime (BDM; a myosin inhibitor). To quantify the results, the number of rapid actin patch movements was counted in 20 second time courses, made 30 minutes after the addition of CCCP, BDM or DMSO (control). Treatment with both CCCP and BDM resulted in a reduction of F-actin cables but other F-actin structures were unperturbed, similar to the effects of *myo-5* deletion (Figure 3.12). CCCP treatment caused a 50% decrease in the frequency of rapid actin patch movements, while treatment with BDM did not have any detectable effect on patch movement. These data, and the reduction in frequency of rapid patch movement when *myo-5* was deleted, suggests that MYO-5 contributes to rapid translocation of actin patches.

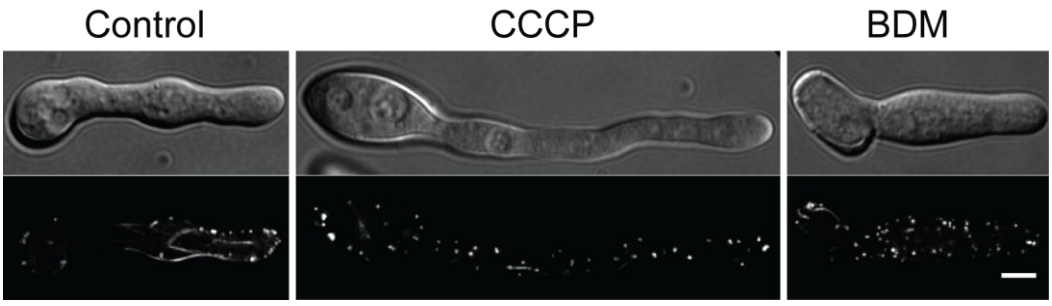

Figure 3.12. Treatment with CCCP and BDM perturbs F-actin organisation. Cells expressing Lifeact-GFP were incubated in liquid VMM for 3 h then treated with 100 µM CCCP, 10 mM BDM, or 0.1% DMSO (control) and imaged 30 mins later. Treatment with both CCCP and BDM resulted in a reduction of actin cables but other F-actin structures were unaffected. Bar, 2 µm.

3.1.9 MYO-5 localises at the hyphal tip in an actin-dependent manner

To visualise MYO-5, strain *Pccg-1-sgfp-myo-5* was created in which a GFP-MYO-5 fusion construct was expressed under the control of the *ccg-1* promoter. However, no clear GFP localisation was observed and the signal to noise ratio was very low. Therefore, a new strain was constructed in which the GFP was integrated at the 5' end of the *myo-5* gene to be expressed under control of the native *myo-5* promoter. This strain, *sgfp-myo-5*, displayed a clear GFP-MYO-5 signal, normal morphology and had germination and fusion rates similar to wild-type (Figure 3.9).

GFP-MYO-5 localised as a small crescent or spot at the tips of germ tubes and CATs (Figure 3.13). During cell fusion GFP-MYO-5 remained at CAT tips and was gradually lost after cell fusion (Figure 3.13D and E). Therefore, GFP-MYO-5 shows close association with sites of active growth. The tip of the fungal hyphae is the site of exocytosis and deposition of new cell wall (Bartnicki-Garcia et al., 2000; Taheri-Talesh et al., 2008) which suggests that MYO-5 participates in these processes. We were also able to observe the movement of GFP-MYO-5 particles throughout the length of germ tubes. These particles moved predominately towards the tip, seemingly along underlying linear tracks (Supplementary movie 6). The velocities of these particles were determined to be 0.34 ± 0.07 µm/s (n = 26, 9 germlings). We attempted to create a dual-labelled GFP-MYO-5 and Lifeact-tagRFP-T strain, however, the resulting transformants exhibited a gross perturbation of cell morphology, inadequate co-expression, and mislocalisation of one or both fusion constructs. The velocity of GFP-MYO-5 particles, 0.34 µm/s, was markedly lower than that observed for rapid actin patches, 1.2 µm/s, however this does not rule out the involvement of MYO-5 in rapid patch movement; it is possible that the observed GFP-MYO-5 particles only represent a subset of MYO-5 motors which could be associated with cargoes other than actin patches.

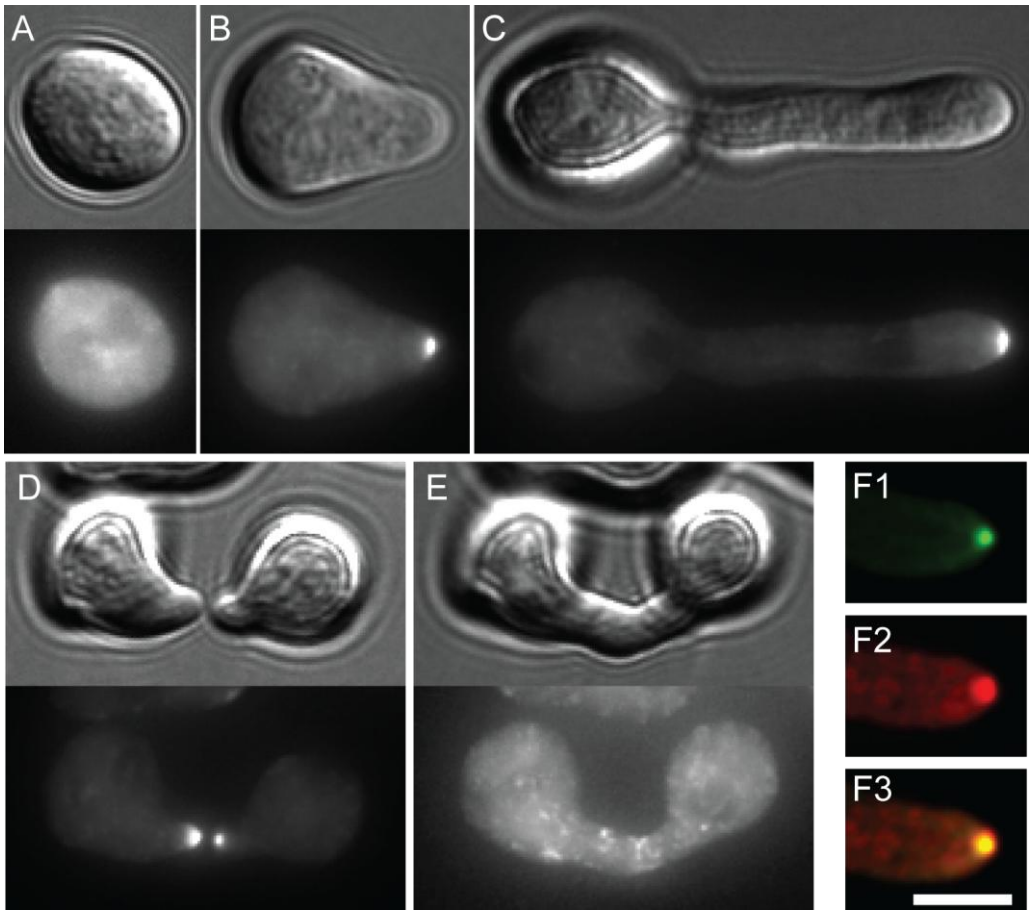

Figure 3.13. GFP-MYO-5 localises at germ tube tips and colocalises with the Spk in mature hyphae. The *sgfp-myo-5* strain was incubated in liquid VMM for 3 h or overnight to obtain representative images of germination or mature hyphae, respectively, then imaged with fluorescence and DIC microscopy. (A, B, C) At germ tube tips GFP-MYO-5 localised as a spot/crescent. (D, E) During CAT-mediated cell fusion GFP-MYO-5 localised to the tips of CATs (D) and following cell fusion was lost from the fusion site (E). (F) At the tips of mature hyphae GFP-MYO-5 (F1) colocalised with the Spk (F2), stained with FM4-64. (F3) Merged image of F1 and F2. Bar, 5 µm.

To determine if GFP-MYO-5 particles are indeed associated with actin patches, I attempted to generate a strain co-expressing GFP-MYO-5 and Lifeact-tagRFP-T. To visualise the localisation of both actin and myosin-5 in *N. crassa*, *sgfp-myo-5* was transformed with a Lifeact-tagRFP-T construct, pAL5 (Lichius and Read, 2010). However, the resulting strain *sgfp-myo-5*, *lifeact-rfp* displayed a gross perturbation of cell morphology, inadequate co-expression, and mislocalisation artefacts, which precluded its use for further analysis.

In mature hyphae of *N. crassa*, GFP-MYO-5 localised as a spot at the tip of hyphae and colocalised with FM4-64 at the Spk (Figure 3.13F). The Spk is a complex, multicomponent structure dominated by vesicles and in close proximity to the apical plasma membrane of mature hyphae (Verdin et al., 2009) and the presence of MYO-5 in this structure suggests that this motor may be responsible for transporting vesicles to the Spk. Occasionally, GFP-MYO-5 was associated with septa (Figure 3.14) where, conceivably, it may participate in septum formation.

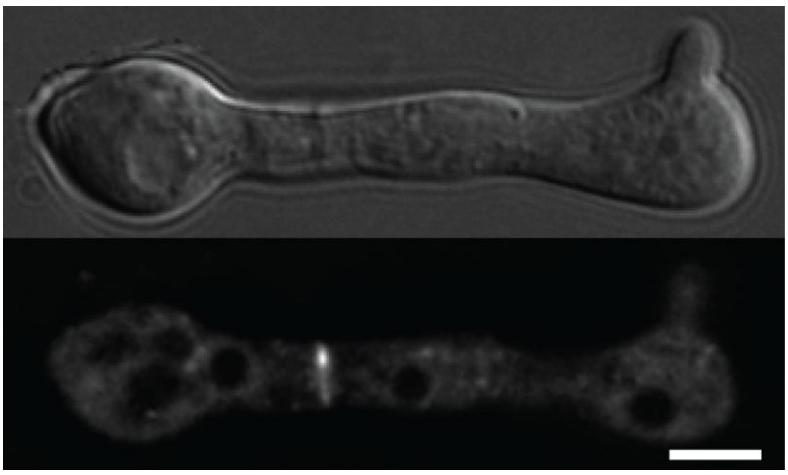

Figure 3.14. GFP-MYO-5 occasionally localises at septa. The *sgfp-myo-5* strain was incubated in liquid VMM for 3 h then imaged with fluorescence and DIC microscopy. Bar, 5 µm.

The *sgfp-myo-5* strain was treated with a range of pharmacological inhibitors to better understand how MYO-5 is organised. Four inhibitors were used: Benomyl, which disrupts microtubules; Lat A, which inhibits actin polymerisation; CCCP, which depletes ATP; and BDM, which is a broad-range myosin inhibitor. Figure 3.15 shows the result of the treatments and quantitative analysis of the effects. Incubation of *sgfp-myo-5* germlings with CCCP or BDM resulted in a loss of tip-associated GFP-MYO-5, but a GFP-MYO-5 signal could still be seen as motile cytoplasmic dots with a tip-high gradient or in some cases fluorescence was entirely dispersed in the cytoplasm, demonstrating that ATP and myosin activity are required for localisation of the fusion protein (Figure 3.15). Following treatment with Lat A the GFP-MYO-5 signal was entirely cytoplasmic, showing that an intact actin cytoskeleton is needed for MYO-5 localisation at hyphal tips (Figure 3.15). Treatment with benomyl caused a loss of most tip-associated MYO-5 and resulted in a dispersed gradient of the fusion protein suggesting that microtubules contribute to MYO-5 transport (Figure 3.15).

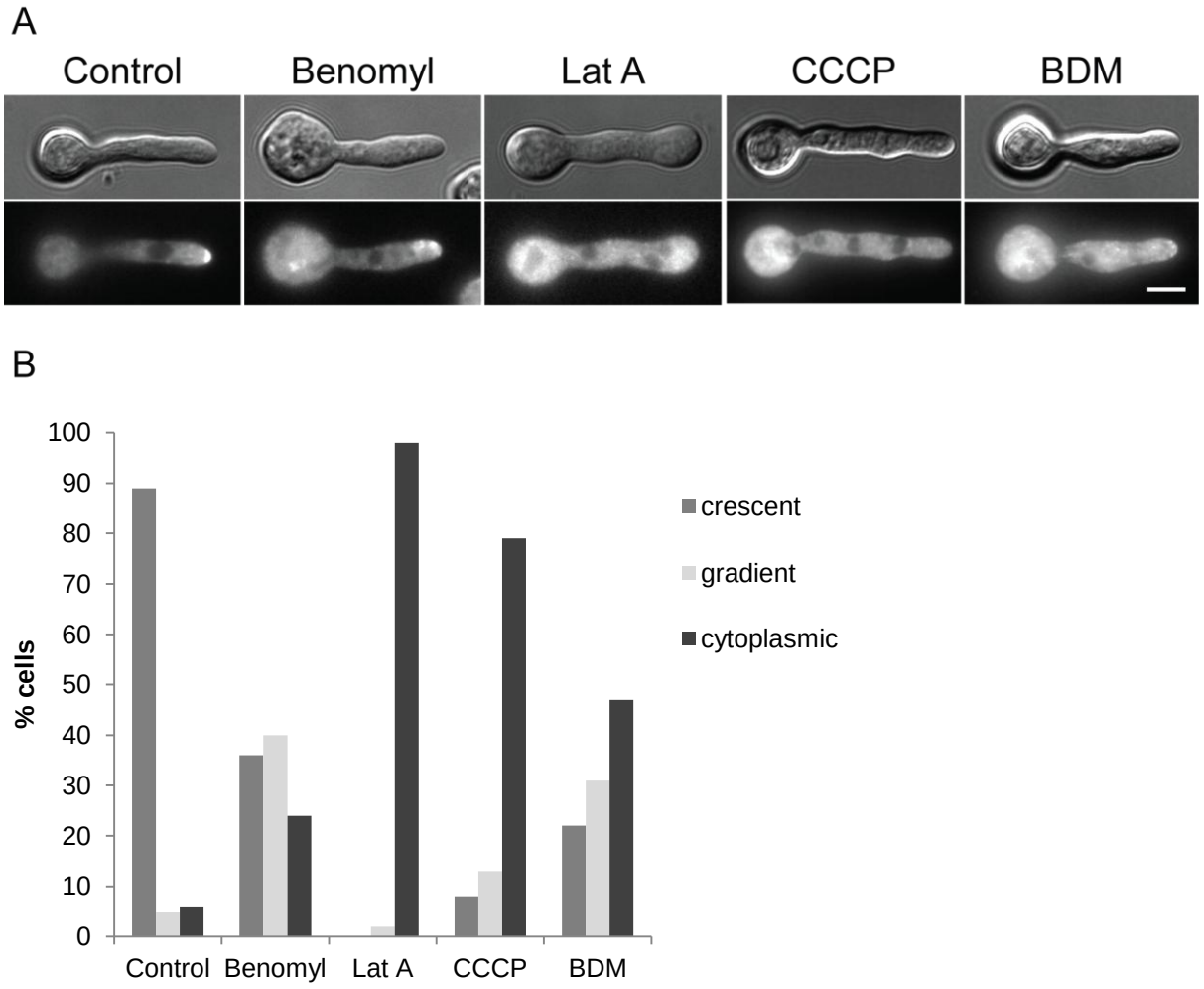

Figure 3.15. GFP-MYO-5 localisation is dependent on actin and myosin activity. Cells expressing GFP-MYO-5 were incubated in liquid VMM for 3 h then treated with 3 µg/ml Benomyl, 10 µM Lat A, 100 µM CCCP, 10 mM BDM, or 0.1% DMSO (control) and imaged 30 mins later. (A) Representative images of treated cells. (B) Graph indicating the percentage of cells with altered GFP-MYO-5 localisation (*n* = 50). Bar, 5 µm.

3.2 Discussion

Considerable effort has been expended in attempts to visualise F-actin distribution and dynamics in living fungal cells and have mostly relied on fusions between FPs and actin or ABPs (Doyle and Botstein, 1996; Waddle et al., 1996; Yang and Pon, 2002). The use of FP-actin fusions as reporters for F-actin is problematic as only a fraction of actin is present in microfilaments resulting in a low signal-to-noise ratio, and, more importantly, the relatively large FP moiety has been shown to perturb actin dynamics in a variety of cell types (Aizawa et al., 1997; Riedl et al., 2008; Yang and Pon, 2002). Thus, FP-actin fusion constructs are likely to alter actin dynamics in filamentous fungi. Fluorescent protein tagging of ABPs is preferable as there is generally less perturbation of actin dynamics *in vivo* but this approach may only reveal a small population of F-actin and the fusion protein may compete with unlabelled endogenous ABPs (Washington and Knecht, 2008; Wu and Pollard, 2005). Therefore, the Lifeact peptide was utilised as a reporter for F-actin in *N. crassa*, which has been shown to provide clear labelling of F-actin in various cell types without interfering with actin dynamics (Era et al., 2009; Riedl et al., 2008; Riedl et al., 2010; Ueda et al., 2009; Vidali et al., 2009). Expression of Lifeact-FP from the *ccg-1* or *tef*-1 promoter had no noticeable effect on radial extension rates, cell morphology, germination or cell fusion rates, colony development or conidiation. The pattern of actin localisation revealed by Lifeact-FP was consistent with previous reports in filamentous fungi using immunofluorescence, phalloidin staining, and FP-based live-cell imaging (Barja et al., 1991; Heath et al., 2000; Virag and Griffiths, 2004), and allowed visualisation of F-actin reorganisation and polarisation in *N. crassa*.

I confirmed the specificity of Lifeact-FP for F-actin with the drug Latrunculin A, which prevents F-actin polymerisation (Ayscough et al., 1997). Treatment with 10 µM Lat A led to a rapid loss of Lifeact-FP-labelled patches and cables demonstrating a high rate of F-actin turnover in *N. crassa*. Interestingly, although all cables disassembled within 10 min of Lat A

treatment, some cables appeared to be initially insensitive to Lat A implying that different subpopulations of actin cables with different turnover rates exist in *N. crassa*.

In budding yeast, actin cables form tracks for myosin-V-dependent transport of secretory vesicles, whereas actin patches are involved in endocytosis and membrane invagination (Moseley and Goode, 2006). Both patches and cables localise to new buds in *S. cerevisiae* but only actin cables are required for polarised secretion (Huckaba et al., 2004; Pruyne et al., 1998; Yang and Pon, 2002). The localisation of actin patches and cables to the tips of germ tubes and CATs in *N. crassa* suggests active exo- and endocytosis in these regions and indicates a tight coupling of these two processes at this stage of development. Accumulation of actin cables and patches at sites of active growth in *N. crassa* confirms that polarisation of the actin cytoskeleton underlies apical extension.

Interestingly, the marked differences observed in F-actin architecture in tip growing regions suggests that the spatial organisation of exo- and endocytosis changes during development. A bright focal point of F-actin, colocalising with the core region of the Spk, and an F-actin-depleted zone followed by a collar of actin patches were present in the tips of mature hyphae compared to the actin arrays and concentration of patches at the extreme apex of germ tubes. The F-actin spot represents formin-mediated actin nucleation, presumably creating tracks for exocytic vesicles; the formin BNI-1 is found as a spot at hyphal tips of *N. crassa* that co-localises with the Spk (Lichius et al., 2012). In contrast, subapical collars of actin patches are known to be involved in endocytosis in filamentous fungi (Araujo-Bazan et al., 2008; Upadhyay and Shaw, 2008). Thus it seems the sites of exo- and endocytosis are well separated in mature hyphae while they have tight association in germlings. Extension rates in mature hyphae are 10-fold more rapid than germlings (Araujo-Palomares et al., 2007) and the spatial segregation of endocytosis and exocytosis indicates that reorganisation of the secretory machinery underlies rapid extension, as has been reported in *A. gossypii* (Koehli et al., 2008).

Consistent with models of actin cable-mediated transport of secretory vesicles in budding yeast (Moseley and Goode, 2006), in *N. crassa* we found that dense arrays of actin cables were present at sites of germ tube emergence and branch formation. Interestingly, cable arrays persisted at the tips of elongating germ tubes and CATs whereas during branch formation and outgrowth in the mature colony cables were gradually lost from the tip to be replaced by an F-actin spot and collar of patches. Lifeact-FP allowed us to monitor the formation of these complex arrays of actin cables during germ tube elongation and observe their subsequent retrograde movement. This phenomenon was recurrent and was commonly observed during the initial stages of germ tube emergence and elongation but was not observed during branch formation or tip extension in the mature colony. The formation of actin arrays probably represents *de novo* assembly of cables at the tip, eventually leading to backflow of cable arrays. It was possible to observe the movement of a relatively intact array along the length of a germ tube and monitor its eventual dissolution. It is likely that the disassembly of actin arrays is necessary for reincorporation of resulting actin subunits into new cables at sites of active growth.

The importance of actin cables for polarised growth is also highlighted by cable localisation during and after CAT-mediated cell fusion; dense actin arrays were shown to assemble at the cell cortex prior to CAT formation and intensify during CAT extension and homing. Shortly after cell fusion, actin cables gradually disappeared from the fusion site while patches persisted. It has been proposed that the polarised secretion of biosynthetic materials is compensated by endocytosis, maintaining the polarised state of cortical markers and receptors (Altschuler et al., 2007; Steinberg, 2007b; Upadhyay and Shaw, 2008). Given the role of actin patches in endocytosis, it is possible that the accumulation of actin patches at the tips of homing CATs and their persistence shortly after fusion facilitates the recycling of membrane receptors and polarity factors no longer required at this site.

Furthermore, Lifeact-FP also showed that actin cables are not always associated with tip growth, but have an additional role in septum formation. The formins, SepA and BNI-1 are required for actin ring formation and septation in *A. nidulans* and *N. crassa*, respectively (Justa-Schuch et al., 2010; Lichius et al., 2012; Sharpless and Harris, 2002). Interestingly, in *N. crassa*, actin rings were formed by the gradual accumulation of pre-existing actin cables and their concentration into a ring rather than by *de novo* assembly of F-actin into a ring. This suggests that ring formation involves both formin-mediated cable production and regulation of the spatial organisation of actin cables post-production.

Three dimensional reconstruction and time-lapse microscopy demonstrated a close association of patches and cables (Figure 3.2 and 3.5). Generally we observed two types of patch behavior: slow/non-linear and fast/linear movement. Patch formation occurred at the cell cortex and was followed by a short period of undirected movement, then patches traveled out of the plane of focus presumably towards the interior of the cell. The measured velocities and lifetimes of slow/non-linear patches, 0.26 µm/s and 14 s, respectively, were similar to values obtained for endocytic patches of *A. nidulans* (velocity: 0.19 µm/s; lifetime: 24 s) (Upadhyay and Shaw, 2008), *Schizosaccharomyces pombe* (velocity: 0.31 µm/s; lifetime: not determined) (Pelham and Chang, 2001; Sirotkin et al., 2010), and *S. cerevisiae* (velocity: 0.1 – 0.5 µm/s; lifetime: 10-20 s) (Doyle and Botstein, 1996; Smith et al., 2001; Waddle et al., 1996) and thus these patches probably represent endocytic vesicles decorated with F-actin. Lifeact-FP-labelled patches also underwent directional movement along cables in a discontinuous manner and occasionally we observed the movement of patches from the cell surface onto actin cables, along which they were transported. These observations strongly indicate that in *N. crassa*, F-actin decorated endocytic vesicles form at the plasma membrane and, following invagination and scission, can be transported along actin cables. The observations of patch dynamics in *N. crassa* are consistent with current

models of patch formation which describe how patch movement correlates with their maturation state (Robertson et al., 2009b).

The movement of actin patches along cables has been shown in budding yeast and fission yeast, and in *A. nidulans* actin patches have been shown to undergo linear directed movement along unidentified structures (Huckaba et al., 2004; Pelham and Chang, 2001; Upadhyay and Shaw, 2008). Most interestingly, in *N. crassa* transport of patches along cables was bidirectional, which contrasts with previous findings, where it was reported that in budding yeast, directional movement of patches along cables is always retrograde to the site of polarised growth (Huckaba et al., 2004). Based on their findings, Huckaba et al. (2004) concluded that retrograde patch movement is coupled to the retrograde flow of cables. As the saltatory nature and rapid speed (1.2 µm/s) of actin patch transport along cables in *N. crassa* suggested the involvement of motor proteins, presumably myosins, I investigated the role of the single class-V myosin present in the genome of *N. crassa*. To study MYO-5 organisation, I N-terminally tagged MYO-5 with GFP, allowing the observation of MYO-5 localisation at various stages of development. MYO-5 localised at germ tube tips and CATs as a small crescent or spot. Occasionally we observed germ tubes that did not show a distinct MYO-5 localisation at the tip. Given the known role of class-V myosins in transporting secretory vesicles (Jin et al., 2011; Pruyne et al., 1998; Schott et al., 2002), it is likely that these germ tubes were not growing at this stage; CATs, which grow continuously, typically displayed a persistent MYO-5 spot at the tip. In mature hyphae, which grow at a more rapid rate than germ tubes, GFP-MYO-5 accumulated at the core of the Spk, suggesting that it transports vesicles to this location. Normal cellular distribution of myosin-5 was found to depend on F-actin and myosin activity, with MTs also participating in MYO-5 localisation.

Key roles for class-V myosins have been demonstrated in *C. albicans*, *U. maydis* and *A. nidulans*. In *C. albicans* and *A. nidulans* a class-V myosin is required for efficient secretion

and normal hyphal growth (Taheri-Talesh et al., 2012; Woo et al., 2003; Zhang et al., 2011). In *U. maydis*, Myo5 is needed for normal cell separation, mating, hyphal growth and pathogenicity (Weber et al., 2003). In *C. albicans, U. maydis* and *A. nidulans*, *myo-5* is not essential for survival, whereas in *S. cerevisiae* the class-V myosin Myo2 is essential. Similar to *C. albicans, U. maydis* and *A. nidulans*, the *myo-5* gene is not essential in *N. crassa*, suggesting that in filamentous fungi, an absence of myosin-5 activity is compensated for by the presence of additional mechanisms and/or motors proteins. Indeed, recent evidence suggests that the secretion of chitin synthases involves both F-actin and microtubules in addition to the concerted action of kinesin-1 and myosin-5 (Schuster et al., 2012).

In the absence of *myo-5*, *N. crassa* germlings produce multiple germ tubes, suggesting that MYO-5 is involved in cell polarity. Secretion and growth still occur in the absence of MYO-5 as evidenced by the elaboration of polar germ tubes and branches. Germ tubes were often swollen and misshapen when in the absence of *myo-5*, demonstrating that MYO-5 is required for proper cell morphogenesis, which is in keeping with its known roles in transporting secretory vesicles in other eukaryotes (Jin et al., 2011; Pruyne et al., 1998; Schott et al., 2002). The rate of cell fusion rates is lower in the *Δmyo-5* mutant compared to wild-type (Figure 3.9). Taken together with the fact that MYO-5 is localised in CATs and fused CATs (Figure 3.13), this finding suggests that MYO-5 plays a role in CAT fusion. Indeed, in *S. pombe*, two class-V myosins, Myo51 and Myo52, have been implicated in cell fusion (Doyle et al., 2009).

Class-V myosins have been shown to have important roles in organelle transport in the unicellular yeasts *S. cerevisiae* and *S. pombe*. In *S. cerevisiae*, the majority of organelles are translocated along the actin cytoskeleton in a Myo2-dependent manner. Importantly the rapid anterograde translocation of secretory vesicles by Myo2 is thought to overcome the retrograde flow of F-actin from its site of nucleation in growing buds into the cell body. In *S. pombe*, the class-V myosin, Myo52 transports α glucan synthase (Mok1), β 1,3 glucan

synthase (Bgs1) and the SNARE protein, synaptobrevin, to regions of active growth (Mulvihill et al., 2006; Win et al., 2001).

To address the role of *myo-5* in actin patch transport, I generated Lifeact-GFP-expressing *myo-5* null mutant strain. The absence of *myo-5* caused a drastic perturbation of F-actin distribution (Figure 3.11). Instead of forming dense arrays of actin cables at the germ tube tip, F-actin was concentrated at germ tube tips as a crescent. A similar localisation pattern was previously reported in a ∆myo-5 *U. maydis* mutant (Weber et al., 2003). Furthermore, less actin cables were present and the frequency of rapid actin patch movement was reduced. The altered organisation of actin cables could be due to an absence of MYO-5-mediated delivery of formin to the cell tip, which would hinder efficient cable nucleation. Additionally, although F-actin organisation was altered in the absence of myo-5 and actin cables were rarely visible, the actin cytoskeleton was still distributed in a polar manner which suggests that other mechanisms contribute to cell polarity, such as MT-based transport. Indeed, in *U. maydis* both kinesin and myosin-5 support hyphal growth – cell polarity is completely lost in Δ*myo5* and Δ*kin1* mutants and a Δ*myo5*, Δ*kin3* double mutant (Schuchardt et al., 2005). It is possible that MYO-5 contributes to normal cell polarity by targeting secretion to distinct sites at the plasma membrane thereby restricting the number of growth foci.

Treatment with the ATP-depleting agent CCCP and BDM, which inhibits myosin activity, resulted in a loss of normal actin localisation. Lifeact-GFP-expressing cells treated with CCCP showed a 50% decrease in the frequency of rapid actin patch translocation, however, BDM did not seem to have any effect on rapid actin patch movement. BDM has a broad effect on many non-myosin proteins and does not completely abrogate myosin ATPase activity (Ostap, 2002), therefore it is possible that MYO-5 still retains some activity following treatment. Taken together these data imply that MYO-5 is involved in F-actin organisation and rapid actin patch movement but is not the sole motor responsible for patch

translocation. Alternatively, the reduction in the frequency in actin patch transport could stem from the perturbed F-actin organisation caused by loss of *myo-5*.

Chapter 4:

Septin function and organisation in in *Neurospora crassa*

4.1 Results

4.1.1 Septins limit the emergence of germ tubes and are involved in conidiation

Bioinformatic and phylogenetic analysis of the *N. crassa* genome has revealed the presence of six putative septins (Pan et al., 2007). Four ORFS, NCU8207, NCU3515, NCU2464, and NCU3795, are orthologs of the core *S. cerevisiae* septins, *cdc3*, *cdc10*, *cdc11*, and *cdc12*, respectively, so we adopted this nomenclature as recommended by Pan et al. (2007). Two hypothetical proteins were found to contain canonical septin sequences but are only found in filamentous fungi (Pan et al., 2007). These two ORFs, NCU1998 and NCU6414, were named ASP-1 and ASP-2, respectively. To determine the role of septins in *N. crassa* I constructed strains in which individual septins were deleted or where a combination of core septins were deleted. Genotyping analysis of deletion strains and others is shown in Figures A.1 and A.2. Previous studies in *A. nidulans* have shown that septins delay and limit the emergence of germ tubes and are involved in septation (Lindsey et al., 2010a). To understand if this is a general function of septins in filamentous fungi we initially assessed the rates of germination and cell fusion and the morphology of septin null mutants and compared these with the wild type (Figures 4.1 and 4.2). A slight but significant ($p = <0.05$) decrease in the rate of germination in Δ*cdc-10* and Δ*cdc-11* strains was observed, which suggests that in these strains germ tubes emerge later than in the wild-type. No significant differences in germination and fusion rates were observed for *cdc-3*, *cdc-12*, *asp-1* and *asp-2* deletion mutants.

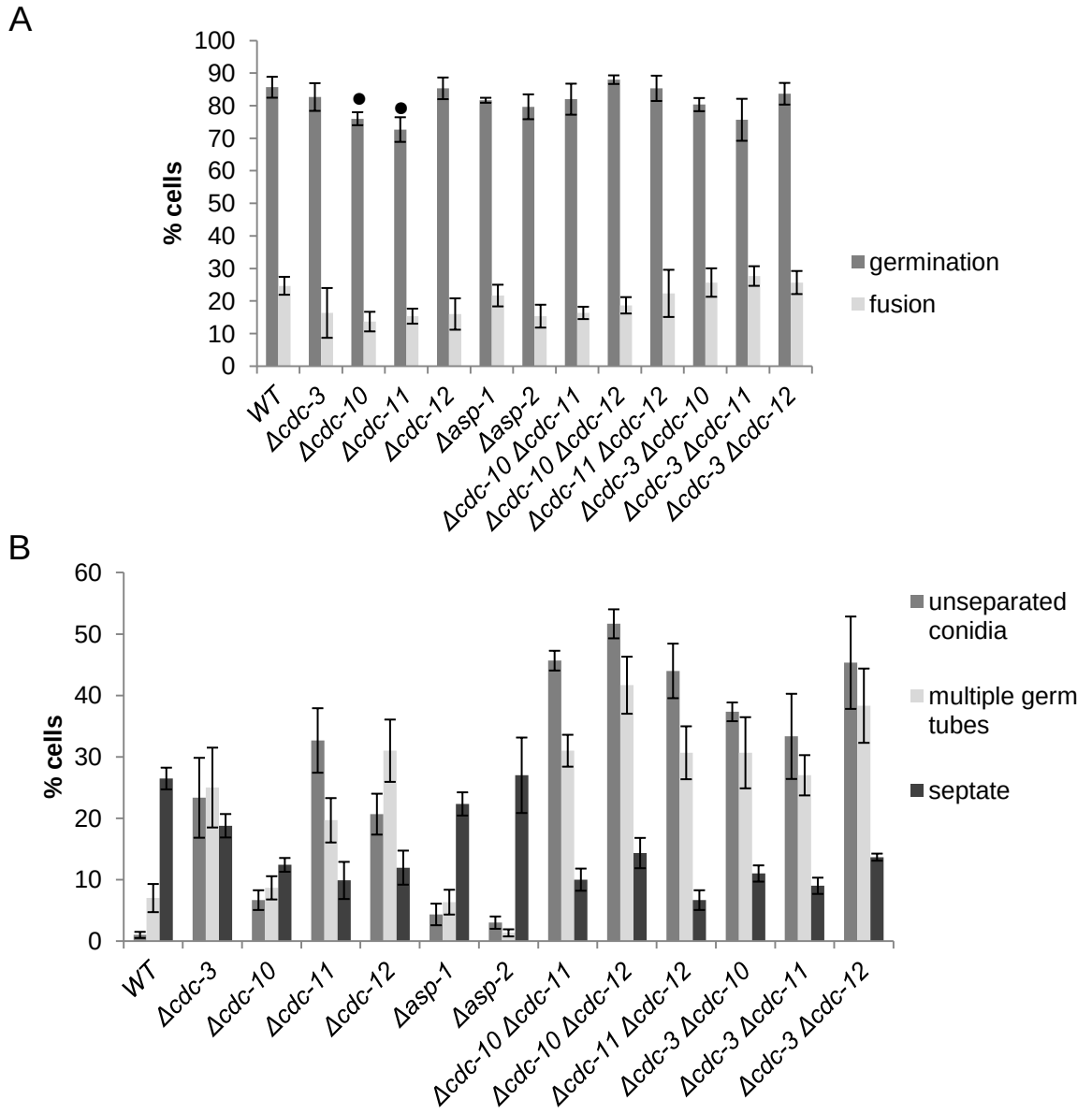

Figure 4.1. Septin deletion strains display an increase in germ tube emergence and unseparated conidia and a reduction in septation compared to wild-type. (**A**)The number of unseparated cells in was counted before incubation, the number of cells with more than two germ tubes was counted following 3 h of incubation in liquid VMM and the number of septate cells was determined with DIC microscopy after 5 h of incubation in liquid VMM (*n* = 300). There was a significant increase (p = <0.05) in the percentage of unseparated conidia and cells with multiple germ tubes compared to wild-type for all strains with the exception of Δ*cdc10*, Δ*asp-1* and Δ*asp-2*. Similarly, there was a significant decrease (p = <0.05) in the percentage of septate cells for all strains compared to the wild-type except for Δ*asp-1* and Δ*asp-2*. (**B**) Strains were incubated in liquid VMM for 3 h then counted for germination and cell fusion (*n* = 300). A black dot above bars indicate a significance difference (p = <0.05) compared to the wild-type control. The germination rates of Δ*cdc-10* and Δ*cdc-11* was slightly reduced compared to wild-type. The error bars indicate standard deviations.

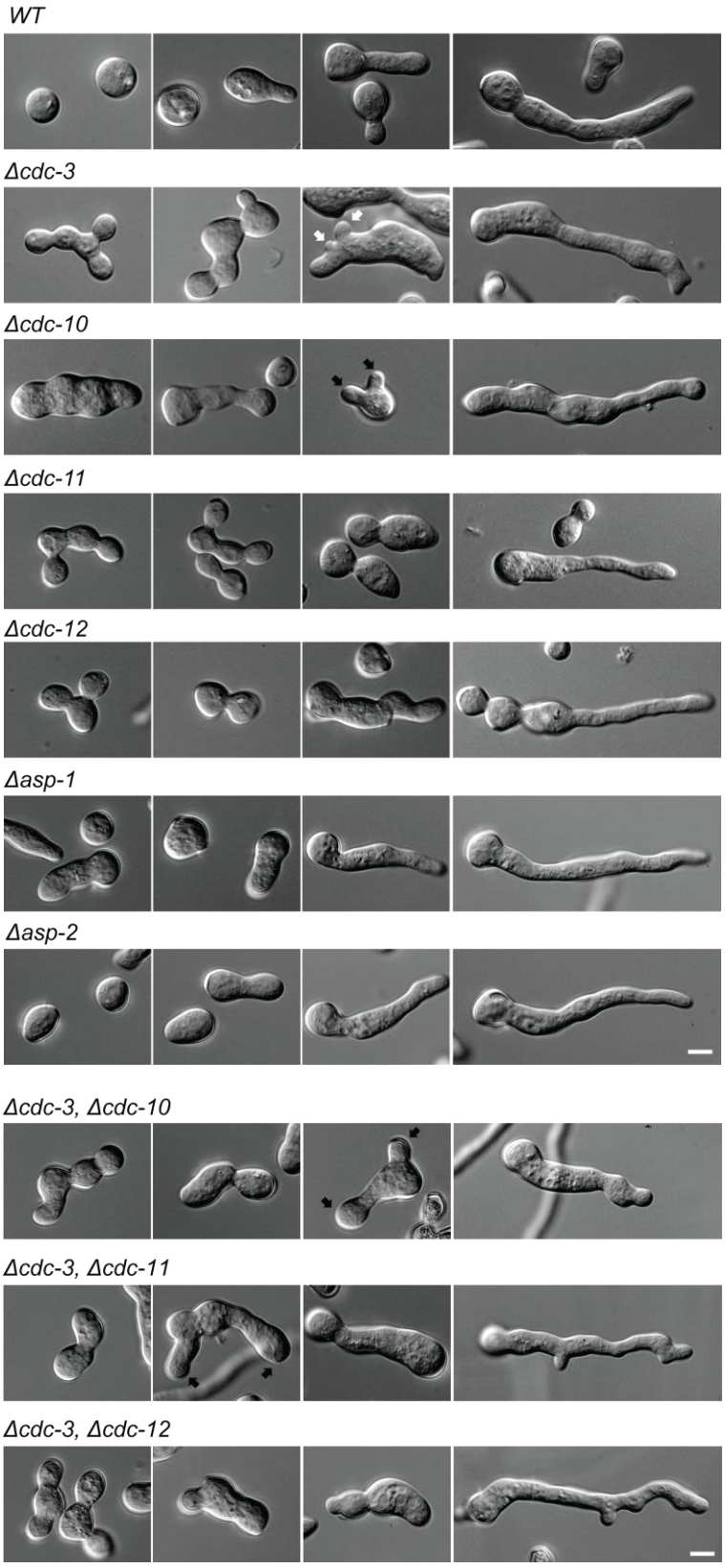
WT
Δcdc-3
Δcdc-10
Δcdc-11
Δcdc-12
Δasp-1
Δasp-2
Δcdc-3, Δcdc-10
Δcdc-3, Δcdc-11
Δcdc-3, Δcdc-12

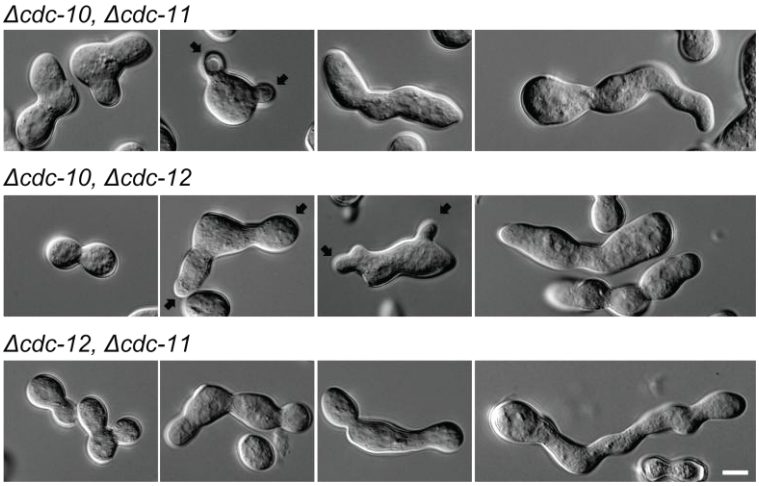

Figure 4.2 Septin deletion strains have altered morphologies. Wild-type and septin deletion strains were incubated in liquid VMM for up to 5 h then imaged by DIC microscopy to obtain representative images of germination and development. Septin deletion strains, with the exception of *Δasp-2* and *Δasp-1*, fail to properly separate conidia and often appear swollen and misshapen. Black arrows denote multiple germ tube emergence. White arrows show multiple CAT emergence Bar, 5 µm.

Despite the relatively minor effects of the absence of individual septins on germination and fusion rates, the morphologies of the *cdc-3*, *cdc-10*, *cdc-11*, and *cdc-12* deletion strains were markedly different from that of the wild-type. There were no obvious morphological defects for Δ*asp-1* and Δ*asp-2* strains. The major morphological defects displayed by strains lacking core septins included joined conidia, swelling, and multiple germ tube and CAT emergence (Figures 4.1 and 4.2). The presence of joined conidia was probably due to defects during conidiation and most likely stems from a failure of conidia to separate during budding due to lack of a functional septin ring.

I quantified the amount of conidia that were unseparated or exhibited more than one site of germ tube outgrowth and found a drastic increase in Δ*cdc-3*, Δ*cdc-10*, Δ*cdc-11*, and Δ*cdc-12* strains compared to wild-type. Strains lacking the core septins produced significantly (Figure 4.1B, $p = <0.05$) more germ tubes and unseparated cells than the wild-type although the phenotype of the *cdc-10* null mutant was not as severe. The Δ*asp-1* and Δ*asp-2* strains, however, were similar to wild-type.

An increase in sites of germ tube outgrowth is usually accompanied by a reduction in radial extension due to hyperbranching so the radial extension rate of the septin mutants was measured (Table 4.2). Strains lacking the core septin showed a marked reduction in radial extension compared to the wild-type with Δ*cdc-3* extending 25% slower than wild-type. Again the Δ*cdc-10* strain showed a less severe phenotype, with an extension rate only 5% slower than wild type. The colony morphologies of Δ*cdc-3*, Δ*cdc-11*, and Δ*cdc-12* were slightly denser than the wild-type and showed areas of cell lysis whereas the Δ*cdc-10*, Δ*asp-1*, and Δ*asp-2* mutants appeared unaffected (Figure 4.3).

Given the role for septins in septation and cytokinesis I assessed whether septation still occurred in the deletion mutants and if so whether there was any reduction in their formation. Septa still formed in null mutants and appeared identical to wild-type septa suggesting that septins are not required for septum formation *per se*; however, there was a significant reduction ($p = <0.05$) in the number of septate germ tubes formed after 5 h in the Δ*cdc-3*, Δ*cdc-10,* Δ*cdc-11* and Δ*cdc-12* mutants suggesting that septins contribute to septation. Research in *U. maydis* and *C. albicans* has shown that in the absence of septins the cell wall is abnormal (Alvarez-Tabares and Perez-Martin, 2010; Warenda and Konopka, 2002). However, calcofluor white staining of *N. crassa* septin deletion mutants did not reveal any defects in cell wall formation (Figure 4.4).

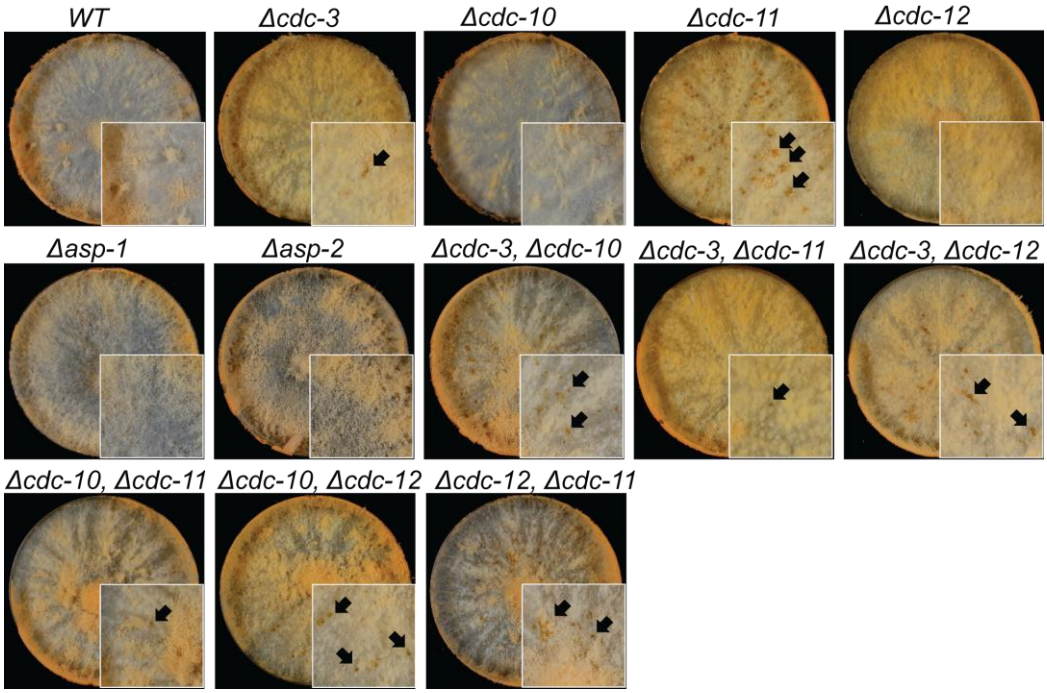

Figure 4.3. Colony morphology is altered in septin deletion strains. Wild-type and septin deletion strains were inoculated onto solid VMM, incubated for 3 d at 24 °C then photographed. Septin deletion strains, with the exception of *Δasp-1* and *Δasp-2*, do not produce as many aerial hyphae as wild-type and occasionally visible are regions of cell lysis (black arrows).

Table 4.2 Radial extension of *N. crassa* septin mutants

Strain	Extension rate ± Stdev (mm/hour)*
WT	2.4±0.6
Δcdc-3	1.8±0.4
Δcdc-10	2.2±0.4
Δcdc-11	1.7±0.6
Δcdc-12	1.7±0.4
Δasp-1	2.5±0.5
Δasp-2	2.4±0.4
Δcdc-10 Δcdc-11	1.6±0.3
Δcdc-10 Δcdc-12	1.7±0.4
Δcdc-11 Δcdc-12	1.7±0.4
Δcdc-3 Δcdc-10	1.8±0.3
Δcdc-3 Δcdc-11	1.6±0.4
Δcdc-3 Δcdc-12	1.6±0.4

*The radial extension of mycelia was assessed after 8 h growth on VMM plates at 35 °C. Colony extension was measured along four randomly chosen radii on duplicate plates; *n* = 8 for each.

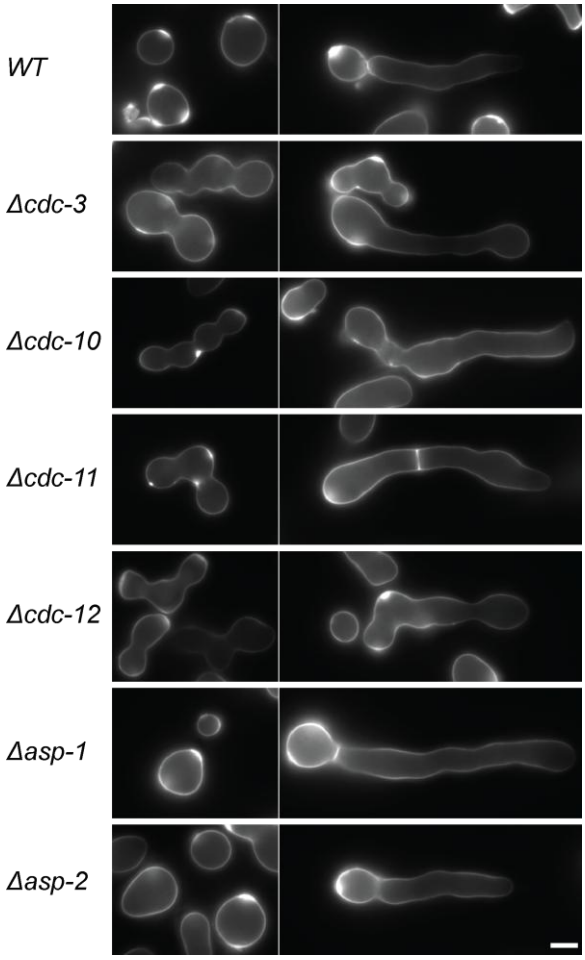

Figure 4.4. Cell wall deposition is unaffected in septin deletion strains. Wild-type and septin deletion strains were incubated in liquid VMM for up to 5 h, stained with calcofluor white then imaged with fluorescence microscopy. Bar, 5 µm.

To further dissect the functional roles of the *N. crassa* core septins I constructed double mutants lacking two core septins in different combinations. The resulting strains were all viable and exhibited similar germination and fusion rates to the wild-type (Figure 4.1). Colony morphologies of the double deletion strains were comparable to the single null mutants (Figure 4.3). However, the amount of unseparated cells and germ tubes was significantly increased ($p = <0.05$) and septation significantly reduced ($p = <0.05$) in the double mutants compared to single deletion strains suggesting that individual core septins may have non-overlapping roles (Figure 4.1B).

To determine the effects of septin deletion on the actin cytoskeleton we generated a *cdc-11* null mutant expressing GFP-Lifeact, which labels F-actin in *N. crassa* (Berepiki et al., 2010; Riedl et al., 2008). F-actin structures were unaffected in the absence of septin complexes although due to the polarity defects of the *cdc-11* null mutant, F-actin accumulated at the growing tip and in the spore body where new growth had presumably been initiated (Figure 4.5).

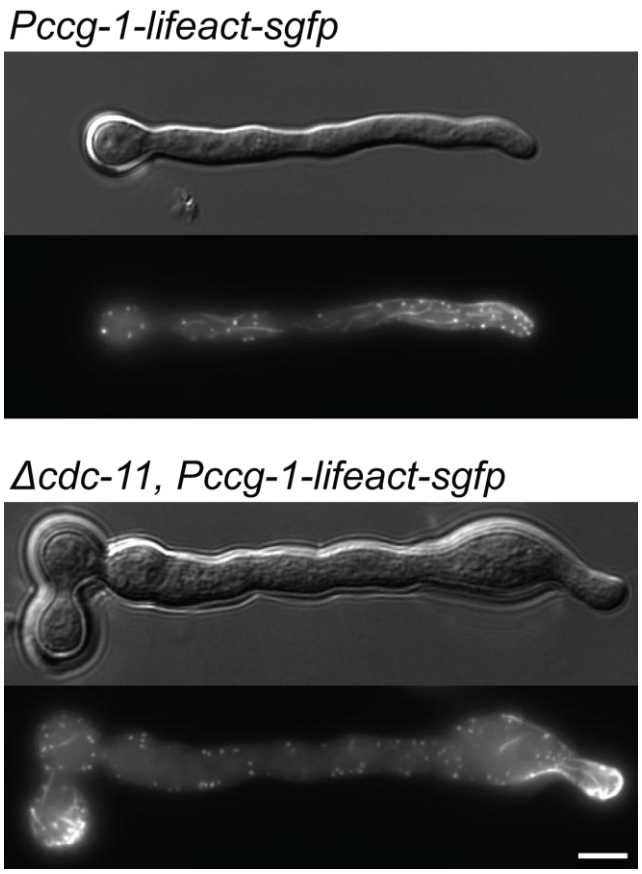

Figure 4.5. F-actin structures are unaffected in the absence of *cdc-11*. Lifeact-GFP-expressing wild-type and *Δcdc-11* strains were incubated in liquid VMM for 3 h then imaged with fluorescence microscopy. F-actin structures appear as normal although due to the polarity defects of the *cdc-11* null mutant, actin accumulated at the tip and in the spore body. Bar, 5 µm.

4.1.2 Septins show different patterns of localisation at the hyphal tip and form rings, fibres, bar-like structures and caps

To visualise the septin cytoskeleton in *N. crassa* I made in-frame fusions of GFP to the 3' ends of the open reading frames of CDC-3, CDC-10, CDC-11, CDC-12, ASP-1 and ASP-2 so that each resulting fusion protein was expressed from their endogenous promoter as the only copy of the gene. GFP-expressing strains were imaged by wide-field microscopy followed by iterative deconvolution. We were unable to visualise CDC-10, ASP-1 and ASP-2 by C-terminal integration of GFP or via overexpression of CDC-10-GFP, ASP-1-GFP and ASP-2-GFP from the *ccg-1* promoter. Overexpression of CDC-10 and ASP-1 tagged at their N-terminal ends with GFP was successful but we were still unable to visualise ASP-2 even when the expression of the ORF was driven by the strong *ccg-1* promoter suggesting that this hypothetical gene may not be a *bona fide* ORF. Given that N-terminal overexpression of GFP-CDC-10 and GFP-ASP-1 was efficacious, I generated N-terminal GFP integration cassettes for these genes to ensure that expression level of the fusion construct was as close to wild-type levels as possible. Endogenous expression of GFP-CDC-10 gave an adequate signal-to-noise ratio so this strain was used for further experiments. However, the expression level of the GFP-ASP-1 fusion was too low to allow visualisation so the *Pccg1-sgfp-asp-1* strain was used for imaging instead. To determine whether the GFP tag might interfere with septin function, I compared the phenotypes of the septin GFP fusion strains (*cdc-3-gfp*, *gfp-cdc-10*, *cdc-11-gfp*, *cdc-12-gfp*, and *Pccg1-gfp-asp-1*) with those of wild-type and septin-deleted strains. Germination, cell fusion, conidiation, and septation were all similar to wild-type in the septin-GFP strains, indicating that the GFP tag does not interfere with function (Figure 4.6).

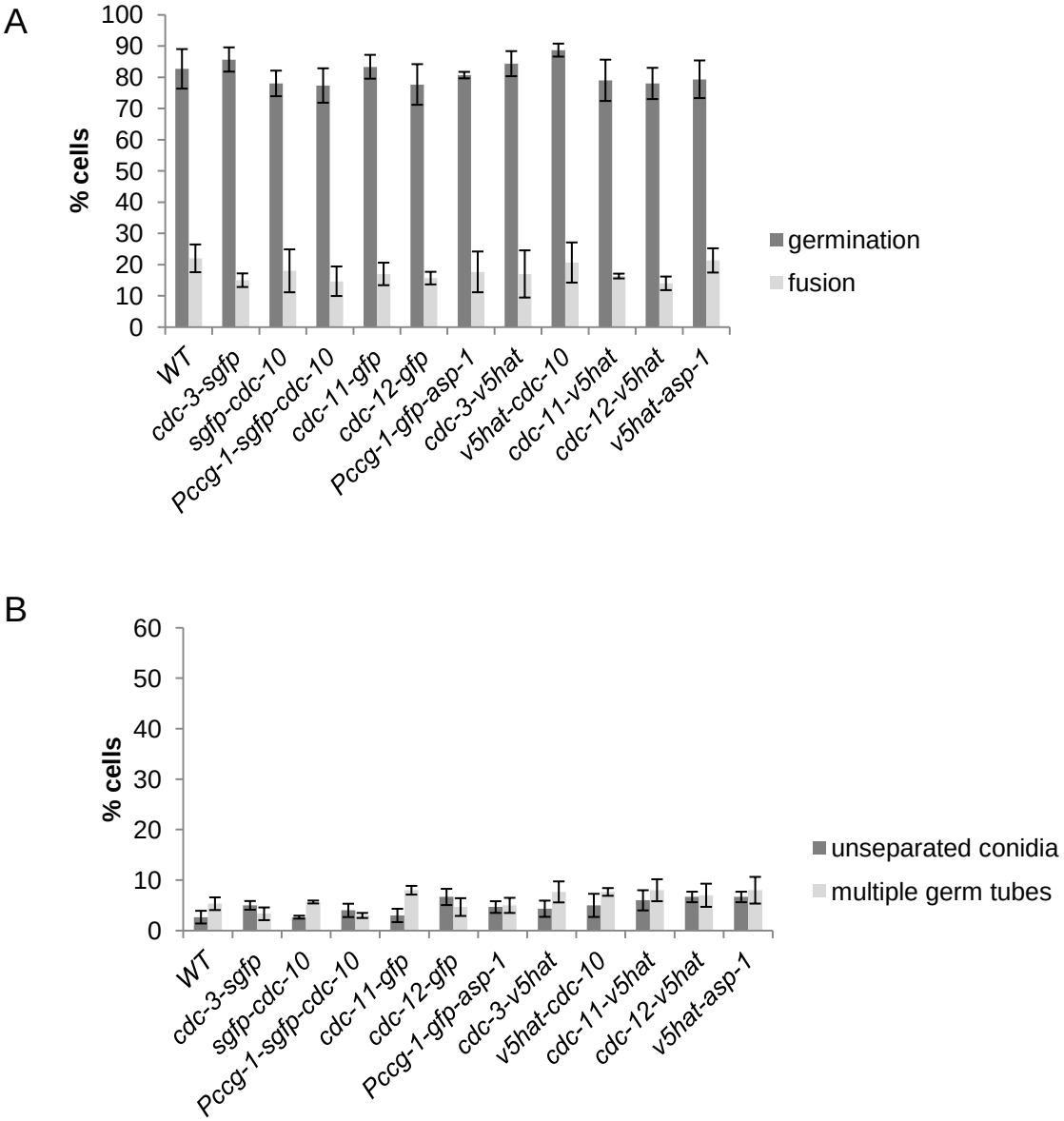

Figure 4.6. Germination, cell fusion, septation, and conidiation are unaffected in septin-GFP or septin-V5-HAT strains. (A, B) Strains were incubated in liquid VMM for 3 h (A) or 5 h (B) then counted for germination and cell fusion (*n* = 300). (C) The number of unseparated cells was counted before incubation, cells with more than two germ tubes was counted following 3 h of incubation in liquid VMM and the number of septate cells was determined with DIC microscopy after 5 h incubation in liquid VMM (*n* = 300). Differences in the assed parameters between transformant strains and wild-type were statistically not significant (all p > 0.1). The error bars indicate standard deviations.

Strikingly, at the tips of germ tubes the septins had varied patterns of localisation (Figure 4.7). CDC3-GFP and CDC12-GFP were present as a crescent at the germ tube tip whereas GFP-CDC10 and CDC11-GFP localised in the form of multiple bar-like structures in the tip region but the signal was noticeably weaker at the tip apex and more intense at the plasma membrane zone approximately 1 µM from the apex. GFP-ASP-1 localised to the plasma membrane but the fluorescent signal was evenly distributed forming a cap that extended ~ 5 µM back from the tip.

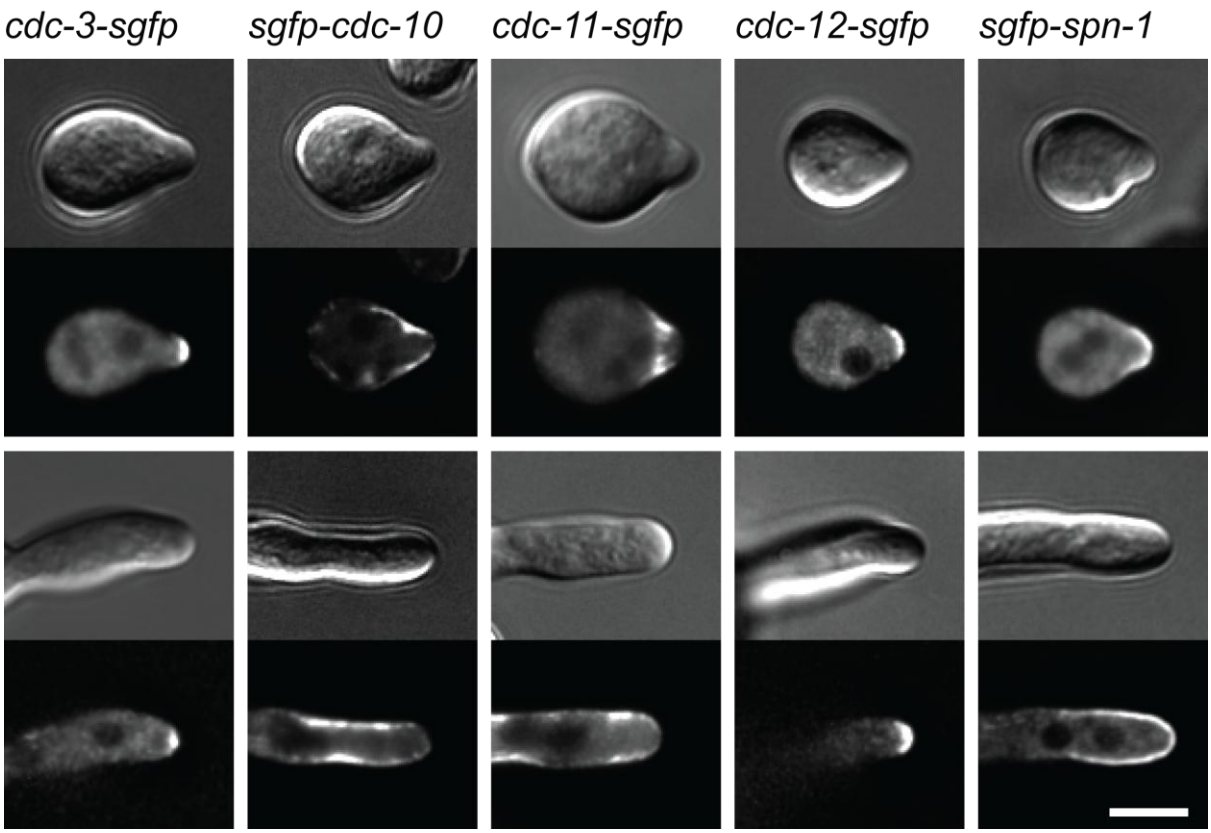

Figure 4.7. Septins show different patterns of localisation at germ tube tips. Septin-GFP strains were incubated in liquid VMM for 3 h then imaged with fluorescence and DIC microscopy to obtain representative images of germination and development. At the hyphal tip septins localise as a cap (CDC-3-GFP and CDC-12-GFP), an extended cap (GFP-ASP-1) or as a bar-like structures (GFP-CDC-10 and CDC-11-GFP). Bar, 5 µm.

To my knowledge this is the first report of individual septins displaying varied localisation patterns in hyphal tips. These findings suggest that septins play a role in tip growth and/or maintaining the tip growth apparatus and that, given their localisation, individual septins could play different roles in hyphal growth. The localisation pattern was broadly similar throughout the period of germ tube emergence and outgrowth. A near identical spatial organisation was observed for septins in CATs before and up to the point of making contact (Figure 4.8). After fusion, however, I observed that the characteristic bar-like structures for one septin, CDC-11, became concentrated around the fusion pore, indicating a possible role for septins in the terminal stages of cell fusion (Figure 4.8). CDC-11-GFP became dispersed in the cytoplasm following fusion. All septins localised as rings at sites of septation suggesting that the heteromeric septin ring complex in *N. crassa* consists of five distinct septins (Figure 4.8). Ring formation was preceded by an accumulation of septin fibres associated with the cell cortex which eventually concentrated as a ring. We also observed two other HO septin assemblies in *N. crassa*: fibres and loops (Figure 4.7).

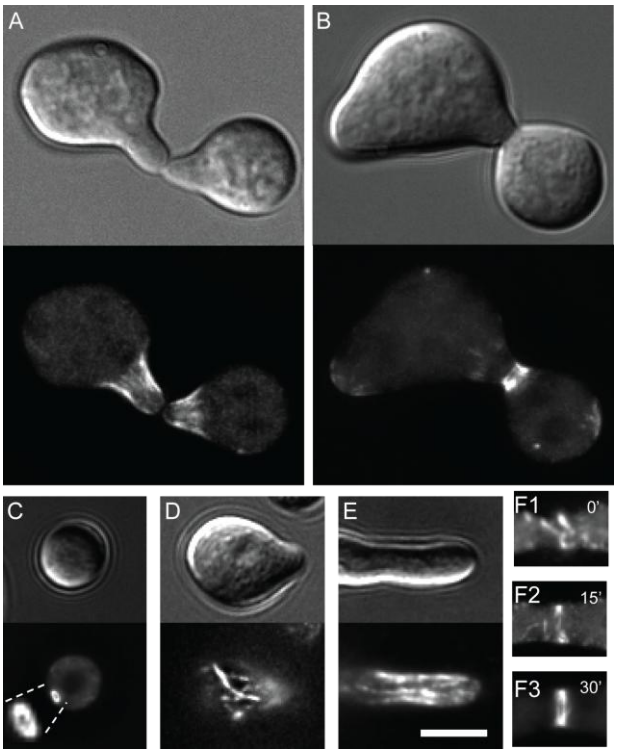

Figure 4.8. Septin localise to the tips of conidial anastomosis tubes (CATs) and form diverse HO structures. Cells expressing CDC-11-GFP (A, B, C, and F) or GFP-CDC-10 (D and E) were incubated in liquid VMM for 3 h then imaged with fluorescence and DIC microscopy to obtain representative images of HO structures, septin ring formation and cell fusion. (A, B) CDC-11 localises as bar-like structures at the tips of CATs prior to cell fusion (A) and following this process become concentrated around the fusion pore (B). (C) Dense septin loop associated with the cell cortex. (D, E) Septin fibres are present in the cytoplasm. (F1, F2, F3) Septin rings formed by the accumulation of septin fibres. Bar, 5 µm.

Fibres were approximately 0.2-0.5 µM thick and varied in length from 0.5-5 µM and were found throughout the cytoplasm with some being associated with the cell cortex. Septin fibres were observed with CDC-11-GFP or GFP-CDC-10 but not with other septins, and were more prevalent in ungerminated or slowly growing cells. The number of fibres increased drastically when GFP-CDC-10 was overexpressed by the *ccg-1* promoter compared to endogenous levels (Figure 4.9). It has been suggested that fibres inhibit new growth (Hernandez-Rodriguez et al., 2012), however, we did not observe any inhibition of germination in strain *Pccg-1-sgfp-cdc-10* compared to wild-type or *sgfp-cdc-10* (Figure 4.6).

To determine if these fibres colocalise with MTs or F-actin, we attempted to generate strains co-expressing GFP-tagged septins and βtub-mCherry or Lifeact-tagRFPT. However, the resulting strains exhibited a gross perturbation of cell morphology, inadequate co-expression, and mislocalisation of one or both polymers.

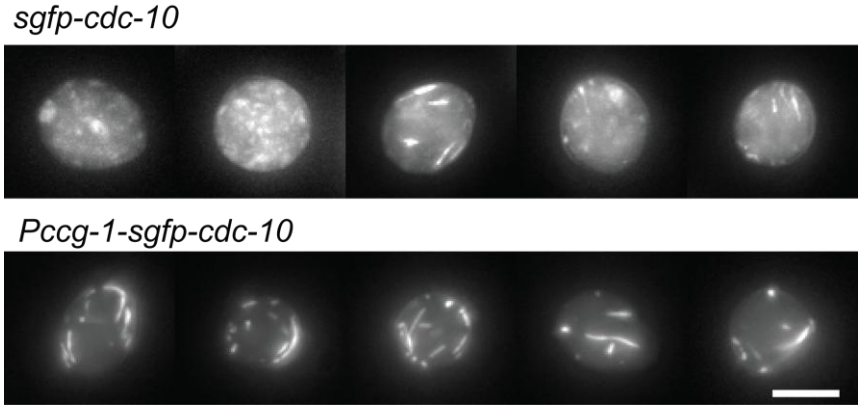

Figure 4.9. Septins fibres are more abundant when GFP-CDC-10 is overexpressed. Conidia from two GFP-CDC-10 strains were harvested then imaged with fluorescence and DIC microscopy to obtain representative images of septin fibres. When GFP-CDC-10 is expressed from the *Pccg-1* promoter instead of its native promoter septin fibres are more abundant. Bar, 5 µm.

Dense loops with a diameter of ~ 1 µM were found in *cdc-11-gfp* but not in other GFP-expressing strains. Similar to fibres, these structures were more commonly observed in ungerminated spores and did not appear to show an association with actively growing regions. To determine if HO septin structures form in the absence of an individual septin we analysed the ability of CDC-11-GFP and CDC-12-GFP to form rings in null mutants. In null mutants lacking *cdc-3*, *cdc-11*, and *cdc-12*, CDC-11-GFP and CDC-12-GFP were only localised to the cytoplasm and HO assemblies were completely absent (Figure 4.10). Interestingly, although CDC-11-GFP and CDC-12-GFP display different patterns of localisation at germ tube tips, it appears that CDC-11 requires CDC-12 for proper tip distribution and conversely, CDC-12 requires CDC-11 for proper tip distribution. In Δ*cdc*-10, Δ*asp-1* and Δ*asp-2* strains the localisation of CDC-11-GFP rings and tip-associated complexes were indistinguishable from wild-type (Figure 4.10). These findings suggest that CDC-3, CDC-11, and CDC-12 are essential for oligomerisation and HO structure assembly whereas CDC-10, ASP-1 and ASP-1 are not.

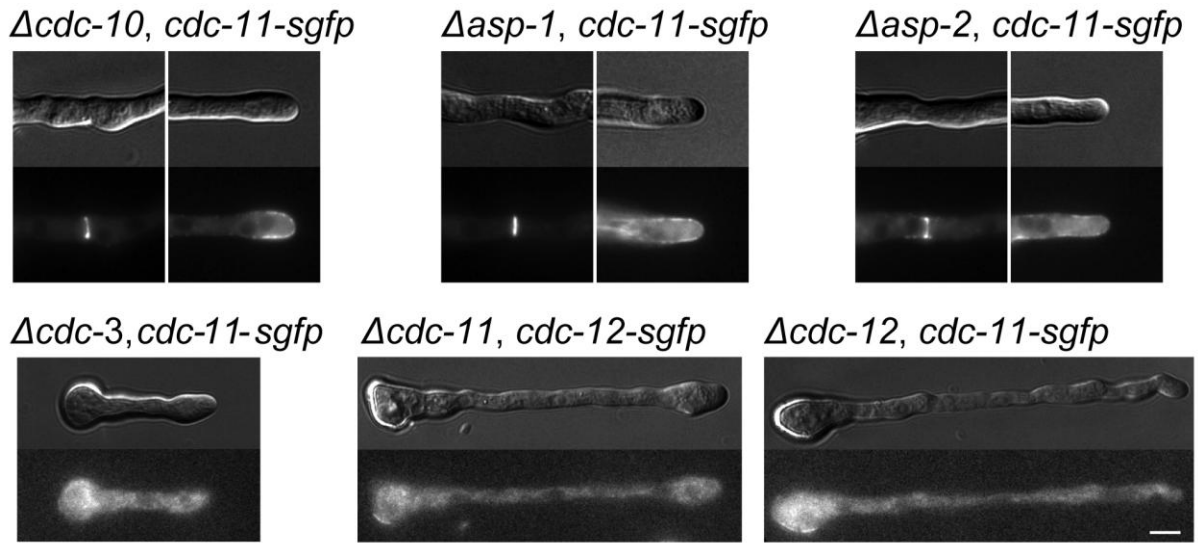

Figure 4.10. Higher-order septin structures fail to form in the absence of CDC-3, CDC-11, or CDC-12. Septin deletion strains expressing CDC-11-GFP were incubated in liquid VMM for 5 h then imaged with fluorescence and DIC microscopy to obtain representative images of septin localisation. Bar, 5 µm.

4.1.3 Purification and analysis of septin complexes

Tandem affinity purification (TAP) with magnetic beads was utilised to detect protein-protein interactions in septin complexes. Protein purification using magnetic beads offers several advantages over conventional column chromatography such as ease of use, rapidity and lower non-specific binding of proteins (Sousa et al., 2011; Trinkle-Mulcahy et al., 2008). To purify protein complexes I used anti-V5 antibody conjugated Dynabeads and charged His tag isolation (HTI) Dynabeads. Two epitopes were used to label the *N. crassa* septin complexes; a V5 epitope, derived from the V5 simian virus and a poly-histidine sequence from chicken lactate dehydrogenase (HAT), which is known to be a superior alternative to the commonly used 6xHis tag (Chaga et al., 1999). The double epitope tag was created *de novo* using three overlapping synthetic oligonucleotides that were combined using YRC. Single native genomic loci were tagged by the introduction of an integration cassette containing the V5-HAT epitope and hygromycin selection marker. Confirmation of correct integration into the genome by homologous recombination was confirmed by genotyping PCR of transformants. Next, I examined the expression of the different epitope-tagged septins. Western blot analysis of whole cell extracts with a monoclonal anti-V5 antibody demonstrated that all of the V5-HAT-tagged septins were expressed with the exception of V5-HAT-ASP-2 (Figure 4.11). Western analysis demonstrated the presence of two isoforms of CDC-3 and CDC-10 which could represent sumoylated or phosphorylated isoforms of these proteins as has been shown for *S. cerevisiae* Cdc3, Cdc11, and Shs1 (Johnson and Blobel, 1999; Mortensen et al., 2002; Takahashi et al., 1999).

Figure 4.11. Western blot analysis of septin-V5-HAT-expressing strains. Whole-cell extracts from various strains (in italics) were separated by SDS-PAGE then probed with αV5. The positions of the molecular mass markers (M, in kDa) are shown at the left of the panel.

Following confirmation of expression, I analysed the respective strains for phenotypic defects. In V5-HAT-expressing strains, germination, fusion, septation, and germ tube emergence was unchanged from wild-type (Figure 4.6), suggesting that the V5-HAT tag does not interfere with septin function. I compared the efficacy of one-step and two-step affinity purification in immunoprecipitating CDC-12 and also differences in the eluted protein profiles using two buffers: 0.1 M glycine-HCl (pH 2.5) and hot (70 °C) SDS sample loading buffer. The profiles of proteins isolated using the one-step purification with anti-V5 beads were identical to that obtained with the two-step method (Figure 4.12). In both cases negligible non-specific interactions were detected in untagged wild-type whole cell extract control using anti-V5 beads, whereas HTI bead purification of whole cell extracts from wild-type and CDC-12-V5-HAT gave similar profiles. The HAT tag is functional, as demonstrated by the subsequent pulldown of the CDC-12-V5-HAT complex by anti-V5 beads. However, the large degree of non-specific contaminants bound to the HTI beads and the efficacy of the one-step anti-V5 bead IP, allowed me to exclude this step from the purification method.

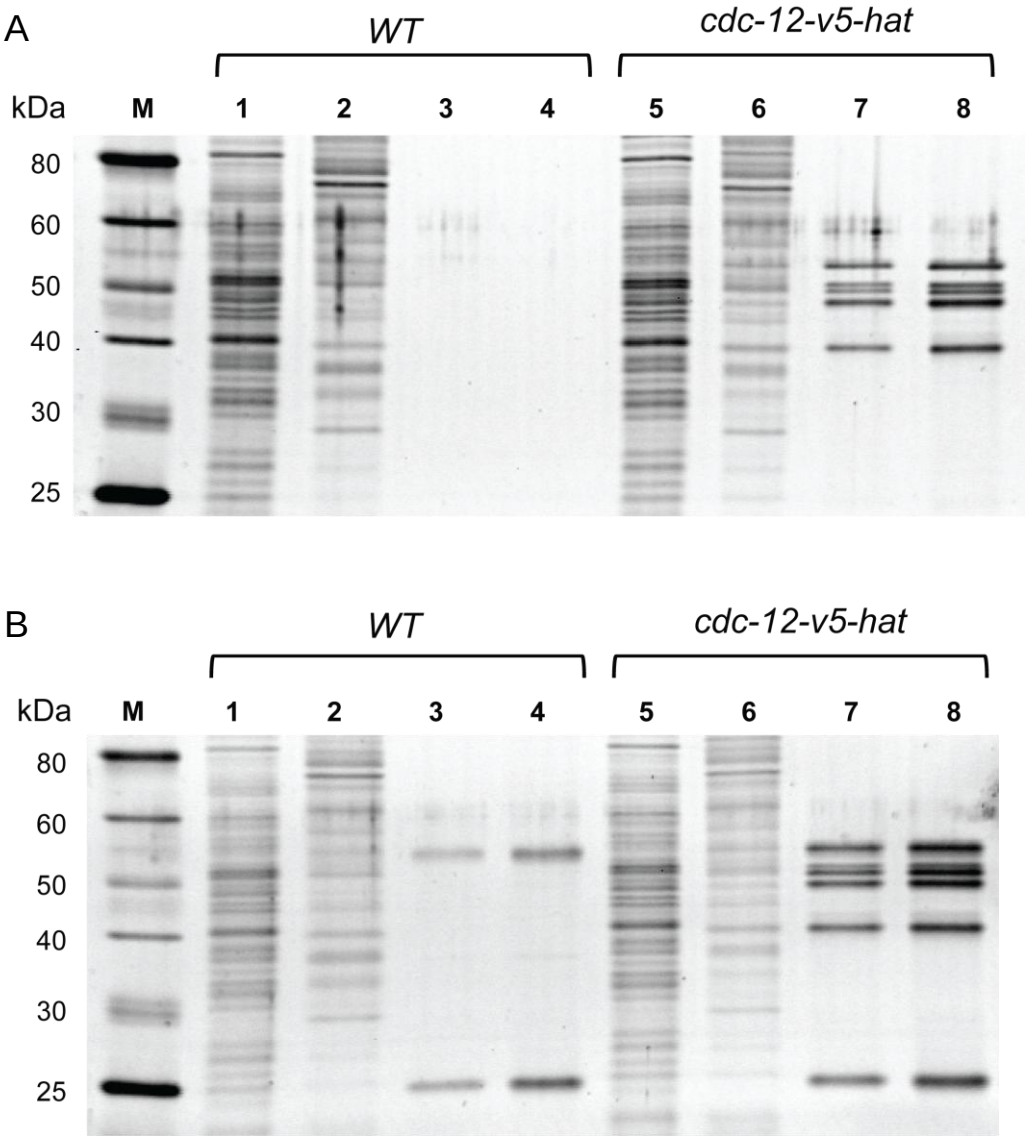

Figure 4.12. Comparison of one- and two-step purification and elution buffers. (A) Comparison of one- and two-step purification of whole-cell extracts from wild-type and *cdc-12-v5-hat* strains with elution in 0.1M glycine-HCl (pH 2.5). Lanes 1 and 5, whole cell extract. Lanes 2 and 6, first step of two-step purification using HTI beads. Lanes 3 and 7, second step of two-step purification using αV5-beads. Lanes 4 and 8, one-step purification using αV5-beads. (B) Comparison of one- and two-step purification of whole-cell extracts from wild-type and *cdc-12-v5-hat* strains with elution in hot SDS buffer . Lanes 1 and 5, whole cell extract. Lanes 2 and 6, first step of two-step purification using HTI beads. Lanes 3 and 7, second step of two-step purification using αV5-beads. Lanes 4 and 8, one-step purification using αV5-beads. The positions of the molecular mass markers (M, in kDa) are shown at the left of the panel.

To determine if the protein complex was completely eluted from the beads and to test for the elution of non-specific interactants from the beads the protein profiles of IPs eluted in 0.1 M glycine-HCl (pH 2.5) and hot (70 °C) SDS sample loading buffer were monitored. Elution in glycine-HCl allows reuse of the beads but may leave proteins bound to the beads whereas elution in hot SDS sample loading buffer completely strips beads of protein but precludes their reuse. A comparison of elution profiles is shown in Figure 4.12. The elution profiles for both buffers are essentially identical demonstrating that all bound proteins are eluted in both cases. However, an additional 25 kDa interactant is present in the SDS eluate in both the wild-type and *cdc-12-v5-hat* strains, which suggests that this is a non-specific interactant and binds to the bead surface rather than to the bead-bound complex. This contaminant was absent from the glycine-HCl eluate, and therefore all further elutions were carried out using 0.1 M glycine-HCl (pH 2.5). IPs were carried out for the five V5-HAT-labelled septins CDC-3, CDC-10, CDC-11, CDC-12, and ASP-1. Following elution, the purified protein complexes were separated by SDS-PAGE and visualised by coomassie blue staining. Protein bands were excised then identified by tandem mass spectrometry by the SynthSys Institute at the University of Edinburgh. CDC-3, CDC-10, CDC-11, CDC-12 were detected in all five purifications. ASP-1 was only detected when V5-HAT-ASP-1 was used as the IP target. Figure 4.13 shows a SYPRO ruby-stained gel with protein profiles of the various IPs. No additional proteins were identified as specific components of septin complexes. These results demonstrate that the core septins form an oligomeric complex and suggests that ASP-1, although it probably does not constitute a subunit of the septin polymer, interacts with it nonetheless, possibly in a similar manner to Shs1/Sep7 in *S. cerevisiae* and Sep7 *C. albicans* (Johnson and Blobel, 1999; Kaneko et al., 2004; Mortensen et al., 2002).

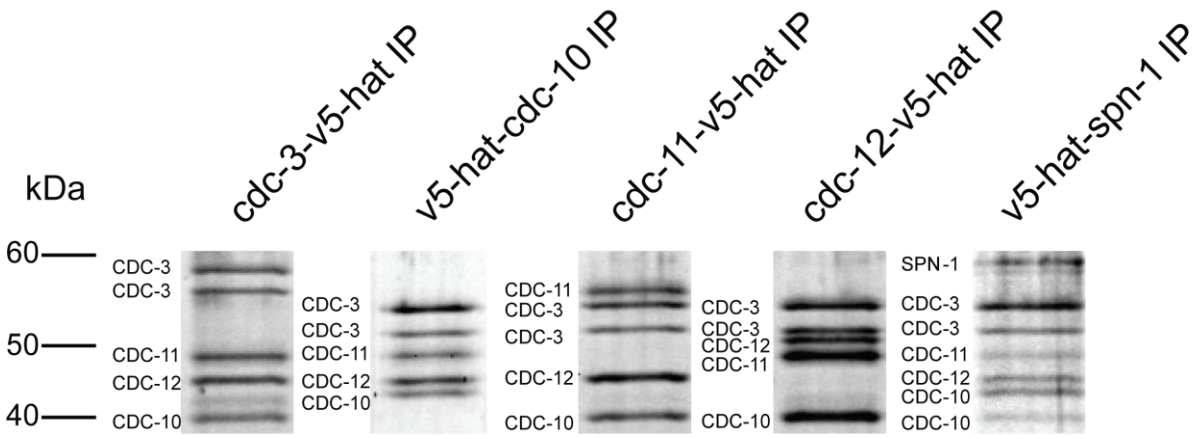

Figure 4.13. Identification of constituents of septin complexes. SYPRO Ruby-stained SDS PAGE gel of septin complexes. Protein were purified from septin-V5-HAT expressing strains and identified by mass spectrometry. The positions of the molecular mass markers (M, in kDa) are shown at the left of the panel.

4.2 Discussion

Septins have been well-studied in budding yeast and are known to have important roles in cytokinesis, cell polarity, morphogenesis and cell wall synthesis (Spiliotis and Gladfelter, 2012). The study of septins in filamentous fungi is still in its infancy but recent reports have revealed new roles for these cytoskeletal polymers. Of particular interest is the finding that in filamentous fungi septins form a variety of HO structures in a single cell and that these structures are regulated by different mechanisms and display different dynamics (DeMay et al., 2009). In addition, two septins specific to filamentous fungi have been identified in a recent phylogenetic study suggesting that septins may have evolved novel functions in these organisms (Pan et al., 2007). To better define the roles of septins in filamentous fungi the six septins present in the *N. crassa* genome were analysed using a combination of null mutants, microscopic analysis of GFP tagged alleles, and mass spectrometry of purified complexes.

None of the *N. crassa* septins were essential for cell viability. Similarly, in other filamentous fungi such as *A. nidulans*, *A. gossypii* and *C. albicans* and the fission yeast *S. pombe* none of the septins studied are essential (Berlin et al., 2003; DeMay et al., 2009; Helfer and Gladfelter, 2006; Hernandez-Rodriguez et al., 2012; Lindsey et al., 2010a; Tasto et al., 2003; Warenda and Konopka, 2002; Wu et al., 2010). This in the stark contrast to the situation in *S. cerevisiae*, where deletion of *cdc3* and *cdc12* is lethal, and *cdc10* and *cdc11* null mutants are viable only at low temperatures (Hartwell, 1971; McMurray et al., 2011). Interestingly, the pathogenic basidomycetes *C. neoformans* and *U. maydis*, which both grow by budding in their yeast phases, require core septins for growth at elevated temperatures. Cumulatively these findings highlight a seemingly important link between cell geometry and growth mode and the requirement of septins in a particular cell type or species. The phenotypes of *N. crassa* strains lacking the core septins (*cdc-3*, *cdc-10*, *cdc-11*, and *cdc-12*) were indistinguishable with all exhibiting reduced septation, increased germ tube emergence, defective separation of conidia, and swollen and misshapen germ tubes.

Although the *Δcdc-10* mutant showed the same phenotype as *cdc-3*, *cdc-11*, and *cdc-12* deletion strains, quantification of multipolarisation, septation, and conidiation defects revealed these were not as greatly perturbed. The *Δasp-1* and *Δasp-2* null mutants did not show any detectable phenotype and behaved as wild-type. Calcofluor white staining of septin mutants showed that despite the misshapen and swollen phenotype of deletion strains, cell walls or septa did not appear to be thickened or abnormal compared to the wild-type suggesting that the phenotypes observed were not due to defective cell wall deposition. This contrasts with *U. maydis* where septin null mutants grown at a restrictive temperature showed a distinctly altered morphology associated with a thickening of the cell wall in the middle of the cell. Similarly, in *C. albicans*, cell wall deposition is perturbed in the absence of *cdc10* or *cdc11*. Taken together these results suggest that *N. crassa*, unlike *U. maydis* and *C. albicans*, does not share the strict requirement for septins in guiding the localisation of the cell wall synthesis machinery.

Given the similarity of the phenotypes for the *cdc-3*, *cdc-10*, *cdc-11*, and *cdc-12* deletion mutants it is likely that these core septins form a heteromeric complex whose function depends on the presence of these four septins. However, the less severe phenotype observed for the *Δcdc-10* mutant suggests the role played by different septins in the assembly or function of a septin complex varies. Indeed, analysis of double mutants lacking two of the core septins in different combinations revealed an exacerbation of phenotypic defects compared to single deletion mutants, suggesting that some septin function is non-overlapping. It has been shown that in *S. cerevisiae* Cdc10 is phosphorylated by Cla4 and that Cdc10 is thought to link polymeric septin rods together (Weirich et al., 2008), whereas Cdc3 is phosphorylated by the cyclin-dependent kinase Cdc28 and is thought to occupy a different part of the heteroctamer with different binding partners.

The distinct cell polarity defects in *N. crassa* core septins null mutants are reminiscent of the aberrant branching patterns observed in septin deletion strains of *A.*

nidulans, and *A. gossypii* (Helfer and Gladfelter, 2006; Lindsey et al., 2010a). We observed an increased number of germ tubes emerging from conidia and the formation of multiple CATs during cell fusion whereas typically only one CAT is formed per germling in the wild type (Roca et al., 2005). These findings suggest that septins influence the maintenance and fidelity of the cell polarity machinery presumably by constraining and corralling this machinery to distinct locations on the plasma membrane, in keeping with the known function of septins functioning as a molecular boundary. The absence of a functional septin complex could feasibly alter the dynamics and/or localisation of important polarity components causing multiple germ tube and/or CAT emergence. Multiple bud emergence has been described in certain *S. cerevisiae* septin mutants (Longtine et al., 2000) and has been ascribed to a failure to successfully corral the polarity machinery.

Although none of the core septins are essential in *N. crassa*, disruption of these genes singly or in combination produces pronounced morphological defects such as misshapen, wider germ tubes that are swollen at the tip. In *C. albicans*, deletion of either of the two non-essential core septins *cdc10* and *cdc11* produced hyphae that appeared as the wild-type but grew with a greater degree of curvature. In *N. crassa*, based on calcofluor white staining, the morphological defects do not appear to stem from altered cell wall deposition. These morphological changes are therefore likely caused by defects in targeted secretion. Septins are known to interact with the exocyst and polarisome in *S. cerevisiae* (Orlando et al., 2011), and, as such, it is possible that these components are mislocalised or improperly regulated in *N. crassa* in the absence of core septins.

Septation in *N. crassa* initially involves the assembly of a CAR followed by septum formation and subsequent ingrowth, but does not result in complete cytokinesis and cell separation (Berepiki et al., 2010; Calvert et al., 2011). *N. crassa* core septins are involved in but are not essential for septation. Septa form in core septin null mutants, albeit at a reduced rate, and have a similar appearance to those found in the wild-type as shown by calcofluor

white staining. The involvement of core septins in septation is unsurprising given their known roles in cytokinesis in other fungi (Hartwell, 1971; Wu et al., 2010). *Saccharomyces cerevisiae* has a strict requirement for core septins to form septa and complete cytokinesis, whereas in *A. nidulans*, *A. gossypii*, *C. albicans* and *S. pombe* core septin mutants septa are still formed but in some instances they appear abnormal (Berlin et al., 2003; Helfer and Gladfelter, 2006; Lindsey et al., 2010a; Tasto et al., 2003; Warenda and Konopka, 2002). As with other phenotypic behaviour, *N. crassa Δcdc-10* mutants did not display as severe a septation defect as *cdc-3*, *cdc-11*, and *cdc-12* deletion strains again suggesting that it has a slightly different role to other core septins in complex formation.

The marked defect in cell separation during conidiation is in sharp contrast to the relatively mild defect in septation in *N. crassa* core septin deletion mutants. The majority of conidia in *N. crassa* are formed by macroconidiation which involves the formation of specialised aerial hyphae (conidiophores) and the subsequent formation of proconidial chains by repeated apical budding followed by sepatation between proconidia and their separation into spores (Springer and Yanofsky, 1989). *Neurospora crassa* core septin deletion mutants produce chains of unseparated conidia which suggests that CAR contraction and cell wall/plasma membrane ingrowth fails to occur between proconidia. A role for septins in spore formation has been reported in *A. nidulans* and *C. neoformans*. In these organisms the production of the specialised spore-forming structure, a conidiophore or basidium, respectively, is perturbed rather than the separation of spores. These differences are most likely due to differences in the sequence of events during macroconidium-formation in *N. crassa* compared to *A. nidulans* and *C. neoformans*. In the latter two organisms, septins are probably necessary for the initial cytokinetic events during the morphogenesis of the spore-forming structure and failure to undergo cytokinesis terminates the process. A fraction of cytokinetic events during spore-formation are successful hence the production of

separated spores albeit at a reduced rate (Kozubowski and Heitman, 2010; Lindsey et al., 2010a).

All of the *N. crassa* septins were labelled by integrating GFP at the endogenous locus of the respective genes, with the exception of ASP-2, which I was unable to visualise either by either integration of knock-in cassette or overexpression. Due to the weak fluorescence of GFP-ASP-1 we used an overexpression fusion construct controlled by the *ccg-1* promoter. In keeping with a previous proposition (Lindsey and Momany, 2006), septin localisation fell into 3 patterns: localisation to partition as septin rings, localisation to foci of new growth as caps and bar-like structures, and cytosolic localisation as loops and fibres. All septins localised as a ring and were all present at hyphal tips as has been shown for other fungal septins. However, at the tips of germ tubes and CATs we observed three specific patterns of septin localisation: a cap formed by CDC-3 and CDC-12, a band of bar-like structures formed by CDC-10 and CDC-11, and an extended cap formed by ASP-1. These structures/patterns marked the site of germ tube emergence prior to outgrowth and persisted during tip extension. I did not observe the formation of septin rings from these tip-associated complexes as has been found in *A. gossypii*. This is the first report demonstrating the co-existence of different patterns of septin localisation at a hyphal tip. It is possible that the different patterns observed represent different functional roles for septins in maintaining and/or regulating the tip growth apparatus. The presence of septins at the hyphal tip is consistent with their proposed roles as scaffold and boundaries at the plasma membrane. Interestingly, in *C. albicans* the exact pattern of septin localisation at hyphal tips is determined by the cell type; a diffuse band of Cdc10-GFP is found at the tips of germ tubes whereas in pseudohyphae the band is absent and instead Cdc10-GFP is organised into a cap. In this instance different patterns of septin organisation are due to changes in septin regulation during the elaboration of different hyphal types (Warenda and Konopka, 2002).

Another possible role for septins in *N. crassa* comes from their localisation during CAT-mediated cell fusion. During cell fusion, septin localisation at CAT tips is identical to that of germ tubes. Once contact between two CATs is made septins became enriched at the tip apex then were gradually rearranged to form the perimeter of the nascent fusion pore, suggesting that they participate in the fusion process.

In addition to rings, caps, and bar-like structures, we observed septins organised into loops and fibres. The dense septins loops, ~ 1 µM in diameter, were in ungerminated conidia expressing CDC-11-GFP and a similar structure has been observed in *A. nidulans*, *A. gossypii*, *A. fumigatus* and in mammalian cells treated anti-actin drugs (Kinoshita et al., 2002). In *A. gossypii*, an increase in the number of loops was associated with growth, arrest, heat shock, and treatment with anti-actin drugs led the authors to suggest that these structures are self-assembling reservoirs of septins that form above a certain concentration of free subunits (DeMay et al., 2009). In *N. crassa*, these loops are not observed in the presence of other HO septin structures or during growth and, as such, it is likely they serve a similar function.

Septin fibres were commonly observed in cells expressing CDC-11-GFP or GFP-CDC-10 but not with other septin-GFP fusions. Septin fibres are present in a range of mammalian cells and have been recently found in *A. nidulans*, *A. gossypii*, *A. fumigatus*, *C. neoformans*, *U. maydis*, and chlamydiospores of *C. albicans* (Alvarez-Tabares and Perez-Martin, 2010; DeMay et al., 2009; Hernandez-Rodriguez et al., 2012; Juvvadi et al., 2011; Kaufmann and Philippsen, 2009; Kozubowski and Heitman, 2010; Martin et al., 2005d). In mammalian cells septin fibres colocalise with actin stress filaments and/or microtubules and in *C. neoformans* and *U. maydis* partially colocalise with microtubules, although colocalisation of fibres with actin cables was not carried out in these latter two organisms (Alvarez-Tabares and Perez-Martin, 2010; Kozubowski and Heitman, 2010). My attempts to generate strains co-expressing GFP-tagged septins and βtub-mCherry or Lifeact-tagRFPT

were unsuccessful due to the resultant gross perturbation of cell morphology, inadequate co-expression, and mislocalisation.

The septin fibres observed in *N. crassa* appear very similar to those present in *A. nidulans* and *A. fumigatus*; they were 0.2-0.5 µM thick and 0.5-5 µM long, and are associated with the plasma membrane and found in the cytosol. When we overexpressed GFP-CDC-10 we saw a drastic increase in the number of fibres. The accumulation in septin fibres upon overexpression of GFP-CDC-10 suggests that these fibres could serve as storage reservoirs of free GFP-CDC-10 monomers, similar to the proposed role of the septin loops found in quiescent regions/cells. Alternatively, based on the absence of septin fibres in budding yeast and the finding that yeast septin mutants do not produce extra growth foci, it has been proposed that septin fibres may have a role in suppressing new growth (Hernandez-Rodriguez et al., 2012). Indeed, the presence of fibres in non-growing regions and cells in *N. crassa* supports the notion that fibres are storage reservoirs. However, as overexpression of GFP-CDC-10 in *N. crassa* does not supress germination or germ tube emergence, this implies that fibres are not a growth repressing structure.

To investigate the relationship of the various septins in the assembly of HO structures I analysed the ability of CDC-11-GFP or CDC-12-GFP to form rings and other structures in null mutants. Typically in *S. cerevisiae*, *A. nidulans*, and *A. gossypii* the absence of a single core septin abrogates the formation of HO structures (Byers and Goetsch, 1976; DeMay et al., 2009; Kim et al., 1991; Lindsey et al., 2010a) whereas in *U. maydis*, *C. albicans*, and *S. pombe* these structures persist in septin null mutants (Alvarez-Tabares and Perez-Martin, 2010; An et al., 2004; Warenda and Konopka, 2002). I found that in *N. crassa* CDC-3, CDC-11, and CDC-12 are required for ring formation and proper localisation of septin complexes; in their absence the only fluorescence observed was cytoplasmic. Interestingly, although CDC-11-GFP and CDC-12-GFP display different patterns of organisation in the tip growth apparatus, it appears that CDC-11 requires CDC-

12 for proper tip localisation and vice versa, CDC-12 requires CDC-11 for proper tip localisation. Conversely, deletion of *cdc-10*, *asp-1*, or *asp-2* did not impede the formation and localisation of septin complexes. From these findings it can be expected that ASP-1 and possibly ASP-2 (see Discussion below) are "peripheral" septins that could modify or influence septin complexes but are not core constituents as has been demonstrated for Shs1 (Garcia et al., 2011). Interestingly, *A. nidulans* mutants lacking AspE, the ASP-1 ortholog showed a marked reduction of septin fibres while other structures are mostly unaffected, suggesting a specific role for this septin in fibre assembly. The ability of *cdc-10* null mutants to form HO structures is consistent with models of septin polymer formation in *S. cerevisiae*, where Cdc10 links septin oligomers together (McMurray et al., 2011). Similarly, in *U. maydis* the CDC-10 ortholog, Sep4, is not required to form HO assemblies.

Septins have been shown to associate with actin in mammalian cells. To determine the effects of septin deletion on the actin cytoskeleton we generated a *cdc-11* null mutant expressing GFP-Lifeact, which is a marker for F-actin (Berepiki et al., 2010; Riedl et al., 2008). F-actin structures appeared as normal although due to the polarity defects of the *cdc-11* null mutant, F-actin accumulated at the tip and in the spore body.

I was able to efficiently purify septin complexes from *N. crassa* cell extracts using five of the six septins as the target. The failure to detect expression of V5-HAT-tagged ASP-2 in western blots or in IP experiments, the lack of a phenotype for the *asp-2* null mutant, the inability to express GFP fusions for ASP-2 by knock-in or by overexpression, and the failure to detect ASP-2 in subsequent IP of various septins, indicate that the *asp-2* ORF probably does not encode a *bona fide* septin. Septin complexes were isolated in a convenient, rapid dynabead-based method with almost a complete absence of contaminants, confirming that the V5 epitope is highly efficacious for protein purification from *N. crassa*.

The composition of the purified *N. crassa* septin complex is similar to that obtained for *S. cerevisiae* and *C. albicans*; the septin oligomer is composed of CDC-3, CDC-10, CDC-

11, and CDC-12 with ASP-1 present as an associating partner but is probably not an integral component of the septin complex. It is possible that ASP-1 performs a similar regulatory role to Shs1 in *S. cerevisiae*, which binds to and interacts with the septin complex. It has been shown that Shs1 is phosphorylated (Mortensen et al., 2002) and that it plays a role in regulating the formation and stability of the septin ring complex (Garcia et al., 2011).

Chapter 5:

Final discussion

5.1 Concluding remarks and outlook

Lifeact-FP gave clear and robust labelling of F-actin in *N. crassa* without any detectable toxic side-effects and provided novel insights into the dynamic reorganisation and polarisation of the actin cytoskeleton during germ tube formation and elongation, and CAT-mediated cell fusion. Lifeact constructs clearly labelled actin patches, cables and rings, and revealed a direct association of F-actin structures with sites of cell polarisation and active tip growth. It is likely that Lifeact will become an invaluable tool for studying the regulation, dynamics and organisation of the fungal actin cytoskeleton in the future. The results of this study shed some light on the function of MYO-5 in *N. crassa*; MYO-5 associated with growing regions of cells, is involved in CAT fusion and participates in the correct organisation of the actin cytoskeleton. Due to the reduction in the frequency of rapid patch movements in the absence of *myo-5*, it is possible that MYO-5 contributes to the translocation of actin patches along actin cables.

Several important aspects of actin organisation and dynamics remain poorly understood in filamentous fungi. The functional roles of patch transport within hyphae need to be defined. In both *N. crassa* and *A. nidulans*, actin patches undergo rapid linear transport. Although I have provided some evidence for the involvement of MYO-5 in this process, the purpose of this transport, and additional motors involved have not been determined. An analysis of Lifeact-FP dynamics in motor protein null mutants (myosins, kinesins, and dynein) will be important to answer this question.

The finding that the tip growth apparatus is highly structured and changes over time is most interesting. Rearrangements in the tip growth apparatus are often observed during changes in growth rate or developmental state, but a causal, mechanistic relationship has not been established.

Additionally, the precise roles of F-actin in the Spk need to be determined. The concentration of F-actin within the core of the Spk probably represents a fourth type of

higher-order F-actin structure in filamentous fungi. F-actin is thought to be important for the short range targeting of secretory vesicles from the Spk to the plasma membrane. However, it may also have additional roles such as maintaining the structural integrity of the Spk and/or regulating Spk movement within the hyphal tip. The generation of temperature-sensitive ABPs combined with live-cell imaging of Spk dynamics under permissive and repressive conditions could be carried out to address the functional roles of actin in the Spk.

Six septins are present in the genome of *N. crassa*. None of the *N. crassa* septins are essential for cell viability, however, analysis of null mutants revealed that septins limit germ tube emergence and are required for correct patterns of morphogenesis and conidiation. The absence of the *asp-2* gene, which on the basis of phylogenetic studies has been identified as a septin (Pan et al., 2007), failed to cause a detectable phenotype and it was not possible to detect or tag the putative ASP-2 protein, suggesting that this ORF is not a bona fide septin. All septins localised as a ring and were all present at hyphal tips as has been shown for other fungal septins. Bars, collars and fibres were also formed by septins. Interestingly, the tips of germ tubes and CATs, septins displayed three specific patterns of localisation. It is possible that the different patterns observed represent different function roles for septins in maintaining and/or regulating the tip growth apparatus. Isolation and mass spectrometry of purified septin complexes demonstrated that the septin complex consists predominantly of CDC-3, CDC-10, CDC-11 and CDC-12. Immunoprecipitation of ASP-1 revealed that this septin interacts with the core septin complex.

The failure to generate healthy *N. crassa* strains expressing GFP-tagged septins and RFP-tagged Lifeact, tubulin or other septins precluded any co-labelling microscopic analysis, which will be important to determine septin fibre organisation and the sequence of protein recruitment during septation. Alternative RFPs to tagRFP-T and mCherry might resolve this impediment; alternatively, GFP and RFP could be replaced by CFP and YFP.

Due to the pronounced cell polarity defects in septin null mutants, it will be interesting to determine if the localisation and dynamics of polarisome and exocyst components are altered in the absence of a functional septin complex. This question could be addressed by the introduction of GFP-tagged markers, such as SPA-2-GFP and GFP-SEC-3, into septin null mutants followed by FRAP analysis to determine if the mobility of these markers is increased.

Bibliography

Abenza, J.F., A. Pantazopoulou, J.M. Rodriguez, A. Galindo, and M.A. Penalva. 2009. Long-distance movement of *Aspergillus nidulans* early endosomes on microtubule tracks. *Traffic*. 10:57-75.

Adams, A.E., and J.R. Pringle. 1984. Relationship of actin and tubulin distribution to bud growth in wild-type and morphogenetic mutant *Saccharomyces cerevisiae*. *J Cell Biol*. 98:934-945.

Aghamohammadzadeh, S., and K.R. Ayscough. 2009. Differential requirements for actin during yeast and mammalian endocytosis. *Nat Cell Biol*. 11:1039-1042.

Aizawa, H., M. Sameshima, and I. Yahara. 1997. A green fluorescent protein-actin fusion protein dominantly inhibits cytokinesis, cell spreading, and locomotion in *Dictyostelium*. *Cell Struct Funct*. 22:335-345.

Altschuler, S.J., E. Marco, R. Wedlich-Soldner, R. Li, and L.F. Wu. 2007. Endocytosis optimizes the dynamic localization of membrane proteins that regulate cortical polarity. *Cell*. 129:411-422.

Alvarez-Tabares, I., and J. Perez-Martin. 2010. Septins from the phytopathogenic fungus *Ustilago maydis* are required for proper morphogenesis but dispensable for virulence. *PLoS One*. 5:e12933.

An, H., J.L. Morrell, J.L. Jennings, A.J. Link, and K.L. Gould. 2004. Requirements of fission yeast septins for complex formation, localization, and function. *Mol Biol Cell*. 15:5551-5564.

Araujo-Bazan, L., M.A. Penalva, and E.A. Espeso. 2008. Preferential localization of the endocytic internalization machinery to hyphal tips underlies polarization of the actin cytoskeleton in *Aspergillus nidulans*. *Mol Microbiol*. 67:891-905.

Araujo-Palomares, C.L., E. Castro-Longoria, and M. Riquelme. 2007. Ontogeny of the Spitzenkorper in germlings of *Neurospora crassa*. *Fungal Genet Biol*. 44:492-503.

Araujo-Palomares, C.L., M. Riquelme, and E. Castro-Longoria. 2009. The polarisome component SPA-2 localizes at the apex of *Neurospora crassa* and partially colocalizes with the Spitzenkorper. *Fungal Genet Biol*. 46:551-563.

Asakura, T., T. Sasaki, F. Nagano, A. Satoh, H. Obaishi, H. Nishioka, H. Imamura, K. Hotta, K. Tanaka, H. Nakanishi, and Y. Takai. 1998. Isolation and characterization of a novel actin filament-binding protein from *Saccharomyces cerevisiae*. *Oncogene*. 16:121-130.

Ayad-Durieux, Y., P. Knechtle, S. Goff, F. Dietrich, and P. Philippsen. 2000. A PAK-like protein kinase is required for maturation of young hyphae and septation in the filamentous ascomycete *Ashbya gossypii*. *J Cell Sci*. 113 Pt 24:4563-4575.

Ayscough, K.R. 2000. Endocytosis and the development of cell polarity in yeast require a dynamic F-actin cytoskeleton. *Curr Biol*. 10:1587-1590.

Ayscough, K.R., D.M. Gheorghe, S. Aghamohammadzadeh, L.I.S.D. Rooij, E.G. Allwood, and S.J. Winder. 2008. Interactions between the yeast SM22 homologue Scp1 and actin demonstrate the importance of actin bundling in endocytosis. *J Biol Chem*. 283:15037-15046.

Ayscough, K.R., J. Stryker, N. Pokala, M. Sanders, P. Crews, and D.G. Drubin. 1997. High rates of actin filament turnover in budding yeast and roles for actin in establishment and maintenance of cell polarity revealed using the actin inhibitor latrunculin A. *J Cell Biol*. 137:399-416.

Balguerie, A., P. Sivadon, M. Bonneu, and M. Aigle. 1999. Rvs167p, the budding yeast homolog of amphiphysin, colocalizes with actin patches. *J Cell Sci*. 112:2529-2537.

Barja, F., M.L. Chappuis, and G. Turian. 1993. Differential effects of anticytoskeletal compounds on the localization and chemical patterns of actin in germinating conidia of *Neurospora crassa*. *FEMS Microbiol Lett*. 107:261-266.

Barja, F., B.N. Thi, and G. Turian. 1991. Localization of actin and characterization of its isoforms in the hyphae of *Neurospora crassa*. *FEMS Microbiol Lett*. 61:19-24.

Barral, Y., V. Mermall, M.S. Mooseker, and M. Snyder. 2000. Compartmentalization of the cell cortex by septins is required for maintenance of cell polarity in yeast. *Mol Cell Biol*. 5:841-851.

Bartnicki-Garcia, S. 2002. Hyphal tip growth: outstanding questions. *In* Molecualr Biology of Fungal Development. H.D. Osiewaqcz, editor. Marcel Dekker, New York. 29-58.

Bartnicki-Garcia, S., C.E. Bracker, G. Gierz, R. Lopez-Franco, and H. Lu. 2000. Mapping the growth of fungal hyphae: orthogonal cell wall expansion during tip growth and the role of turgor. *Biophysical journal*. 79:2382-2390.

Bartnicki-Garcia, S., F. Hergert, and G. Gierz. 1989. Computer-simulation of fungal morphogenesis and the mathematical basis for hyphal (tip) growth. *Protoplasma*. 153:46-57.

Berepiki, A., A. Lichius, and N.D. Read. 2011. Actin organization and dynamics in filamentous fungi. *Nat Rev Microbiol*. 9:876-887.

Berepiki, A., A. Lichius, J.Y. Shoji, J. Tilsner, and N.D. Read. 2010. F-actin dynamics in *Neurospora crassa*. *Eukaryot Cell*. 9:547-557.

Berlin, A., A. Paoletti, and F. Chang. 2003. Mid2p stabilizes septin rings during cytokinesis in fission yeast. *J Cell Biol*. 160:1083-1092.

Bertin, A., M.A. McMurray, P. Grob, S.S. Park, G. Garcia, 3rd, I. Patanwala, H.L. Ng, T. Alber, J. Thorner, and E. Nogales. 2008. *Saccharomyces cerevisiae* septins: supramolecular organization of heterooligomers and the mechanism of filament assembly. *Proc Natl Acad Sci U S A*. 105:8274-8279.

Bertrand, E., P. Chartrand, M. Schaefer, S.M. Shenoy, R.H. Singer, and R.M. Long. 1998. Localization of ASH1 mRNA particles in living yeast. *Mol Cell*. 2:437-445.

Borkovich, K.A., L.A. Alex, O. Yarden, M. Freitag, G.E. Turner, N.D. Read, S. Seiler, D. Bell-Pedersen, J. Paietta, N. Plesofsky, M. Plamann, M. Goodrich-Tanrikulu, U. Schulte, G. Mannhaupt, F.E. Nargang, A. Radford, C. Selitrennikoff, J.E. Galagan, J.C. Dunlap, J.J. Loros, D. Catcheside, H. Inoue, R. Aramayo, M. Polymenis, E.U. Selker, M.S. Sachs, G.A. Marzluf, I. Paulsen, R. Davis, D.J. Ebbole, A. Zelter, E.R. Kalkman, R. O'Rourke, F. Bowring, J. Yeadon, C. Ishii, K. Suzuki, W. Sakai, and R. Pratt. 2004. Lessons from the genome sequence of *Neurospora crassa*: tracing the path from genomic blueprint to multicellular organism. *Microbiol Mol Biol Rev*. 68:1-108.

Bourett, T.M., and R.J. Howard. 1991. Ultrastructural immunolocalization of actin in a fungus. *Protoplasma*. 163:199-202.

Boyce, K.J., H. Chang, C.A. D'Souza, and J.W. Kronstad. 2005. An *Ustilago maydis* septin is required for filamentous growth in culture and for full symptom development on maize. *Eukaryot Cell*. 4:2044-2056.

Boyce, K.J., M.J. Hynes, and A. Andrianopoulos. 2003. Control of morphogenesis and actin localization by the *Penicillium marneffei* RAC homolog. *J Cell Sci*. 116:1249-1260.

Bracker, C.E., D.J. Murphy, and R. Lopez-Franco. 1997. Laser beam micromanipulation of cell morphogenesis in growing fungal hyphae. *In* Functional Imaging of Optical Manipulation of Living Cells. Proceedings of SPIE. Vol. 2983. D.L. Farkas and B.J. Tromberg, editors. International Society of Optical Engineering, Bellingham, Washington, USA. 67-80.

Bretscher, A. 2003. Polarized growth and organelle segregation in yeast: the tracks, motors, and receptors. *J Cell Biol*. 160:811-816.

Byers, B., and L. Goetsch. 1976. A highly ordered ring of membrane-associated filaments in budding yeast. *J Cell Biol*. 69:717-721.

Calvert, M.E., G.D. Wright, F.Y. Leong, K.H. Chiam, Y. Chen, G. Jedd, and M.K. Balasubramanian. 2011. Myosin concentration underlies cell size-dependent scalability of actomyosin ring constriction. *J Cell Biol*. 195:799-813.

Casamayor, A., and M. Snyder. 2003. Molecular dissection of a yeast septin: distinct domains are required for septin interaction, localization, and function. *Mol Cell Biol*. 23:2762-2777.

Chaga, G., D.E. Bochkariov, G.G. Jokhadze, J. Hopp, and P. Nelson. 1999. Natural poly-histidine affinity tag for purification of recombinant proteins on cobalt(II)-carboxymethylaspartate crosslinked agarose. *J Chrom. A*. 864:247-256.

Chang, F., D. Drubin, and P. Nurse. 1997. cdc12p, a protein required for cytokinesis in fission yeast, is a component of the cell division ring and interacts with profilin. *J Cell Biol*. 137:169-182.

Chesarone, M.A., A.G. DuPage, and B.L. Goode. 2010. Unleashing formins to remodel the actin and microtubule cytoskeletons. *Nat Rev Mol Cell Biol*. 11:62-74.

Chiu, W.L., Y. Niwa, W. Zeng, T. Hirano, H. Kobayashi, and J. Sheen. 1996. Engineered GFP as a vital reporter in plants. *Curr Biol*. 6:325-330.

Cooper, J.A. 1987. Effects of cytochalasin and phalloidin on actin. *J Cell Biol*. 105:1473-1478.

Coue, M., S.L. Brenner, I. Spector, and E.D. Korn. 1987. Inhibition of actin polymerization by latrunculin A. *FEBS letters*. 213:316-318.

Dagdas, Y.F., K. Yoshino, G. Dagdas, L.S. Ryder, E. Bielska, G. Steinberg, and N.J. Talbot. 2012. Septin-mediated plant cell invasion by the rice blast fungus, *Magnaporthe oryzae*. *Science*. 336:1590-1595.

Davis, R.H. 2000. *Neurospora* : contributions of a model organism. Oxford University Press, New York. xii, 333 p. pp.

Davis, R.H., and D.D. Perkins. 2002. *Neurospora*: a model of model microbes. *Nat Rev Genet*. 3:397-403.

Delgado-Alvarez, D.L., O.A. Callejas-Negrete, N. Gomez, M. Freitag, R.W. Roberson, L.G. Smith, and R.R. Mourino-Perez. 2010. Visualization of F-actin localization and dynamics with live cell markers in *Neurospora crassa*. *Fungal Genet Biol*. 47:573-586.

DeMay, B.S., X. Bai, L. Howard, P. Occhipinti, R.A. Meseroll, E.T. Spiliotis, R. Oldenbourg, and A.S. Gladfelter. 2011. Septin filaments exhibit a dynamic, paired organization that is conserved from yeast to mammals. *J Cell Biol*. 193:1065-1081.

DeMay, B.S., R.A. Meseroll, P. Occhipinti, and A.S. Gladfelter. 2009. Regulation of distinct septin rings in a single cell by Elm1p and Gin4p kinases. *Mol Biol Cell*. 20:2311-2326.

DeMay, B.S., R.A. Meseroll, P. Occhipinti, and A.S. Gladfelter. 2010. Cellular requirements for the small molecule forchlorfenuron to stabilize the septin cytoskeleton. *Cytoskeleton (Hoboken)*. 67:383-399.

Dobbelaere, J., and Y. Barral. 2004. Spatial coordination of cytokinetic events by compartmentalization of the cell cortex. *Science*. 305:393-396.

Dominguez, R., and K.C. Holmes. 2011. Actin structure and function. *Annual review of biophysics*. 40:169-186.

Doyle, A., R. Martin-Garcia, A.T. Coulton, S. Bagley, and D.P. Mulvihill. 2009. Fission yeast Myo51 is a meiotic spindle pole body component with discrete roles during cell fusion and spore formation. *J Cell Sci*. 122:4330-4340.

Doyle, T., and D. Botstein. 1996. Movement of yeast cortical actin cytoskeleton visualized *in vivo*. *Proc Natl Acad Sci U S A*. 93:3886-3891.

Ebbole, D., and M.S. Sachs. 1990. A simple method to obtain microconidia. *Fungal Genet Newsl*. 37:17-18.

Epp, E., A. Walther, G. Lepine, Z. Leon, A. Mullick, M. Raymond, J. Wendland, and M. Whiteway. 2010. Forward genetics in *Candida albicans* that reveals the Arp2/3 complex is required for hyphal formation, but not endocytosis. *Mol Microbiol*. 75:1182-1198.

Era, A., M. Tominaga, K. Ebine, C. Awai, C. Saito, K. Ishizaki, K.T. Yamato, T. Kohchi, A. Nakano, and T. Ueda. 2009. Application of Lifeact reveals F-actin dynamics in *Arabidopsis thaliana* and the liverwort, *Marchantia polymorpha*. *Plant Cell Physiol*. 50:1041-1048.

Evangelista, M., K. Blundell, M.S. Longtine, C.J. Chow, N. Adames, J.R. Pringle, M. Peter, and C. Boone. 1997. Bni1p, a yeast formin linking Cdc42p and the actin cytoskeleton during polarized morphogenesis. *Science*. 276:118-122.

Evangelista, M., D. Pruyne, D.C. Amberg, C. Boone, and A. Bretscher. 2002. Formins direct Arp2/3-independent actin filament assembly to polarize cell growth in yeast. *Nat Cell Biol*. 4:260-269.

Fang, X., J. Luo, R. Nishihama, C. Wloka, C. Dravis, M. Travaglia, M. Iwase, E.A. Vallen, and E. Bi. 2010. Biphasic targeting and cleavage furrow ingression directed by the tail of a myosin II. *J Cell Biol*. 191:1333-1350.

Fehrenbacher, K.L., I.R. Boldogh, and L.A. Pon. 2003. Taking the A-train: actin-based force generators and organelle targeting. *Trends Cell Biol*. 13:472-477.

Fischer-Parton, S., R.M. Parton, P.C. Hickey, J. Dijksterhuis, H.A. Atkinson, and N.D. Read. 2000. Confocal microscopy of FM4-64 as a tool for analysing endocytosis and vesicle trafficking in living fungal hyphae. *J Microsc*. 198:246-259.

Frazier, J.A., M.L. Wong, M.S. Longtine, J.R. Pringle, M. Mann, T.J. Mitchison, and C. Field. 1998. Polymerization of purified yeast septins: evidence that organized filament arrays may not be required for septin function. *J Cell Biol*. 143:737-749.

Freitag, M., P.C. Hickey, N.B. Raju, E.U. Selker, and N.D. Read. 2004. GFP as a tool to analyze the organization, dynamics and function of nuclei and microtubules in *Neurospora crassa*. *Fungal Genet Biol*. 41:897-910.

Fuchs, F., H. Prokisch, W. Neupert, and B. Westermann. 2002. Interaction of mitochondria with microtubules in the filamentous fungus *Neurospora crassa*. *J Cell Sci*. 115:1931-1937.

Fuchs, U., I. Manns, and G. Steinberg. 2005. Microtubules are dispensable for the initial pathogenic development but required for long-distance hyphal growth in the corn smut fungus *Ustilago maydis*. *Mol Biol Cell*. 16:2746-2758.

Garcia, G., 3rd, A. Bertin, Z. Li, Y. Song, M.A. McMurray, J. Thorner, and E. Nogales. 2011. Subunit-dependent modulation of septin assembly: budding yeast septin Shs1 promotes ring and gauze formation. *J Cell Biol*. 195:993-1004.

Garrill, A., and S. Suei. 2008. An F-actin-depleted zone is present at the hyphal tip of invasive hyphae of *Neurospora crassa*. *Protoplasma*. 232:165-172.

Gietz, R.D., and R.A. Woods. 2001. Genetic transformation of yeast. *Biotechniques*. 30:816-820, 822-816, 828 passim.

Girbardt, M. 1957. Der Spitzenkörper von *Polysticus versicolor*. *Planta*. 50:47-59.

Gladfelter, A.S. 2006. Nuclear anarchy: asynchronous mitosis in multinucleated fungal hyphae. *Curr Opin Microbiol*. 9:547-552.

Gladfelter, A.S., J.J. Moskow, T.R. Zyla, and D.J. Lew. 2001. Isolation and characterization of effector-loop mutants of CDC42 in yeast. *Mol Biol Cell*. 12:1239-1255.

Hall, P.A., S.E.H. Russell, and J.R. Pringle. 2008. The septins. John Wiley-Blackwell, Oxford ; Hoboken, NJ. ix, 370 p., 378 p. of plates pp.

Harispe, L., C. Portela, C. Scazzocchio, M.A. Penalva, and L. Gorfinkiel. 2008. Ras GTPase-activating protein regulation of actin cytoskeleton and hyphal polarity in *Aspergillus nidulans*. *Eukaryot Cell*. 7:141-153.

Harris, S.D. 2006. Cell polarity in filamentous fungi. *Int Rev Cytol*. 251:41-77.

Harris, S.D. 2011. Cdc42/Rho GTPases in fungi: variations on a common theme. *Mol Microbiol*. 79:1123-1127.

Harris, S.D., L. Hamer, K.E. Sharpless, and J.E. Hamer. 1997. The *Aspergillus nidulans* sepA gene encodes an FH1/2 protein involved in cytokinesis and the maintenance of cellular polarity. *EMBO J*. 16:3474-3483.

Harris, S.D., and M. Momany. 2004. Polarity in filamentous fungi: moving beyond the yeast paradigm. *Fungal Genet Biol*. 41:391-400.

Harris, S.D., J.L. Morrell, and J.E. Hamer. 1994. Identification and characterization of *Aspergillus nidulans* mutants defective in cytokinesis. *Genetics*. 136:517-532.

Harris, S.D., N.D. Read, R.W. Roberson, B. Shaw, S. Seiler, M. Plamann, and M. Momany. 2005. Polarisome meets spitzenkorper: microscopy, genetics, and genomics converge. *Eukaryot Cell*. 4:225-229.

Hartwell, L.H. 1971. Genetic control of the cell division cycle in yeast. IV. Genes controlling bud emergence and cytokinesis. *Experimental cell research*. 69:265-276.

Heath, I.B., G. Gupta, and S. Bai. 2000. Plasma membrane-adjacent actin filaments, but not microtubules, are essential for both polarization and hyphal tip morphogenesis in *Saprolegnia ferax* and *Neurospora crassa*. *Fungal Genet Biol*. 30:45-62.

Helfer, H., and A.S. Gladfelter. 2006. AgSwe1p regulates mitosis in response to morphogenesis and nutrients in multinucleated *Ashbya gossypii* cells. *Mol Biol Cell*. 17:4494-4512.

Hernandez-Rodriguez, Y., S. Hastings, and M. Momany. 2012. The septin AspB in *Aspergillus nidulans* forms bars and filaments and plays roles in growth emergence and conidiation. *Eukaryot Cell*. 11:311-323.

Hickey, P.C., D. Jacobson, N.D. Read, and N.L. Louise Glass. 2002. Live-cell imaging of vegetative hyphal fusion in *Neurospora crassa*. *Fungal Genet Biol*. 37:109-119.

Honda, S., and E.U. Selker. 2009. Tools for fungal proteomics: multifunctional neurospora vectors for gene replacement, protein expression and protein purification. *Genetics*. 182:11-23.

Howard, R.J. 1981. Ultrastructural analysis of hyphal tip cell growth in fungi: Spitzenkorper, cytoskeleton and endomembranes after freeze-substitution. *J Cell Sci*. 48:89-103.

Hu, Q., W.J. Nelson, and E.T. Spiliotis. 2008. Forchlorfenuron alters mammalian septin assembly, organization, and dynamics. *J Biol Chem*. 283:29563-29571.

Hubbard, M.A., and S.G. Kaminskyj. 2008. Rapid tip-directed movement of Golgi equivalents in growing *Aspergillus nidulans* hyphae suggests a mechanism for delivery of growth-related materials. *Microbiology*. 154:1544-1553.

Huckaba, T.M., A.C. Gay, L.F. Pantalena, H.C. Yang, and L.A. Pon. 2004. Live cell imaging of the assembly, disassembly, and actin cable-dependent movement of endosomes and actin patches in the budding yeast, *Saccharomyces cerevisiae*. *J Cell Biol*. 167:519-530.

Irelan, J., V. Miao, and E.U. Selker. 1993. Small scale DNA preps for *Neurospora crassa*. *Fungal Genet Newsl*. 40:24.

Ishibashi, K., K. Suzuki, Y. Ando, C. Takakura, and H. Inoue. 2006. Nonhomologous chromosomal integration of foreign DNA is completely dependent on MUS-53 (human Lig4 homolog) in *Neurospora*. *Proc Natl Acad Sci U S A*. 103:14871-14876.

Jin, Y., A. Sultana, P. Gandhi, E. Franklin, S. Hamamoto, A.R. Khan, M. Munson, R. Schekman, and L.S. Weisman. 2011. Myosin V transports secretory vesicles via a Rab GTPase cascade and interaction with the exocyst complex. *Dev Cell*. 21:1156-1170.

John, C.M., R.K. Hite, C.S. Weirich, D.J. Fitzgerald, H. Jawhari, M. Faty, D. Schlapfer, R. Kroschewski, F.K. Winkler, T. Walz, Y. Barral, and M.O. Steinmetz. 2007. The *Caenorhabditis elegans* septin complex is nonpolar. *EMBO J*. 26:3296-3307.

Johnson, E.S., and G. Blobel. 1999. Cell cycle-regulated attachment of the ubiquitin-related protein SUMO to the yeast septins. *J Cell Biol*. 147:981-994.

Jones, L.A., and P.E. Sudbery. 2010. Spitzenkorper, exocyst, and polarisome components in *Candida albicans* hyphae show different patterns of localization and have distinct dynamic properties. *Eukaryot Cell*. 9:1455-1465.

Jonsdottir, G.A., and R. Li. 2004. Dynamics of yeast myosin I: evidence for a possible role in scission of endocytic vesicles. *Curr Biol*. 14:1604-1609.

Jorde, S., A. Walther, and J. Wendland. 2011. The *Ashbya gossypii* fimbrin SAC6 is required for fast polarized hyphal tip growth and endocytosis. *Microbiol Res*. 166:137-145.

Justa-Schuch, D., S. Seiler, Y. Heilig, and C. Richthammer. 2010. Septum formation is regulated by the RHO4-specific exchange factors BUD3 and RGF3 and by the landmark protein BUD4 in *Neurospora crassa*. *Mol Microbiol*. 76:220-235.

Juvvadi, P.R., J.R. Fortwendel, L.E. Rogg, and W.J. Steinbach. 2011. Differential localization patterns of septins during growth of the human fungal pathogen *Aspergillus fumigatus* reveal novel functions. *Biochem Biophys Res Comm*. 405:238-243.

Kaksonen, M., Y. Sun, and D.G. Drubin. 2003. A pathway for association of receptors, adaptors, and actin during endocytic internalization. *Cell*. 115:475-487.

Kaksonen, M., C.P. Toret, and D.G. Drubin. 2005. A modular design for the clathrin- and actin-mediated endocytosis machinery. *Cell*. 123:305-320.

Kaneko, A., T. Umeyama, N. Hanaoka, B.C. Monk, Y. Uehara, and M. Niimi. 2004. Tandem affinity purification of the *Candida albicans* septin protein complex. *Yeast*. 21:1025-1033.

Kaufmann, A., and P. Philippsen. 2009. Of bars and rings: Hof1-dependent cytokinesis in multiseptated hyphae of *Ashbya gossypii*. *Mol Cell Biol*. 29:771-783.

Kemper, M., L. Mohlzahn, M. Lickfeld, C. Lang, S. Wahlisch, and H.P. Schmitz. 2011. A Bnr-like formin links actin to the spindle pole body during sporulation in the filamentous fungus *Ashbya gossypii*. *Mol Microbiol*. 80:1276-1295.

Kilmartin, J.V., and A.E. Adams. 1984. Structural rearrangements of tubulin and actin during the cell cycle of the yeast *Saccharomyces*. *J Cell Biol*. 98:922-933.

Kim, H.B., B.K. Haarer, and J.R. Pringle. 1991. Cellular morphogenesis in the *Saccharomyces cerevisiae* cell cycle: localization of the CDC3 gene product and the timing of events at the budding site. *J Cell Biol*. 112:535-544.

Kinoshita, M. 2003. Assembly of mammalian septins. *J Biol Chem*. 134:491-496.

Kinoshita, M., C.M. Field, M.L. Coughlin, A.F. Straight, and T.J. Mitchison. 2002. Self- and actin-templated assembly of mammalian septins. *Dev Cell*. 3:791-802.

Kinoshita, M., S. Kumar, A. Mizoguchi, C. Ide, A. Kinoshita, T. Haraguchi, Y. Hiraoka, and M. Noda. 1997. Nedd5, a mammalian septin, is a novel cytoskeletal component interacting with actin-based structures. *Genes & development*. 11:1535-1547.

Kitamoto, K., Y. Higuchi, J.Y. Shoji, and M. Arioka. 2009. Endocytosis is crucial for cell polarity and apical membrane recycling in the filamentous fungus *Aspergillus oryzae*. *Eukaryot Cell*. 8:37-46.

Knechtle, P., P. Philippsen, and J. Wendland. 2006. The SH3/PH domain protein AgBoi1/2 collaborates with the Rho-type GTPase AgRho3 to prevent nonpolar growth at hyphal tips of *Ashbya gossypii*. *Eukaryot Cell*. 5:1635-1647.

Koehli, M., P. Philippsen, V. Galati, K. Boudier, and R.W. Roberson. 2008. Growth-speed-correlated localization of exocyst and polarisome components in growth zones of *Ashbya gossypii* hyphal tips. *J Cell Sci*. 121:3878-3889.

Konopka, J.B., L.M. Douglas, and S.W. Martin. 2009. BAR Domain Proteins Rvs161 and Rvs167 contribute to *Candida albicans* endocytosis, morphogenesis, and virulence. *Infect Immun*. 77:4150-4160.

Kovar, D.R., J.R. Kuhn, A.L. Tichy, and T.D. Pollard. 2003. The fission yeast cytokinesis formin Cdc12p is a barbed end actin filament capping protein gated by profilin. *J Cell Biol*. 161:875-887.

Kovar, D.R., V. Sirotkin, and M. Lord. 2011. Three's company: the fission yeast actin cytoskeleton. *Trends Cell Biol*. 21:177-187.

Kovar, D.R., J.Q. Wu, and T.D. Pollard. 2005. Profilin-mediated competition between capping protein and formin Cdc12p during cytokinesis in fission yeast. *Mol Biol Cell*. 16:2313-2324.

Kozubowski, L., and J. Heitman. 2010. Septins enforce morphogenetic events during sexual reproduction and contribute to virulence of *Cryptococcus neoformans*. *Mol Microbiol*. 75:658-675.

Krappmann, S., C. Sasse, and G.H. Braus. 2006. Gene targeting in *Aspergillus fumigatus* by homologous recombination is facilitated in a nonhomologous end-joining-deficient genetic background. *Eukaryot Cell*. 5:212-215.

Kreis, T.E., K.H. Winterhalter, and W. Birchmeier. 1979. *In vivo* distribution and turnover of fluorescently labeled actin microinjected into human fibroblasts. *Proc Natl Acad Sci U S A*. 76:3814-3818.

Kubler, E., and H. Riezman. 1993. Actin and fimbrin are required for the internalization step of endocytosis in yeast. *EMBO J*. 12:2855-2862.

Kück, U., and B. Hoff. 2010. Application of the nourseothricin acetyltransferase (*nat1*) as dominant marker for the transformation of filamentous fungi. *Fungal Genet Newsl*. 53:9-11.

Kwon, M.J., M. Arentshorst, E.D. Roos, C.A. van den Hondel, V. Meyer, and A.F. Ram. 2011. Functional characterization of Rho GTPases in *Aspergillus niger* uncovers conserved and diverged roles of Rho proteins within filamentous fungi. *Mol Microbiol*. 79:1151-1167.

Larrondo, L.F., H.V. Colot, C.L. Baker, J.J. Loros, and J.C. Dunlap. 2009. Fungal functional genomics: tunable knockout-knock-in expression and tagging strategies. *Eukaryot Cell*. 8:800-804.

Lebrun, M.H., F. Villalba, J. Collemare, P. Landraud, K. Lambou, V. Brozek, B. Cirer, D. Morin, C. Bruel, and R. Beffa. 2008. Improved gene targeting in *Magnaporthe grisea* by inactivation of MgKU80 required for non-homologous end joining. *Fungal Genet Biol*. 45:68-75.

Lees-Miller, J.P., G. Henry, and D.M. Helfman. 1992. Identification of Act2, an essential gene in the fission yeast *Schizosaccharomyces pombe* that encodes a protein related to actin. *Proc Natl Acad Sci U S A*. 89:80-83.

Leipe, D.D., Y.I. Wolf, E.V. Koonin, and L. Aravind. 2002. Classification and evolution of P-loop GTPases and related ATPases. *J Mol Biol*. 317:41-72.

Li, C.R., Y.M. Wang, X. De Zheng, H.Y. Liang, J.C. Tang, and Y. Wang. 2005. The formin family protein CaBni1p has a role in cell polarity control during both yeast and hyphal growth in *Candida albicans*. *J Cell Sci*. 118:2637-2648.

Li, R. 1997. Bee1, a yeast protein with homology to Wiscott-Aldrich syndrome protein, is critical for the assembly of cortical actin cytoskeleton. *J Cell Biol*. 136:649-658.

Lichius, A., A. Berepiki, and N.D. Read. 2011. Form follows function - the versatile fungal cytoskeleton. *Fungal Biol*. 115:518-540.

Lichius, A., and N.D. Read. 2010. A versatile set of Lifeact-RFP expression plasmids for live-cell imaging of F-actin in filamentous fungi. *Fungal Genet Rep*. 57:8-14.

Lichius, A., M.E. Yanez-Gutierrez, N.D. Read, and E. Castro-Longoria. 2012. Comparative live-cell imaging analyses of SPA-2, BUD-6 and BNI-1 in *Neurospora crassa* reveal novel features of the filamentous fungal polarisome. *PLoS One*. 7:e30372.

Lindsey, R., S. Cowden, Y. Hernandez-Rodriguez, and M. Momany. 2010a. Septins AspA and AspC are important for normal development and limit the emergence of new growth foci in the multicellular fungus *Aspergillus nidulans*. *Eukaryot Cell*. 9:155-163.

Lindsey, R., Y. Ha, and M. Momany. 2010b. A septin from the filamentous fungus *Aspergillus nidulans* induces atypical pseudohyphae in the budding yeast *Saccharomyces cerevisiae*. *PLoS One*. 5:e9858.

Lindsey, R., and M. Momany. 2006. Septin localization across kingdoms: three themes with variations. *Curr Opin Microbiol*. 9:559-565.

Liu, Y.J., and B.D. Hall. 2004. Body plan evolution of ascomycetes, as inferred from an RNA polymerase II phylogeny. *Proc Natl Acad Sci U S A*. 101:4507-4512.

Longtine, M.S., C.L. Theesfeld, J.N. McMillan, E. Weaver, J.R. Pringle, and D.J. Lew. 2000. Septin-dependent assembly of a cell cycle-regulatory module in *Saccharomyces cerevisiae*. *Mol Cell Biol*. 20:4049-4061.

Lord, M., E. Laves, and T.D. Pollard. 2005. Cytokinesis depends on the motor domains of myosin-II in fission yeast but not in budding yeast. *Mol Biol Cell*. 16:5346-5355.

Luedeke, C., S.B. Frei, I. Sbalzarini, H. Schwarz, A. Spang, and Y. Barral. 2005. Septin-dependent compartmentalization of the endoplasmic reticulum during yeast polarized growth. *J Cell Biol*. 169:897-908.

Lukoyanova, N., S.A. Baldwin, and J. Trinick. 2008. 3D reconstruction of mammalian septin filaments. *J Mol Biol*. 376:1-7.

Madania, A., P. Dumoulin, S. Grava, H. Kitamoto, C. Scharer-Brodbeck, A. Soulard, V. Moreau, and B. Winsor. 1999. The *Saccharomyces cerevisiae* homologue of human Wiskott-Aldrich syndrome protein Las17p interacts with the Arp2/3 complex. *Mol Biol Cell*. 10:3521-3538.

Mahlert, M., L. Leveleki, A. Hlubek, B. Sandrock, and M. Bolker. 2006. Rac1 and Cdc42 regulate hyphal growth and cytokinesis in the dimorphic fungus *Ustilago maydis*. *Mol Microbiol*. 59:567-578.

Margolin, B.S., M. Freitag, and E.U. Selker. 1997. Improved plasmids for gene targeting at the *his-3* locus of *Neurospora crassa* by electroporation. *Fungal Genet Newsl* 44:112.

Marks, J., I.M. Hagan, and J.S. Hyams. 1986. Growth polarity and cytokinesis in fission yeast: the role of the cytoskeleton. *J Cell Sci* 5:229-241.

Martin, A.C., X.P. Xu, I. Rouiller, M. Kaksonen, Y. Sun, L. Belmont, N. Volkmann, D. Hanein, M. Welch, and D.G. Drubin. 2005a. Effects of Arp2 and Arp3 nucleotide-binding pocket mutations on Arp2/3 complex function. *J Cell Biol*. 168:315-328.

Martin, R., A. Walther, and H. Wendland. 2005b. Ras1-induced hyphal development in *Candida albicans* requires the formin Bni1. *Eukaryot Cell*. 4:1712-1724.

Martin, S.G., W.H. McDonald, J.R. Yates, 3rd, and F. Chang. 2005c. Tea4p links microtubule plus ends with the formin for3p in the establishment of cell polarity. *Dev Cell*. 8:479-491.

Martin, S.W., L.M. Douglas, and J.B. Konopka. 2005d. Cell cycle dynamics and quorum sensing in *Candida albicans* chlamydospores are distinct from budding and hyphal growth. *Eukaryot Cell*. 4:1191-1202.

May, G.S., and T.H. Adams. 1997. The importance of fungi to man. *Genome Res*. 7:1041-1044.

McMurray, M.A., A. Bertin, G. Garcia, 3rd, L. Lam, E. Nogales, and J. Thorner. 2011. Septin filament formation is essential in budding yeast. *Dev Cell*. 20:540-549.

McMurray, M.A., and J. Thorner. 2008. Septin stability and recycling during dynamic structural transitions in cell division and development. *Curr Biol*. 18:1203-1208.

McMurray, M.A., and J. Thorner. 2009. Reuse, replace, recycle. Specificity in subunit inheritance and assembly of higher-order septin structures during mitotic and meiotic division in budding yeast. *Cell Cycle*. 8:195-203.

Mendoza, M., A.A. Hyman, and M. Glotzer. 2002. GTP binding induces filament assembly of a recombinant septin. *Curr Biol*. 12:1858-1863.

Merzlyak, E.M., J. Goedhart, D. Shcherbo, M.E. Bulina, A.S. Shcheglov, A.F. Fradkov, A. Gaintzeva, K.A. Lukyanov, S. Lukyanov, T.W. Gadella, and D.M. Chudakov. 2007. Bright monomeric red fluorescent protein with an extended fluorescence lifetime. *Nat Methods*. 4:555-557.

Mitchison, T.J., and C.M. Field. 2002. Cytoskeleton: what does GTP do for septins? *Curr Biol*. 12:R788-790.

Momany, M., J. Zhao, R. Lindsey, and P.J. Westfall. 2001. Characterization of the *Aspergillus nidulans* septin (asp) gene family. *Genetics*. 157:969-977.

Mortensen, E.M., H. McDonald, J. Yates, 3rd, and D.R. Kellogg. 2002. Cell cycle-dependent assembly of a Gin4-septin complex. *Mol Biol Cell*. 13:2091-2105.

Moseley, J.B., and B.L. Goode. 2006. The yeast actin cytoskeleton: from cellular function to biochemical mechanism. *Microbiol Mol Biol Rev*. 70:605-645.

Moseley, J.B., I. Sagot, A.L. Manning, Y.W. Xu, J. Eck, D. Pellman, and B.L. Goode. 2004. A conserved mechanism for Bni1-and mDia1-induced actin assembly and dual regulation of Bni1 by Bud6 and profilin. *Mol Biol Cell*. 15:896-907.

Motegi, F., R. Arai, and I. Mabuchi. 2001. Identification of two type V myosins in fission yeast, one of which functions in polarized cell growth and moves rapidly in the cell. *Mol Biol Cell*. 12:1367-1380.

Mulholland, J., D. Preuss, A. Moon, A. Wong, D. Drubin, and D. Botstein. 1994. Ultrastructure of the yeast actin cytoskeleton and Its association with the plasma membrane. *J Cell Biol*. 125:381-391.

Mulvihill, D.P., S.R. Edwards, and J.S. Hyams. 2006. A critical role for the type V myosin, Myo52, in septum deposition and cell fission during cytokinesis in *Schizosaccharomyces pombe*. *Cell Motil Cytoskeleton*. 63:149-161.

Munn, A.L., B.J. Stevenson, M.I. Geli, and H. Riezman. 1995. End5, End6, and End7 - mutations that cause actin delocalization and block the internalization step of endocytosis in *Saccharomyces cerevisiae*. *Mol Biol Cell*. 6:1721-1742.

Murray, J.M., P.L. Appleton, J.R. Swedlow, and J.C. Waters. 2007. Evaluating performance in three-dimensional fluorescence microscopy. *J Microsc*. 228:390-405.

Nakahira, M., J.N. Macedo, T.V. Seraphim, N. Cavalcante, T.A. Souza, J.C. Damalio, L.F. Reyes, E.M. Assmann, M.R. Alborghetti, R.C. Garratt, A.P. Araujo, N.I. Zanchin, J.A. Barbosa, and J. Kobarg. 2010. A draft of the human septin interactome. *PLoS One*. 5:e13799.

Nayak, T., E. Szewczyk, C.E. Oakley, A. Osmani, L. Ukil, S.L. Murray, M.J. Hynes, S.A. Osmani, and B.R. Oakley. 2006. A versatile and efficient gene-targeting system for *Aspergillus nidulans*. *Genetics*. 172:1557-1566.

Ninomiya, Y., K. Suzuki, C. Ishii, and H. Inoue. 2004. Highly efficient gene replacements in *Neurospora* strains deficient for nonhomologous end-joining. *Proc Natl Acad Sci U S A*. 101:16391-16391.

Novick, P., and D. Botstein. 1985. Phenotypic analysis of temperature-sensitive yeast actin mutants. *Cell*. 40:405-416.

Oberholzer, U., A. Marcil, E. Leberer, D.Y. Thomas, and M. Whiteway. 2002. Myosin I is required for hypha formation in *Candida albicans*. *Eukaryot Cell*. 1:213-228.

Oldenburg, K.R., K.T. Vo, S. Michaelis, and C. Paddon. 1997. Recombination-mediated PCR-directed plasmid construction in vivo in yeast. *Nucleic Acids Res*. 25:451-452.

Oliferenko, S., and M. Mishra. 2008. Cytokinesis: catch and drag. *Curr Biol* 18:R247-R250.

Opekarova, M., G. Grossmann, J. Malinsky, W. Stahlschmidt, M. Loibl, I. Weig-Meckl, W.B. Frommer, and W. Tanner. 2008. Plasma membrane microdomains regulate turnover of transport proteins in yeast. *J Cell Biol*. 183:1075-1088.

Orlando, K., X. Sun, J. Zhang, T. Lu, L. Yokomizo, P. Wang, and W. Guo. 2011. Exo-endocytic trafficking and the septin-based diffusion barrier are required for the maintenance of Cdc42p polarization during budding yeast asymmetric growth. *Mol Biol Cell*. 22:624-633.

Osherov, N., R.A. Yamashita, Y.S. Chung, and G.S. May. 1998. Structural requirements for *in vivo* myosin I function in *Aspergillus nidulans*. *J Biol Chem*. 273:27017-27025.

Ostap, E.M. 2002. 2,3-Butanedione monoxime (BDM) as a myosin inhibitor. *J Mus Rres Cell Motility*. 23:305-308.

Pan, F., R.L. Malmberg, and M. Momany. 2007. Analysis of septins across kingdoms reveals orthology and new motifs. *BMC Evol Biol*. 7:103-109.

Pantazopoulou, A., and M.A. Penalva. 2009. Organization and dynamics of the *Aspergillus nidulans* Golgi during apical extension and mitosis. *Mol Biol Cell*. 20:4335-4347.

Pearson, C.L., K.M. Xu, K.E. Sharpless, and S.D. Harris. 2004. MesA, a novel fungal protein required for the stabilization of polarity axes in *Aspergillus nidulans*. *Mol Biol Cell*. 15:3658-3672.

Pelham, R.J., Jr., and F. Chang. 2001. Role of actin polymerization and actin cables in actin-patch movement in *Schizosaccharomyces pombe*. *Nat Cell Biol*. 3:235-244.

Penalva, M.A. 2010. Endocytosis in filamentous fungi: Cinderella gets her reward. *Curr Opin Microbiol*. 13:684-692.

Penalva, M.A., and A. Hervas-Aguilar. 2010. Endocytic machinery protein SlaB is dispensable for polarity establishment but necessary for polarity maintenance in hyphal tip cells of *Aspergillus nidulans*. *Eukaryot Cell*. 9:1504-1518.

Peter, B.J., H.M. Kent, I.G. Mills, Y. Vallis, P.J.G. Butler, P.R. Evans, and H.T. McMahon. 2004. BAR domains as sensors of membrane curvature: the amphiphysin BAR structure. *Science*. 303:495-499.

Philippsen, P., P. Knechtle, A. Kaufmann, and D. Cavicchioli. 2008. The paxillin-like protein AgPxl1 is required for apical branching and maximal hyphal growth in *Ashbya gossypii*. *Fungal Genet Biol*. 45:829-838.

Pollard, T.D. 2010. Mechanics of cytokinesis in eukaryotes. *Curr Opin Cell Biol*. 22:50-56.

Pollard, T.D., J.Q. Wu, V. Sirotkin, D.R. Kovar, M. Lord, C.C. Beltzner, and J.R. Kuhn. 2006. Assembly of the cytokinetic contractile ring from a broad band of nodes in fission yeast. *J Cell Biol*. 174:391-402.

Pruyne, D., and A. Bretscher. 2000. Polarization of cell growth in yeast. I. Establishment and maintenance of polarity states. *J Cell Sci*. 113 365-375.

Pruyne, D., M. Evangelista, C.S. Yang, E.F. Bi, S. Zigmond, A. Bretscher, and C. Boone. 2002. Role of formins in actin assembly: nucleation and barbed-end association. *Science*. 297:612-615.

Pruyne, D., L. Gao, E. Bi, and A. Bretscher. 2004. Stable and dynamic axes of polarity use distinct formin isoforms in budding yeast. *Mol Biol Cell*. 15:4971-4989.

Pruyne, D.W., D.H. Schott, and A. Bretscher. 1998. Tropomyosin-containing actin cables direct the Myo2p-dependent polarized delivery of secretory vesicles in budding yeast. *J Cell Biol*. 143:1931-1945.

Ram, A.F.J., V. Meyer, M. Arentshorst, A. El-Ghezal, A.C. Drews, R. Kooistra, and C.A.M.J.J. van den Hondel. 2007. Highly efficient gene targeting in the *Aspergillus niger* kusA mutant. *J Biotechnol*. 128:770-775.

Rasmussen, C.G., and N.L. Glass. 2005. A rho-type GTPase, rho-4, is required for septation in *Neurospora crassa*. *Eukaryot Cell*. 4:1913-1925.

Rasmussen, C.G., and N.L. Glass. 2007. Localization of RHO-4 indicates differential regulation of conidial versus vegetative septation in the filamentous fungus *Neurospora crassa*. *Eukaryot Cell*. 6:1097-1107.

Read, N.D. 2006. Environmental sensing and the filamentous fungal lifestyle. *In* Fungi and the Environment. G.M. Gadd, S.C. Watkinson, and P.S. Dyer, editors. Cambridge University Press, Cambridge. 38-57.

Read, N.D., A. Lichius, J.Y. Shoji, and A.B. Goryachev. 2009. Self-signalling and self-fusion in filamentous fungi. *Curr Opin Microbiol*. 12:608-615.

Reijnst, P., A. Walther, and J. Wendland. 2011. Dual-colour fluorescence microscopy using yEmCherry-/GFP-tagging of eisosome components Pil1 and Lsp1 in *Candida albicans*. *Yeast*. 28:331-338.

Ren, B., F. Robert, J.J. Wyrick, O. Aparicio, E.G. Jennings, I. Simon, J. Zeitlinger, J. Schreiber, N. Hannett, E. Kanin, T.L. Volkert, C.J. Wilson, S.P. Bell, and R.A. Young. 2000. Genome-wide location and function of DNA binding proteins. *Science*. 290:2306-2312.

Rida, P.C.G., A. Nishikawa, G.Y. Won, and N. Dean. 2006. Yeast-to-hyphal transition triggers formin-dependent golgi localization to the growing tip in *Candida albicans*. *Mol Biol Cell*. 17:4364-4378.

Riedl, J., A.H. Crevenna, K. Kessenbrock, J.H. Yu, D. Neukirchen, M. Bista, F. Bradke, D. Jenne, T.A. Holak, Z. Werb, M. Sixt, and R. Wedlich-Soldner. 2008. Lifeact: a versatile marker to visualize F-actin. *Nat Methods*. 5:605-607.

Riedl, J., K.C. Flynn, A. Raducanu, F. Gartner, G. Beck, M. Bosl, F. Bradke, S. Massberg, A. Aszodi, M. Sixt, and R. Wedlich-Soldner. 2010. Lifeact mice for studying F-actin dynamics. *Nat Methods*. 7:168-169.

Riquelme, M., C.G. Reynaga-Pena, G. Gierz, and S. Bartnicki-Garcia. 1998. What determines growth direction in fungal hyphae? *Fungal Genet Biol*. 24:101-109.

Roberson, R.W. 1992. The actin cytoskeleton in hyphal cells of *Sclerotium rolfsii*. *Mycologia*. 84:41-51.

Robertson, A.S., E.G. Allwood, A.P. Smith, F.C. Gardiner, R. Costa, S.J. Winder, and K.R. Ayscough. 2009a. The WASP homologue Las17 activates the novel actin-regulatory activity of Ysc84 to promote endocytosis in yeast. *Mol Biol Cell*. 20:1618-1628.

Robertson, A.S., E. Smythe, and K.R. Ayscough. 2009b. Functions of actin in endocytosis. *Cell Mol Life Sci*. 66:2049-2065.

Robzyk, K., and Y. Kassir. 1992. A simple and highly efficient procedure for rescuing autonomous plasmids from yeast. *Nucleic Acids Res*. 20:3790.

Roca, M.G., J. Arlt, C.E. Jeffree, and N.D. Read. 2005. Cell biology of conidial anastomosis tubes in *Neurospora crassa*. *Eukaryot Cell*. 4:911-919.

Roca, M.G., H.C. Kuo, A. Lichius, M. Freitag, and N.D. Read. 2010. Nuclear dynamics, mitosis, and the cytoskeleton during the early stages of colony initiation in *Neurospora crassa*. *Eukaryot Cell*. 9:1171-1183.

Rodal, A.A., L. Kozubowski, B.L. Goode, D.G. Drubin, and J.H. Hartwig. 2005. Actin and septin ultrastructures at the budding yeast cell cortex. *Mol Biol Cell*. 16:372-384.

Rolke, Y., and P. Tudzynski. 2008. The small GTPase Rac and the p21-activated kinase Cla4 in *Claviceps purpurea*: interaction and impact on polarity, development and pathogenicity. *Mol Microbiol*. 68:405-423.

Rossanese, O.W., C.A. Reinke, B.J. Bevis, A.T. Hammond, I.B. Sears, J. O'Connor, and B.S. Glick. 2001. A role for actin, Cdc1p, and Myo2p in the inheritance of late Golgi elements in *Saccharomyces cerevisiae*. *J Cell Biol*. 153:47-62.

Sagot, I., S.K. Klee, and D. Pellman. 2002. Yeast formins regulate cell polarity by controlling the assembly of actin cables. *Nat Cell Biol*. 4:42-50.

Sanchez-Ferrero, J.C., and M.A. Peñalva. 2007. Endocytosis. *In* The Aspergilli: genomics, medical applications, biotechnology, and research methods. S. Osmani and G. Goldman, editors. CRC Press, Boca Raton, FL.

Saunders, D.G., Y.F. Dagdas, and N.J. Talbot. 2010. Spatial uncoupling of mitosis and cytokinesis during appressorium-mediated plant infection by the rice blast fungus *Magnaporthe oryzae*. *Plant Cell*. 22:2417-2428.

Schmitz, H.P., A. Kaufmann, M. Kohli, P.P. Laissue, and P. Philippsen. 2006. From function to shape: a novel role of a formin in morphogenesis of the fungus *Ashbya gossypii*. *Mol Biol Cell*. 17:130-145.

Schott, D.H., R.N. Collins, and A. Bretscher. 2002. Secretory vesicle transport velocity in living cells depends on the myosin-V lever arm length. *J Cell Biol*. 156:35-39.

Schuchardt, I., D. Assmann, E. Thines, C. Schuberth, and G. Steinberg. 2005. Myosin-V, Kinesin-1, and Kinesin-3 cooperate in hyphal growth of the fungus Ustilago maydis. *Mol Biol Cell*. 16:5191-5201.

Schuster, M., S. Treitschke, S. Kilaru, J. Molloy, N.J. Harmer, and G. Steinberg. 2012. Myosin-5, kinesin-1 and myosin-17 cooperate in secretion of fungal chitin synthase. *EMBO J*. 31:214-227.

Schwob, E., and R.P. Martin. 1992. New yeast actin-like gene required late in the cell cycle. *Nature*. 355:179-182.

Seger, S., R. Rischatsch, and P. Philippsen. 2011. Formation and stability of eisosomes in the filamentous fungus *Ashbya gossypii*. *J Cell Sci*. 124:1629-1634.

Seiler, S., and D. Justa-Schuch. 2010. Conserved components, but distinct mechanisms for the placement and assembly of the cell division machinery in unicellular and filamentous ascomycetes. *Mol Microbiol*. 78:1058-1076.

Seiler, S., F.E. Nargang, G. Steinberg, and M. Schliwa. 1997. Kinesin is essential for cell morphogenesis and polarized secretion in *Neurospora crassa*. *EMBO J*. 16:3025-3034.

Seiler, S., and M. Plamann. 2003. The genetic basis of cellular morphogenesis in the filamentous fungus *Neurospora crassa*. *Mol Biol Cell*. 14:4352-4364.

Shaner, N.C., R.E. Campbell, P.A. Steinbach, B.N. Giepmans, A.E. Palmer, and R.Y. Tsien. 2004. Improved monomeric red, orange and yellow fluorescent proteins derived from *Discosoma* sp. red fluorescent protein. *Nat Biotech*. 22:1567-1572.

Shaner, N.C., M.Z. Lin, M.R. McKeown, P.A. Steinbach, K.L. Hazelwood, M.W. Davidson, and R.Y. Tsien. 2008. Improving the photostability of bright monomeric orange and red fluorescent proteins. *Nat Methods*. 5:545-551.

Sharpless, K.E., and S.D. Harris. 2002. Functional characterization and localization of the *Aspergillus nidulans* formin SEPA. *Mol Biol Cell*. 13:469-479.

Shcheprova, Z., S. Baldi, S.B. Frei, G. Gonnet, and Y. Barral. 2008. A mechanism for asymmetric segregation of age during yeast budding. *Nature*. 454:728-734.

Sheffield, P.J., C.J. Oliver, B.E. Kremer, S. Sheng, Z. Shao, and I.G. Macara. 2003. Borg/septin interactions and the assembly of mammalian septin heterodimers, trimers, and filaments. *J Biol Chem*. 278:3483-3488.

Si, H., D. Justa-Schuch, S. Seiler, and S.D. Harris. 2010. Regulation of septum formation by the Bud3-Rho4 GTPase module in *Aspergillus nidulans*. *Genetics*. 185:165-176.

Sikorski, R.S., and P. Hieter. 1989. A system of shuttle vectors and yeast host strains designed for efficient manipulation of DNA in Saccharomyces cerevisiae. *Genetics*. 122:19-27.

Sirajuddin, M., M. Farkasovsky, F. Hauer, D. Kuhlmann, I.G. Macara, M. Weyand, H. Stark, and A. Wittinghofer. 2007. Structural insight into filament formation by mammalian septins. *Nature*. 449:311-315.

Sirotkin, V., J. Berro, K. Macmillan, L. Zhao, and T.D. Pollard. 2010. Quantitative analysis of the mechanism of endocytic actin patch assembly and disassembly in fission yeast. *Mol Biol Cell*. 21:2894-2904.

Smith, M.G., S.R. Swamy, and L.A. Pon. 2001. The life cycle of actin patches in mating yeast. *J Cell Sci*. 114:1505-1513.

Sophianopoulou, V., I. Vangelatos, K. Roumelioti, C. Gournas, T. Suarez, and C. Scazzocchio. 2010. Eisosome organization in the filamentous ascomycete *Aspergillus nidulans*. *Eukaryot Cell*. 9:1441-1454.

Sousa, M.M., K.W. Steen, L. Hagen, and G. Slupphaug. 2011. Antibody cross-linking and target elution protocols used for immunoprecipitation significantly modulate signal-to noise ratio in downstream 2D-PAGE analysis. *Prot Sci*. 9:45.

Spiliotis, E.T., and A.S. Gladfelter. 2012. Spatial guidance of cell asymmetry: septin GTPases show the way. *Traffic*. 13:195-203.

Spiliotis, E.T., M. Kinoshita, and W.J. Nelson. 2005. A mitotic septin scaffold required for mammalian chromosome congression and segregation. *Science*. 307:1781-1785.

Spring, K.R. 2007. Cameras for digital microscopy. *Methods in cell biology*. 81:171-186.

Springer, M.L., and C. Yanofsky. 1989. A morphological and genetic analysis of conidiophore development in *Neurospora crassa*. *Genes Dev*. 3:559-571.

Steinberg, G. 2007a. Hyphal growth: a tale of motors, lipids, and the Spitzenkorper. *Eukaryot Cell*. 6:351-360.

Steinberg, G. 2007b. On the move: endosomes in fungal growth and pathogenicity. *Nat Rev Microbiol*. 5:309-316.

Suelmann, R., and R. Fischer. 2000. Mitochondrial movement and morphology depend on an intact actin cytoskeleton in *Aspergillus nidulans*. *Cell Motil Cytoskeleton*. 45:42-50.

Sun, Y.D., A.C. Martin, and D.G. Drubin. 2006. Endocytic internalization in budding yeast requires coordinated actin nucleation and myosin motor activity. *Dev Cell*. 11:33-46.

Surka, M.C., C.W. Tsang, and W.S. Trimble. 2002. The mammalian septin MSF localizes with microtubules and is required for completion of cytokinesis. *Mol Biol Cell*. 13:3532-3545.

Swedlow, J.R. 2007. Quantitative fluorescence microscopy and image deconvolution. *Methods in cell biology*. 81:447-465.

Taheri-Talesh, N., T. Horio, L. Araujo-Bazan, X. Dou, E.A. Espeso, M.A. Penalva, S.A. Osmani, and B.R. Oakley. 2008. The tip growth apparatus of *Aspergillus nidulans*. *Mol Biol Cell*. 19:1439-1449.

Taheri-Talesh, N., Y. Xiong, and B.R. Oakley. 2012. The functions of myosin II and myosin V homologs in tip growth and septation in Aspergillus nidulans. *PLoS One*. 7:e31218.

Takahashi, Y., M. Iwase, M. Konishi, M. Tanaka, A. Toh-e, and Y. Kikuchi. 1999. Smt3, a SUMO-1 homolog, is conjugated to Cdc3, a component of septin rings at the mother-bud neck in budding yeast. *Biochem Biophys Res Comm*. 259:582-587.

Takeshita, N., Y. Higashitsuji, S. Konzack, and R. Fischer. 2008. Apical sterol-rich membranes are essential for localizing cell end markers that determine growth directionality in the filamentous fungus *Aspergillus nidulans*. *Mol Biol Cell*. 19:339-351.

Takizawa, P.A., J.L. DeRisi, J.E. Wilhelm, and R.D. Vale. 2000. Plasma membrane compartmentalization in yeast by messenger RNA transport and a septin diffusion barrier. *Science*. 290:341-344.

Tang, C.S., and S.I. Reed. 2002. Phosphorylation of the septin cdc3 in g1 by the cdc28 kinase is essential for efficient septin ring disassembly. *Cell Cycle*. 1:42-49.

Tasto, J.J., J.L. Morrell, and K.L. Gould. 2003. An anillin homologue, Mid2p, acts during fission yeast cytokinesis to organize the septin ring and promote cell separation. *J Cell Biol*. 160:1093-1103.

Torralba, S., M. Raudaskoski, A.M. Pedregosa, and F. Laborda. 1998. Effect of cytochalasin A on apical growth, actin cytoskeleton organization and enzyme secretion in *Aspergillus nidulans*. *Microbiology*. 144 45-53.

Trinkle-Mulcahy, L., S. Boulon, Y.W. Lam, R. Urcia, F.M. Boisvert, F. Vandermoere, N.A. Morrice, S. Swift, U. Rothbauer, H. Leonhardt, and A. Lamond. 2008. Identifying specific protein interaction partners using quantitative mass spectrometry and bead proteomes. *J Cell Biol*. 183:223-239.

Ueda, T., A. Era, M. Tominaga, K. Ebine, C. Awai, C. Saito, K. Ishizaki, K.T. Yamato, T. Kohchi, and A. Nakano. 2009. Application of Lifeact Reveals F-Actin Dynamics in *Arabidopsis thaliana* and the Liverwort, *Marchantia polymorpha*. *Plant Cell Physiol*. 50:1041-1048.

Upadhyay, S., and B.D. Shaw. 2008. The role of actin, fimbrin and endocytosis in growth of hyphae in *Aspergillus nidulans*. *Mol Microbiol*. 68:690-705.

Vavylonis, D., J.Q. Wu, S. Hao, B. O'Shaughnessy, and T.D. Pollard. 2008. Assembly mechanism of the contractile ring for cytokinesis by fission yeast. *Science*. 319:97-100.

Verdin, J., S. Bartnicki-Garcia, and M. Riquelme. 2009. Functional stratification of the Spitzenkorper of *Neurospora crassa*. *Mol Microbiol*. 74:1044-1053.

Versele, M., and J. Thorner. 2004. Septin collar formation in budding yeast requires GTP binding and direct phosphorylation by the PAK, Cla4. *J Cell Biol*. 164:701-715.

Vidali, L., C.M. Rounds, P.K. Hepler, and M. Bezanilla. 2009. Lifeact-mEGFP reveals a dynamic apical F-actin network in tip growing plant cells. *PLoS One*. 4:e5744.

Virag, A., and A.J. Griffiths. 2004. A mutation in the *Neurospora crassa* actin gene results in multiple defects in tip growth and branching. *Fungal Genet Biol*. 41:213-225.

Virag, A., and S.D. Harris. 2006. Functional characterization of *Aspergillus nidulans* homologues of *Saccharomyces cerevisiae* Spa2 and Bud6. *Eukaryot Cell*. 5:881-895.

Virag, A., M.P. Lee, H. Si, and S.D. Harris. 2007. Regulation of hyphal morphogenesis by cdc42 and rac1 homologues in *Aspergillus nidulans*. *Mol Microbiol*. 66:1579-1596.

Vrabioiu, A.M., S.A. Gerber, S.P. Gygi, C.M. Field, and T.J. Mitchison. 2004. The majority of the *Saccharomyces cerevisiae* septin complexes do not exchange guanine nucleotides. *J Biol Chem*. 279:3111-3118.

Vrabioiu, A.M., and T.J. Mitchison. 2006. Structural insights into yeast septin organization from polarized fluorescence microscopy. *Nature*. 443:466-469.

Vrabioiu, A.M., and T.J. Mitchison. 2007. Symmetry of septin hourglass and ring structures. *J Mol Biol*. 372:37-49.

Waddle, J.A., T.S. Karpova, R.H. Waterston, and J.A. Cooper. 1996. Movement of cortical actin patches in yeast. *J Cell Biol*. 132:861-870.

Wallace, W., L.H. Schaefer, and J.R. Swedlow. 2001. A workingperson's guide to deconvolution in light microscopy. *Biotechniques*. 31:1076-1078, 1080, 1082 passim.

Walther, A., and J. Wendland. 2004a. Apical localization of actin patches and vacuolar dynamics in *Ashbya gossypii* depend on the WASP homolog Wal1p. *J Cell Sci*. 117:4947-4958.

Walther, A., and J. Wendland. 2004b. Polarized hyphal growth in *Candida albicans* requires the Wiskott-Aldrich Syndrome protein homolog Wal1p. *Eukaryot Cell*. 3:471-482.

Walther, T.C., J.H. Brickner, P.S. Aguilar, S. Bernales, C. Pantoja, and P. Walter. 2006. Eisosomes mark static sites of endocytosis. *Nature*. 439:998-1003.

Walther, T.C., and M. Mann. 2010. Mass spectrometry-based proteomics in cell biology. *J Cell Biol*. 190:491-500.

Wang, J., H. Hu, S. Wang, J. Shi, S. Chen, H. Wei, X. Xu, and L. Lu. 2009. The important role of actinin-like protein (AcnA) in cytokinesis and apical dominance of hyphal cells in *Aspergillus nidulans*. *Microbiology*. 155:2714-2725.

Warenda, A.J., S. Kauffman, T.P. Sherrill, J.A. Becker, and J.B. Konopka. 2003. *Candida albicans* septin mutants are defective for invasive growth and virulence. *Infect Immun*. 71:4045-4051.

Warenda, A.J., and J.B. Konopka. 2002. Septin function in *Candida albicans* morphogenesis. *Mol Biol Cell*. 13:2732-2746.

Washington, R.W., and D.A. Knecht. 2008. Actin binding domains direct actin-binding proteins to different cytoskeletal locations. *BMC Cell Biol*. 9:10.

Waters, J.C. 2007. Live-cell fluorescence imaging. *Methods Cell Biol*. 81:115-140.

Weber, I., D. Assmann, E. Thines, and G. Steinberg. 2006. Polar localizing class V myosin chitin synthases are essential during early plant infection in the plant pathogenic fungus *Ustilago maydis*. *Plant Cell*. 18:225-242.

Weber, I., C. Gruber, and G. Steinberg. 2003. A class-V myosin required for mating, hyphal growth, and pathogenicity in the dimorphic plant pathogen *Ustilago maydis*. *Plant Cell*. 15:2826-2842.

Wedlich-Soldner, R., M. Bolker, R. Kahmann, and G. Steinberg. 2000. A putative endosomal t-SNARE links exo- and endocytosis in the phytopathogenic fungus *Ustilago maydis*. *EMBO J*. 19:1974-1986.

Wehland, J., and K. Weber. 1981. Actin rearrangement in living cells revealed by microinjection of a fluorescent phalloidin derivative. *Eur J Cell Biol*. 24:176-183.

Weirich, C.S., J.P. Erzberger, and Y. Barral. 2008. The septin family of GTPases: architecture and dynamics. *Nat Rev Mol Cell Biol*. 9:478-489.

Wendland, J., and A. Walther. 2005. *Ashbya gossypii*: A model for fungal developmental biology. *Nat Rev Microbiol*. 3:421-429.

Westfall, P.J., and M. Momany. 2002. *Aspergillus nidulans* septin AspB plays pre- and postmitotic roles in septum, branch, and conidiophore development. *Mol Biol Cell*. 13:110-118.

Win, T.Z., Y. Gachet, D.P. Mulvihill, K.M. May, and J.S. Hyams. 2001. Two type V myosins with non-overlapping functions in the fission yeast Schizosaccharomyces pombe: Myo52 is concerned with growth polarity and cytokinesis, Myo51 is a component of the cytokinetic actin ring. *J Cell Sci*. 114:69-79.

Winston, F., C. Dollard, and S.L. Ricupero-Hovasse. 1995. Construction of a set of convenient *Saccharomyces cerevisiae* strains that are isogenic to S288C. *Yeast*. 11:53-55.

Woo, M., K. Lee, and K. Song. 2003. MYO2 is not essential for viability, but is required for polarized growth and dimorphic switches in *Candida albicans*. *FEMS Microbiol Lett*. 218:195-202.

Wu, J.Q., V.C. Coffman, A.H. Nile, I.J. Lee, and H.Y. Liu. 2009. Roles of formin nodes and myosin motor activity in Mid1p-dependent contractile-ring assembly during fission yeast cytokinesis. *Mol Biol Cell*. 20:5195-5210.

Wu, J.Q., and T.D. Pollard. 2005. Counting cytokinesis proteins globally and locally in fission yeast. *Science*. 310:310-314.

Wu, J.Q., Y. Ye, N. Wang, T.D. Pollard, and J.R. Pringle. 2010. Cooperation between the septins and the actomyosin ring and role of a cell-integrity pathway during cell division in fission yeast. *Genetics*. 186:897-915.

Yamashita, R.A., and G.S. May. 1998. Constitutive activation of endocytosis by mutation of myoA, the myosin I gene of *Aspergillus nidulans*. *J Biol Chem*. 273:14644-14648.

Yamashita, R.A., N. Osherov, and G.S. May. 2000. Localization of wild type and mutant class I myosin proteins in *Aspergillus nidulans* using GFP-fusion proteins. *Cell Motil Cytoskeleton*. 45:163-172.

Yang, H.C., and L.A. Pon. 2002. Actin cable dynamics in budding yeast. *Proc Natl Acad Sci U S A*. 99:751-756.

Yokoyama, K., H. Kaji, K. Nishimura, and M. Miyaji. 1990. The role of microfilaments and microtubules in apical growth and dimorphism of *Candida albicans*. *J Gen Microbiol*. 136:1067-1075.

Zhang, J., C. Kong, H. Xie, P.S. McPherson, S. Grinstein, and W.S. Trimble. 1999. Phosphatidylinositol polyphosphate binding to the mammalian septin H5 is modulated by GTP. *Curr Biol*. 9:1458-1467.

Zhang, J., K. Tan, X. Wu, G. Chen, J. Sun, S.L. Reck-Peterson, J.A. Hammer, 3rd, and X. Xiang. 2011. Aspergillus myosin-V supports polarized growth in the absence of microtubule-based transport. *PLoS One*. 6:e28575.

Zigmond, S.H., M. Evangelista, C. Boone, C.S. Yang, A.C. Dar, F. Sicheri, J. Forkey, and M. Pring. 2003. Formin leaky cap allows elongation in the presence of tight capping proteins. *Curr Biol*. 13:1820-1823.

Appendix

Table A.1. *N. crassa* strains used in this study

Strain	Genotype	Source
Wild-type	*74-OR23-1 A*	FGSC #2489
his-3^{-}	*his-3 A*	FGSC #6103
his-3^{-}, *Δmus-51*	*his-3 Δmus-51*::*bar A*	FGSC #9717
Δmus-51	*Δmus-51*::*bar a*	FGSC #9718
Δmus-52	*Δmus-52*::*bar a*	FGSC #9719
Pccg1-sgfp-lifeact	*his-3*$^{+}$*::Pccg-1-Lifeact-gfp Δmus-51::bar A*	This study
Ptef1-sgfp-lifeact	*his-3*$^{+}$*::Ptef-1-Lifeact-gfp Δmus-51::bar A*	This study
lifeact-rfp	*his-3*$^{+}$*::Ptef-1-lifeact-tagrfpt Δmus-51*::*bar a*	This study
Δmyo-5	*Δmyo-5::hph*	FGSC #11442
sgfp-myo-5	*sgfp-myo-5::hph*	This study
Δmyo-5, *lifeact-sgfp*	*Δmyo-5::hph his-3*$^{+}$*::Pccg-1-lifeact-sgfp*	This study
Δcdc-3, *Δmus-52*	*Δcdc-3::hph Δmus-52::bar*	This study
Δcdc-3	*Δcdc-3::hph*	FGSC #11972
Δcdc-3, *Δcdc-10*	*Δcdc-3::hph Δcdc-10::nat*	This study
Δcdc-3, *Δcdc-11*	*Δcdc-3::hph Δcdc-11::nat*	This study
Δcdc-3, *Δcdc-12*	*Δcdc-3::hph Δcdc-12::nat*	This study
Δcdc-3, *cdc-11-sgfp*	*Δcdc-3::hph cdc-11-sgfp::nat*	This study
cdc-3-sgfp	*cdc-3-sgfp::hph*	This study
cdc-3-v5-hat	*cdc-3-v5-hat::hph*	This study
Δcdc-10, *Δmus-51*	*Δcdc-10::hph Δmus-51::bar*	FGSC #11727
Δcdc-10	*Δcdc-10::hph*	This study
Δcdc-10, *Δcdc-11*	*Δcdc-10::hph Δcdc-11::nat*	This study
Δcdc-10, *Δcdc-12*	*Δcdc-10::hph, Δcdc-12::nat*	This study
Δcdc-10, *cdc-11-sgfp*	*Δcdc-10::hph cdc-11-sgfp::nat*	This study
sgfp-cdc-10	*sgfp-cdc-10::hph*	This study
Pccg1-sgfp-cdc-10	*his-3*$^{+}$*::Pccg-1-sgfp-cdc-10*	This study
sgfp-cdc-10, bml-mch	*his-3*$^{+}$*::Pccg-1-sgfp-cdc-10/Pccg-1-bml mch::nat*	This study
v5-hat-cdc-10	*v5-hat-cdc-10::hph*	This study
Δcdc-11, *Δmus-51*	*Δcdc-11::hph Δmus-51::bar*	This study
Δcdc-11	*Δcdc-11::hph*	FGSC #11971
Δcdc-11, *cdc-12-sgfp*	*Δcdc-11::hph cdc-12-sgfp::nat*	This study
Δcdc-11, *lifeact-sgfp*	*Δcdc-11::hph his-3*$^{+}$*::Pccg-1-lifeact-sgfp*	This study
cdc-11-sgfp	*cdc-11-sgfp::hph*	This study
cdc-11-v5-hat	*cdc-11-v5-hat::hph*	This study
Δcdc-12, Δmus-51	*Δcdc-12::hph Δmus-51::bar*	This study

Δcdc-12	*Δcdc-12::hph*	This study
Δcdc-12, *cdc-11-sgfp*	*Δcdc-12::hph cdc-11-sgfp::nat*	This study
cdc-12-sgfp	*cdc-12-sgfp::hph*	This study
cdc-12-sgfp, *lifeact-rfp*	*cdc-12-sgfp::hph his-3^{+}::Ptef-1-lifeact-tagrfpt*	This study
cdc-12-v5-hat	*cdc-12-v5-hat::hph*	This study
Δasp-1, *Δmus-51*	*Δasp-1::hph Δmus-51::bar*	This study
Δasp-1	*Δasp-1::hph*	This study
Δasp-1, *cdc-11-sgfp*	*Δasp-1::hph cdc-11-sgfp::nat*	This study
Pccg1-sgfp-asp-1	*his-3^{+}::Pccg-1-sgfp-asp-1*	This study
v5-hat-asp-1	*v5-hat-asp-1::hph*	This study
Δasp-2, *Δmus-51*	*Δasp-2::hph Δmus-51::bar*	This study
Δasp-2	*Δasp-2::hph*	This study
Δasp-2, *cdc-11-sgfp*	*Δasp-2::hph cdc-11-sgfp::nat*	This study
v5-hat-asp-2	*v5-hat-asp-2::hph*	This study

Table A.2. Oligonucleotide primers used in this study

Primer name	Sequence
LA Fw	GATCTCTAGAATGGGCGTCGCTGACCTCATCAAGAAGTTCGAGTCCATCTCCAAGGAGG AGTTAATTAACTAG
LA Rv	CTAGTTAATTAACTCCTCCTTGGAGATGGACTCGAACTTCTTGATGAGGTCAGCGACGCC CATTCTAGAGATC
TEF1 IF Fw	ACCGCGGTGGCGGCCGCGATATCCCGTGACCACTGAACTA
TEF1 IF Rv	CGACGCCCATTCTAGATAACCCGGGGATCCGATAT
MYO-5 P1	GTAATACGACTCACTATAGGGCGAATTGGGTACCgagtgtagacttggacatcg
MYO-5 P2	ATCCACTTAACGTTACTGAAATCTCCAACaggtctaggagttcgaaagg
MYO-5 P3	GTAATACGACTCACTATAGGGCGAATTGGGTACCcgacaagttacgcaccaa
MYO-5 P4	GCCTCCGCCTCCGCCTCCGCCGCCTCCGCCataaagcgtgtaatgcctgcc
MYO-5 P5	CAAAGGAATAGAGTAGATGCCGACCGGGATAACgccgcttaagtgcatatcatg
MYO-5 P6	CTCACTAAAGGGAACAAAAGCTGGAGCTCCcgtcgtatgagtcgcgg
MYO-5 N1	GTAATACGACTCACTATAGGGCGAATTGGGGCGGCCGCcgacctaaaggtggaaggaagac
MYO-5 N2	GCTATACGAAGTTATGGATCCGAGCTCGGTACcaaatgtgtctctggaggctc
MYO-5 N3	CGATAAGCTTGATATCGAATTCTTACTTGTAgagtgtagacttggacatcgtgac
MYO-5 N4 GFP	AGTGAACAATTCCTCGCCTTTTGAAACcattggatgcgcttgtatcgg
MYO-5 N5	GGCGGAGGCGGCGGAGGCGGAGGCGGAGGCatgtcggagagctatgatgttg
MYO-5 N6	CAAAAGCTGGAGCTCCACCGCGGTGGCGGCCGCgtgttaccctggttgaggtact
CDC-3 P1	GTAATACGACTCACTATAGGGCGAATTGGGTACCacccgtcaggccagtggaca
CDC-3 P2	CGATAAGCTTGATATCGAATTCTTACTTGTAtgcacccggcatgtgtcttc
CDC-3 P3	GTAATACGACTCACTATAGGGCGAATTGGGTACCcttctaccttgagcgacaacc
CDC-3 P4	GCCTCCGCCTCCGCCTCCGCCGCCTCCGCCtcggagagaaaatcccttcc
CDC-3 P5	CAAAGGAATAGAGTAGATGCCGACCGGGATAACcatgttatcccgcatacacc
CDC-3 P6	CTCACTAAAGGGAACAAAAGCTGGAGCTCCtgagacagatgagaaccacc
CDC-10 P1	GTAATACGACTCACTATAGGGCGAATTGGGGCGGCCGCtgaagtatcccagcagttcc
CDC-10 P2	CGATAAGCTTGATATCGAATTCTTACTTGTAcaggcaacctaacctaactgg
CDC-10 P3	GTAATACGACTCACTATAGGGCGAATTGGGGCGGCCGCgtttcgacagcatcacct
CDC-10 P4	GCCTCCGCCTCCGCCTCCGCCGCCTCCGCCgtagccgttcatggtcat
CDC-10 P5	GCTATACGAAGTTATGGATCCGAGCTCGGTACgtggagtggacttcttaacc
CDC10 P6	CAAAAGCTGGAGCTCCACCGCGGTGGCGGCCGCcctcccaagtaggattcatgc
CDC-10 N1	GTAATACGACTCACTATAGGGCGAATTGGGGCGGCCGCgggagggaagttgtttggagaa
CDC-10 N2	GCTATACGAAGTTATGGATCCGAGCTCGGTACccctcaacttcgccgtgc
CDC-10 N3	CGATAAGCTTGATATCGAATTCTTACTTGTAgctgtgtcctgagggtttgg
CDC-10 N4 GFP	GGTGAACAGCTCCTCGCCCTTGCTCACCATgattgcgaacttgatggggg
CDC-10 N4 V5	CCGAGGAGGGGGTTGGGGATGGGCTTGCCCATgattgcgaacttgatggggg
CDC-10 N5	GGCGGAGGCGGCGGAGGCGGAGGCGGAGGCatgtcgaccatgggccct
CDC-10 N6	CAAAAGCTGGAGCTCCACCGCGGTGGCGGCCGCcctccacgttgatcacgcc
CDC-10 CCG1 P9	TTCACAACCCCTCACATCAACCAAATCTAGatgtcgaccatgggccct
CDC-10 P9 IFNTERM	GGAGGCGGCGGAGGCGGCatgtcgaccatgggccct
CDC-10 P2 IF NTERM	TGGCGGCCGCTCTAGActagtagccgttcatggtcatgcg
CDC-11 P1	GTAATACGACTCACTATAGGGCGAATTGGGGCGGCCGCatgacagcagagacttgagc

CDC-11 P2	CGATAAGCTTGATATCGAATTCTTACTTGTAtagaggtgaggtagtgttgg
CDC-11 P3 V2	GTAATACGACTCACTATAGGGCGAATTGGGGCGGCCGCgattaaccattgcattatctcccaggc
CDC-11 P4 V2	GCCTCCGCCTCCGCCTCCGCCGCCTCCGCCgtttccatctggggaaccgttaatttc
CDC-11 P5	GCTATACGAAGTTATGGATCCGAGCTCGGTACacgacactagcacacacatacc
CDC-11 P6	CAAAAGCTGGAGCTCCACCGCGGTGGCGGCCGCcaagtatcatgtggaggagg
CDC-12 P1	GTAATACGACTCACTATAGGGCGAATTGGGGCGGCCGCgaagttcagttacaggctgc
CDC-12 P2	CGATAAGCTTGATATCGAATTCTTACTTGTAgggtagaggattaagtcacg
CDC-12 P3	GTAATACGACTCACTATAGGGCGAATTGGGGCGGCCGCcacaaaggctgagctcgaggag
CDC-12 P4	GCCTCCGCCTCCGCCTCCGCCGCCTCCGCCgcggcgaccgtggctg
CDC-12 P5	GCTATACGAAGTTATGGATCCGAGCTCGGTACaactgggcgacttacatacc
CDC-12 P6	CAAAAGCTGGAGCTCCACCGCGGTGGCGGCCGCcgtacttgtggtcctttagc
ASP-1 P1	GTAATACGACTCACTATAGGGCGAATTGGGGCGGCCGCctatcctcctcttccctttcc
ASP-1 P2	CGATAAGCTTGATATCGAATTCTTACTTGTAagaggtaactaaagccgacc
ASP-1 P3	GTAATACGACTCACTATAGGGCGAATTGGGGCGGCCGCcaagagtgccttggcac
ASP-1 P4	GCCTCCGCCTCCGCCTCCGCCGCCTCCGCCacggatctttgcgcc
ASP-1 P5	GCTATACGAAGTTATGGATCCGAGCTCGGTACccatgttatggagacagagc
ASP-1 P6	CAAAAGCTGGAGCTCCACCGCGGTGGCGGCCGCgatagagacagggacagagg
ASP-1 N1	GTAATACGACTCACTATAGGGCGAATTGGGGCGGCCGCgcggatttggcctggctt
ASP-1 N2	GCTATACGAAGTTATGGATCCGAGCTCGGTACctttggaccgatggaggtgag
ASP-1 N3	CGATAAGCTTGATATCGAATTCTTACTTGTAcgtctatcctcctcttcctttccc
ASP-1 N4 GFP	GGTGAACAGCTCCTCGCCCTTGCTCACCATagctctcggtgagagactgaatgc
ASP-1 N4 V5	CCGAGGAGGGGGTTGGGGATGGGCTTGCCCATagctctcggtgagagactgaatgc
ASP-1 N5	GGCGGAGGCGGCGGAGGCGGAGGCGGAGGCatgaaccagtctcctgctcgc
ASP-1 N6	CAAAAGCTGGAGCTCCACCGCGGTGGCGGCCGCcccagaccgccctctttagc
ASP-1 CCG1 P9	TTCACAACCCCTCACATCAACCAAATCTAGatgaaccagtctcctgctcg
ASP-1 P9 IF NTERM	GGAGGCGGCGGAGGCGGCatgaaccagtctcctgctcg
ASP-1 P2 IF NTERM	TGGCGGCCGCTCTAGActaacggatctttgcgcc
ASP-2 P1	GTAATACGACTCACTATAGGGCGAATTGGGGCGGCCGCgacacatcttggttgacagc
ASP-2 P2	CGATAAGCTTGATATCGAATTCTTACTTGTAggaatgggtagctagtatgg
ASP-2 P3	GTAATACGACTCACTATAGGGCGAATTGGGGCGGCCGCgctgggtggagagggtggt
ASP-2 P4	GCCTCCGCCTCCGCCTCCGCCGCCTCCGCCccgccaaatccgattccac
ASP-2 P5	GCTATACGAAGTTATGGATCCGAGCTCGGTACggttgatcctctgctactgg
ASP-2 P6	CAAAAGCTGGAGCTCCACCGCGGTGGCGGCCGCatcagctgtcgtagtcttgg
ASP-2 N1	GTAATACGACTCACTATAGGGCGAATTGGGGCGGCCGCcgcttccacgtcgatccttt
ASP-2 N2	GCTATACGAAGTTATGGATCCGAGCTCGGTACgattccccgacggtgttactc
ASP-2 N3	CGATAAGCTTGATATCGAATTCTTACTTGTAgacacatcttggttgacagcg
ASP-2 N4 GFP	GGTGAACAGCTCCTCGCCCTTGCTCACCATcgcaaagagagcaatctacatacac
ASP-2 N4 V5	CCGAGGAGGGGGTTGGGGATGGGCTTGCCCATcgcaaagagagcaatctacatacac
ASP-2 N5	GGCGGAGGCGGCGGAGGCGGAGGCGGAGGCatgcgctcaaacaacgatgc
ASP-2 N6	CAAAAGCTGGAGCTCCACCGCGGTGGCGGCCGCgaccttgaaccgcctttagtctg
ASP-2 CCG1 P9	TTCACAACCCCTCACATCAACCAAATCTAGatgcgctcaaacaacgatg
ASP-2 IF NTERM P9	GGAGGCGGCGGAGGCGGCatgcgctcaaacaacgatg
ASP-2 P2 IF NTERM	TGGCGGCCGCTCTAGAtcaccgccaaatccgatt

HPH Y HR Fw CC	TACAAGTAAGAATTCGATATCAAGC
HPH Y HR Rv DD	GTACCGAGCTCGGATCC
NAT Y HR Fw CC	TACAAGTAAGAATTCGATATCAAGCTTATCGcaactgatattgaaggagcatttt
NAT Y HR Rv DD	GTACCGAGCTCGGATCCATAACTTCGTATAGCcttgtcgacgaattcagatg
NAT Y HR Rv YY	CAAAAGCTGGAGCTCCACCGCGGTGGCGGCCGCcttgtcgacgaattcagatg
YRC BB GFP TAGT Fw	GGCGGAGGCGGCGGAGGCGGAGGCGGAGGCATGGTG
YRC CC Rv	CGATAAGCTTGATATCGAATTCTTACTTGTA
MCHERRY Fw BB YRC	GGCGGAGGCGGCGGAGGCGGAGGCGGAGGCatggtgagcaagggcgagg
MCHERRY Rv CC YRC	CGATAAGCTTGATATCGAATTCTTACTTGTACAGCTCGTCCATGCC
V5 HAT YRC A Fw	GGCGGAGGCGGCGGAGGCGGAGGCGGAGGCGGCAAGCCCATCCCCAACCCCCTCCTC GGACTCGACAGCACC
V5 HAT YRC B Rv V2	CTTGTGGACGTTGTGGATGAGGTGGTCCTTGGCGCCGGCGCCGGCGCCGGTGCTGTCG AGTCCGAGGAGGGGGTTGGG
V5 HAT YRC C Fw V2	AAGGACCACCTCATCCACAACGTCCACAAGGAGGAGCACGCCCACGCCCACAACAAGTA ATACAAGTAAGAATTCGATATCAAGCTTATCG
YRC NT FP START Fw	ATGGTGAGCAAGGGCGAGG
YRC NT V5-HAT START Fw	ATGGGCAAGCCCATCCCCAAC
YRC NT FP Rv BB	GCCTCCGCCTCCGCCTCCGCCGCCTCCGCCcttgtacagctcgtccatgcc
YRC NT V5-HAT Rv BB	GCCTCCGCCTCCGCCTCCGCCGCCTCCGCCcttgttgtgggcgtgggc
TAGRFP IF Fw	CCCCGGGTTAATTAAGGGAGCTGGTGCAATGGTGTCTAAGGGCGAAGA
TAGRFP IF Rv	CGATAAGCTTGATATCGAATTCTTACTTGTACAGCTCGTCC
PCCG1 Fw YRC XX	GTAATACGACTCACTATAGGGCGAATTGGGGCGGCCGCgctagaaggagcagtccatc
BTUB Rv YRC BB	GCCTCCGCCTCCGCCTCCGCCGCCTCCGCCgttaattaactcctcgccctc
MYO-5 G1	GCTCTTTGACGCTGGATGA
MYO-5 G2	CACTTGGCAAATTCTGGAG
MYO-5 G3	CCCTCCTCAACAATGTCTACC
MYO-5 G4	CCCATTGCCATTACTCATC
CDC-3 G1	TCCCCTTAGCATGTCCTTTT
CDC-3 G2	AAGAGAGTGTTAACGAGGGTC
CDC-3 G3	CTTCTACCTTGAGCGACAACC
CDC-3 G4	GGGGCATAGACAAATTTCCT
CDC-10 G1	CTTCACACATGGACACCTAGA
CDC-10 G2	GGGGTGTCGACAATGTT
CDC-10 G3	GTTTCGACAGCATCACCT
CDC-10 G4	CTTATCCTTCCACCTGGAGT
CDC-11 G1	CTCGGTTACCAAGTGGAATG
CDC-11 G2	TGATGAAGTAGAGCATGGC
CDC-11 G3	CCTTTGTCAACACCCTCTG
CDC-11 G4	CATCTTCGTCTTCCTCACAG
CDC-12 G1	GAACTGGAGGACTCTTTCGAG
CDC-12 G2	AAACCTACCCTGGACTTGAA
CDC-12 G3	GTTCTTCAAGGGTACGACAG
CDC-12 G4	CAGCCATCTCGAGTACATCAT
ASP-1 G1	GTCGTTTGTGATCTCATCGA

ASP-1 G2	GCTAGCATAGCTGTAACGTCC
ASP-1 G3	CAAGAGTGCCTTGGCAC
ASP-1 G4	GCCAACATCTCGAGTACTTTC
ASP-2 G1	CAACACCAGGGATTCGCT
ASP-2 G2	CGACGATGTGTCACTGACA
ASP-2 G3	GACTAAAGGCGGTTCAAGGTC
ASP-2 G4	CCTGAGATCAAATTGCCAACG
MUS-51 Fw	CTTGGAGGAAGGATCAGGAT
MUS-51 Rv	CTCTCAACTAGCTCAGCC
MUS-52 Fw	GACAAGGAAGCCACAGTCTA
MUS-52 Rv	CTCCGAGAGAAGGGCGTC
ACT-1 Fw	GACGACATGGAGAAGATTTGG
ACT-1 Rv	CCTAGCCTATACTGCCATCTCC
HPH 1 Fw	TCACTGGCAAACTGTGATG
HPH 2 Rv	ACACATGGGGATCAGCAATC
NAT 1 Fw	CTTCGTGGTCGTCTCGTA
NAT 2 Rv	CGCCAGGTCGCCGTCG
HIS-3 3' Fw	TTGCCATCTCCACCATCC
HIS-3 5' Rv	GCTGTAGACCAGACCCAGAGC
GFP Fw	CAAGATCCGCCACAACATCG
GFP Rv	ATGTGGTCGGGGTAGCGG

Table A.3. Plasmids used in this study

Plasmid name	Vector backbone	Target/epitiope	Source
pAB221	pCCG::C-Gly::GFP	*his-3-Pccg-1-lifeact-sgfp*	This study
pAB261	pCCG::C-Gly::GFP	*his-3-Ptef-1-lifeact-sgfp*	This study
pAB271	pAB261	*his-3-Ptef-1-lifeact-tagrfpt*	This study
pAB414	pRS426	*myo-5-5f-hph-myo-5-3f*	This study
pAB224	pCCG::C-Gly::GFP	*his-3-Pccg-1- myo-5-sgfp*	This study
pAB324	pCCG::C-Gly::GFP	*his-3-Pccg-1-sgfp-myo-5*	This study
pSP524	pRS426	*myo-5-5f-hph-Pmyo-5-v5hat-myo-5-3f*	This study
pAB415	pRS426	*cdc-3-5f-hph-cdc-3-3f*	This study
pAB425	pRS426	*cdc-3-5f-sgfp-hph-cdc-3-3f*	This study
pAB455	pRS426	*cdc-3-5f-v5hat-hph-cdc-3-3f*	This study
pAB416	pRS426	*cdc-10-5f-hph-cdc-10-3f*	This study
pAB616	pRS426	*cdc-10-5f-nat-cdc-10-3f*	This study
pAB426	pRS426	*cdc-10-5f-sgfp-hph-cdc-10-3f*	This study
pAB226	pCCG::C-Gly::GFP	*his-3-Pccg-1- cdc-10-sgfp*	This study
pAB326	pCCG::N-GFP	*his-3-Pccg-1-sgfp-cdc-10*	This study
pAB526	pRS426	*cdc-105f-hph-Pcdc-10-sgfp-cdc-10ff*	This study
pAB556	pRS426	*cdc-105f-hph-Pcdc-10-v5hat-cdc-10ff*	This study
pAB417	pRS426	*cdc-11-5f-hph-cdc-11-3f*	This study
pAB617	pRS426	*cdc-11-5f-nat-cdc-11-3f*	This study
pAB427	pRS426	*cdc-11-5f-sgfp-hph-cdc-11-3f*	This study
pAB627	pRS426	*cdc-11-5f-sgfp-nat-cdc-11-3f*	This study
pAB647	pRS426	*cdc-11-5f-mch-nat-cdc-11-3f*	This study
pAB457	pRS426	*cdc-11-5f-v5hat-hph-cdc-11-3f*	This study
pAB418	pRS426	*cdc-12-5f-hph-cdc-12-3f*	This study
pAB618	pRS426	*cdc-12-5f-nat-cdc-12-3f*	This study
pAB428	pRS426	*cdc-12-5f-sgfp-hph-cdc-12-3f*	This study
pAB628	pRS426	*cdc-12-5f-sgfp-nat-cdc-12-3f*	This study
pAB458	pRS426	*cdc-12-5f-v5hat-hph-cdc-12-3f*	This study
pAB419	pRS426	*asp-1-5f-hph-asp-1-3f*	This study
pAB429	pRS426	*asp-1-5f-sgfp-hph-asp-1-3f*	This study
pAB229	pCCG::C-Gly::GFP	*his-3-Pccg-1-asp-1-sgfp*	This study
pAB329	pCCG::N-GFP	*his-3-Pccg-1-sgfp-asp-1*	This study
pAB529	pRS426	*asp-1-5f-hph-Pasp-1-sgfp-asp-1-3f*	This study
pAB559	pRS426	*asp-1-5f-hph-Pasp-1-v5hat-asp-1-3f*	This study
pAB412	pRS426	*asp-2-5f-hph-asp-2-3f*	This study
pAB422	pRS426	*asp-2-5f-sgfp-hph-asp-2-3f*	This study
pAB222	pCCG::C-Gly::GFP	*his-3-Pccg-1- asp-2-sgfp*	This study
pAB322	pCCG::N-GFP	*his-3-Pccg-1-sgfp-asp-2*	This study
pAB552	pRS426	*asp-2-5f-hph-Pasp-2-v5hat-asp-2-3f*	This study
pAB84BT	pRS426	*Pccg-1-bml-mch-nat*	This study

Table A.4. Number of unique tryptic peptides identified by MS/MS					
	Strains				
	cdc-3-v5hat	*v5hat-cdc-10*	*cdc-11-v5hat*	*cdc-12-v5hat*	*v5hat-asp-1*
Protein					
CDC-3	17	23	15	11	26
CDC-10	33	37	37	24	37
CDC-11	36	33	33	25	33
CDC-12	37	36	36	26	37
ASP-1	0	0	0	0	15

Figure A.1

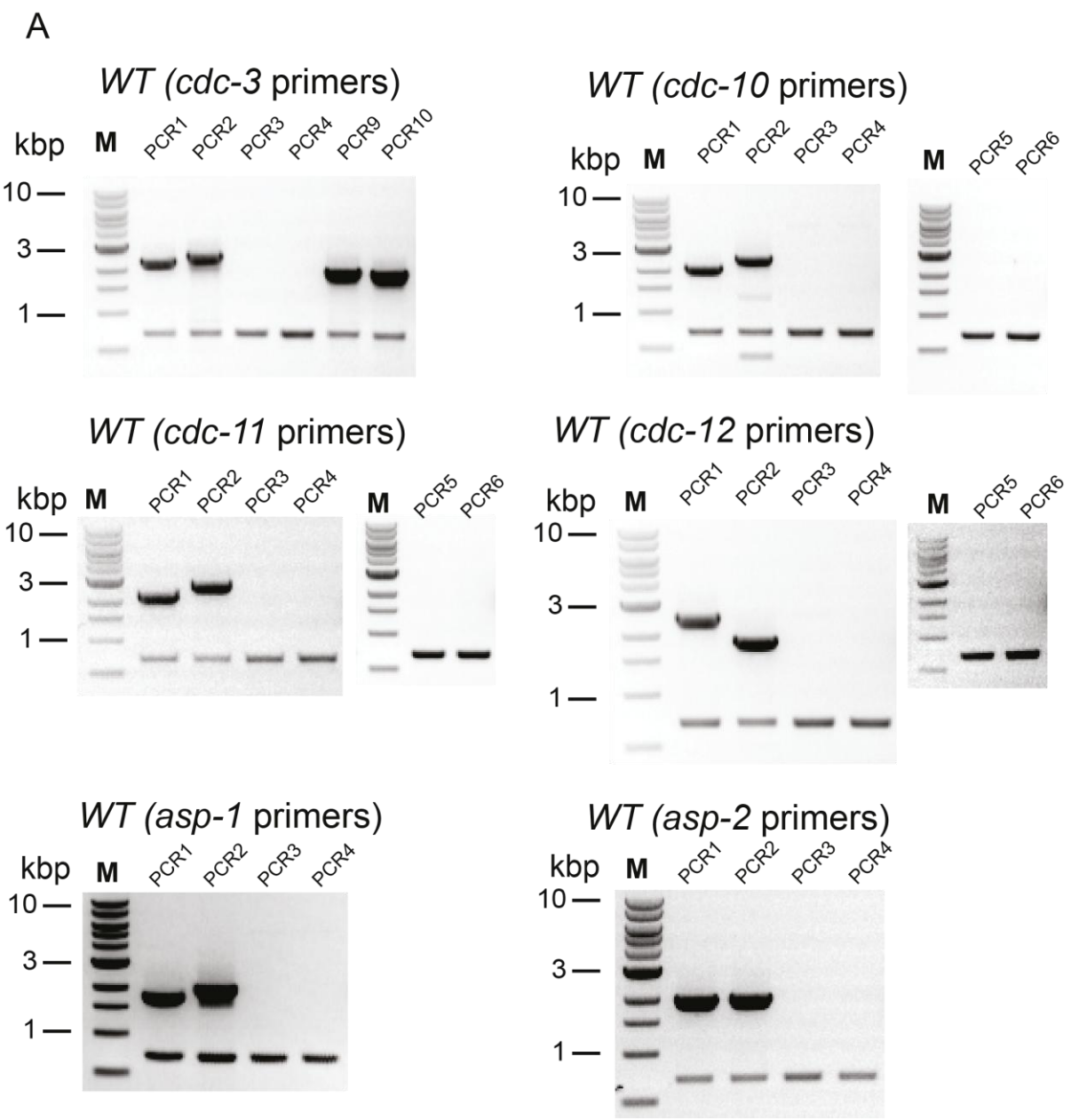
A
WT (cdc-3 primers)
kbp
M
PCR1
PCR2
PCR3
PCR4
PCR9
PCR10
10
3
1
WT (cdc-10 primers)
kbp
M
PCR1
PCR2
PCR3
PCR4
M
PCR5
PCR6
10
3
1
WT (cdc-11 primers)
kbp
M
PCR1
PCR2
PCR3
PCR4
M
PCR5
PCR6
10
3
1
WT (cdc-12 primers)
kbp
M
PCR1
PCR2
PCR3
PCR4
M
PCR5
PCR6
10
3
1
WT (asp-1 primers)
kbp
M
PCR1
PCR2
PCR3
PCR4
10
3
1
WT (asp-2 primers)
kbp
M
PCR1
PCR2
PCR3
PCR4
10
3
1

Figure A.1

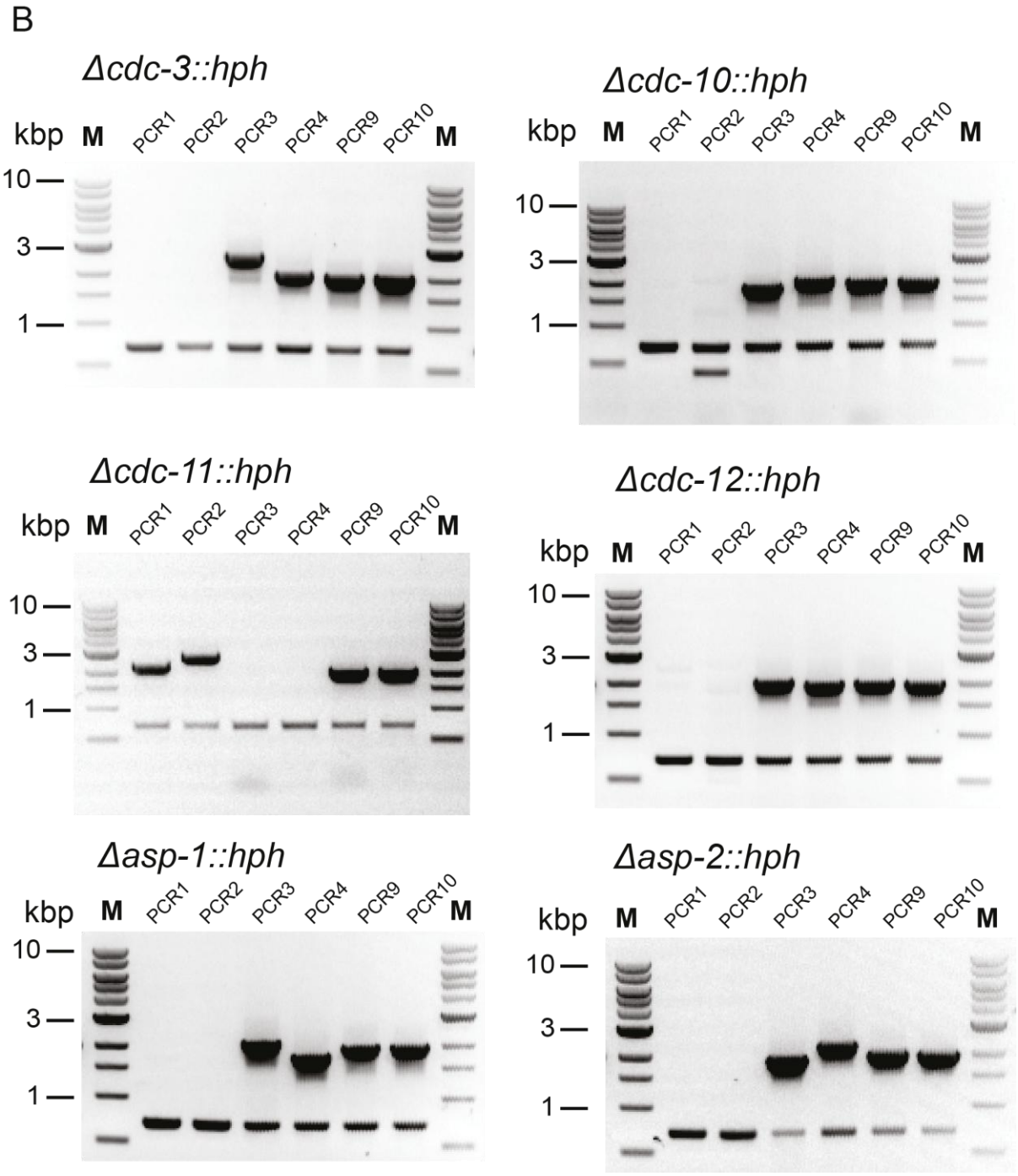
B
Δcdc-3::hph
kbp M PCR1 PCR2 PCR3 PCR4 PCR9 PCR10 M
10
3
1
Δcdc-10::hph
kbp M PCR1 PCR2 PCR3 PCR4 PCR9 PCR10 M
10
3
1
Δcdc-11::hph
kbp M PCR1 PCR2 PCR3 PCR4 PCR9 PCR10 M
10
3
1
Δcdc-12::hph
kbp M PCR1 PCR2 PCR3 PCR4 PCR9 PCR10 M
10
3
1
Δasp-1::hph
kbp M PCR1 PCR2 PCR3 PCR4 PCR9 PCR10 M
10
3
1
Δasp-2::hph
kbp M PCR1 PCR2 PCR3 PCR4 PCR9 PCR10 M
10
3
1

Figure A.1

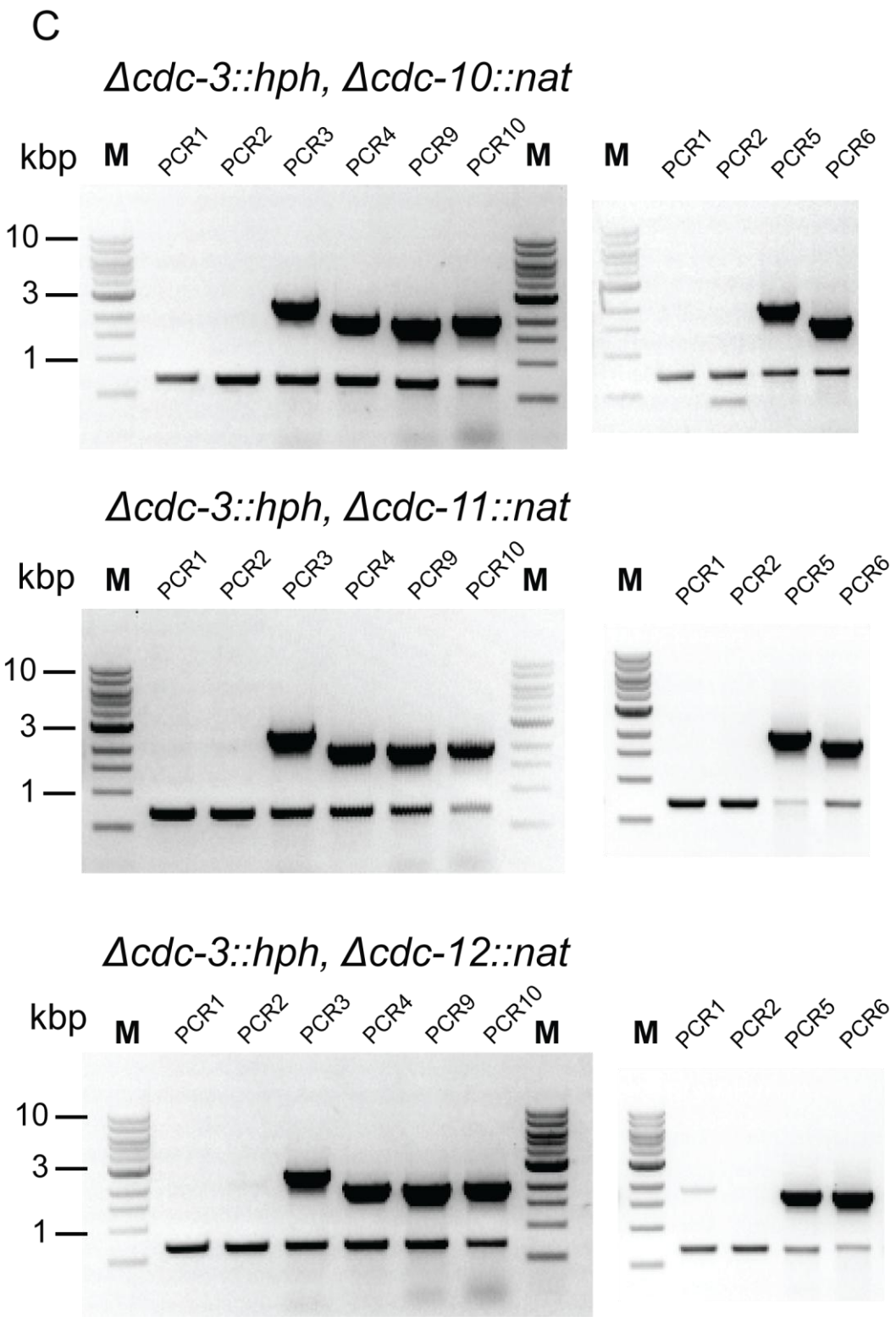
C
Δcdc-3::hph, Δcdc-10::nat
kbp
M
PCR1
PCR2
PCR3
PCR4
PCR9
PCR10
M
M
PCR1
PCR2
PCR5
PCR6
10
3
1
Δcdc-3::hph, Δcdc-11::nat
kbp
M
PCR1
PCR2
PCR3
PCR4
PCR9
PCR10
M
M
PCR1
PCR2
PCR5
PCR6
10
3
1
Δcdc-3::hph, Δcdc-12::nat
kbp
M
PCR1
PCR2
PCR3
PCR4
PCR9
PCR10
M
M
PCR1
PCR2
PCR5
PCR6
10
3
1

Figure A.1

C

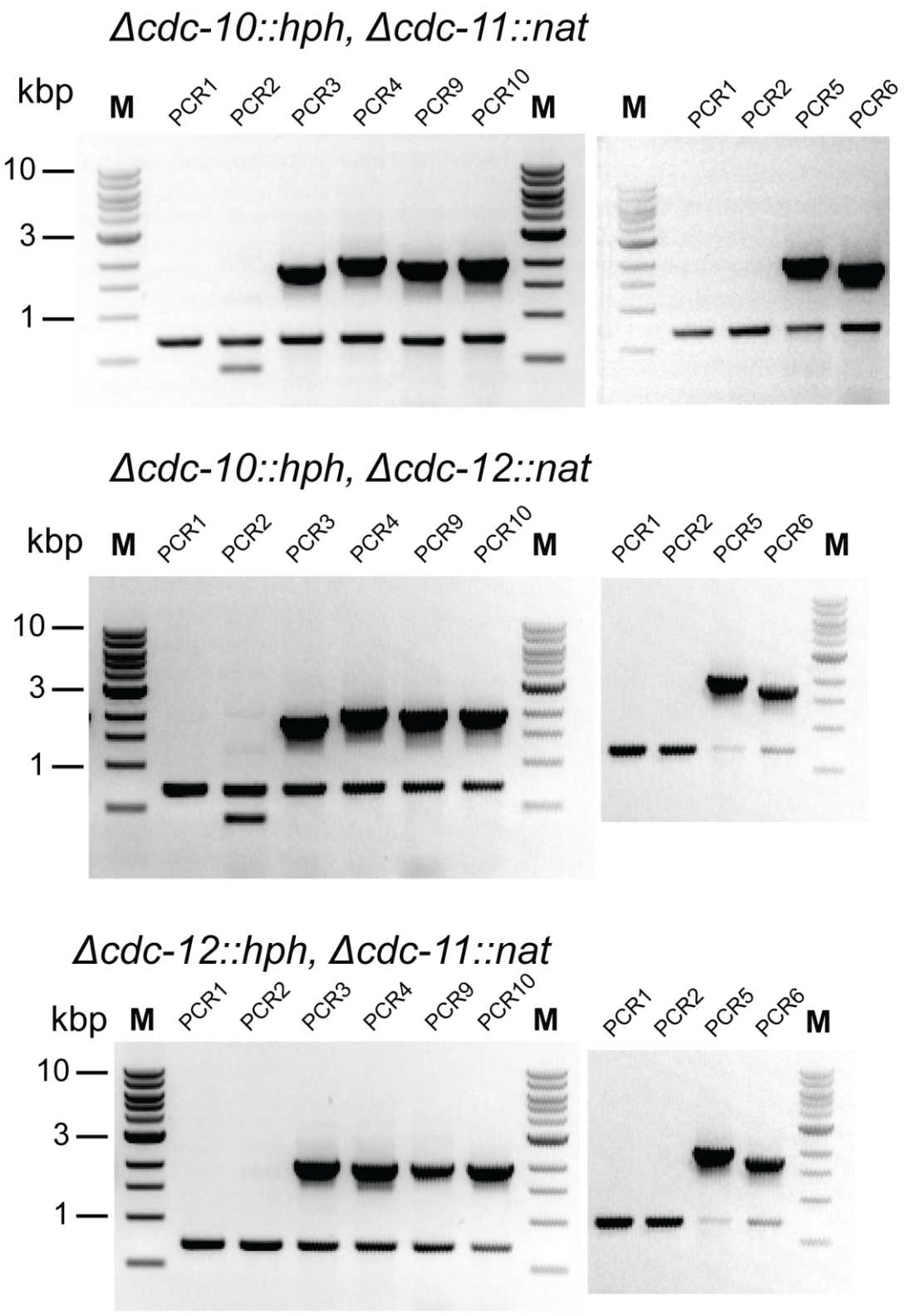
Δcdc-10::hph, Δcdc-11::nat
kbp
M
PCR1
PCR2
PCR3
PCR4
PCR9
PCR10
M
M
PCR1
PCR2
PCR5
PCR6
10
3
1
Δcdc-10::hph, Δcdc-12::nat
kbp
M
PCR1
PCR2
PCR3
PCR4
PCR9
PCR10
M
PCR1
PCR2
PCR5
PCR6
M
10
3
1
Δcdc-12::hph, Δcdc-11::nat
kbp
M
PCR1
PCR2
PCR3
PCR4
PCR9
PCR10
M
PCR1
PCR2
PCR5
PCR6
M
10
3
1

Figure A.1

D

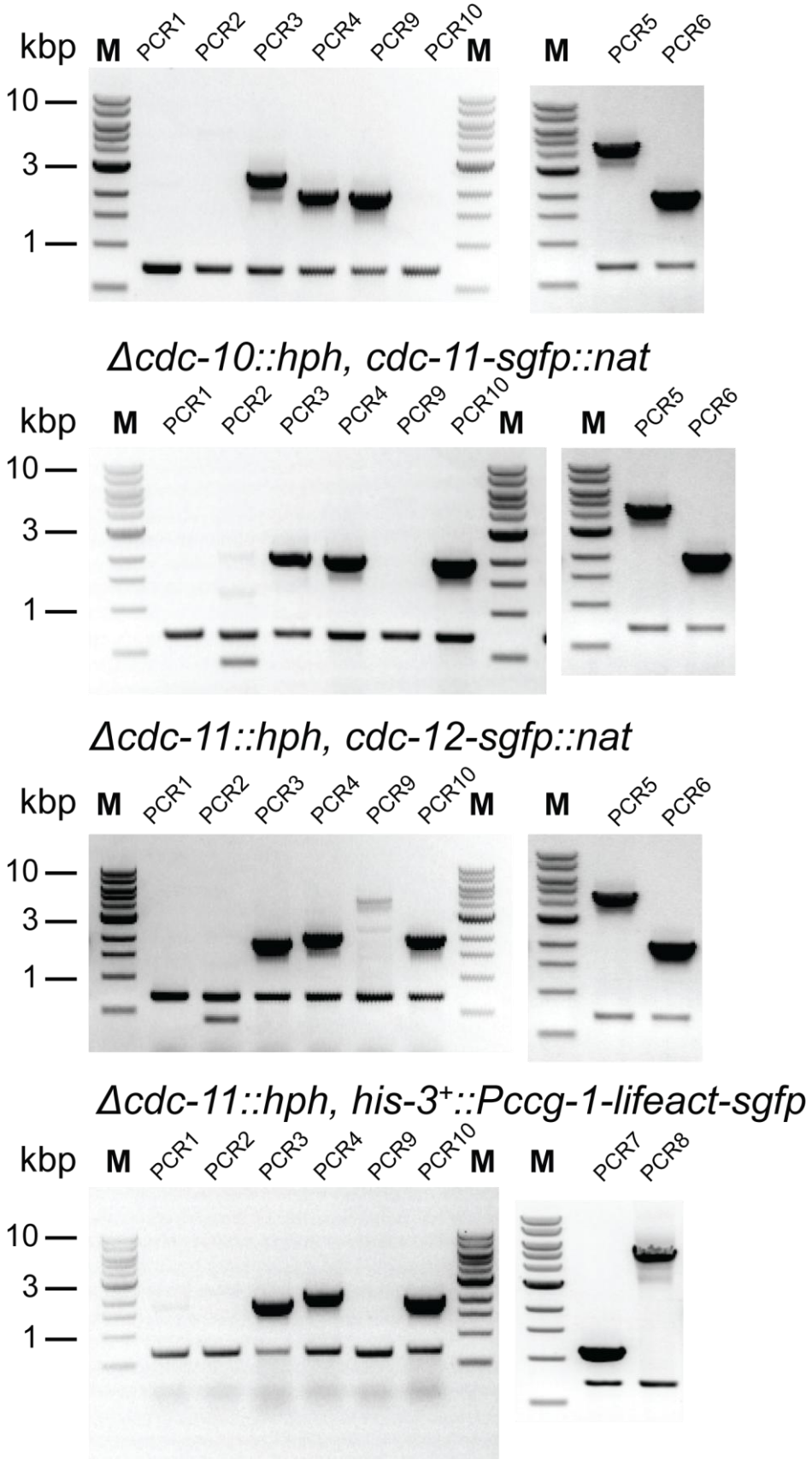
Δcdc-3::hph, cdc-11-sgfp::nat
kbp
M
PCR1
PCR2
PCR3
PCR4
PCR9
PCR10
M
M
PCR5
PCR6
10
3
1
Δcdc-10::hph, cdc-11-sgfp::nat
kbp
M
PCR1
PCR2
PCR3
PCR4
PCR9
PCR10
M
M
PCR5
PCR6
10
3
1
Δcdc-11::hph, cdc-12-sgfp::nat
kbp
M
PCR1
PCR2
PCR3
PCR4
PCR9
PCR10
M
M
PCR5
PCR6
10
3
1
Δcdc-11::hph, his-3+::Pccg-1-lifeact-sgfp
kbp
M
PCR1
PCR2
PCR3
PCR4
PCR9
PCR10
M
M
PCR7
PCR8
10
3
1

Figure A.1

D

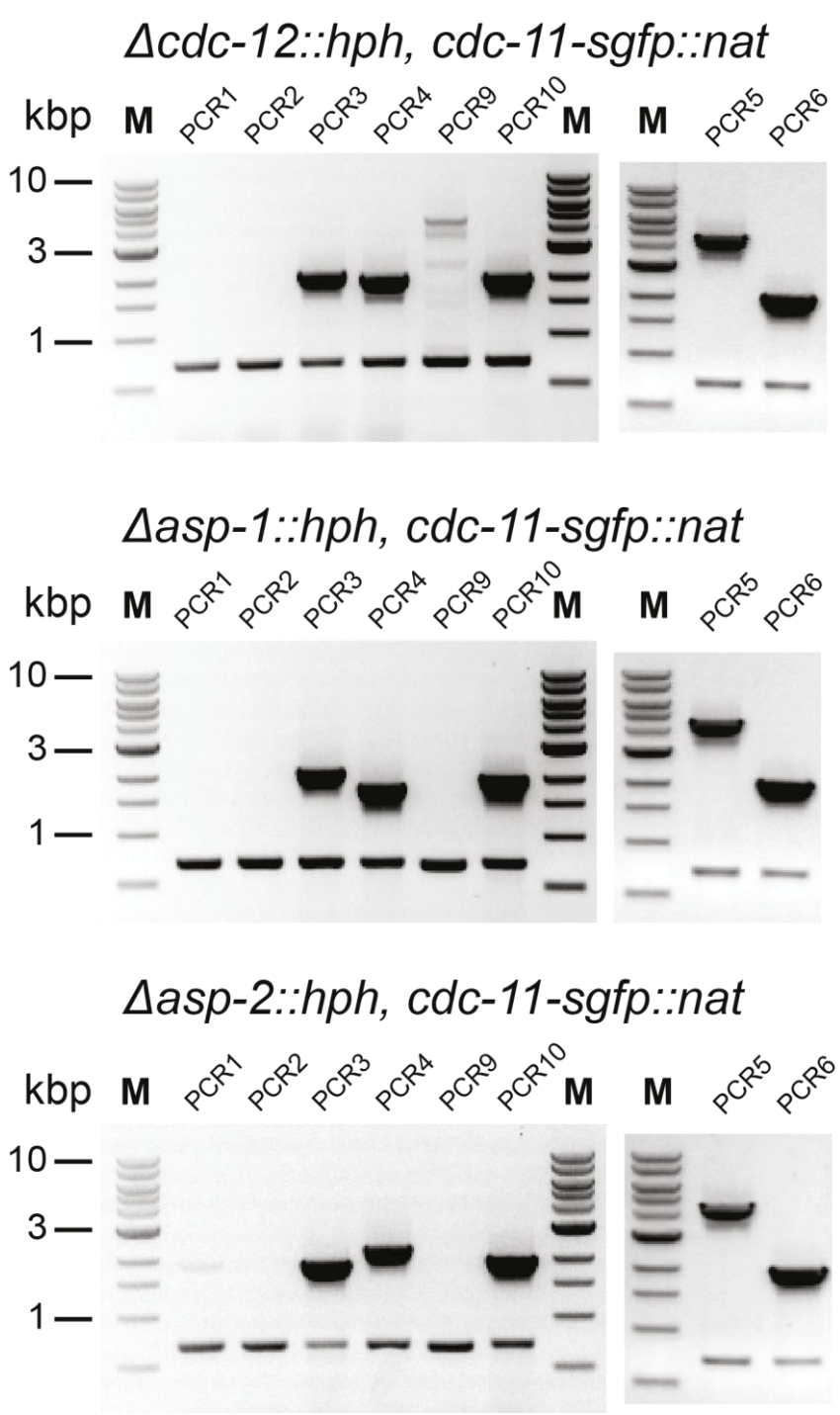
Δcdc-12::hph, cdc-11-sgfp::nat
kbp
M
PCR1
PCR2
PCR3
PCR4
PCR9
PCR10
M
M
PCR5
PCR6
10
3
1
Δasp-1::hph, cdc-11-sgfp::nat
kbp
M
PCR1
PCR2
PCR3
PCR4
PCR9
PCR10
M
M
PCR5
PCR6
10
3
1
Δasp-2::hph, cdc-11-sgfp::nat
kbp
M
PCR1
PCR2
PCR3
PCR4
PCR9
PCR10
M
M
PCR5
PCR6
10
3
1

Figure A.1

E

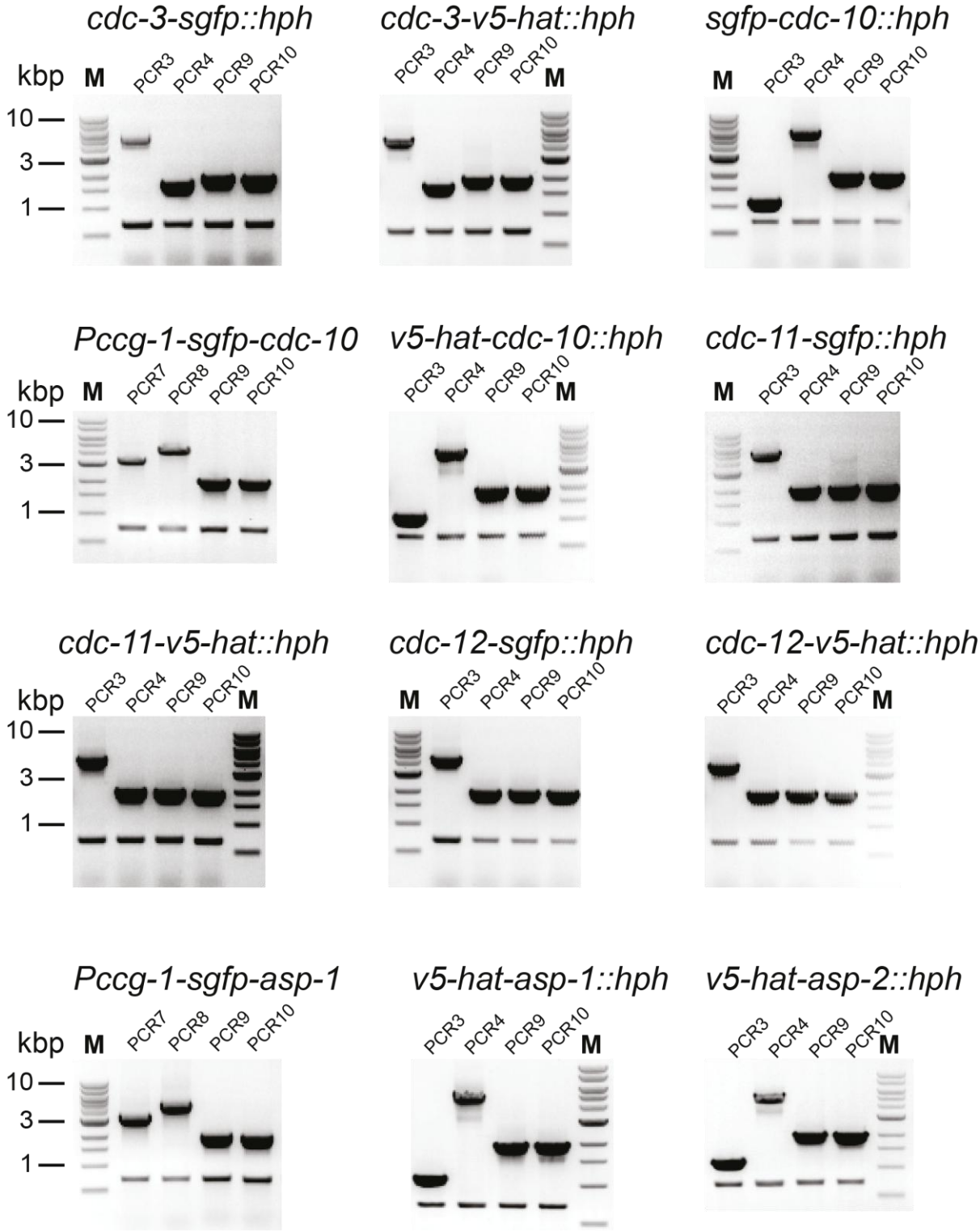
cdc-3-sgfp::hph
kbp
M
PCR3
PCR4
PCR9
PCR10
10
3
1
cdc-3-v5-hat::hph
PCR3
PCR4
PCR9
PCR10
M
sgfp-cdc-10::hph
M
PCR3
PCR4
PCR9
PCR10
Pccg-1-sgfp-cdc-10
kbp
M
PCR7
PCR8
PCR9
PCR10
10
3
1
v5-hat-cdc-10::hph
PCR3
PCR4
PCR9
PCR10
M
cdc-11-sgfp::hph
M
PCR3
PCR4
PCR9
PCR10
cdc-11-v5-hat::hph
kbp
PCR3
PCR4
PCR9
PCR10
M
10
3
1
cdc-12-sgfp::hph
M
PCR3
PCR4
PCR9
PCR10
cdc-12-v5-hat::hph
PCR3
PCR4
PCR9
PCR10
M
Pccg-1-sgfp-asp-1
kbp
M
PCR7
PCR8
PCR9
PCR10
10
3
1
v5-hat-asp-1::hph
PCR3
PCR4
PCR9
PCR10
M
v5-hat-asp-2::hph
PCR3
PCR4
PCR9
PCR10
M

Figure A.1. PCR-based genotyping of deletion strains, septin-GFP strains and septin-V5-HAT strains. Refer to Figure 2.2 for details of primer binding locations. Primers sets were chosen to confirm the presence of the wild-type gene (primers set G1+G2 = PCR1 and primers set G3+G4 = PCR2), integration of the deletion or epitope cassette (primers set G1 + HPH2 = PCR3, primers set G4 + HPH1 = PCR4, primers set G1 + NAT2 = PCR5, primers set G4 + NAT1 = PCR6), integration of His-3 Pccg-1 GFP overexpression cassette (primers set GFP Fw + His3 Rv = PCR7, primers set GFP Rv + His3 Fw = PCR8) or to check the presence of mus-51 (primers set MUS-51 Fw + MUS-51 Rv = PCR9) and mus-52 (MUS-51 Fw + MUS-51 Rv = PCR10). For strains with two integration events two gel pictures are shown – on the left is confirmation of integration of the hygromycin resistance cassette while on the right is shown the absence of the second deleted gene and confirmation of integration of the nourseothricin resistance cassette or *his*-3-based cassette. The lower band in the gels is an actin amplicon internal control to confirm the presence of genomic DNA. The positions of DNA size markers (M, in kbp) are shown at the left or right of the panels and the template DNA used for the PCR is in italics above the gel. (A) PCR-based genotyping of wild-type genomic DNA to confirm lack of non-specific primer binding. (B) Genotyping PCRs on single septin deletion strains. (C) Genotyping PCRs on double septin deletion strains. (D) Genotyping PCRs on septin null mutants expressing GFP-tagged septins or Lifeact-GFP. (E) Genotyping PCRs on septin-GFP and septin-V5-HAT strains.

Figure A.2

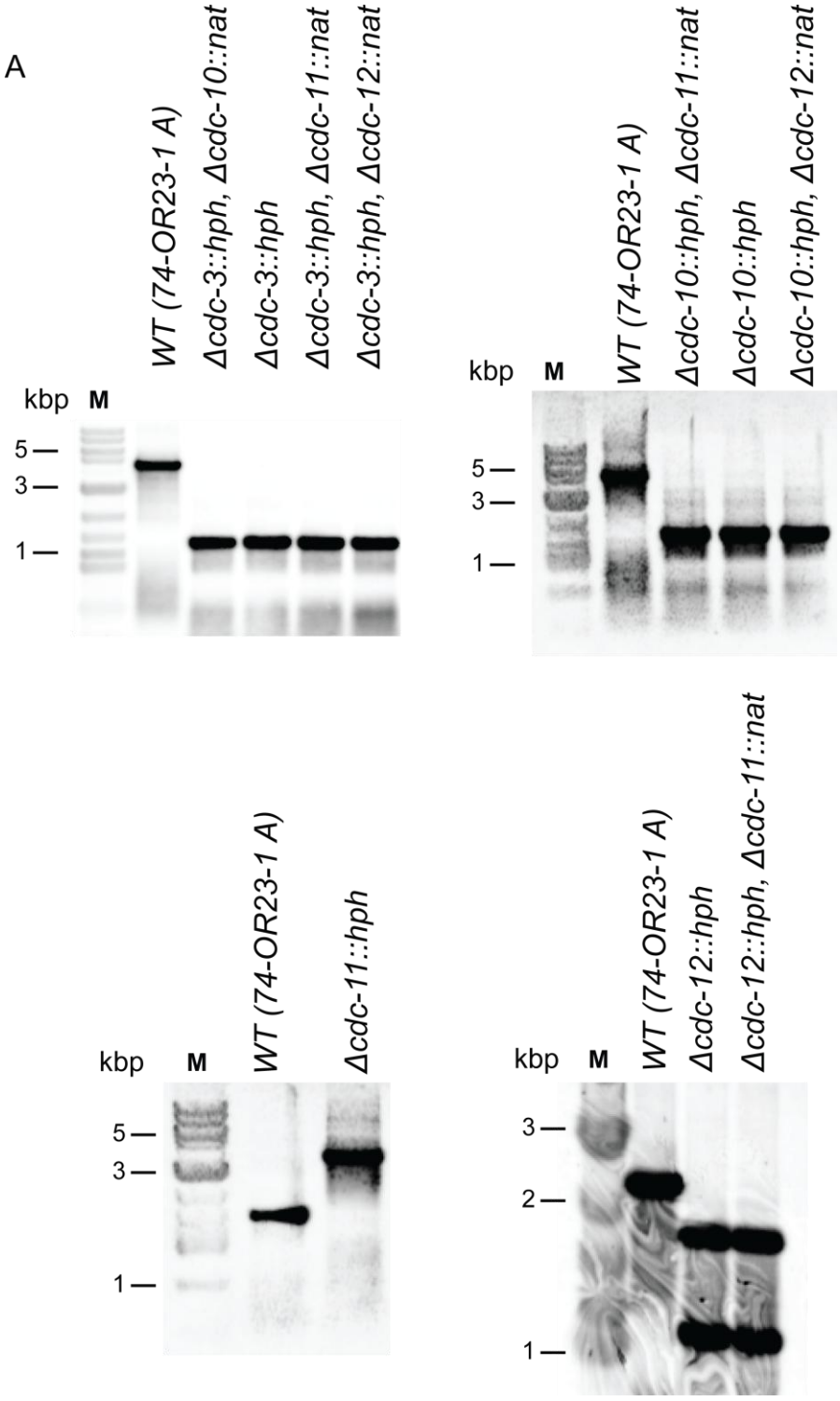
A
WT (74-OR23-1 A)
Δcdc-3::hph, Δcdc-10::nat
Δcdc-3::hph
Δcdc-3::hph, Δcdc-11::nat
Δcdc-3::hph, Δcdc-12::nat
kbp
M
5
3
1
WT (74-OR23-1 A)
Δcdc-10::hph, Δcdc-11::nat
Δcdc-10::hph
Δcdc-10::hph, Δcdc-12::nat
kbp
M
5
3
1
WT (74-OR23-1 A)
Δcdc-11::hph
kbp
M
5
3
1
WT (74-OR23-1 A)
Δcdc-12::hph
Δcdc-12::hph, Δcdc-11::nat
kbp
M
3
2
1

Figure A.2

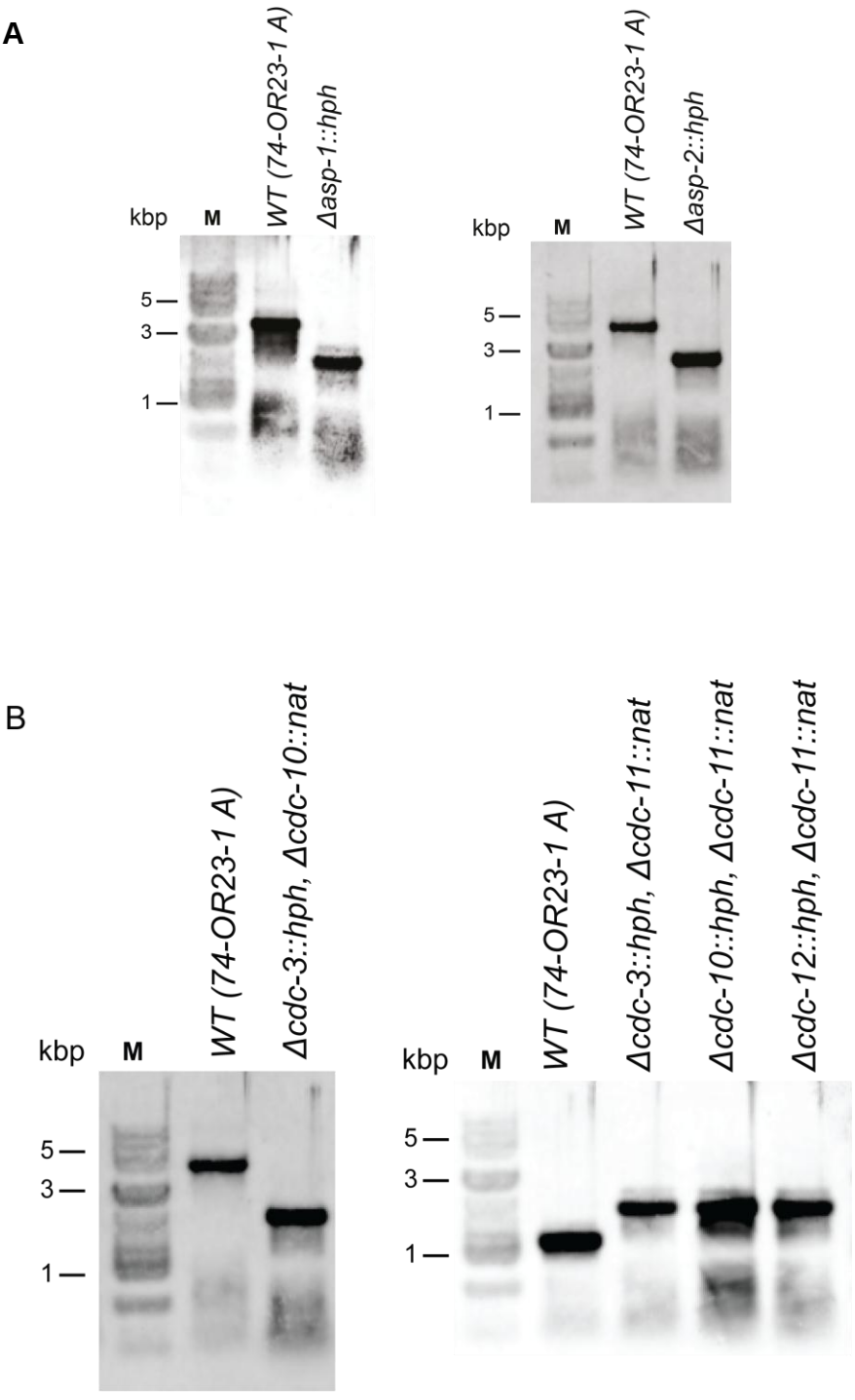
A
kbp
M
WT (74-OR23-1 A)
Δasp-1::hph
5
3
1
kbp
M
WT (74-OR23-1 A)
Δasp-2::hph
5
3
1
B
kbp
M
WT (74-OR23-1 A)
Δcdc-3::hph, Δcdc-10::nat
5
3
1
kbp
M
WT (74-OR23-1 A)
Δcdc-3::hph, Δcdc-11::nat
Δcdc-10::hph, Δcdc-11::nat
Δcdc-12::hph, Δcdc-11::nat
5
3
1

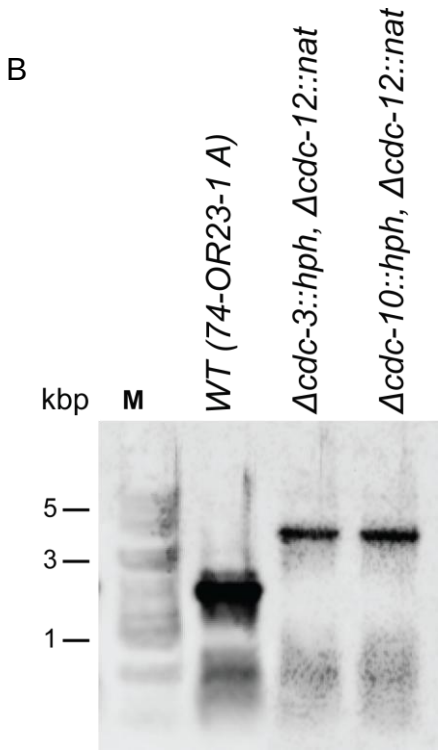

Figure A.2. Southern blotting analysis of septin deletion strains. The positions of DNA size markers (M, in kbp) are shown at the left or right of the panels. (A) Genomic DNA from wild-type and septin deletion strains generated with a hygromycin resistance cassette was probed with *hph*-3'UTR-based probe. DNA fragments detected in deletion strains matches the predicted fragment sizes (see Table 2.1). (B) Genomic DNA from wild-type and septin deletion strains generated with a nourseothricin resistance cassette was probed with *nat*-3'UTR-based probe. DNA fragments detected in deletion strains matches the predicted fragment sizes (see Table 2.1).

Supplementary movie 1. Actin cables are in constant flux and exhibit 'exploratory' movement when untethered or severed. The arrow denotes cable becomes untethering. Bar, 2 µm.

Supplementary movie 2. Complex arrays of actin cables form at the tip of germ tubes and undergo retrograde movement. The extension rate of the germ tube was 0.37 µm/min. Bar, 2 µm.

Supplementary movie 3. Actin cable dynamics in an elongating germ tube. Actin arrays are continually formed at the tip and exhibit retrograde movement while the germ tube is growing. The extension rate of the germ tube was 1.5 µm/min. Bar, 2 µm.

Supplementary movie 4. F-actin dynamics in the tip of a mature hypha. Actin is concentrated within the core of the Spitzenkörper and actin patches are localised in a subapical collar. The extension rate of the hypha was 11.4 µm/min. Bar, 2 µm.

Supplementary movie 5. Actin patches travel along actin cables in a discontinuous manner. Bar, 2 µm.

Supplementary movie 6. MYO-5-GFP particles travel along underlying linear tracks towards the hyphal tip. Bar, 5µm.

List of publications

Berepiki, A., A. Lichius, and N.D. Read. 2011. Actin organization and dynamics in filamentous fungi. *Nat Rev Microbiol*. 9:876-887

Lichius, A., A. Berepiki, and N.D. Read. 2011. Form follows function - the versatile fungal cytoskeleton. *Fungal Biol*. 115:518-540

Hoi, J.W., C. Lamarre, R. Beau, I. Meneau, A. Berepiki, A. Barre, E. Mellado, N.D. Read, and J.P. Latge. 2011. A novel family of dehydrin-like proteins is involved in stress response in the human fungal pathogen *Aspergillus fumigatus*. Mol Biol Cell. 22:1896-1906

Berepiki, A., A. Lichius, J.Y. Shoji, J. Tilsner, and N.D. Read. 2010. F-actin dynamics in *Neurospora crassa*. *Eukaryot Cell*. 9:547-557